NUMERICAL MODELLING OF DYNAMICAL SYSTEMS IN ISOTHERMAL CHEMICAL REACTIONS AND MORPHOGENESIS

A thesis submitted for the degree of Doctor of Philosophy

by

Zeynep Aysun Çınar

Department of Mathematics and Statistics, Brunel University

July 1999

Abstract

Mathematical models of isothermal chemical systems in reactor problems and Turing's theory of morphogenesis with an application in sea-shell patterning are studied. The reaction-diffusion systems describing these models are solved numerically. First- and second-order difference schemes are developed, which are economical and reliable in comparison to classical numerical methods. The linearization process decouples the reaction-diffusion equations thereby allowing the use of different time steps for each differential equation, which may be large due to the excellent stability properties of the methods. The methods avoid having to solve a non-linear algebraic system at each time step. The schemes are suitable for implementation on a parallel machine.

Contents

List of Tables

List of Figures

Acknowledgements

I wish to express my special gratitude to my supervisior Prof. E. H. Twizell for his excellent supervision and professionalism and for always having an open door throughout this period of my thesis. I wish to thank him for making this thesis possible and for his unwavering support on bad as well as good days.

This is a pleasant opportunity to thank Dr S. Matar for his invaluable positive assistance and encouragement throughout my stay at Brunel. I am also grateful to Dr J. Furter for his valuable suggestions. I would like to take the opportunity to also thank Dr E. L. Short from the Department of Chemistry, Brunel for his informative discussion in chemical dynamics during the first year of my research. I wish to express my gratitude to University of Dokuz Eylül for the scholarship and support provided throughout the duration of this thesis. Special gratitude goes to Prof. Güzin Gökmen and Dr Şennur Somalı for their support. I also would like to thank the staff in the Mathematics and Statistics Department here at Brunel and friends both in academia and elsewhere for providing continual support and enjoyment throughout my research time.

My very special gratitude goes to Dr U. S. Herges for his constant support, encouragement and always being there for me. Thank you!

I wish to dedicate this thesis to my mother and the memory of my father who dedicated his life to us. They are not mathematicians, yet I have learnt from them all the really important things that motivated me to become one: love of scholarship and admiration for the beauty of science.

"The waves of the sea, the little ripples on the shore, the sweeping curve of the sand bay between the headlands, the outline of the hills, the shape of the clouds, all these are so many riddles of form, so many problems of morphology, and all of them the physicist can more or less easily read and adequately solve... Nor is it otherwise with the form of living things. "

D' Arcy Wentworth Thompson.

TO MY MOTHER AND

IN LOVING MEMORY OF MY FATHER

Chapter 1

Introduction

Human beings live in a universe of patterns. Every night the stars move in circles across the sky. No two snowflakes are ever exactly the same, but they all have sixfold symmetry. Tigers and zebras are covered in patterns of stripes, leopards are covered in patterns of spots. Intricate trains of waves march across the oceans, very similar trains of sand-dunes march across the desert.

Morphogenesis can be applied to describe any of the dynamic processes by which form and pattern are generated in biological systems. One of the main characteristic of morphogenetic processes is the fact that particular forms and patterns of obvious similarity can arise in completely unrelated organisms. Much has been made of the universal occurrence of DNA, RNA, and protein in all organisms, and in the universality of the mechanism by which genetic message, carried at least in part in DNA, are transcribed into functional protein.

After 1950 Turing thought most about his own, completely original, mathematical theory of morphogenesis. He was the first to use a computer for hands-on mathematical research of this kind. His work can now be seen as the beginning of the huge field of non-linear systems involving chaos, fractals and complexity. He was certainly very aware of how a small change in parameters could tip a dynamical system from stability into instability. Turing theory is concerned with one of the basic questions in this morphogenetic behaviour in biological systems such as "how

is it possible for an initially homogeneous aggregate of cells to acquire differentiated characteristics?"

By using mathematics all these patterns can be recognized, classified and modelled. By doing this one can understand that patterns are actually vital clues to the rules that govern natural processes.

As well as nature's patterns, nature's rhythms, such as heart beats, are also not random but regular processes. The organizing principle behind these and many other biological cycles is the mathematical concept of an oscillator. The most obvious oscillators are an animal's limb, but the main oscillators that concern us are found in the creature's nervous system, the neural circuitry that generates the rhythmic electrical signals that stimulate and control the limb's activity.

In this thesis, mathematical models of these fascinating phenomena of nature together with Turing's celebrated theory of morphogenesis are discussed and studied. First the principles of chemical reactions are studied and then uncoupled and coupled oscillatory chemical systems are examined and finally these systems are investigated in pattern formation.

The thesis aims to derive mathematical models of some of these chemical and biological systems and develop finite-difference schemes for the numerical solution of the ordinary and partial differential equations which model those systems.

Since the discovery and development of powerful computers the finite-difference method has become the most, or at least one of the most, commonly used methods in computation, especially in large-scale scientific computation of many practical problems. The numerical schemes are implicit in nature but are applied explicitly; therefore they are convenient, appropriate and easy to implement for the solution of various problems of non-linear, stationary or non-stationary partial differential equations.

For numerical computation of ordinary differential equations the error analysis, and stability properties of particular finite-difference schemes are investigated. The Routh-Hurwitz criterion is used when the Jacobian has order greater than

two; stability conditions are given in terms of Routh-Hurwitz inequalities May [36]. Throughout the numerical experiments Mathematica v3.0.2 (Solaris 2.x) is used to do simple but lengthy calculations, such as finding the eigenvalues of some Jacobians.

For the numerical solution of reaction-diffusion systems, the error analysis, the convergence and von Neumann type stability analyses are investigated. The von Neumann method for stability is applied succesfully for all numerical schemes developed.

The convergence of the discrete solutions to a generalized solution of the reaction-diffusion problems is stated in detail. As the grid size tends to zero, the discrete solution and its difference quotients appearing in the scheme converge respectively to a limiting vector function and its appropriate derivatives. The limiting vector function is just the unique generalized global vector solution for the original problem of those non-linear parabolic systems which arrise as mathematical models of the chemical and biological problems. This yields the existence and uniqueness of the generalized global solution of the problem of the general non-linear parabolic system and shows that the finite-difference schemes converge in a certain sense in the space of the generalized global solutions.

Some of the numerical methods developed in this thesis can be applied by using several processors working in parallel. This is an important feature in terms of efficiency and speed in computing. Programs are designed and written in the FORTRAN 90 programming language.

An introduction to chemical dynamics is given in §1.1 of this chapter of the thesis.

In Chapter 2, various preliminary definitions as well as theorems referred to in the rest of the thesis are explained.

Chapter 3 deals with relatively simple molecular mechanisms, general order of autocatalysis and decay in isothermal chemical system. These chemical reactions are studied in general and account for a primary pattern of morphogenesis to determine pattern formation of tissue and sea shells in Chapters 7 and 8, respectively. First-

and second-order numerical methods are proposed to solve the well-stirred model. Double-zero eigenvalue degeneracy is discovered and studied. A family of finite-difference schemes are used to solve the reaction-diffusion system.

Chapter 4 outlines the principles of oscillatory systems in a pooled chemical reaction. The chemical reactions are studied and a mathematical model is derived. The Hopf bifurcation phenomenon is discovered and studied in detail. An unconditionally stable first-order numerical method is developed and a second-order method is also obtained.

Chapter 5 describes the coupled version of a pooled chemical reaction problem which is a simple example of Turing's equations of cellular biology studied in Chapter 7. Coupling through a reactant $\mathcal{A}$ and through autocatalysis $\mathcal{B}$ creates sytems of ordinary differential equations which are all studied qualitatively and numerically in detail by using first- and second-order finite-difference schemes. An unconditionally stable first-order numerical scheme is developed for the case of coupling through autocatalysis $\mathcal{B}$. Complex dynamical behaviour such as periodic transitions to quasi-periodic transitions, Hopf, flip and fold type of bifurcations, hysteresis phenomenon, secondary Hopf bifurcation are investigated.

Chapter 6 gives an introduction to the development of organisms. It describes the basic network structures including Turing's ring-of-isolated-cells model which is studied in Chapter 7.

Chapter 7 is devoted to the fascinating problem of Turing's model for the growing embryo. Turing's theory of morphogenesis is described and his two approaches, ring of cells and continuous ring of tissue, are analysed in detail. First-order finite-difference schemes are developed and applied for Turing's suggested numerical example, a six-cell problem. A family of numerical methods is developed and applied to solve the reaction-diffusion system which models the numerical example of twenty-cell problem. The mathematical framework outlined in this chapter may be used for the description of many other dynamical systems. To create a random effect for initial conditions the random number generator, RANDOM(), is used to create

initial conditions. The RANDOM() routine returns a uniformly distributed random number between 0.0D0 and 1.0D0.

Chapter 8 is a special application of Turing's theory of pattern formation to sea shell patterning. The activator-inhibitor scheme, a reaction-diffusion system, is studied and a set of chemical reactions is proposed to explain the model. A family of numerical schemes are developed and analysed to approximate the reaction-diffusion equations of the model.

Parts of the contents of Chapter 4 have been contained in a technical report Çınar and Twizell [8]. Parts of the contents of Chapter 5 were presented at a numerical analysis conference in Dundee in 1997 and will appear in the proceedings of the "Conference on Finite-difference methods: Theory and Applications", held in August 1997 in Rousse, Bulgaria.

1.1 Chemical Dynamics

A chemical reaction is a process in which one or more substances, the reactants, combine or separate to form one or more other substances, the products. Mass is conserved in such a process but energy is not. The conservation of mass in one such reaction is represented by the symbolic equation

$$\mathcal{A} + \mathcal{B} \rightarrow \mathcal{P}, \quad \text{rate} = kab. \tag{1.1}$$

This says that one molecule of substance $\mathcal{A}$ combines with one molecule of substance $\mathcal{B}$ to form one molecule of substance $\mathcal{P}$. Due to the microscopic nature of molecules, however, one prefers to count them in units of approximately 6.024×10^{23} (Avagadro's Number). This amount of molecules of substance $\mathcal{X}$ is called a **mole** of $\mathcal{X}$. Then (1.1) may also be read as saying that a mole of $\mathcal{A}$ combines with a mole of $\mathcal{B}$ to produce a mole of $\mathcal{P}$. Due to the random motion of molecules, collisions occur. Such collisions give rise to combinations of molecules. But the greater the concentration of each substance the greater the number of collisions between respective molecules. It

therefore seems reasonable to assume that the rate at which $\mathcal{A}$ and $\mathcal{B}$ are converted into $\mathcal{P}$ will be proportional to the concentration of substance $\mathcal{X}$, in moles per unit volume. This could be expressed in the following form

$$\begin{aligned} \text{Rate of Increase of Product} &= \text{Rate of Conversion of Reactant} \\ \frac{d}{dt}[\mathcal{P}] &= k[\mathcal{A}][\mathcal{B}], \end{aligned} \tag{1.2}$$

where k is a constant. Suppose that $\varpi(t)$ moles of $\mathcal{A}$ and $\mathcal{B}$ are converted to $\mathcal{P}$ in time t, that is, $\varpi(t)$ moles of $\mathcal{A}$ plus $\varpi(t)$ moles of $\mathcal{B}$ become $\varpi(t)$ moles of $\mathcal{P}$. Then, if a_0 and b_0 denote the initial concentrations of $\mathcal{A}$ and $\mathcal{B}$, (1.2) becomes

$$\frac{d\varpi}{dt} = k(a_0 - \varpi(t))(b_0 - \varpi(t)). \tag{1.3}$$

Equation (1.3) is a mathematical model for the dynamics of the chemical reaction that is described symbolically by (1.1). One should check that, as $t \to \infty$ in the solution, the product concentration ϖ tends to $\min(a_0, b_0)$, whereas the reactant concentrations tend to 0 and $\max(a_0, b_0) - \min(a_0, b_0)$. In other words, the lesser abundant of the two reactants is completely converted into a constituent of the product. The simplest form of flow system is "CSTR", continuous flow, stirred-tank reactor, represented schematically in Fig. 1.1. "Continuous" refers to a continuous flow entering (and leaving) the reactor, in other words, a CSTR is an open system. Human beings and other living organisms that have input of reactants (nutrients) and output of products (wastes) are complex examples of CSTRs.

It is in open systems that truly stationary states can be realized or oscillatory behaviour sustained indefinitely. Stationary states arise as a balance between the production or consumption of species by chemical reaction and their net rates of departure and arrival by flow or diffusion. The simplest of open systems to analyse mathematically is the continuous flow, stirred-tank reactor where compositions are uniform and there is no need to solve partial differential equations to describe spatial behaviour.

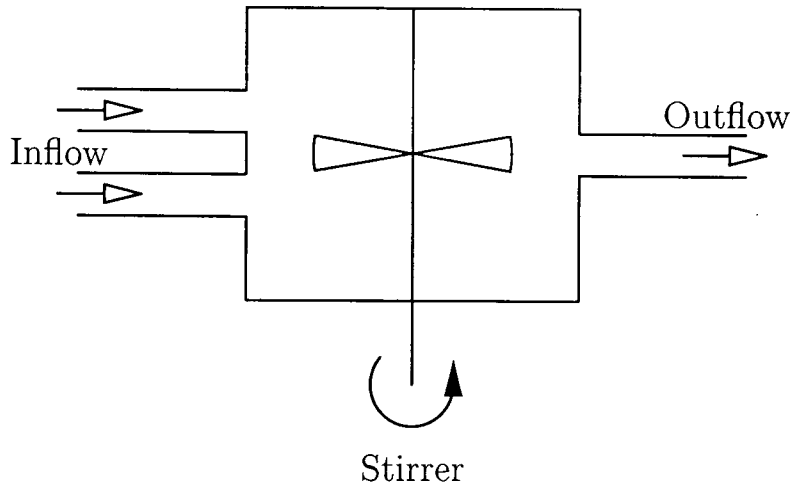

Figure 1.1: Schematic diagram of a continuous-flow well-stirred tank reactor.

1.1.1 Autocatalytic reactions in diffusion reactors

Well-stirred systems are particularly convenient for the theoretician but are often less easy to realize in practice. For example, the cubic autocatalytic process

$$\mathcal{A} + 2\mathcal{B} \to 3\mathcal{B}, \quad \text{rate} = k_1 ab^2 \tag{1.4}$$

is taken into consideration in a reaction-diffusion cell, represented schematically in Fig. 1.2.

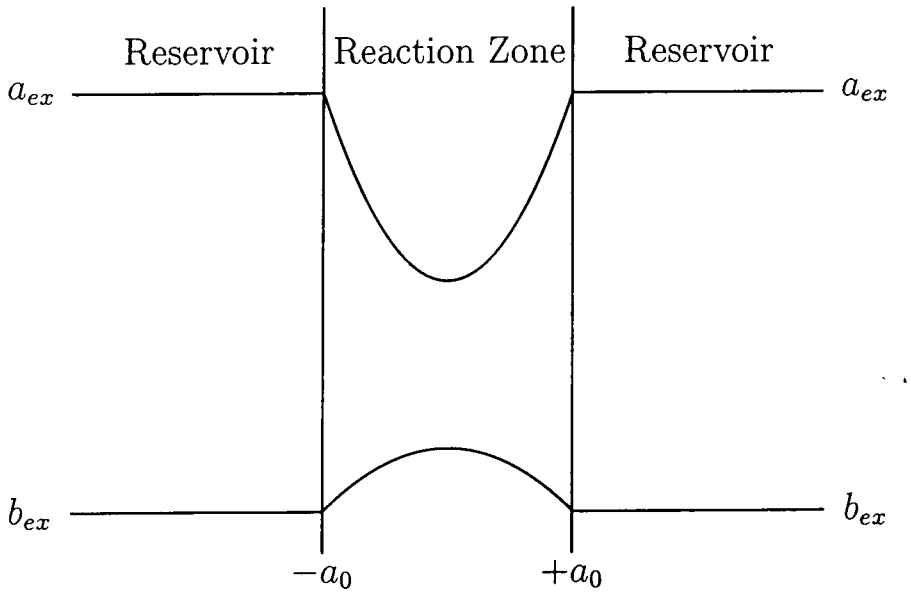

Figure 1.2: A reaction-diffusion cell.

The reactants and products, here denoted $\mathcal{A}$ and $\mathcal{B}$, have constant concentrations a_{ex} and b_{ex} in the surrounding reservoir, but these vary across the reaction zone,

$-a_0 \leq r \leq +a_0$. For the reaction kinetics of (1.4), the equation forms as follows

$$\begin{array}{lcll} \dfrac{\partial a}{\partial t} & = & D_A \dfrac{\partial^2 a}{\partial r^2} & - \quad k_1 a b^2 \\ \text{rate of change} & & \text{diffusion} & \text{chemistry} \end{array}$$

Here, the first term on the right hand side gives the net diffusive inflow of species $\mathcal{A}$ into the volume element. It is assumed that the diffusive process follows *Fick's law* (see Crank [7], page 2) and that the diffusion coefficient does not vary with position.

Chapter 2

Mathematical Preliminaries

2.1 About the Numerical Methods

Most mathematical models of dynamic systems are formulated in terms of differential equations. Much of the analysis of the solution behaviour of a given differential equation is done by means of constructing numerical solutions. The most important matter is how one may construct finite-difference models such that the solutions do not contain instabilities and/or chaotic behaviour and at the same time reflect the qualitative behaviour of the continuous-time system well. Consider a given first-order ordinary differential equation (ODE) system of the form

$$\frac{dy}{dt} = y'(t) = f(y(t)), \quad t \in I, \quad y(0) = y_0 \in \mathbb{R}^m. \tag{2.1}$$

Here f is a sufficiently well-behaved function that maps $[t_0, \infty) \times \mathbb{R}^m$ to $\mathbb{R}^m$ and the initial condition $y_0 \in \mathbb{R}^m$ is a given vector; $\mathbb{R}^m$ denotes $m-$ dimensional real Euclidean space. A numerical solution of (2.1) will be computed either in a compact interval $I = [t_0, t_0+t^*]$, or the half-line $I = [0, \infty)$ with some time-stepping numerical methods. In other words, the interval will be covered by an equidistant grid and the time-stepping procedure is employed to produce a numerical solution. Each grid is associated with a different numerical sequence and the critical question is whether, as $\ell \to 0$ and the grid is refined, the numerical solution tends to the exact

solution of (2.1) Jordan and Smith [21]. All numerical methods for (2.1) generate approximations $y_0, y_1, \ldots, y_n, \ldots$ to the true values $y(t_0), y(t_1), \ldots, y(t_n), \ldots$, where $0 = t_0 < t_1 < \ldots < t_n < \ldots$ is a grid in I. If I is bounded, the grid is assumed to have a finite number of grid-points t_n. If $I = [0, \infty)$ then n takes all positive integer values and $t_n \to \infty$ while it is clearly not feasible to actually compute infinitely many y_n, it is convenient to conceive of numerical integrations that cover arbitrarily long time intervals. More formally, it expresses the dependence of the numerical solution upon the step size by the notation $y_n = y_{n,\ell}$, $n = 0, 1, \ldots, \lfloor t^*/\ell \rfloor$ where $\lfloor \alpha \rfloor \in \mathbb{Z}$ is the integer part of $\alpha \in \mathbb{R}$. This discrete finite-difference model may be constructed by means of the following set of rules:

$$t \to t_n = (\Delta t)n = \ell n, \quad \ell = \Delta t, \tag{2.2}$$

$$y(t) \to y(t_n) = y_n, \tag{2.3}$$

$$\frac{dy}{dt} \to \begin{cases} \dfrac{y_{n+1} - y_n}{\ell} & , \text{ forward-Euler} \\ \dfrac{y_n - y_{n-1}}{\ell} & , \text{ backward-Euler} \\ \dfrac{y_{n+1} - y_{n-1}}{2\ell} & , \text{ central-difference} \end{cases} \tag{2.4}$$

It should also be noted that the derivative, $\dfrac{dy}{dt}$, can be modelled by more general expressions, such as

$$\frac{dy}{dt} \to \begin{cases} \dfrac{y_{n+1} - y_n}{\phi(\ell)} \\ \dfrac{y_n - y_{n-1}}{\phi(\ell)} \\ \dfrac{y_{n+1} - y_{n-1}}{2\phi(\ell)} \end{cases} \tag{2.5}$$

with $\phi(\ell)$ has the property

$$\lim_{\ell \to 0} \phi(\ell) = \ell + O(\ell^2).$$

Possible finite-difference models for non-linear terms such as y^2 or y^3 can be

$$y^2 \to \begin{cases} y_n^2 \\ y_{n+1} y_n \\ \dfrac{y_{n+1}^2 + y_{n+1} y_n + y_n^2}{3} \end{cases} \tag{2.6}$$

$$y^3 \to \left\{ y_{n+1} y_n \left(\frac{y_{n+1} + y_n}{2} \right) \right. \tag{2.7}$$

Most of the time, the best difference equation models the non-linear terms as non-local, that is y^2 is evaluated at two different lattice points [73]

$$y^2 \to y_n y_{n+1}. \tag{2.8}$$

Note that

$$\lim_{\ell \to 0} y_n y_{n+1} = \lim_{\ell \to 0} y_n^2 = y^2(t); \tag{2.9}$$

however, for finite, fixed, non-zero ℓ, the two representations may not be equal, that is,

$$y_n y_{n+1} \neq y_n^2. \tag{2.10}$$

When the modelling rules of equations are applied, the difference equation is given by

$$\frac{y_{n+1} - y_n}{\ell} = f(y_n, n\ell), \tag{2.11}$$

which has the structure

$$y_{n+1} = f(y_n, n, \ell). \tag{2.12}$$

If the function $f(y,t)$ depends on a set of parameters, $(c_1, c_2, \ldots, c_n)$, then the function $f(y_n, n, \ell)$ depends on the parameter set $(c_1, c_2, \ldots, c_n, \ell)$. Therefore, the dimension of the parameter space for the discrete finite-difference model is larger than the corresponding parameter space for the differential equation. This fact leads to the possibility of a greater variety of solution behaviour for the difference equation model as opposed to the differential equation. Within this framework, "numerical instabilities" can be defined as solutions to the difference equation model that have no qualitative correspondence to the solutions of the differential equation Mickens [49].

A method is said to be convergent if, for every ordinary differential equation (2.1) with a Lipschitz function f and every $t^* > 0$ it is true that

$$\lim_{\ell \to 0^+} \max_{n=0,1,\ldots,\lfloor t^*/\ell^* \rfloor} \| y_{n,\ell} - y(t_n) \| = 0.$$

For this reason, convergence means that, for every Lipschitz function, the numerical solution tends to the true solution as the grid becomes increasingly fine. In general, given an arbitrary time-stepping method

$$y_{n+1} = \mathscr{F}(f, \ell, y_0, y_1, \ldots, y_n), \quad n = 0, 1, \ldots, \tag{2.13}$$

for the ODE (2.1), the method is of order p if

$$y(t_{n+1}) - \mathscr{F}(f, \ell, y(t_0, y(t_1), \ldots, y(t_n))) = O(\ell^{p+1}) \tag{2.14}$$

for every analytic f and $n = 0, 1, \ldots$ The order of a numerical method provides the information about its local behaviour advancing from t_n to t_{n+1}, where $\ell > 0$ is sufficiently small, producing an error of $O(\ell^{p+1})$. In general, the global behaviour of the method is important rather than the local one. The local error decays as $O(\ell^{p+1})$ but the number of steps increases as $O(\ell^{-1})$. The naive expectation is that the global error decreases as $O(\ell^p)$ but it cannot be taken for granted for each and every numerical method. As far as Euler's method is concerned, it is indeed the case that the error decays as $O(\ell)$. Important questions that need to be considered are the following : How well is the numerical method doing in a fixed bounded interval of integration as $\ell \to 0$? Whether it converges to the true solution or not? And if it does how fast? These are essential questions that should be taken into consideration during the development of numerical schemes.

As discussed so far, the continous flow solution of (2.1) is approximated by a discrete map. In order to analyse the effectiveness of the numerical method for long-term computations, one therefore has to compare the long-term behaviour of the map and flow. The following definitions and theorems are the necessary tools to study the qualitative analysis of experimental dynamical systems.

2.2 Some Definitions and Theorems

Definition 1 (Fixed point) *If $y^* \in \mathbb{R}^n$ satisfies $f(y^*) = 0$ then y^* is a fixed point (equilibrium point, critical point, steady state) of the flow (2.1).*

Definition 2 (Locally attractive) *A fixed point y^* of (2.1) is locally attractive (linearly stable) if there exists a neighbourhood around y^* such that any solution $y(t)$ entering the neighbourhood satisfies $y(t) \to y^*$ as $t \to \infty$.*

Here the phrase neighbourhood around y^* means the set of points z such that $\|y^* - z\| < \delta$ for some norm $\|\cdot\|$ and some $\delta > 0$. The local attractivity of a fixed point may be analysed by writing $y(t) = y^* + \epsilon(t)$ and linearizing around the fixed point to obtain

$$\epsilon'(t) = y'(t) = f(y(t)) = f(y^* + \epsilon(t)) \approx f(y^*) + \frac{\partial f(y^*)}{\partial y}\,\epsilon(t). \qquad (2.15)$$

Since $f(y^*) = 0$, (2.15) becomes up to first order,

$$\epsilon'(t) = \frac{\partial f(y^*)}{\partial y}\,\epsilon(t),$$

which is a constant coefficient, linear system for $\epsilon(t)$, the long-term dynamics of which are determined by the eigenvalues of the Jacobian matrix. A result by Poincaré and Liapunov [27] shows that this linearization process determines local attractivity. Under mild assumptions about f, a sufficient condition for a fixed point y^* of (2.1) to be locally stable (attractive) is

$$\Re(\lambda) < 0, \quad \text{for every eigenvalue} \quad \lambda \quad \text{of} \quad \frac{\partial f(y^*)}{\partial y}\,. \qquad (2.16)$$

Further, replacing " $<$ " by " $\leq$ " in (2.16) yields the necessary condition for local attractivity. The definiton of local attractivity also includes the phrase " there exists a neighbourhood ...". Of course it is not known in advance how large this neighbourhood will be. The set

$$\{y_0 \in \mathbb{R}^m : y(t) \to y^* \quad \text{as} \quad t \to \infty \quad \text{in} \quad (2.1)\}$$

is called the basin of attraction of the fixed point y^*. If y^* is locally attractive then this means that the basin of attraction contains a neighbourhood of y^*.

The analogous definition of a fixed point for the map (2.13) is as follows.

Definition 3 *If $y^* \in \mathbb{R}^m$ satisfies $y^* = \mathscr{F}(y^*)$ then y^* is a fixed point of the map (2.13).*

Local stability may be defined in a similar manner to the continuous case.

Definition 4 *A fixed point y^* of (2.13) is locally attractive (linearly stable) if there exists a neighbourhood around y^* satisfies $y_n \to y^*$ as $n \to \infty$.*

Perturbing to $y_n = y^* + \epsilon_n$, and linearizing, gives

$$y^* + \epsilon_{n+1} = \mathscr{F}(y^* + \epsilon_n) \approx \mathscr{F}(y^*) + \frac{\partial \mathscr{F}(y^*)}{\partial y}\,\epsilon_n. \tag{2.17}$$

Since $y^* = \mathscr{F}(y^*)$, (2.17) becomes up to first order,

$$\epsilon_{n+1} = \frac{\partial \mathscr{F}(y^*)}{\partial y}\,\epsilon_n, \tag{2.18}$$

which is a constant coefficient, linear iteration for ϵ_n, the long-term dynamics of which are determined by the eigenvalues of the Jacobian.

Ostrowski's Theorem shows that the linearization process determines local attractivity. Under mild assumptions about $\mathscr{F}$, a sufficient condition for a fixed point y^* of (2.13) to be locally stable is

$$\rho\left(\frac{\partial \mathscr{F}(y^*)}{\partial y}\right) < 1, \tag{2.19}$$

where $\rho(\cdot)$ denotes the spectral radius, that is, the largest eigenvalue in modulus. Replacing " $<$ " by " $\leq$ " in (2.19) gives a necessary condition for local attractivity.

Definition 5 (Spurious Solutions) *Suppose a numerical method applied to the flow (2.1) produces the map (2.13). Then a fixed point y^* of the map is said to be "spurious" if it is not a fixed point of the flow.*

Spurious fixed points are undesirable since they represent numerical approximations that are wrong.

Definition 6 (Regular Method) *A method of the form (2.13) is said to be a regular method if the method is free of spurious fixed points.*

As far as Euler's method is concerned, $y_{n+1} = y_n + \ell f(y_n)$, y^* is a fixed point of the map if and only if $f(y^*) = 0$. Hence, Euler's method will never produce a spurious fixed point.

In many systems of differential equations, particularly models of chemical and biological processes, the phenomenon of Hopf bifurcation has been observed. Hopf bifurcation stands for the appearance of periodic solutions to the differential equation out of a steady state solution when varying a bifurcation parameter. The following theorem is an extension of Hopf's original theorem, Hassard *et al.* [18]. It deals with an autonomous system of the form $dX/dt = F(X, \mu), X \in \mathbb{R}, \mu \in \mathbb{R}, F : \mathbb{R}^n \times \mathbb{R}^n$ with steady-state solution $X = 0$ and critical bifurcation value $\mu = 0$.

Theorem 1 (Hopf Bifurcation Theorem) *Let* $dX/dt = F(X, \mu), F : \mathbb{R}^n \times \mathbb{R}^n$ *be a system of differential equations with isolated stationary solution* $0 \in \mathbb{R}$ *for* $\mu \in (-\delta, \delta), \delta > 0$ *and let* $\lambda(\mu) = \alpha(\mu) \pm i\omega(\mu)$ *such that* $\alpha(0) = 0, \omega(0) = \omega_0 > 0$ *and* $d\alpha(0)/d\mu \neq 0$ *be two eigenvalues. Let the remaining* $(n-2)$ *eigenvalues of* $J(\mu)$ *have strictly negative real parts. Then* $dX/dt = F(X, \mu)$ *has a family of periodic solutions and* $\exists\, \varepsilon_P > 0$ *and functions* $\mu(\varepsilon), T(\varepsilon), \beta(\varepsilon) \in C^{L+1}$ *such that*

$$\mu(\varepsilon) = \sum_{i=1}^{\lfloor L/2 \rfloor} \mu_{2i}\varepsilon^{2i} + O(\varepsilon^{L+1}), \quad 0 < \varepsilon < \varepsilon_P \tag{2.20}$$

and $\forall\, \varepsilon \in (0, \varepsilon_P)$ *there exists a periodic solution* $p_\varepsilon(t) \in \mathbb{R}^n$ *occurring for* $\mu = \mu(\varepsilon)$ *(direction of Hopf bifurcation).*

The period of $p_\varepsilon(t)$ *is given by*

$$T(\varepsilon) = \frac{2\pi}{\omega_0}\left[1 + \sum_{i=1}^{\lfloor L/2 \rfloor} \tau_{2i}\varepsilon^{2i}\right] + O(\varepsilon^{L+1}), \quad 0 < \varepsilon < \varepsilon_P, \tag{2.21}$$

and stability is determined by the function $\beta(\varepsilon)$ *with*

$$\beta(\varepsilon) = \sum_{i=1}^{\lfloor L/2 \rfloor} \beta_{2i}\varepsilon^{2i} + O(\varepsilon^{L+1}), \quad 0 < \varepsilon < \varepsilon_P. \tag{2.22}$$

The periodic solution $p_\varepsilon(t)$ *is asymptotically stable if* $\beta(\varepsilon) < 0$ *and unstable if* $\beta(\varepsilon) > 0$. *If there exists a first non-vanishing coefficient* $\mu_{2k}, 1 \leq k \leq \lfloor L/2 \rfloor$ *in equation (2.20) then the first non-vanishing coefficient* β_{2k} *in (2.22) is given by*

$$\beta_{2k} = -2\alpha'(0)\mu_{2k}.$$

The terms *supercritical* and *subcritical bifurcation* appear in the literature with different definitions. Following Seydel [62] a (Hopf) bifurcation is called supercritical if stable solutions of the corresponding differential equation can be found on both sides of the bifurcation. That is, if a bifurcation takes place for the parameter value $\mu = \mu_c$ then there exists a stable solution (constant or periodic) for $\mu = \mu_c - \varepsilon$ and $\mu = \mu_c + \varepsilon$, ε sufficiently small. A bifurcation is called subcritical if a stable solution on one side of the bifurcation cannot be continued to a stable solution on the other side of the bifurcation.

Theorem 2 (The Routh-Hurwitz Theorem) *The real polynomial $D_n(s)$ given by*

$$D_n(s) = a_n s^n + a_{n-1} s^{n-1} + \ldots + a_1 s + a_0 = 0$$

is a Routh-Hurwitz polynomial if and only if all principal minors of H are positive. That is,

$$\begin{aligned}
\Delta_1 &= a_{n-1} > 0, \\
\Delta_2 &= det \begin{bmatrix} a_{n-1} & a_{n-3} \\ a_n & a_{n-2} \end{bmatrix} > 0, \\
\Delta_3 &= det \begin{bmatrix} a_{n-1} & a_{n-3} & a_{n-5} \\ a_n & a_{n-2} & a_{n-4} \\ 0 & a_{n-1} & a_{n-3} \end{bmatrix} > 0, \\
&\cdots \\
\Delta_n &= detH > 0,
\end{aligned} \tag{2.23}$$

where

$$H = \begin{bmatrix} a_{n-1} & a_{n-3} & a_{n-5} & a_{n-7} & \dots & 0 \\ a_n & a_{n-2} & a_{n-4} & a_{n-6} & \dots & 0 \\ 0 & a_{n-1} & a_{n-3} & a_{n-5} & \dots & 0 \\ 0 & a_n & a_{n-2} & a_{n-4} & \dots & 0 \\ \dots & \dots & \dots & \dots & \dots & \dots \\ 0 & \dots & a_5 & a_3 & a_1 & 0 \\ 0 & \dots & a_6 & a_4 & a_2 & a_0 \end{bmatrix}\Bigg|_{(x_{1,s},y_{1,s})}$$

The necessary and sufficient conditions for the roots of

$$P(r) := a_0 r^k + a_1 r^{k-1} + \ldots + a_k$$

to lie in the half-plane $\Re r < 0$ are summarized in Table 2.1 for $k = 2, 3, 4$.

Table 2.1: The Routh-Hurwitz stability criteria

n	Stability Criteria
2	$a_j > 0;\ j = 0, 1, 2$
3	$a_j > 0;\ j = 0, 1, 2, 3;\ a_1 a_2 - a_3 a_0 > 0$
4	$a_j > 0;\ j = 0, 1, 2, 3, 4;\ a_1 a_2 a_3 - a_0 a_3^2 - a_1^2 a_4 > 0$

Theorem 3 (The Liénard-Chipart Theorem) *The real polynomial $D_n(s)$ given by*

$$D_n(s) = a_n s^n + a_{n-1} s^{n-1} + \ldots + a_1 s + a_0 = 0,$$

is a Routh-Hurwitz polynomial if and only if the $\Delta_i > 0$ in (2.23) hold for all i odd or all i even, when $a_i > 0$ for all i.

Stability analysis of a discrete-time system may be studied by methods analogous to those for a continuous-time system. The continuous system is stable if and only if all the eigenvalues lie in the left half complex plane. Stability of the corresponding discrete system requires more stringent condition that all the eigenvalues lie inside the unit circle. In order to apply the Routh-Hurwitz theorem to a discrete-time system the characteristic polynomial needs to be a Schur polynomial Lambert [28].

Definition 7 (Schur Polynomial) *A polynomial $\pi(r)$ of degree k is said to be Schur if its roots r_t satisfy $|r_t| < 1$, $t = 1, 2, \ldots, k$.*

In order to provide the stability conditions for discrete-time systems it is necessary first to make the transformation $r \to z, \quad r, z \in \mathbb{C}$, where $r = (1+z)/(1-z)$. This transformation maps the boundary of the circle $|r| = 1$ onto the imaginary axis $\Re z = 0$, and the interior of the circle $|r| = 1$ onto the left half-plane $\Re z < 0$. Hence

$$P(z) := (1-z)^k \pi[(1+z)/(1-z)] = a_0 z^k + a_1 z^{k-1} + \ldots + a_k,$$

and it is assumed without loss of generality that $a_0 > 0$. Now, the problem is to find the necessary and sufficient conditions for the roots of $P(z)$ to lie in the half-plane $\Re z < 0$.

Many problems in chemistry and biology requiring numerical solution involve special cases of the linear parabolic differential equation

$$\sigma(x,t)\frac{\partial u}{\partial t} = \frac{\partial}{\partial x}\Big(a(x,t)\frac{\partial u}{\partial x}\Big) + b(x,t)\frac{\partial u}{\partial x} - c(x,t)u, \tag{2.24}$$

which holds within some prescribed region R of the (x,t) plane. Within this region, the functions σ, a are strictly positive and c is non-negative Twizell [70].

The problem of stability of a finite-difference calculation used to solve equation (2.24) is introduced as consisting of finding a condition under which

$$U_m^n - \tilde{U}_m^n (\equiv Z_m^n),$$

the difference between the theoretical solution and numerical solutions of the difference equation, remains bounded as n tends to infinity. The latter occurs in a calculation where either

(i) ℓ remains fixed for all n and $t \to \infty$, or

(ii) $h, \ell \to 0$ (ℓ/h^2 fixed) for a fixed value of $t = n\ell$.

The von Neumann method is used for examining this notion of stability of a finite-difference calculation.

A harmonic decomposition is made of the error Z at grid points at a given time level, leading to the error function

$$E(x) = \sum_j A_j e^{i\beta_j x},$$

where in general the frequencies $|\beta_j|$ and j are arbitrary. It is necessary to consider only the single term $e^{i\beta x}$ where β is any real number. For convenience, suppose that the time level being considered corresponds to $t = 0$. To investigate the error propagation as t increases, it is necessary to find a solution of the finite-difference equation which reduces to $e^{i\beta x}$ when $t = 0$. Let such a solution be

$$e^{\alpha t} e^{i\beta x}$$

where $\alpha = \alpha(\beta)$ is, in general, complex. The original error component $e^{i\beta x}$ will not grow with time if

$$e^{\alpha \ell} \leq 1$$

for all α. This is von Neumann's criterion for stability. In order to allow for exponentially growing solutions of the partial differential equation itself, a more general form is $|e^{\alpha \ell}| \leq 1 + O(\ell)$.

The following important points should be noted concerning the von Neumann method of examining stability Mitchell and Griffiths [51].

(i) The method which is based on Fourier series applies only if the coefficients of the linear difference equation are constant. If the difference equation has variable coefficients, the method can still be applied locally and it might be expected that a method will be stable if the von Neumann condition, derived as though the coefficients were constant, is satisfied at every point of the field. There is much numerical evidence to support this contention.

(ii) For two level difference schemes with one dependent variable and any number of independent variables, the von Neumann condition is sufficient as well as necessary for stability. Otherwise, the condition is necessary only.

(iii) Boundary conditions are neglected by the von Neumann method which applies

in theory only to pure initial-value problems with periodic initial data. It does however provide necessary conditions for stability of constant coefficient problems regardless of the type of boundary condition.

Chapter 3

Isothermal Chemical Systems

3.1 Introduction

Chemical reactions with autocatalytic or thermal feedback play a central role in many biological and biochemical systems. In a series of papers, Merkin and Needham [41], [42], [43] have considered the development of travelling waves in simple isothermal chemical systems with a variation of autocatalytic and decay schemes. The quadratic autocatalytic scheme

$$\mathcal{A} + \mathcal{B} \longrightarrow 2\mathcal{B}, \quad \text{rate} = k_1 ab, \tag{3.1}$$

where a is the concentration of the fuel $\mathcal{A}$ and b is the concentration of the product (and catalyst) $\mathcal{B}$ has been proposed as a model for many biological and biochemical systems, Murray [52]. This chemical scheme also leads to a study of the Fisher-Kolmogorov equation (Fisher [10]; Kolmogorov *et al.* [26]) which explains the advance of an advantageous gene through a population. In chemical systems, kinetic scheme (3.1) has been suggested as a mechanism by Voronkov and Semenov [75] to show how almost isothermal flames in the carbon-sulphide-oxygen reaction arising from quadratic branching could be described in terms of simple autocatalysis. Equation (3.1) together with the linear decay step

$$\mathcal{B} \longrightarrow \mathcal{C}, \quad \text{rate} = k_2 b, \tag{3.2}$$

has been considered as a model for the spread of infectious diseases by Kermack and McKendrick [25] and Kendall [24]. This coupled reaction kinetic scheme has been studied numerically by using first-order finite-difference methods by Twizell *et al.* [73]. The cubic autocatalytic rate law

$$\mathcal{A} + 2\mathcal{B} \longrightarrow 3\mathcal{B}, \quad \text{rate} = k_3 a b^2, \tag{3.3}$$

has been used to describe certain liquid-phase reactions by Hanna *et al.* [17] and Showalter [60]. Dixon-Lewis and Williams [9] have also shown that cubic autocatalysis plays an important role in the hydrogen-oxygen reaction. Further work on travelling waves with quadratic autocatalysis with quadratic decay,

$$\mathcal{B} + \mathcal{B} \longrightarrow \mathcal{C}, \quad \text{rate} = k_4 b^2, \tag{3.4}$$

has been studied by Merkin and Needham [48]. A chemical scheme with quadratic autocatalysis coupled with quadratic decay was studied extensively by using first- and second-order finite-difference methods by Al-Mannai [1].

The clear need for a careful appraisal of the actual kinetics that should be used in modelling these processes drives Merkin and Needham [44] to study the constraint which describes all such systems by considering general autocatalytic schemes of the form

$$\mathcal{A} + r\mathcal{B} \longrightarrow (r+1)\mathcal{B}, \quad \text{rate} = k_1 a b^r, \tag{3.5}$$

and allowing for autocatalyst decay via

$$s\mathcal{B} \longrightarrow \mathcal{C}, \quad \text{rate} = k_2 b^s, \tag{3.6}$$

where r and s are the autocatalysis exponent and decay rate exponent, respectively. These exponents are general (not necessarily integer) powers subject only to the restriction that $r, s \geq 1$. Applications can be found in modelling core kinetics in gas-phase radical chain-branching oxidation such as carbon monoxide-oxygen as well as in solution phase branching kinetics, for example iodate-arsenous acid reaction,

Needham and Chamberlain [53]. Reaction schemes (3.5)-(3.6) lead to reaction-diffusion equations, which in dimensionless form and for plane geometry, are

$$\frac{\partial \alpha}{\partial t} = \frac{\partial^2 \alpha}{\partial x^2} - \alpha\beta^r, \tag{3.7}$$

$$\frac{\partial \beta}{\partial t} = \frac{\partial^2 \beta}{\partial x^2} + \alpha\beta^r - \kappa\beta^s, \tag{3.8}$$

with initial and boundary conditions as used by Merkin and Needham [44]

$$\alpha(x,0) = 1 \quad \text{for all values of} \quad x$$

$$\beta(x,0) = \begin{cases} \beta_0 g(x) & , \quad |x| \leq \sigma, \\ 0 & , \quad |x| > \sigma, \end{cases} \tag{3.9}$$

$$\alpha \to 1, \quad \beta \to 0 \quad \text{as} \quad |x| \to \infty, \quad \text{for all} \quad t \geq 0, \tag{3.10}$$

where $g(x)$ is a positive, continuous function of x in $|x| \leq \sigma$, with maximum value $\{g(x)\} = 1$, for example $g(x) = e^{-x^2}$. The reaction terms $-\alpha\beta^r$ in (3.7) and $\alpha\beta^r - \kappa\beta^s$ in (3.8) satisfy Lipschitz condition, Burden [5]. The non-dimensionalization of the original equations follows that used by Merkin and Needham [41], [42], [43], [45], [48]. Here $\alpha = \alpha(x,t)$ and $\beta = \beta(x,t)$ are the dimensionless concentrations of reactant $\mathcal{A}$ and autocatalyst $\mathcal{B}$, respectively. These have been made dimensionless with respect to a_0, the initial concentration of $\mathcal{A}$. The coordinates x and t are dimensionless space and time variables, defined so as to keep the length scale l, associated with the initial input $\mathcal{B}$, and the diffusion coefficient D in the parameter $\sigma = (k_1 a_0 l^2/D)^{\frac{1}{2}}$. Here equal diffusion coefficients are assumed for reactants $\mathcal{A}$ and $\mathcal{B}$ as $D_{\mathcal{A}} = D_{\mathcal{B}} = D = 1$. The parameter $\kappa = \dfrac{k_2}{k_1} a_0^{1+r-s}$ can be regarded as a chain-branching factor and represents the relative strength of the decay rate to the autocatalytic production step. The parameter $\beta_0 = \dfrac{b_0}{a_0}$ represents the maximum value of the initial input of autocatalyst $\mathcal{B}$ relative to $\mathcal{A}$, where a_0 and b_0 are the initial uniform concentrations of $\mathcal{A}$ and $\mathcal{B}$, respectively.

3.2 The Well-stirred Model

The simplest form of flow system, the well-stirred analogue of the reaction-diffusion problem (3.7), (3.8) and initial conditions (3.9), in the continuously-fed, well-stirred tank reactor is

$$\frac{d\alpha}{dt} = -\alpha\beta^r, \tag{3.11}$$

$$\frac{d\beta}{dt} = \alpha\beta^r - \kappa\beta^s, \tag{3.12}$$

subject to $\alpha(0) = 1,\ \beta(0) = \beta_0 \geq 0$.

3.2.1 Local stability analysis of the well-stirred model

The reaction rate equations which describe the evolution of two concentration variables α and β can be written in general terms as

$$\frac{d\alpha}{dt} = f_1(\alpha, \beta; \kappa), \tag{3.13}$$

$$\frac{d\beta}{dt} = f_2(\alpha, \beta; \kappa), \tag{3.14}$$

where κ presents the parameter involved in the system. The functions f_1 and f_2 are given by

$$f_1(\alpha, \beta; \kappa) = -\alpha\beta^r, \tag{3.15}$$

$$f_2(\alpha, \beta; \kappa) = \alpha\beta^r - \kappa\beta^s. \tag{3.16}$$

The equilibrium points (α_e, β_e) are obtained by evaluating $f_1(\alpha_e, \beta_e) = f_2(\alpha_e, \beta_e) = 0$. The positive quadrant of the (α, β) phase plane equations (3.11) and (3.12) have a line of equilibrium points

$$\alpha = \alpha_e, \quad \beta = 0, \quad \text{for all} \quad \alpha_e \geq 0.$$

Every point on the α axis, $\beta = 0$ is an equilibrium point. Local stability is determined by considering the Jacobian, J_w, of the pair of equations (3.15) and (3.16). This is defined as

$$J_w = \begin{bmatrix} \partial f_1/\partial\alpha & \partial f_1/\partial\beta \\ \partial f_2/\partial\alpha & \partial f_2/\partial\beta \end{bmatrix},$$

so that

$$J_w = \begin{bmatrix} -\beta^r & -r\alpha\beta^{r-1} \\ \beta^r & r\alpha\beta^{r-1} - \kappa s\beta^{s-1} \end{bmatrix}.$$

At the steady-state, $(\alpha_e, 0)$, J_w becomes

$$J_w = \begin{bmatrix} 0 & 0 \\ 0 & 0 \end{bmatrix}.$$

The system, (3.11), (3.12), has non-simple equilibrium points, since J_w is singular. Therefore the local behaviour in phase space cannot be determined by the usual linearization theorem. As can easily be seen the eigenvalues of the linearized flow about the equilibrium point vanish then the local dynamics is dominated by the non-linear terms in the given equation. This case is also known as a degenerate case in the literature and a literature search has as yet revealed no general technique for finding the phase portrait of it. According to Luenberger [33] since there are no eigenvalues in the right half of the complex plane, but all are equal to zero, this special intermediate situation may referred to as "marginally stable". Other than this approach there exists geometrical devices which could be used for obtaining more information directly from the given ODEs Arrowsmith [2], Burden [5], Glendinning [13]. One way is to look at the behaviour of $\frac{d\beta}{d\alpha}$ on trajectories. If this can be solved then the equation of the trajectories can be obtained in the phase space which can then be sketched. Another way is finding the curves in phase space on which $\dot{\alpha} = 0$ and $\dot{\beta} = 0$ and hence dividing the phase space into regions where $\dot{\alpha} > 0$ and $\dot{\beta} > 0$, $\dot{\alpha} < 0$ and $\dot{\beta} > 0$ and so on. This information could be used to obtain a rough picture of the behaviour of trajectories in phase space. Finally, some invariant curves might also help to organize the sketch of phase space, Verhulst [74]. Here, a combination of the suggested techniques will be applied to analyse the stability of the given ODE system (3.11), (3.12). There are three possible cases to analyse depending on the sign of $r - s$.

• **Case 1 :** $r = s$

The equation for the trajectories of the system in the (α, β) phase plane is

$$\frac{d\beta}{d\alpha} = \frac{(\kappa - \alpha)}{\alpha}, \quad \beta = \beta_0 \quad \text{at} \quad \alpha = 1 \tag{3.17}$$

which is a separable equation leading to

$$\int_{\beta_0}^{\beta} d\beta = \int_1^{\alpha} \frac{\kappa - \alpha}{\alpha} d\alpha$$

or

$$\beta = -\alpha + \kappa \ln|\alpha| + C_0 \tag{3.18}$$

where C_0 is a constant of integration. The particular trajectory that is

$$\beta = 1 - \alpha + \kappa \ln|\alpha| + \beta_0 \tag{3.19}$$

has a maximum value at $\alpha = \kappa$ since $\beta'' = -\frac{1}{\kappa} < 0$ so that

$$\beta \to \kappa \ln\alpha \quad \text{as} \quad \alpha \to 0$$

and

$$\beta \to -\alpha \quad \text{as} \quad \alpha \to \infty.$$

If $\kappa > 1$, the trajectory starts to the left of the maximum at $\alpha = \kappa$ and for all β_0, β decreases monotonically to zero as $\alpha \to \alpha_e$, one of the two real roots of the equation $1 - \alpha + \kappa \ln|\alpha| + \beta_0 = 0$. If $\kappa < 1$, the phase trajectory starts to the right of the maximum and β increases to a maximum value of $1 - \alpha + \kappa \ln|\alpha| + \beta_0$ at $\alpha = \kappa$ before decreasing to zero as $\alpha \to \alpha_e$. Phase-plane presentation of this situation for $\kappa = 0.9$ for quadratic autocatalysis and linear decay, $r = 1, s = 1$, is presented in Fig. 3.1.

By using this information and (3.11), (3.12), it then follows that the equilibrium points in $0 \leq \alpha_e < \kappa$ are all stable while those in the interval $\alpha_e \geq \kappa$ are unstable.

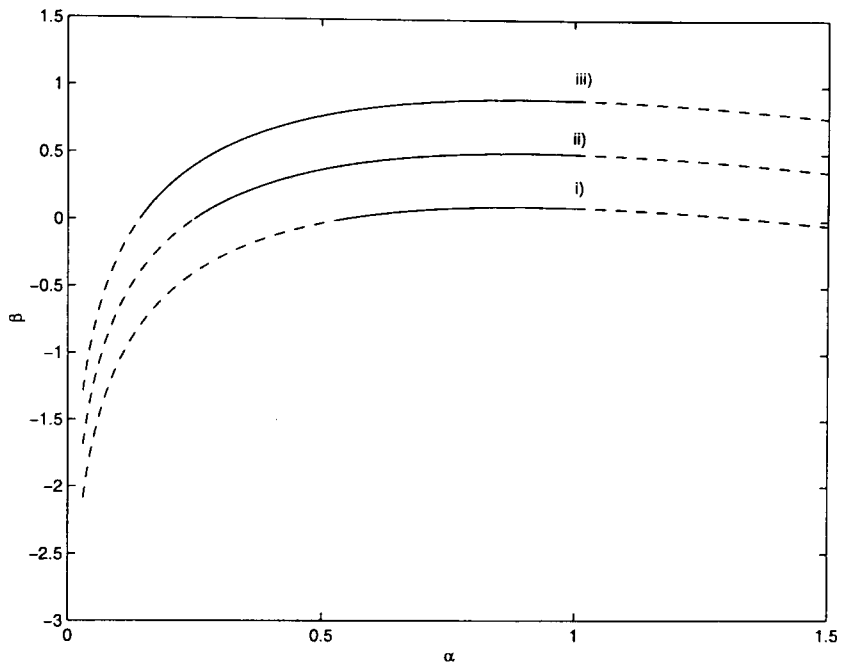

Figure 3.1: Phase-plane trajectories for $\kappa = 0.9$ with initial conditions $\alpha = 1$ and i) $\beta_0 = 0.1$, ii) $\beta_0 = 0.5$, iii) $\beta_0 = 0.9$.

- **Case 2 :** $r < s$

i) $s - r = 1$: (e.g. $r = 1, s = 2$)

The system, (3.11)-(3.12), can be written as

$$\begin{aligned} \frac{d\alpha}{dt} &= -\alpha\beta^r, \\ \frac{d\beta}{dt} &= \beta^r(\alpha - \kappa\beta), \end{aligned} \tag{3.20}$$

the trajectory equation of the system in the phase plane reduces to

$$\frac{d\beta}{d\alpha} = \kappa\frac{\beta}{\alpha} - 1, \quad \beta = \beta_0 \quad \text{at} \quad \alpha = 1. \tag{3.21}$$

The resulting family of solutions can be written as

$$\beta = \begin{cases} \dfrac{\alpha}{\kappa - 1} + C_0\alpha^\kappa & , \quad \kappa \neq 1, \\ -\alpha \ln|\alpha| + C_0\alpha & , \quad \kappa = 1, \end{cases} \tag{3.22}$$

where C_0 is a constant of integration. All trajectories obtained by (3.22), shows that all the equilibrium points $\alpha = \alpha_e > 0$, $\beta = 0$ are unstable, with a single trajectory leaving each point $\alpha = \alpha_e, \beta = 0$ and moving into the quadrant α, $\beta > 0$ with

decreasing α. On the same trajectory β increases until it reaches its maximum then it decreases by approaching the origin $\alpha = 0, \beta = 0$ as $\alpha \to 0^+$. Here the parameter κ determines the way in which the origin is approached. The behaviour of β for small α can be summarized as

$$\begin{aligned} \beta &\sim C_0 \alpha^{\kappa} \quad , \quad 0 < \kappa < 1, \\ \beta &\sim C_0 \alpha - \alpha \ln\alpha \quad , \quad \kappa = 1, \\ \beta &\sim C_0 \frac{\alpha}{\kappa - 1} \quad , \quad \kappa > 1. \end{aligned}$$

ii) General values of r and s for $r < s$:

The corresponding equation for the integral path is

$$\frac{d\beta}{d\alpha} = \frac{\alpha\beta^r - \kappa\beta^s}{-\alpha\beta^r}.$$

Since $r < s$ this may be rewritten as

$$\frac{d\beta}{d\alpha} = \frac{\kappa\beta^{s-r} - \alpha}{\alpha}, \quad \beta = \beta_0 \quad \text{at} \quad \alpha = 1. \tag{3.23}$$

The approximate integral paths can be obtained from (3.23) by considering the method of isoclines. It can be concluded that the behaviour of β for small α depends on whether $s - r > 1$ or $s - r < 1$, with, as $\alpha \to 0$, Merkin *et al.* [44].

If $s - r > 1$ then as $\alpha \to 0$

$$\beta \sim (\kappa M)^{-\frac{1}{M}} (-\ln\alpha)^{-\frac{1}{M}}, \quad M = s - r > 0,$$

if $s - r < 1$ then as $\alpha \to 0$

$$\beta \sim (\frac{\alpha}{\kappa})^{-\frac{1}{N}}, \quad N = s - r > 0, N < 1.$$

As a result, all trajectories in the positive quadrant approach the origin, that is $(0, 0)$ is an attractor, so $(0, 0)$ is stable.

- **Case 3:** $r > s$

The corresponding equation for the integral path is

$$\frac{d\beta}{d\alpha} = \frac{\kappa - \alpha\beta^{r-s}}{\alpha\beta^{r-s}}. \tag{3.24}$$

The horizontal and vertical isoclines are given by $\beta = (\frac{\kappa}{\alpha})^{\frac{1}{r-s}}$ and $\alpha = 0$, $\beta = 0$ respectively. This yields

$$\beta > (\frac{\kappa}{\alpha})^{\frac{1}{r-s}} \quad \text{when} \quad \frac{d\beta}{d\alpha} < 0$$

and

$$\beta < (\frac{\kappa}{\alpha})^{\frac{1}{r-s}} \quad \text{when} \quad \frac{d\beta}{d\alpha} > 0;$$

when α decreases β grows until the maximum value is reached, then decreases to zero at a finite value of α. So $(\alpha_e, 0)$ is an attractor for the positive quadrant of the (α, β) phase plane.

3.2.2 First-order numerical methods

The well-stirred form of the reaction-diffusion model is

$$\alpha' \equiv \frac{d\alpha}{dt} = -\alpha\beta^r, \quad t > 0, \tag{3.25}$$

$$\beta' \equiv \frac{d\beta}{dt} = \alpha\beta^r - \kappa\beta^s, \quad t > 0, \tag{3.26}$$

subject to $\alpha(0) = 1, \beta(0) = \beta_0$, in $\alpha \geq 0, \beta \geq 0$ where r and s are general powers subject only to the restriction that $r, s \geq 1$. The functions α and β are the dimensionless concentrations of reactants $\mathcal{A}$ and $\mathcal{B}$ together with a dimensionless parameter κ. The independent variable $t \geq 0$ (time) is discretized at the points $t_n = n\ell$, $(n = 0, 1, 2, \ldots)$, where ℓ is a fixed time step. The theoretical solution of the system (3.25) and (3.26) at the point $t = t_n$ is denoted by $\alpha(t_n)$ and $\beta(t_n)$ while the solution of an approximating numerical method will be denoted by A_n, B_n at the same point t_n, where A and B denote approximations to α and β, respectively. One-step methods are developed by approximating the derivatives $d\alpha(t)/dt$ and $d\beta(t)/dt$ by the first-order replacements (forward-difference approximants)

$$\frac{d\alpha(t)}{dt} = \frac{\alpha(t+\ell) - \alpha(t)}{\ell} + O(\ell) \quad \text{as} \quad \ell \to 0, \tag{3.27}$$

$$\frac{d\beta(t)}{dt} = \frac{\beta(t+\ell) - \beta(t)}{\ell} + O(\ell) \quad \text{as} \quad \ell \to 0, \tag{3.28}$$

at $t = t_n$. Evaluating α and β at the same points gives Method 1 (Euler)

$$\begin{aligned}(A_{n+1} - A_n)/\ell &= -A_n B_n^r, \\ (B_{n+1} - B_n)/\ell &= A_n B_n^r - \kappa B_n^s,\end{aligned} \tag{3.29}$$

which give the alternative explicit formulations

$$A_{n+1} = A_n(1 - \ell B_n^r); \quad n = 0, 1, 2, \ldots \tag{3.30}$$

$$B_{n+1} = B_n + \ell(A_n B_n^r - \kappa B_n^s); \quad n = 0, 1, 2, \ldots \tag{3.31}$$

where $A_0 = \alpha_0$ and $B_0 = \beta_0$. Evaluating some of the α and β on the right hand side of (3.25)-(3.26) at the advanced time level gives Method 2 (alternative finite-difference method) Twizell *et al.* [72], [73].

$$(A_{n+1} - A_n)/\ell = -A_{n+1} B_n^r, \tag{3.32}$$

$$(B_{n+1} - B_n)/\ell = A_{n+1} B_{n+1}^r - \kappa B_{n+1}^s. \tag{3.33}$$

Before arranging as explicit formulation to avoid non-linearity, B_{n+1}^r is approximated at base and advanced time levels. Hence, B_{n+1}^r can be rearranged in the form $B_n^{r-1} B_{n+1}$ to give

$$A_{n+1} = A_n/(1 + \ell B_n^r)\ ; \quad n = 0, 1, 2, \ldots \tag{3.34}$$

$$B_{n+1} = B_n/[1 - \ell(A_{n+1} B_n^{r-1} - \kappa B_n^{s-1})]; \quad n = 0, 1, 2, \ldots \tag{3.35}$$

with $A_0 = \alpha_0$ and $B_0 = \beta_0$.

3.2.3 Local truncation errors

The LTEs associated with Method 1 are presented by $\{\mathscr{L}1_\alpha, \mathscr{L}1_\beta\}$ and obtained from (3.30) and (3.31) and are given by

$$\begin{aligned}\mathscr{L}1_\alpha[\alpha(t), \beta(t); \ell] &= \alpha(t + \ell) - \alpha(t) + \ell\alpha(t)[\beta(t)]^r \\ &= \frac{1}{2}\alpha''\ell^2 + O(\ell^3) \quad \text{as} \quad \ell \to 0,\end{aligned} \tag{3.36}$$

$$\begin{aligned}\mathscr{L}1_\beta[\alpha(t),\beta(t);\ell] &= \beta(t+\ell)-\beta(t)-\ell\alpha(t)[\beta(t)]^r+\ell\kappa[\beta(t)]^s \\ &= \frac{1}{2}\beta''\ell^2+O(\ell^3) \quad \text{as} \quad \ell\to 0. \end{aligned} \tag{3.37}$$

The LTEs associated with Method 2 are presented by $\{\mathscr{L}2_\alpha, \mathscr{L}2_\beta\}$ and obtained from (3.34) and (3.35) and are given by

$$\begin{aligned}\mathscr{L}2_\alpha[\alpha(t),\beta(t);\ell] &= \alpha(t+\ell)-\alpha(t)+\ell\alpha(t+\ell)[\beta(t)]^r \\ &= \left(\frac{1}{2}\alpha''-\alpha'\beta^r\right)\ell^2+O(\ell^3) \quad \text{as} \quad \ell\to 0. \end{aligned} \tag{3.38}$$

$$\begin{aligned}\mathscr{L}2_\beta[\alpha(t),\beta(t);\ell] &= \beta(t+\ell)-\beta(t)-\ell\alpha(t+\ell)[\beta(t)]^{r-1}\beta(t+\ell)+\ell\kappa[\beta(t)]^{s-1}\beta(t+\ell) \\ &= \left(\frac{1}{2}\beta''-\alpha\beta^{r-1}\beta'-\alpha'\beta^r+\kappa\beta'\beta^{s-1}\right)\ell^2+O(\ell^3) \quad \text{as} \quad \ell\to 0. \end{aligned} \tag{3.39}$$

The expressions in (3.36), (3.37) and (3.38), (3.39) verify that the numerical methods Method 1 and Method 2 are first-order accurate.

3.2.4 Stability analysis of numerical methods

The numerical methods (3.30), (3.31) and (3.34), (3.35) all have steady-state solutions which will be denoted by $\alpha = \alpha_e$ and $\beta = \beta_e = 0$. The numerical methods share the same fixed points of the underlying ODEs. In order to examine the stability of these fixed points the one-step methods must be written in the forms

$$\alpha_{n+1} = g_1(\alpha_n, \beta_n);\ n = 0, 1, 2, \dots , \tag{3.40}$$

$$\beta_{n+1} = g_2(\alpha_n, \beta_n);\ n = 0, 1, 2, \dots . \tag{3.41}$$

It is necessary to consider the associated functions

$$\alpha = g_1(\alpha, \beta) \qquad \text{and} \qquad \beta = g_2(\alpha, \beta),$$

from which it may be shown that for Method 1

$$g_1(A, B) = A(1 - \ell B^r), \tag{3.42}$$

$$g_2(A, B) = B + \ell(AB^r - \kappa B^s), \tag{3.43}$$

and for Method 2

$$g_1(A,B) = A/(1+\ell B^r), \tag{3.44}$$

$$g_2(A,B) = B/[1-\ell(AB^{r-1}-\kappa B^{s-1})]. \tag{3.45}$$

In order to examine the stability of the fixed points, (α_e, β_e), of Method 1 and Method 2, the eigenvalues of the matrix

$$J_M = \begin{bmatrix} \partial g_1(\alpha_e,\beta_e)/\partial\alpha & \partial g_1(\alpha_e,\beta_e)/\partial\beta \\ \partial g_2(\alpha_e,\beta_e)/\partial\alpha & \partial g_2(\alpha_e,\beta_e)/\partial\beta \end{bmatrix}$$

must be calculated. The fixed points, (α_e, β_e) of the discrete dynamical systems {(3.30), (3.31)} and {(3.34), (3.35)} are said to be stable or attracting if the spectral radius $\rho(J_M) = \max_{i=1,2}|\lambda_i|$ of the matrix J_M satisfies the condition $\rho(J_M) < 1$ and to be unstable or repelling if $\rho(J_M) > 1$ and marginally stable if $\rho(J_M) = 1$ (see Luenberger [33]). Analysis of the eigenvalues of J_M reveals that eigenvalues of the numerical methods Method 1 and Method 2 are all on the unit circle, that is $|\lambda_1| = |\lambda_2| = 1$. It could be concluded that the fixed points, $(\alpha_e, 0)$, are marginally stable. The case analysis for possible signs of the powers r and s could also be considered in discrete systems. In that way a good insight into the stability analysis may be obtained.

3.2.5 Second-order numerical method

A second-order explicit method is developed for the numerical solution of the initial-value problem which arises from the isothermal chemical system with general orders of autocatalysis and decay which is given by

$$\alpha' = -\alpha\beta^r, \tag{3.46}$$

$$\beta' = \alpha\beta^r - \kappa\beta^s, \tag{3.47}$$

with

$$\alpha(0) = 1,\ \beta(0) = \beta_0 \qquad \text{and} \qquad \alpha \geq 0,\ \beta \geq 0,\ \kappa > 0,\ r, s \geq 1.$$

The second-order method is developed by taking a linear combination of the first-order methods some of which were used in the previous section §3.2.2 to solve the initial-value problem (3.11), (3.12). New first-order methods are introduced to construct the novel second-order method Price *et al.* [57].

Second-order method for A_{n+1}:

The first-order methods used before and the newly introduced methods, named $M1_\alpha, M2_\alpha, M3_\alpha$ and $M4_\alpha$, are

$$M1_\alpha: \quad A_{n+1} = A_n - \ell A_{n+1} B_n^r, \tag{3.48}$$

$$M2_\alpha: \quad A_{n+1} = A_n - \ell A_n B_n^{r-1} B_{n+1}, \tag{3.49}$$

$$M3_\alpha: \quad A_{n+1} = A_n - \ell A_{n+1} B_n^{r-1} B_{n+1}, \tag{3.50}$$

$$M4_\alpha: \quad A_{n+1} = A_n - \ell A_n B_n^r, \tag{3.51}$$

where $n = 0, 1, 2, \ldots$. The local truncation errors, $\mathscr{L}_\alpha^1, \mathscr{L}_\alpha^2, \mathscr{L}_\alpha^3$ and $\mathscr{L}_\alpha^4$, associated with (3.48)-(3.51), respectively, are the functions

$$\begin{aligned}
\mathscr{L}_\alpha^1[\alpha(t), \beta(t); \ell] &= \alpha(t+\ell) - \alpha(t) + \ell\alpha(t+\ell)[\beta(t)]^r \\
&= (\frac{1}{2}\alpha'' + \alpha'\beta^r)\ell^2 + O(\ell^3) \quad \text{as} \quad \ell \to 0, \qquad (3.52) \\
\mathscr{L}_\alpha^2[\alpha(t), \beta(t); \ell] &= \alpha(t+\ell) - \alpha(t) + \ell\alpha(t)[\beta(t)]^{r-1}\beta(t+\ell) \\
&= (\frac{1}{2}\alpha'' + \alpha\beta^{r-1}\beta')\ell^2 + O(\ell^3) \quad \text{as} \quad \ell \to 0, \qquad (3.53) \\
\mathscr{L}_\alpha^3[\alpha(t), \beta(t); \ell] &= \alpha(t+\ell) - \alpha(t) + \ell\alpha(t+\ell)[\beta(t)]^{r-1}\beta(t+\ell) \\
&= (\frac{1}{2}\alpha'' + \alpha'\beta^r + \alpha\beta^{r-1}\beta')\ell^2 + O(\ell^3) \quad \text{as} \quad \ell \to 0, \qquad (3.54) \\
\mathscr{L}_\alpha^4[\alpha(t), \beta(t); \ell] &= \alpha(t+\ell) - \alpha(t) + \ell\alpha(t)[\beta(t)]^r \\
&= (\frac{1}{2}\alpha'')\ell^2 + O(\ell^3) \quad \text{as} \quad \ell \to 0, \qquad (3.55)
\end{aligned}$$

where α, β and their derivatives (denoted by primes) are evaluated at some mesh point $t = t_n$. Define, now, a function $\mathscr{L}_\alpha$ by the formula

$$\mathscr{L}_\alpha = \mathscr{L}_\alpha[\alpha(t), \beta(t); \ell] = \mathscr{L}_\alpha^1 + r\mathscr{L}_\alpha^2 - (r-1)\mathscr{L}_\alpha^4, \tag{3.56}$$

then it is easy to show that

$$\mathscr{L}_\alpha \;=\; \{\frac{1}{2}\alpha'' + \alpha'\beta^r + r[\frac{1}{2}\alpha'' + \alpha\beta^{r-1}\beta'] - \frac{1}{2}(r-1)\alpha''\}\ell^2 + O(\ell^3) \quad \text{as} \quad \ell \to 0. \tag{3.57}$$

Differentiating the differential equation given in (3.46) shows that the coefficient of ℓ^2 in (3.57) vanishes, revealing that

$$\mathscr{L}_\alpha[\alpha(t), \beta(t); \ell] = O(\ell^3) \quad \text{as} \quad \ell \to 0. \tag{3.58}$$

The function $\mathscr{L}_\alpha$ defined by (3.56) is thus the local truncation error of a second-order numerical method for solving the initial-value problem (3.46). The second-order method for A_{n+1} may be constructed from (3.48), (3.49) and (3.51), utilizing (3.52), (3.53) and (3.55). These formulae give

$$\begin{aligned}[A_{n+1} - A_n + \ell A_{n+1}B_n^r] \;&+\; r[A_{n+1} - A_n + \ell A_n B_n^{r-1}B_{n+1}] \\ &-\; (r-1)[A_{n+1} - A_n + \ell A_n B_n^r] = 0,\end{aligned} \tag{3.59}$$

which may be rearranged as

$$M_\alpha: \quad (2 + \ell B_n^r)A_{n+1} + \ell r A_n B_n^{r-1}B_{n+1} = 2A_n + \ell(r-1)A_n B_n^r. \tag{3.60}$$

Second-order method for B_{n+1}:

The second-order numerical method for B_{n+1} can be found in a similar way. The first-order numerical methods, named $M1_\beta, M2_\beta, M3_\beta$ and $M4_\beta$, are

$$M1_\beta: \quad B_{n+1} = B_n + \ell A_{n+1}B_n^r - \ell\kappa B_n^s, \tag{3.61}$$

$$M2_\beta: \quad B_{n+1} = B_n + \ell A_n B_n^{r-1}B_{n+1} - \ell\kappa B_n^s, \tag{3.62}$$

$$M3_\beta: \quad B_{n+1} = B_n + \ell A_n B_n^r - \ell\kappa B_n^{s-1}B_{n+1}, \tag{3.63}$$

$$M4_\beta: \quad B_{n+1} = B_n + \ell A_n B_n^r - \ell\kappa B_n^s, \tag{3.64}$$

where $n = 0, 1, 2, \ldots$. The local truncation errors, $\mathscr{L}_\beta^1, \mathscr{L}_\beta^2, \mathscr{L}_\beta^3$ and $\mathscr{L}_\beta^4$, associated with (3.61)-(3.64), respectively, are the functions

$$\begin{aligned}
\mathscr{L}_\beta^1[\alpha(t), \beta(t); \ell] &= \beta(t+\ell) - \beta(t) - \ell\alpha(t+\ell)[\beta(t)]^r - \ell\kappa[\beta(t)]^s \\
&= (\frac{1}{2}\beta'' - \alpha'\beta^r)\ell^2 + O(\ell^3) \quad \text{as} \quad \ell \to 0, \qquad (3.65) \\
\mathscr{L}_\beta^2[\alpha(t), \beta(t); \ell] &= \beta(t+\ell) - \beta(t) - \ell\alpha(t+\ell)[\beta(t)]^r - \ell\kappa[\beta(t)]^s \\
&= (\frac{1}{2}\beta'' - \alpha\beta^{r-1}\beta')\ell^2 + O(\ell^3) \quad \text{as} \quad \ell \to 0, \qquad (3.66) \\
\mathscr{L}_\beta^3[\alpha(t), \beta(t); \ell] &= \beta(t+\ell) - \beta(t) - \ell\alpha(t)[\beta(t)]^r - \ell\kappa[\beta(t)]^{s-1}\beta(t+\ell) \\
&= (\frac{1}{2}\beta'' + \kappa\beta'\beta^{s-1})\ell^2 + O(\ell^3) \quad \text{as} \quad \ell \to 0, \qquad (3.67) \\
\mathscr{L}_\beta^4[\alpha(t), \beta(t); \ell] &= \beta(t+\ell) - \beta(t) - \ell\alpha(t)[\beta(t)]^r - \ell\kappa[\beta(t)]^s \\
&= (\frac{1}{2}\beta'')\ell^2 + O(\ell^3) \quad \text{as} \quad \ell \to 0, \qquad (3.68)
\end{aligned}$$

where α, β and their derivatives (denoted by primes) are evaluated at some mesh point $t = t_n$. Define, now, a function $\mathscr{L}_\beta$ by the formula

$$\mathscr{L}_\beta = \mathscr{L}_\beta[\alpha(t), \beta(t); \ell] = \mathscr{L}_\beta^1 + r\mathscr{L}_\beta^2 + s\mathscr{L}_\beta^3 - (r+s-1)\mathscr{L}_\beta^4, \qquad (3.69)$$

then it is possible to show that

$$\mathscr{L}_\beta = \{\frac{1}{2}\beta'' - \alpha'\beta^r + r[\frac{1}{2}\beta'' - \alpha\beta^{r-1}\beta'] - \frac{1}{2}(r+s-1)\beta''\}\ell^2 + O(\ell^3) \quad \text{as} \quad \ell \to 0. \qquad (3.70)$$

Differentiating the differential equation given in (3.47) shows that the coefficient of ℓ^2 in (3.58) vanishes, revealing that

$$\mathscr{L}_\beta[\alpha(t), \beta(t); \ell] = O(\ell^3) \quad \text{as} \quad \ell \to 0. \qquad (3.71)$$

The function $\mathscr{L}_\beta$ defined by (3.69) is thus the local truncation error of a second-order numerical method for solving the initial-value problem (3.47). The second-order method for B_{n+1} may be developed from (3.61)-(3.64), utilizing (3.65)-(3.68). These formulae give

$$\begin{aligned}
&[B_{n+1} - B_n - \ell A_{n+1} B_n^r] + r[B_{n+1} - B_n - \ell A_n B_n^{r-1} B_{n+1} + \ell\kappa B_n^s] \\
&\qquad + s[B_{n+1} - B_n - \ell A_n B_n^r + \ell\kappa B_n^{s-1} B_{n+1}] \\
&\qquad - (r+s-1)[B_{n+1} - B_n - \ell A_n B_n^r + \ell\kappa B_n^s] = 0, \qquad (3.72)
\end{aligned}$$

which may be rearranged as

$$M_\beta : \quad -\ell B_n^r A_{n+1} + (2 - r\ell A_n B_n^{r-1} + s\ell\kappa B_n^{s-1}) B_{n+1}$$
$$= 2B_n - (r-1)\ell A_n B_n^r - 2\ell\kappa(2-s)B_n^s. \tag{3.73}$$

Solving the algebraic system (3.60) and (3.73) simultaneously for A_{n+1} and B_{n+1} gives

$$A_{n+1} =$$
$$\frac{A_n\{4 - 2\ell B_n^r[r(B_n^{r-1} - 1) + 1] - r\ell B_n^{r-1}[2A_n - \ell\kappa(2-s)B_n^s] + \ell\kappa s B_n^{s-1}[2 + \ell\kappa(r-1)B_n^r]\}}{(2 + \ell B_n^m)(2 + \ell\kappa s B_n^{s-1}) - 2\ell r A_n B_n^{r-1}} \tag{3.74}$$

$$B_{n+1} =$$
$$\frac{\ell A_n B_n^r[2 + \ell(r-1)B_n] + (2 + \ell B_n^r[2B_n - \ell(r-1)A_n B_n^r - \ell\kappa(2-s)B_n^s]}{(2 + \ell B_n^m)(2 + \ell\kappa s B_n^{s-1}) - 2\ell r A_n B_n^{r-1}}. \tag{3.75}$$

Analyses of the fixed points

Equations (3.74) and (3.75) are of the form of the one-point iteration algorithm

$$A_{n+1} = h_1(A_n, B_n), \quad n = 0, 1, 2, \ldots, \tag{3.76}$$
$$B_{n+1} = h_2(A_n, B_n), \quad n = 0, 1, 2, \ldots. \tag{3.77}$$

It is necessary to consider the associated functions

$$A = h_1(A, B) \qquad \text{and} \qquad B = h_2(A, B),$$

from which it may be shown that $h_1(A, B)$ equals the right-hand side of the expression (3.74) at (A, B) and similarly $h_2(A, B)$ equals the right-hand side of the expression (3.75) at (A, B).

The fixed point of the system is also $(\alpha_e, 0)$ which is a line of fixed points. The stability properties of the second-order method is determined by the position of the eigenvalues of the system matrix

$$J_S = \begin{bmatrix} \partial h_1(\alpha_e, \beta_e)/\partial A & \partial h_1(\alpha_e, \beta_e)/\partial B \\ \partial h_2(\alpha_e, \beta_e)/\partial A & \partial h_2(\alpha_e, \beta_e)/\partial B \end{bmatrix}$$

which must be calculated.

Since all the eigenvalues have a value of unity, it may be concluded that the second-order method is marginally stable, Luenberger [33].

3.2.6 Numerical experiments

First- and second-order finite-difference schemes were suggested to solve the initial-value problem given by the equations (3.11) and (3.12) with the initial conditions $\alpha(0) = \alpha_0 = 1$ and $\beta(0) = \beta_0$. The behaviour of the numerical solution of this IVP was studied with respect to the autocatalysis exponent r and the decay rate exponent s. The development and analysis of the numerical schemes were done by considering general orders of autocatalysis and decay, that is $r, s \geq 1$. Throughout the numerical experiments only the integer values of $1 \leq r, s \leq 3$ were studied. The reason for this is that, in the chemical aspect, there are four possible rates at which the order of reaction can occur, namely zero, first, second and third. The last one occurs rarely due to the low probability in the number of the possible collisions of the bodies in a reaction with the rate higher than three, Short [63]. The phase-plane analyses in Cases 1, 2 and 3 were used for qualitative comparisons with the experimental results. Some of the results given in the literature, for example Merkin *et al.* [48], were also used to establish the reliability of the alternative first-order methods Method 1, Method 2 and second-order method developed in §3.2.2 and §3.2.5. As was shown in §3.2.1 this IVP has a line of equilibrium points given by $\alpha = \alpha_e$ and $\beta = 0$ for all $\alpha \geq 0$. It was observed that this was also the feature of all the suggested numerical methods.

Solutions were obtained for a range of values of κ and β_0 in Cases 1, 2 and 3. The stability intervals of the numerical schemes for all cases are summarized in Table 3.1.

Case 1: $r = s$

The parameter and initial conditions used in Case 1 were taken to be

$$\kappa = 0.9,\ \alpha_0 = 1,\ \beta_0 = 0.1\ . \tag{3.78}$$

Numerical solutions given by Method 1 (Euler) converged monotonically to some equilibrium point, α_e, while β first approached a local maximum at $\kappa = 0.9$, [see also Fig. 3.1] then converged to zero for small values of the time step ℓ, [see Table 3.1]. As ℓ was increased, Method 1 computed negative values of α which is not realistic for a chemical concentration. Convergence still took place, however, while β was approaching the local maximum at a qualitatively wrong value which was less than $\kappa = 0.9$. As ℓ was increased further, Method 1 eventually produced overflow for $\ell > 3.44$ with $1 \leq r = s \leq 3$.

Numerical solutions computed using Method 2 converged to the stationary point, $(\alpha_e, 0)$, for large values of the time step ℓ, $\ell \leq \ell_{\text{large}}$, $(\ell_{\text{large}} = 100)$ for $1 \leq r = s \leq 3$. It was also observed that the higher the value of ℓ, the quicker the stationary point was attained; for instance for $r = s = 2$ with $\ell = 5$ convergence occurred after 2000 iterations and with $\ell = 50$ convergence occurred after 20 iterations while for $\ell = 100$ convergence occurred after 5 iterations.

Using the second-order method convergence to the fixed point, $(\alpha_e, 0)$, was observed to be always monotonic for $\ell \leq 20.0$ for $r = s = 1$. As ℓ was increased further, due to the growing global truncation error, the solution sequence appeared to be being attracted to another fixed point, which was a perturbation of the correct fixed point. The convergence to the steady state was always monotonic for $\ell \leq \ell_{\text{large}}$ for $r = s = 2$ and $r = s = 3$.

Case 2: $r < s$

The same parameter and initial conditions, (3.78), given in Case 1, were also used for Case 2.

Numerical solutions given by Method 1 converged to the stable stationary point, $(0, 0)$, for $\ell \leq 1.8$ for $r = s = 1$, $\ell \leq 1.4$ for $r = s = 2$ and $\ell \leq 3.4$ for $r = s = 3$. As

ℓ was increased further, Method 1 diverged for $1 \leq r \leq 3$.

Numerical solutions produced using Method 2 converged to the stable fixed point, $(0,0)$, for $\ell \leq \ell_{\text{large}}$ used for $1 \leq r < s \leq 3$.

The second-order method converged to the correct stationary state, (0,0), for $\ell \leq \ell_{\text{large}}$ for the values $r = 1, s = 2$ and $r = 1, s = 3$. For the case $r = 2, s = 3$ convergence was observed up to $\ell = 50.0$. As ℓ was increased further a similar phenomenon to that in Case 1 was also observed due to the growing global truncation error.

Case 3: $r > s$

The parameter and initial conditions used in this case were

$$\kappa = 0.0465,\ \alpha_0 = 1,\ \beta_0 = 0.1. \tag{3.79}$$

Here the parameter value of κ was chosen to satisfy the relation $\beta_0 > \kappa^{\frac{1}{r-s}}$, Merkin *et al.* [48].

Method 1 converged monotonically to some equilibrium point, $(\alpha_e, 0)$, while β approached zero for $\ell \leq 2.0$ for $r = 2, s = 1$; $\ell \leq 4.0$ for $r = 3, s = 2$; and $\ell \leq 5.0$ for $r = 3, s = 1$. Method 1 was seen to break down due to overflow for $\ell > 4.0, \ell > 5.0$ and $\ell > 8.0$ respectively.

The alternative finite-difference scheme, Method 2, also performed very well for this case and converged to some stationary point, $(\alpha_e, 0)$, for $\ell \leq \ell_{\text{large}}$ for $1 \leq s < r \leq 3$.

The second-order method converged to the correct fixed point for $\ell \leq \ell_{\text{large}}$ for $r = 2, s = 1$ and $r = 3, s = 2$. For $r = 3, s = 1$ the method seemed to converge for $\ell \leq 75.7$ but as ℓ was increased further the method did not diverge but instead converged to the perturbation of the correct fixed point similar to Cases 2 and 3.

A variety of initial conditions were also used to solve (3.11) and (3.12) with $\alpha_0 = 1$ and for various values of β_0 such as $\beta_0 = 0.1, 0.5, 0.9$, to show the affect of the initial conditions on the convergence of the solutions. The second-order method was used to produce the numerical results which are depicted in Fig. 3.2. From this it can

be observed that β first approaches the local maximum at $\kappa = 0.9$ then converges to zero at $\alpha_e = 0.53$ for $\beta_0 = 0.1$, $\alpha_e = 0.25$ for $\beta_0 = 0.5$, and $\alpha_e = 0.14$ for $\beta_0 = 0.9$.

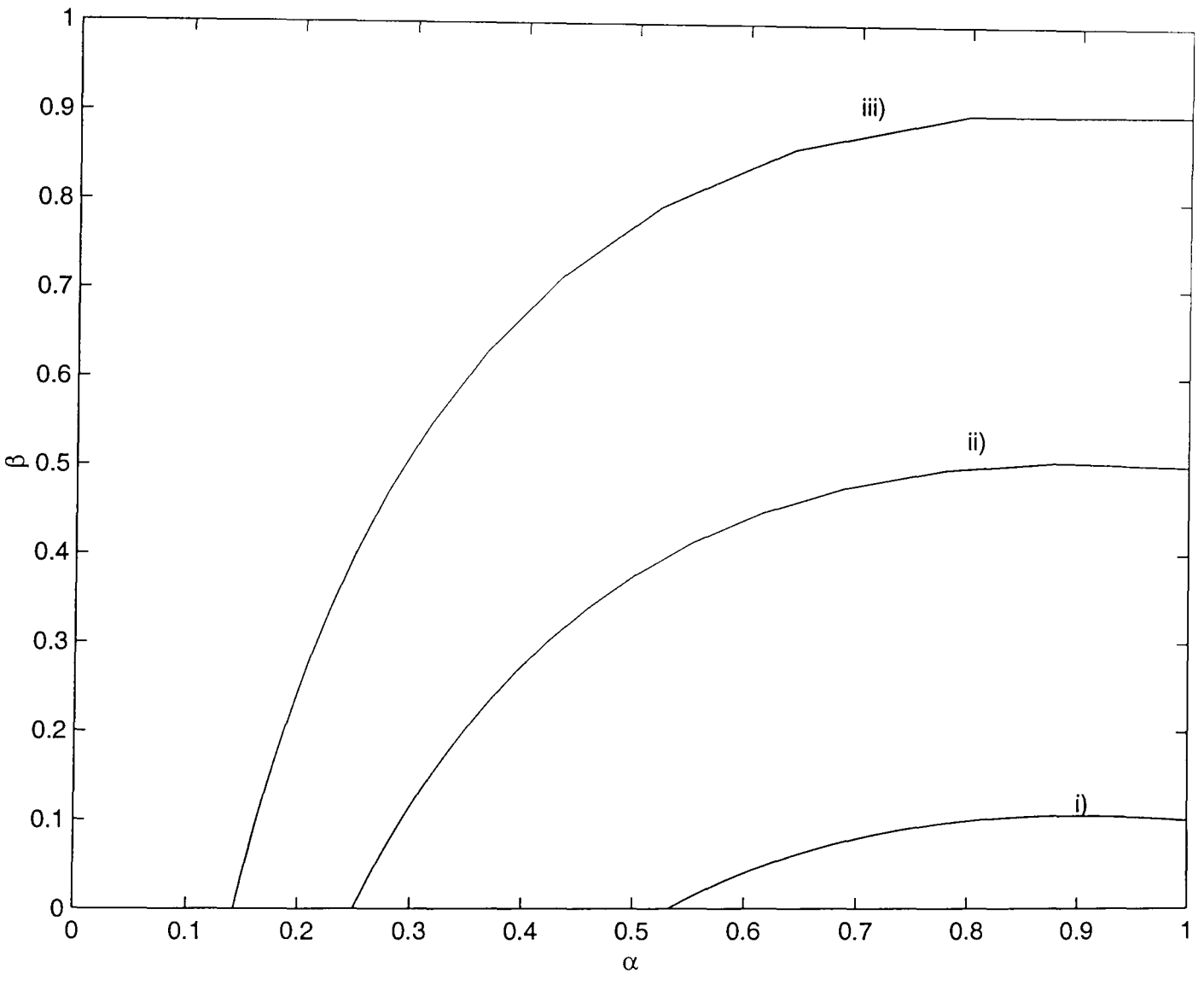

Figure 3.2: The solution profiles of α and β using $\kappa = 0.9$ with initial conditions $\alpha = 1$ and i) $\beta_0 = 0.1$, ii) $\beta_0 = 0.5$, iii) $\beta_0 = 0.9$.

Specific Cases		Interval of Stability		
		Method 1	Method 2	Second-order method
$r = s$	$r = s = 1$	(0, 1.3)	$(0, \ell_{\text{large}})$	(0, 20.0)
	$r = s = 2$	(0, 3.0)	$(0, \ell_{\text{large}})$	$(0, \ell_{\text{large}})$
	$r = s = 3$	(0, 3.0)	$(0, \ell_{\text{large}})$	$(0, \ell_{\text{large}})$
$r < s$	$r = 1, s = 2$	(0, 1.8)	$(0, \ell_{\text{large}})$	$(0, \ell_{\text{large}})$
	$r = 2, s = 3$	(0, 1.4)	$(0, \ell_{\text{large}})$	(0, 50.0)
	$r = 1, s = 3$	(0, 3.4)	$(0, \ell_{\text{large}})$	$(0, \ell_{\text{large}})$
$r > s$	$r = 2, s = 1$	(0, 2.0)	$(0, \ell_{\text{large}})$	$(0, \ell_{\text{large}})$
	$r = 3, s = 2$	(0, 4.0)	$(0, \ell_{\text{large}})$	$(0, \ell_{\text{large}})$
	$r = 3, s = 1$	(0, 5.0)	$(0, \ell_{\text{large}})$	(0, 75.7)

Table 3.1: Stability intervals of the numerical methods.

3.3 Reaction-diffusion Model

The inital-value problem given by equations (3.7)-(3.10) will be solved by applying finite-difference approximations, by discretizing the space interval $-\sigma \leq x \leq \sigma$ into $2(N+1)$ sub-intervals, each of width $h > 0$ such that $2(N+1)h = 2\sigma$, and the time interval into steps each of length $\ell > 0$. The open region $\mathscr{R} = [-\sigma < x < \sigma] \times [t > 0]$ and its boundary $\partial\mathscr{R}$ consisting of the lines $x = -\sigma, x = \sigma$, and $t = 0$ are thus covered by a rectangular grid. The equations will be integrated only in the region $\mathscr{R}$ where $x \geq 0$ with zero-flux boundary conditions across the axis $x = 0$. The outer boundary conditions $\alpha = 1, \beta = 0$ will be applied at $x = 200$; this gives a sufficiently large region for any reaction-diffusion wave to develop and reach its asymptotic speed $v_0 = 2(1-k)^{1/2}$, Merkin [42]. The solutions of the approximating finite-difference scheme at the grid point $(x_m, t_n) = (mh, n\ell)$ with $m = -N-1, -N, \ldots, 0, 1, \ldots, N+1$ and $n = 0, 1, 2, \ldots$. The notations A_m^n and B_m^n will be used to distinguish the solution of an approximating finite-difference scheme

from the theoretical solutions $\alpha(x_m, t_n)$ and $\beta(x_m, t_n)$; $\tilde{A}_m^n$ and $\tilde{B}_m^n$ will denote the actual values obtained by computation which may be subject to round-off errors.

3.3.1 Numerical methods

A family of numerical methods will be developed by approximating the time derivatives in (3.7) by the first-order forward difference approximant

$$\partial\alpha(x,t)/\partial t = \frac{1}{\ell}[\alpha(x,t+\ell) - \alpha(x,t)] + O(\ell) \quad \text{as} \quad \ell \to 0, \tag{3.80}$$

and the space derivative in (3.7) by the weighted second-order approximant

$$\begin{aligned} \partial^2\alpha(x,t)/\partial x^2 \;\simeq\; & \frac{1}{h^2}\{\phi[\alpha(x-h,t+\ell) - 2\alpha(x,t+\ell) + \alpha(x+h,t+\ell)] \\ + \;& (1-\phi)[\alpha(x-h,t) - 2\alpha(x,t) + \alpha(x+h,t)]\} + O(h^2) \quad \text{as} \quad h \to 0 \end{aligned} \tag{3.81}$$

in which $x = x_m$ $(m = -N, \ldots, 0, 1, \ldots, N)$, $t = t_n$ $(n = 0, 1, 2, \ldots)$, and $0 \le \phi \le 1$ is a parameter. Similar approximations are used to approximate the derivatives in (3.8).

Furthermore, the unknown functions α and β, which model general orders of autocatalysis and decay, may be approximated in the three ways which some of them were used in §3.2.2, giving

$$\textbf{a)} - A_m^n(B_m^n)^r \quad \text{and} \quad A_m^n(B_m^n)^r - \kappa(B_m^n)^s \tag{3.82}$$

or

$$\textbf{b)} - A_m^{n+1}(B_m^n)^r \quad \text{and} \quad A_m^{n+1}B_m^{n+1}(B_m^n)^{r-1} - \kappa B_m^{n+1}(B_m^n)^{s-1} \tag{3.83}$$

or

$$\textbf{c)} - A_m^{n+1}(B_m^n)^r \quad \text{and} \quad A_m^n B_m^{n+1}(B_m^n)^{r-1} - \kappa B_m^{n+1}(B_m^n)^{s-1}. \tag{3.84}$$

These approximations, together with the replacement for the derivatives of α and β lead to three families of numerical methods, named $\mathscr{C}_1(\phi)$, $\mathscr{C}_2(\phi)$, and $\mathscr{C}_3(\phi)$ for the

numerical solution of (3.7) and (3.8). These methods are as follows.

Method $\mathscr{C}_1(\phi), 0 \leq \phi \leq 1$:

$$-\phi p A_{m-1}^{n+1} + (1+2\phi p)A_m^{n+1} - \phi p A_{m+1}^{n+1} =$$
$$(1-\phi)pA_{m-1}^n + [1-2(1-\phi)p - \ell(B_m^n)^r]A_m^n + (1-\phi)pA_{m+1}^n, \quad (3.85)$$

$$-\phi p B_{m-1}^{n+1} + (1+2\phi p)B_m^{n+1} - \phi p B_{m+1}^{n+1} =$$
$$(1-\phi)pB_{m-1}^n + [1-2(1-\phi)p + \ell A_m^n (B_m^n)^{r-1} - \kappa\ell(B_m^n)^{s-1}]B_m^n + (1-\phi)pB_{m+1}^n, \quad (3.86)$$

Method $\mathscr{C}_2(\phi), 0 \leq \phi \leq 1$:

$$-\phi p A_{m-1}^{n+1} + [1+2\phi p + \ell(B_m^n)^r]A_m^{n+1} - \phi p A_{m+1}^{n+1} =$$
$$(1-\phi)pA_{m-1}^n + [1-2(1-\phi)p]A_m^n + (1-\phi)pA_{m+1}^n, \quad (3.87)$$

$$-\phi p B_{m-1}^{n+1} + [1+2\phi p - \ell A_m^{n+1}(B_m^n)^{r-1} + \kappa\ell(B_m^n)^{s-1}]B_m^{n+1} - \phi p B_{m+1}^{n+1} =$$
$$(1-\phi)pB_{m-1}^n + [1-2(1-\phi)p]B_m^n + (1-\phi)pB_{m+1}^n, \quad (3.88)$$

Method $\mathscr{C}_3(\phi), 0 \leq \phi \leq 1$:

$$-\phi p A_{m-1}^{n+1} + [1+2\phi p + \ell(B_m^n)^r]A_m^{n+1} - \phi p A_{m+1}^{n+1} =$$
$$(1-\phi)pA_{m-1}^n + [1-2(1-\phi)p]A_m^n + (1-\phi)pA_{m+1}^n, \quad (3.89)$$

$$-\phi p B_{m-1}^{n+1} + [1+2\phi p - \ell A_m^n (B_m^n)^{r-1} + \kappa\ell(B_m^n)^{s-1}]B_m^{n+1} - \phi p B_{m+1}^{n+1} =$$
$$(1-\phi)pB_{m-1}^n + [1-2(1-\phi)p]B_m^n + (1-\phi)pB_{m+1}^n, \quad (3.90)$$

in which $p = \ell/h^2, m = -N, \ldots, 0, 1, \ldots, N$ and $n = 0, 1, 2, \ldots$.

3.3.2 Local truncation errors

The local truncation errors associated with (3.85), (3.87) and (3.89) are given by

$$\mathscr{L}_\alpha[\alpha, \beta; h, \ell] = \frac{1}{\ell}[\alpha(x, t+\ell) - \alpha(x, t)]$$

$$
\begin{aligned}
&- \frac{1}{h^2}\phi[\alpha(x-h,t+\ell) - 2\alpha(x,t+\ell) + \alpha(x+h,t+\ell)] \\
&- \frac{1}{h^2}(1-\phi)[\alpha(x-h,t) - 2\alpha(x,t) + \alpha(x+h,t)] \\
&+ \alpha(x,t+\rho\ell) \times [\beta(x,t)]^r \\
&- \{\partial\alpha(x,t)/\partial t - \partial^2\alpha(x,t)/\partial x^2 + \alpha(x,t)[\beta(x,t)]^r\} \quad \text{as} \quad h,\ell \to 0
\end{aligned}
\tag{3.91}
$$

where **a)** for family $\mathscr{C}_1(\phi), \rho = 0$, and **b)**, **c)** for families $\mathscr{C}_2(\phi)$ and $\mathscr{C}_3(\phi), \rho = 1$. The local truncation errors associated with (3.86), (3.88) and (3.90) are given by

$$
\begin{aligned}
\mathscr{L}_\beta[\alpha,\beta;h,\ell] \;=\; & \frac{1}{\ell}[\beta(x,t+\ell) - \beta(x,t)] \\
&- \frac{1}{h^2}\phi[\beta(x-h,t+\ell) - 2\beta(x,t+\ell) + \beta(x+h,t+\ell)] \\
&- \frac{1}{h^2}(1-\phi)[\beta(x-h,t) - 2\beta(x,t) + \beta(x+h,t)] \\
&- \alpha(x,t+\varrho\ell) \times [\beta(x,t+\tau\ell)]^r + \kappa[\beta(x,t+\tau\ell)]^s \\
&- \{\partial\alpha(x,t)/\partial t - \partial^2\alpha(x,t)/\partial x^2 - \alpha(x,t)[\beta(x,t)]^r + \kappa[\beta(x,t)]^s\} \\
& \qquad\qquad \text{as} \quad h,\ell \to 0
\end{aligned}
\tag{3.92}
$$

in which **a)** for family $\mathscr{C}_1(\phi), \varrho = \tau = 0$, **b)** for family $\mathscr{C}_2(\phi), \varrho = \tau = 1$, and **c)** for family $\mathscr{C}_3(\phi), \varrho = 0$ and $\tau = 1$. The LTEs for all three families are $O(h^2 + \ell)$ as $h, \ell \to 0$ with

i)for family $\mathscr{C}_1(\phi)$:

$$
\mathscr{L}_\alpha[\alpha,\beta;h,\ell] = -\frac{1}{12}h^2\frac{\partial^4\alpha}{\partial x^4} + \left(\frac{1}{2}\frac{\partial^2\alpha}{\partial t^2} - \phi\frac{\partial^3\alpha}{\partial x^2\partial t}\right)\ell + \ldots, \tag{3.93}
$$

$$
\mathscr{L}_\beta[\alpha,\beta;h,\ell] = -\frac{1}{12}h^2\frac{\partial^4\beta}{\partial x^4} + \left(\frac{1}{2}\frac{\partial^2\beta}{\partial t^2} - \phi\frac{\partial^3\beta}{\partial x^2\partial t}\right)\ell + \ldots, \tag{3.94}
$$

ii) for family $\mathscr{C}_2(\phi)$:

$$
\mathscr{L}_\alpha[\alpha,\beta;h,\ell] = -\frac{1}{12}h^2\frac{\partial^4\alpha}{\partial x^4} + \left(\frac{1}{2}\frac{\partial^2\alpha}{\partial t^2} - \phi\frac{\partial^3\alpha}{\partial x^2\partial t} + \beta^r\frac{\partial\alpha}{\partial t}\right)\ell + \ldots, \tag{3.95}
$$

$$
\mathscr{L}_\beta[\alpha,\beta;h,\ell] = -\frac{1}{12}h^2\frac{\partial^4\beta}{\partial x^4} + \left[\frac{1}{2}\frac{\partial^2\beta}{\partial t^2} - \phi\frac{\partial^3\beta}{\partial x^2\partial t} - \alpha\left(\frac{\partial\beta}{\partial t}\right)^r - \beta^r\frac{\partial\alpha}{\partial t} + \kappa\frac{\partial\beta}{\partial t}\right]\ell + \ldots, \tag{3.96}
$$

iii) for family $\mathscr{C}_3(\phi)$:

$$\mathscr{L}_\alpha[\alpha,\beta;h,\ell] = -\frac{1}{12}h^2\frac{\partial^4\alpha}{\partial x^4} + \left(\frac{1}{2}\frac{\partial^2\alpha}{\partial t^2} - \phi\frac{\partial^3\alpha}{\partial x^2\partial t} + \beta^r\frac{\partial\alpha}{\partial t}\right)\ell + \ldots, \tag{3.97}$$

$$\mathscr{L}_\beta[\alpha,\beta;h,\ell] = -\frac{1}{12}h^2\frac{\partial^4\beta}{\partial x^4} + \left[\frac{1}{2}\frac{\partial^2\beta}{\partial t^2} - \phi\frac{\partial^3\beta}{\partial x^2\partial t} - \alpha\left(\frac{\partial\beta}{\partial t}\right)^r + \kappa\left(\frac{\partial\beta}{\partial t}\right)^s\right]\ell + \ldots. \tag{3.98}$$

3.3.3 Numerical stability

The von Neumann (or Fourier series) method will be used to analyse the stability properties of the three families $\mathscr{C}_1(\phi)$, $\mathscr{C}_2(\phi)$ and $\mathscr{C}_3(\phi)$. Expressing the error at $(x,t) = (mh, n\ell)$ of the unknown functions A_m^n and B_m^n in the form

$$Z_{\alpha,m}^n = A_m^n - \tilde{A}_m^n = e^{\gamma\ell}e^{i\delta mh} \tag{3.99}$$

and

$$Z_{\beta,m}^n = B_m^n - \tilde{B}_m^n = e^{\mu\ell}e^{i\nu mh} \tag{3.100}$$

where $\gamma,\delta,\mu,\nu \in \mathbb{R}$; $i = +\sqrt{-1}$ and $\tilde{A}_m^n$ and $\tilde{B}_m^n$ are perturbed numerical solutions, a necessary constraint for the error not to grow as $n \to \infty$ is

$$|e^{\gamma\ell}| \leq 1 + K_\alpha\ell \quad \text{and} \quad |e^{\mu\ell}| \leq 1 + K_\beta\ell \tag{3.101}$$

where K_α and K_β are non-negative constants independent of h,ℓ. Equations (3.101) are the von Neumann necessary conditions for stability. They make no allowance for growing solutions if $K_\alpha = 0$ and $K_\beta = 0$.

Method $\mathscr{C}_1(\phi)$:

Substituting $Z_{\alpha,m}^n$ into (3.85) and linearization [19] leads to the (local) stability equation

$$\left(1 + 4\phi p\sin^2\frac{1}{2}\nu h\right)\xi_\alpha = 1 - 4(1-\phi)p\sin^2\frac{1}{2}\delta h - \ell(\tilde{B}_m^n)^r, \tag{3.102}$$

where $\xi_\alpha = e^{\gamma\ell}$, with the consequent stability restrictions

$$\begin{aligned} 0 \le \phi < \frac{1}{2}, \qquad & p \le \frac{2 - \ell(\tilde{B}_m^n)^r}{4(1-2\phi)}; \\ \phi = \frac{1}{2}, \qquad & \ell(\tilde{B}_m^n)^r \le 2; \\ \frac{1}{2} < \phi \le 1, \qquad & p \ge \frac{\ell(\tilde{B}_m^n)^r - 2}{4(2\phi - 1)}. \end{aligned} \tag{3.103}$$

Substituting $Z_{\beta,m}^n$ into (3.86) and linearization [19] leads to the (local) stability equation

$$\left[1 + 4\phi p \sin^2 \frac{1}{2}\nu h\right] \xi_\beta = 1 - 4(1-\phi)p \sin^2 \frac{1}{2}\nu h + \ell r \tilde{A}_m^n (\tilde{B}_m^n)^{r-1} - \kappa \ell s (\tilde{B}_m^n)^{s-1}, \tag{3.104}$$

where $\xi_\beta = e^{\mu\ell}$, with the consequent stability restrictions

$$\begin{aligned} 0 \le \phi < \frac{1}{2}, \qquad & p \le \frac{2 + \ell r \tilde{A}_m^n (\tilde{B}_m^n)^{r-1} - \kappa \ell s (\tilde{B}_m^n)^{s-1}}{4(1-2\phi)}; \\ \phi = \frac{1}{2}, \qquad & \ell[\kappa s (\tilde{B}_m^n)^{s-1} - r \tilde{A}_m^n (\tilde{B}_m^n)^{r-1}] \le 2; \\ \frac{1}{2} < \phi \le 1, \qquad & p \ge \frac{\kappa \ell s (\tilde{B}_m^n)^{s-1} - \ell r \tilde{A}_m^n (\tilde{B}_m^n)^{r-1} - 2}{4(2\phi - 1)}. \end{aligned} \tag{3.105}$$

Method $\mathscr{C}_2(\phi)$:

Substituting $Z_{\alpha,m}^n$ into (3.87) leads to the (local) stability equation

$$\left[1 + 4\phi p \sin^2 \frac{1}{2}\delta h + \ell(\tilde{B}_m^n)^r\right] \xi_\alpha = 1 - 4(1-\phi)p \sin^2 \frac{1}{2}\delta h, \tag{3.106}$$

from which it may be deduced that, for stability

$$\begin{aligned} 0 \le \phi < \frac{1}{2}, \qquad & p \le \frac{2 + \ell(\tilde{B}_m^n)^r}{4(1-2\phi)}; \\ \phi = \frac{1}{2}, \qquad & \ell(\tilde{B}_m^n)^r > -2; \\ \frac{1}{2} < \phi \le 1, \qquad & p \ge \frac{2 + \ell(\tilde{B}_m^n)^r}{4(1-2\phi)}. \end{aligned} \tag{3.107}$$

Substituting $Z_{\beta,m}^n$ into (3.88) leads to the (local) stability equation

$$\left[1 + 4\phi p \sin^2 \frac{1}{2}\nu h - \ell \tilde{A}_m^{n+1} (\tilde{B}_m^n)^r + \kappa \ell (\tilde{B}_m^n)^{s-1}\right] \xi_\beta = 1 - 4(1-\phi)p \sin^2 \frac{1}{2}\nu h, \tag{3.108}$$

from which the stability restrictions are seen to be

$$0 \leq \phi < \frac{1}{2},$$

$$p \leq \frac{2 + \ell\{\tilde{A}_m^{n+1}(\tilde{B}_m^n)^{r-1}[(r-1)\tilde{B}_m^{n+1}(\tilde{B}_m^n)^{-1} - 1] - \kappa(\tilde{B}_m^n)^{s-1}[(s-1)\tilde{B}_m^{n+1}(\tilde{B}_m^n)^{-1} - 1]\}}{4(1-2\phi)}$$

and

$$p \geq \frac{1}{4}\{\tilde{A}_m^{n+1}(\tilde{B}_m^n)^{r-1}[1 + (r-1)\tilde{B}_m^{n+1}(\tilde{B}_m^n)^{-1}] - \kappa(\tilde{B}_m^n)^{s-1}[1 + (s-1)\tilde{B}_m^{n+1}(\tilde{B}_m^n)^{-1}]\};$$

$$\phi = \frac{1}{2},$$

$$\ell\{\tilde{A}_m^{n+1}(\tilde{B}_m^n)^{r-1}[(r-1)\tilde{B}_m^{n+1}(\tilde{B}_m^n)^{-1} - 1] - \kappa(\tilde{B}_m^n)^{s-1}[(s-1)\tilde{B}_m^{n+1}(\tilde{B}_m^n)^{-1} - 1]\} \geq -2$$

and

$$p \geq \frac{1}{4}\{\tilde{A}_m^{n+1}(\tilde{B}_m^n)^{r-1}[1 + (r-1)\tilde{B}_m^{n+1}(\tilde{B}_m^n)^{-1}] - \kappa(\tilde{B}_m^n)^{s-1}[1 + (s-1)\tilde{B}_m^{n+1}(\tilde{B}_m^n)^{-1}]\};$$

$$\frac{1}{2} < \phi \leq 1,$$

$$p \leq \frac{-2 - \ell\{\tilde{A}_m^{n+1}(\tilde{B}_m^n)^{r-1}[(r-1)\tilde{B}_m^{n+1}(\tilde{B}_m^n)^{-1} - 1] - \kappa(\tilde{B}_m^n)^{s-1}[(s-1)\tilde{B}_m^{n+1}(\tilde{B}_m^n)^{-1} - 1]\}}{4(2\phi - 1)}$$

and

$$p \geq \frac{1}{4}\{\tilde{A}_m^{n+1}(\tilde{B}_m^n)^{r-1}[1 + (r-1)\tilde{B}_m^{n+1}(\tilde{B}_m^n)^{-1}] - \kappa(\tilde{B}_m^n)^{s-1}[1 + (s-1)\tilde{B}_m^{n+1}(\tilde{B}_m^n)^{-1}]\}. \tag{3.109}$$

Method $\mathscr{C}_3(\phi)$:

Substituting $Z_{\alpha,m}^n$ into (3.89) leads to the (local) stability equation

$$\left[1 + 4\phi p \sin^2 \frac{1}{2}\delta h + \ell(\tilde{B}_m^n)^r\right] \xi_\alpha = 1 - 4(1-\phi)p \sin^2 \frac{1}{2}\delta h, \tag{3.110}$$

from which it may be deduced that, for stability

$$\begin{aligned} 0 \leq \phi < \frac{1}{2}, \quad & p \leq \frac{2 + \ell(\tilde{B}_m^n)^r}{4(1-2\phi)}; \\ \phi = \frac{1}{2}, \quad & \ell(\tilde{B}_m^n)^r \geq -2; \\ \frac{1}{2} < \phi \leq 1, \quad & p \geq \frac{2 + \ell(\tilde{B}_m^n)^r}{4(1-2\phi)}. \end{aligned} \tag{3.111}$$

Substituting $Z^n_{\beta,m}$ into (3.90) leads to the (local) stability equation

$$\left[1 + 4\phi p \sin^2 \frac{1}{2}\nu h - \ell \tilde{A}^n_m (\tilde{B}^n_m)^{r-1} + \kappa \ell (\tilde{B}^n_m)^{s-1}\right] \xi_\beta = 1 - 4(1-\phi) p \sin^2 \frac{1}{2}\nu h, \tag{3.112}$$

with the consequent stability restrictions

$$0 \le \phi < \frac{1}{2},$$

$$p \le \frac{2 + \ell\{\tilde{A}^n_m (\tilde{B}^n_m)^{r-1}[(r-1)\tilde{B}^{n+1}_m (\tilde{B}^n_m)^{-1} - 1] - \kappa (\tilde{B}^n_m)^{s-1}[(s-1)\tilde{B}^{n+1}_m (\tilde{B}^n_m)^{-1} - 1]\}}{4(1-2\phi)}$$

and

$$p \ge \frac{1}{4}\{\tilde{A}^n_m (\tilde{B}^n_m)^{r-1}[1 + (r-1)\tilde{B}^{n+1}_m (\tilde{B}^n_m)^{-1}] - \kappa (\tilde{B}^n_m)^{s-1}[1 + (s-1)\tilde{B}^{n+1}_m (\tilde{B}^n_m)^{-1}]\};$$

$$\phi = \frac{1}{2},$$

$$\ell\{\tilde{A}^n_m (\tilde{B}^n_m)^{r-1}[(r-1)\tilde{B}^{n+1}_m (\tilde{B}^n_m)^{-1} - 1] - \kappa (\tilde{B}^n_m)^{s-1}[(s-1)\tilde{B}^{n+1}_m (\tilde{B}^n_m)^{-1} - 1]\} \ge -2$$

and

$$p \ge \frac{1}{4}\{\tilde{A}^n_m (\tilde{B}^n_m)^{r-1}[1 + (r-1)\tilde{B}^{n+1}_m (\tilde{B}^n_m)^{-1}] - \kappa (\tilde{B}^n_m)^{s-1}[1 + (s-1)\tilde{B}^{n+1}_m (\tilde{B}^n_m)^{-1}]\};$$

$$\frac{1}{2} < \phi \le 1,$$

$$p \le \frac{-2 - \ell\{\tilde{A}^n_m (\tilde{B}^n_m)^{r-1}[(r-1)\tilde{B}^{n+1}_m (\tilde{B}^n_m)^{-1} - 1] - \kappa (\tilde{B}^n_m)^{s-1}[(s-1)\tilde{B}^{n+1}_m (\tilde{B}^n_m)^{-1} - 1]\}}{4(2\phi - 1)}$$

and

$$p \ge \frac{1}{4}\{\tilde{A}^n_m (\tilde{B}^n_m)^{r-1}[1 + (r-1)\tilde{B}^{n+1}_m (\tilde{B}^n_m)^{-1}] - \kappa (\tilde{B}^n_m)^{s-1}[1 + (s-1)\tilde{B}^{n+1}_m (\tilde{B}^n_m)^{-1}]\}. \tag{3.113}$$

3.3.4 Implementation

Because of the symmetry property of the IVP (3.7)-(3.10) it is enough to treat only the region $\mathscr{R}$ where $x \ge 0$. This provides considerable savings in storage as well as in CPU time. This imposes the conditions

$$\frac{\partial \alpha(0,t)}{\partial x} = 0 \quad \text{and} \quad \frac{\partial \beta(0,t)}{\partial x} = 0, \quad t > 0 \tag{3.114}$$

on the new boundary $x = 0$. The space derivative $\dfrac{\partial \alpha}{\partial x}$ in (3.114) may be approximated by the second-order, central-difference approximant

$$\frac{\partial \alpha(x,t)}{\partial x} = \frac{1}{2h}\left[\alpha(x+h,t) - \alpha(x-h,t)\right] + O(h^2) \quad \text{as} \quad h \to 0 \tag{3.115}$$

with a similar replacement being made to $\dfrac{\partial \beta}{\partial x}$. These replacements reveal that, to second order,

$$A^n_{-1} = A^n_1 \quad \text{and} \quad B^n_{-1} = B^n_1 \quad \text{for all} \quad n = 0, 1, 2, \ldots. \tag{3.116}$$

Also note that the outer boundary conditions give

$$A^n_{N+1} = 1 \quad \text{and} \quad B^n_{N+1} = 0 \quad \text{for all} \quad n = 0, 1, 2, \ldots. \tag{3.117}$$

The number of mesh points to which each finite-difference scheme of the three families of numerical methods must be applied is reduced from $2N + 2$ to $N + 1$. It will be convenient to define $(N + 1)-$ vectors

$$\mathbf{A}^n = [A^n_0, A^n_1, \ldots, A^n_N]^T \quad \text{and} \quad \mathbf{B}^n = [B^n_0, B^n_1, \ldots, B^n_N]^T \tag{3.118}$$

where T denotes transpose. The modifications to the formulae of the three families of numerical methods, and their implications, are as follows.

Method $\mathscr{C}_1(\phi)$

Considering $m = 0$ in (3.85) and (3.86) and using (3.117) gives

$$(1 + 2\phi p)A^{n+1}_0 - 2\phi p A^{n+1}_1 = [1 - 2(1-\phi)p - \ell(B^n_0)^r]A^n_0 + 2(1-\phi)pA^n_1, \tag{3.119}$$

and

$$(1 + 2\phi p)B^{n+1}_0 - 2\phi p B^{n+1}_1 = \\ [1 - 2(1-\phi)p + \ell A^n_0 (B^n_0)^{r-1} - \kappa\ell(B^n_0)^{s-1}]B^n_0 + 2(1-\phi)pB^n_1. \tag{3.120}$$

The solution vectors $\mathbf{A}^{n+1}$ and $\mathbf{B}^{n+1}$ may be obtained using the following parallel algorithm:

$$\textbf{Processor 1}: \quad \text{solve} \quad E_1\mathbf{A}^{n+1} = F_1\mathbf{A}^n + \mathbf{q} \quad \text{for} \quad \mathbf{A}^{n+1}, \tag{3.121}$$

$$\textbf{Processor 2}: \quad \text{solve} \quad E_1\mathbf{B}^{n+1} = G_1\mathbf{B}^n \quad \text{for} \quad \mathbf{B}^{n+1}, \tag{3.122}$$

where E_1 is a constant, tridiagonal matrix of order $N+1$ given by

$$E_1 = \begin{bmatrix} 1+2\phi p & -2\phi p & 0 & \cdots & 0 \\ -\phi p & 1+2\phi p & -\phi p & & \vdots \\ 0 & \ddots & \ddots & \ddots & 0 \\ \vdots & & -\phi p & 1+2\phi p & -\phi p \\ 0 & \cdots & 0 & -\phi p & 1+2\phi p \end{bmatrix}$$

and $\mathbf{q} = [0, \ldots, 0, p]^T$ is a constant vector of order $N+1$. The matrices

$$F_1 = F_1(\mathbf{B}^n) = \begin{bmatrix} f_0 & 2(1-\phi)p & 0 & \cdots & 0 \\ (1-\phi)p & f_1 & (1-\phi)p & & \vdots \\ 0 & \ddots & \ddots & \ddots & 0 \\ \vdots & & (1-\phi)p & f_{N-1} & (1-\phi)p \\ 0 & \cdots & 0 & (1-\phi)p & f_N \end{bmatrix}$$

with $f_i = 1 - 2(1-\phi)p - \ell(B_i)^r$, $i = 0, 1, \ldots, N$, and

$$G_1 = G_1(\mathbf{A}^n) = \begin{bmatrix} g_0 & 2(1-\phi)p & 0 & \cdots & 0 \\ (1-\phi)p & g_1 & (1-\phi)p & & \vdots \\ 0 & \ddots & \ddots & \ddots & 0 \\ \vdots & & (1-\phi)p & g_{N-1} & (1-\phi)p \\ 0 & \cdots & 0 & (1-\phi)p & g_N \end{bmatrix}$$

with $g_i = 1-2(1-\phi)p+\ell A_i^n (B_i^n)^{r-1} - \kappa\ell (B_i^n)^{s-1}$, $i = 0, 1, \ldots, N$, are also tridiagonal matrices of order $N+1$.

Method $\mathscr{C}_2(\phi)$

Substituting $m = 0$ in (3.87) and (3.88) and using (3.117) gives

$$[1 + 2\phi p + \ell (B_0^n)^r] A_0^{n+1} - 2\phi p A_1^{n+1} = [1 - 2(1-\phi)p] A_0^n + 2(1-\phi)p A_1^n, \tag{3.123}$$

$$[1 + 2\phi p - \ell A_0^{n+1} (B_0^n)^{r-1} + \kappa\ell (B_0^n)^{s-1}] B_0^{n+1} - 2\phi p B_1^{n+1} = [1 - 2(1-\phi)p] B_0^n + 2(1-\phi)p B_1^n. \tag{3.124}$$

The solution vectors $\mathbf{A}^{n+1}$ and $\mathbf{B}^{n+1}$ may be obtained using the following sequential algorithm:

$$\text{Solve} \quad E_2 \mathbf{A}^{n+1} = F_2 \mathbf{A}^n + \mathbf{q} \quad \text{for} \quad \mathbf{A}^{n+1}, \tag{3.125}$$

$$\text{Solve} \quad H_2 \mathbf{B}^{n+1} = G_2 \mathbf{B}^n \quad \text{for} \quad \mathbf{B}^{n+1}, \tag{3.126}$$

where E_2 is a tridiagonal matrix of order $N+1$ given by

$$E_2 = \begin{bmatrix} e_0 & -2\phi p & \cdots & 0 & \\ -\phi p & e_1 & -\phi p & & \vdots \\ 0 & \ddots & \ddots & \ddots & 0 \\ \vdots & & -\phi p & e_{N-1} & -\phi p \\ 0 & \cdots & 0 & -\phi p & e_N \end{bmatrix}$$

with $e_i = 1 + 2\phi p + \ell (B_i^n)^r$, $i = 0, 1, \ldots, N$ and $\mathbf{q} = [0, \ldots, 0, p]^T$ is a constant vector of order $N+1$. The matrices F_2 and G_2 are constant tridiagonal matrices of order $N+1$ and have the forms

$$F_2 = \begin{bmatrix} 1-2(1-\phi)p & 2(1-\phi)p & 0 & \cdots & 0 \\ (1-\phi)p & 1-2(1-\phi)p & (1-\phi)p & & \vdots \\ 0 & \ddots & \ddots & \ddots & 0 \\ \vdots & & (1-\phi)p & 1-2(1-\phi)p & (1-\phi)p \\ 0 & \cdots & 0 & (1-\phi)p & 1-2(1-\phi)p \end{bmatrix}$$

and H_2

$$H_2 = \begin{bmatrix} h_0 & -2\phi p & 0 & \cdots & 0 \\ -\phi p & h_1 & -\phi p & & \vdots \\ 0 & \ddots & \ddots & \ddots & 0 \\ \vdots & & -\phi p & h_{N-1} & -\phi p \\ 0 & \cdots & 0 & -\phi p & h_N \end{bmatrix}$$

with $h_i = 1 + 2\phi p - \ell A_i^{n+1}(B_i^n)^{r-1} + \kappa\ell(B_i^n)^{s-1}$, $i = 0, 1, \ldots, N$, is also tridiagonal matrices of order $N + 1$.

Method $\mathscr{C}_3(\phi)$

Considering $m = 0$ in (3.89) and (3.90) and using (3.117) gives

$$[1 + 2\phi p + \ell(B_0^n)^r]A_0^{n+1} - 2\phi p A_1^{n+1} = [1 - 2(1-\phi)p]A_0^n + (1-\phi)pA_1^n, \tag{3.127}$$

$$[1 + 2\phi p - \ell A_0^n(B_0^n)^{r-1} + \kappa\ell(B_0^n)^{s-1}]B_0^{n+1} - \phi p B_1^{n+1} = [1 - 2(1-\phi)p]B_0^n + (1-\phi)pB_1^n. \tag{3.128}$$

The solution vectors $\mathbf{A}^{n+1}$ and $\mathbf{B}^{n+1}$ may be obtained using the following parallel algorithm:

$$\textbf{Processor 1}: \quad \text{solve} \quad E_3\mathbf{A}^{n+1} = F_3\mathbf{A}^n + \mathbf{q} \quad \text{for} \quad \mathbf{A}^{n+1}, \tag{3.129}$$

$$\textbf{Processor 2}: \quad \text{solve} \quad H_3\mathbf{B}^{n+1} = G_3\mathbf{B}^n \quad \text{for} \quad \mathbf{B}^{n+1}, \tag{3.130}$$

The matrices E_3 and E_2, G_3 and G_2, F_3 and F_2 are identical matrices. The matrix H_3 given by

$$H_3 = \begin{bmatrix} j_0 & -2\phi p & 0 & \cdots & 0 \\ -\phi p & j_1 & -\phi p & & \vdots \\ 0 & \ddots & \ddots & \ddots & 0 \\ \vdots & & -\phi p & j_{N-1} & -\phi p \\ 0 & \cdots & 0 & -\phi p & j_N \end{bmatrix}$$

with $j_i = 1 + 2\phi p - \ell A_i^n (B_i^n)^{r-1} + \kappa\ell (B_i^n)^{s-1}$, $i = 0, 1, \ldots, N$, is also a tridiagonal matrix of order $N + 1$.

3.3.5 Numerical experiments

The model of permanent form travelling waves which can develop from the initial-value problem (3.7)-(3.10) were studied. Numerical experiments were carried out to see the behaviour of the three suggested methods, *Method* $\mathscr{C}_1(\phi)$, *Method* $\mathscr{C}_2(\phi)$ and *Method* $\mathscr{C}_3(\phi)$, with $\phi = 0, \frac{1}{2}, 1$ and $h = \frac{1}{2}$ and with $\beta_0 = 1.0$ and for $\kappa = 0.9$. Here the numerical results are explained by considering Cases 1, 2 and 3. The stability intervals of the numerical methods are summarized in Tables 3.2, 3.3 and 3.4.

Case 1 : $r = s$

It was observed that a travelling wave was initiated in the reaction-diffusion system (3.7), (3.8) for $\kappa < 1$ with no restriction on $\beta_0 > 0$. These numerical results coincide with the result of Merkin *et al.* [42], [43], [44], [48].

In the case of *Method* $\mathscr{C}_1(\phi)$ travelling waves were observed for small values of ℓ, [see Table 3.2]. As ℓ was increased beyond the values in the stability interval (see §3.3.3) contrived oscillations were exhibited leading to overflow.

Using *Method* $\mathscr{C}_2(\phi)$ with $\phi = 0$ oscillations occurred for $\ell > 0.129$ with $r = s = 1$, for $\ell > 0.133$ with $r = s = 2$ and for $\ell > 0.14$ with $r = s = 3$ after which overflow occurred as ℓ was increased further. Using $\phi = \frac{1}{2}$ travelling waves were observed for $\ell \leq \ell_{\text{large}}$, ($\ell_{\text{large}} = 50.0$). As ℓ was increased further the numerical values of α slightly exceeded unity. Using $\phi = 1$ the qualitatively correct behaviour was observed for rather restricted time step values of ℓ, [see Table 3.3]. The method did not induce overflow.

In the case of *Method* $\mathscr{C}_3(\phi)$ similar results to those obtained using *Method* $\mathscr{C}_2(\phi)$ were observed. The only difference was *Method* $\mathscr{C}_3(\phi)$ needed more restricted time value of ℓ with $\phi = \frac{1}{2}$ for $r = s = 1$ compared to *Method* $\mathscr{C}_2(\phi)$, [see Table 3.4].

As an indication of the development of travelling reaction-diffusion waves, profiles of α and β are given at time $t = 100$ using *Method* $\mathscr{C}_2(\phi)$ ($\phi = \frac{1}{2}$) with $h = 0.5$ and

$\ell = 0.125$ in Fig. 3.3 for $\kappa = 0.1, 0.5, 0.9$. These clearly show the appearance of a reaction-diffusion wave with α increasing monotonically from $\alpha = \alpha_e$ at the rear $(x = 0)$ to $\alpha = 1$ at the front. Note that, as expected, α_e increases as κ is increased. The profile of β is seen to exhibit a pulse-like behaviour, with the maximum value of β decreasing considerably as κ increases. This is to be expected as the effect of increasing κ is to increase the relative strength of the decay step (3.6) and the reactant $\mathcal{B}$ is less able to maintain a high concentration.

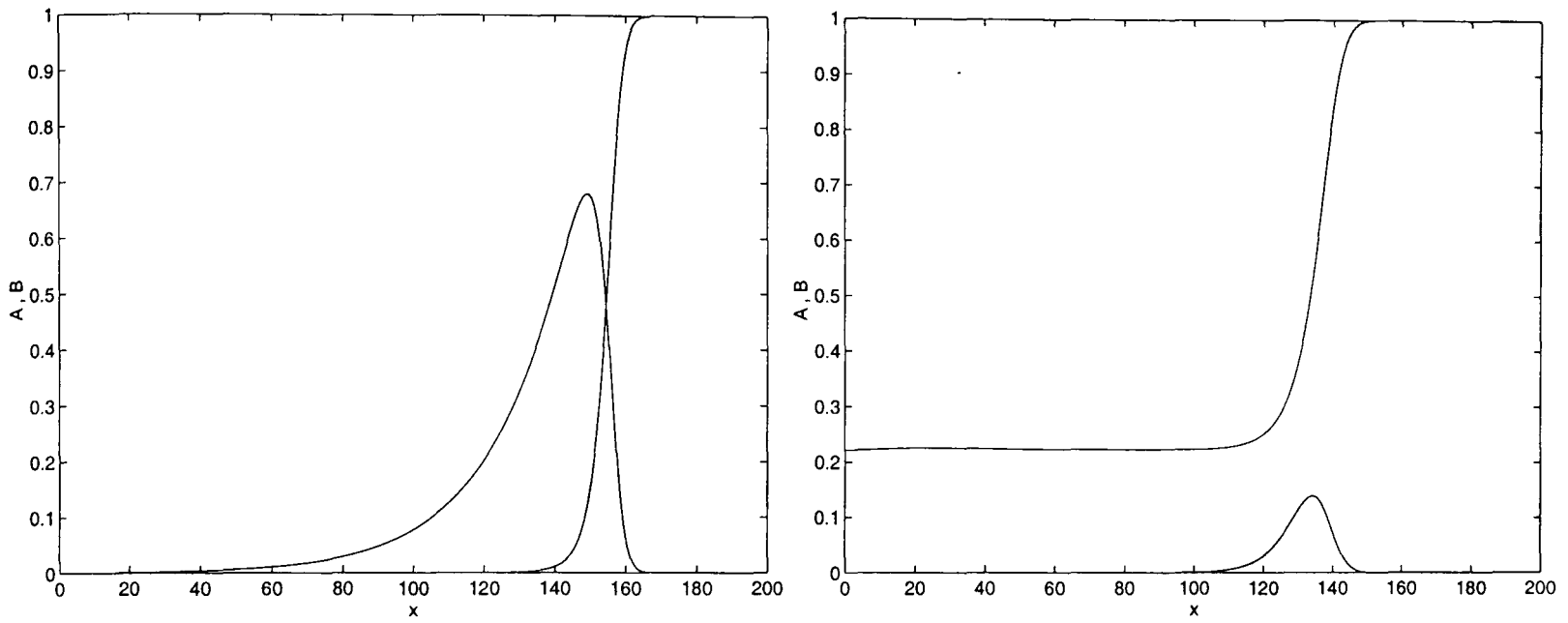

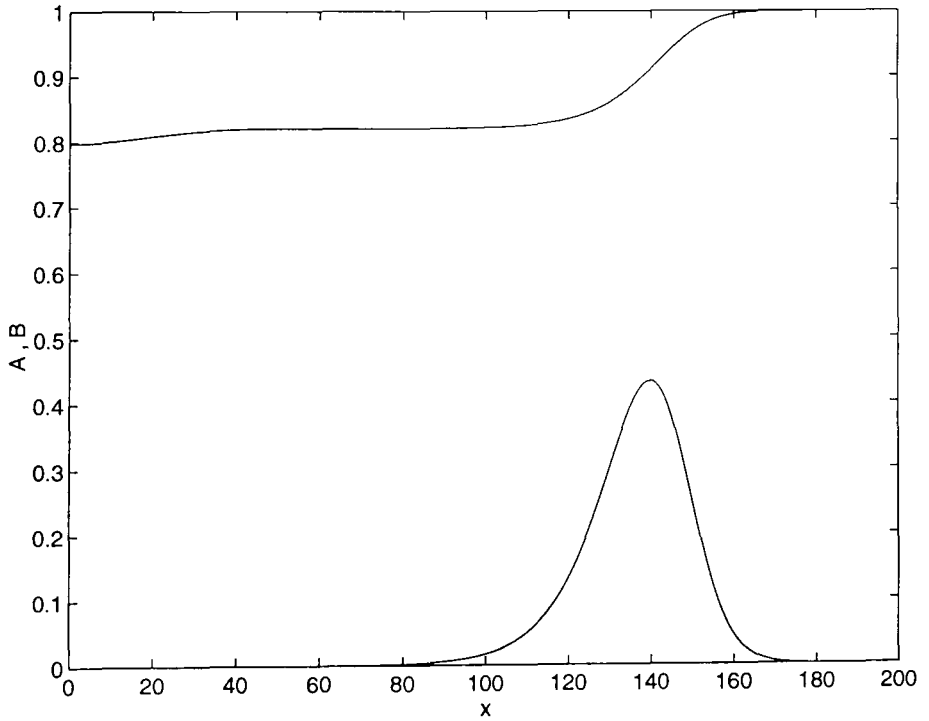

Figure 3.3: The solution profiles of α and β for the case of quadratic autocatalysis and linear decay for i) $\kappa = 0.1$, ii) $\kappa = 0.5$, iii) $\kappa = 0.9$.

Case 2 : $r < s$

In this case, $1 \leq r < s \leq 3$, it was observed that a reaction-diffusion travelling wave developed for all values of κ and for all values of $\beta_0 > 0$. The numerical results obtained are summarized for $\kappa = 0.9$ and $\beta_0 = 1.0$ in Tables 3.2, 3.3, 3.4.

Method $\mathscr{C}_1(\phi)$ produced travelling waves for small time step values of ℓ leading to overflow as ℓ was increased further.

Method $\mathscr{C}_2(\phi)$ and *Method* $\mathscr{C}_3(\phi)$ enjoyed superior stability properties especially for $\phi = \frac{1}{2}$ and $\phi = 1$ with a large time step $\ell \leq \ell_{\text{large}} = 50.0$.

The results are shown in Figs 3.4, 3.5 where the wave profiles, α, β, are given at time $t = 250$ using *Method* $\mathscr{C}_2(\phi)$ $(\phi = \frac{1}{2})$ with $h = 0.5$ and $\ell = 0.125$ for various values of $\kappa = 0.1, 1.0, 10.0$. These profiles show that the maximum value of β decreases as κ increases and that the wave form also becomes more spread out as κ increases, though it is worth noting that the sharp-front structure remains for all κ.

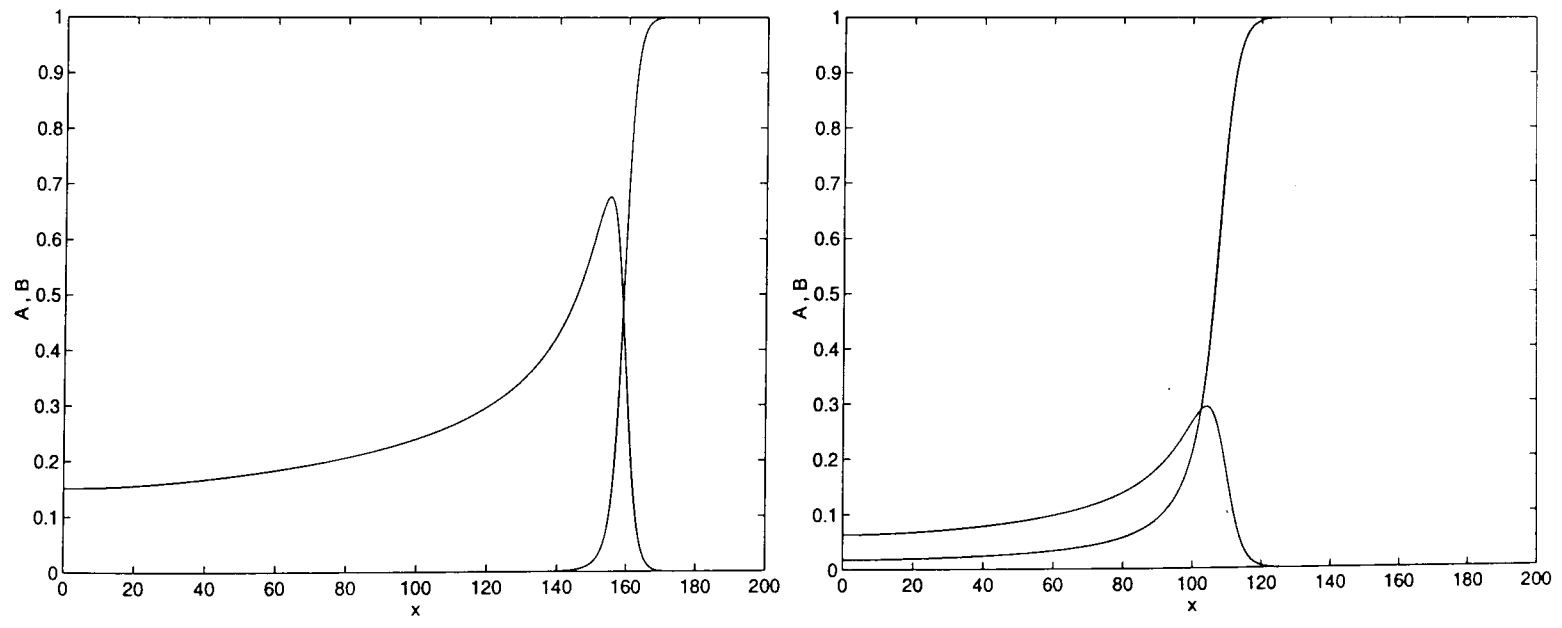

Figure 3.4: The solution profiles of α and β for the case of cubic autocatalysis and cubic decay for i) $\kappa = 0.1$, ii) $\kappa = 1.0$.

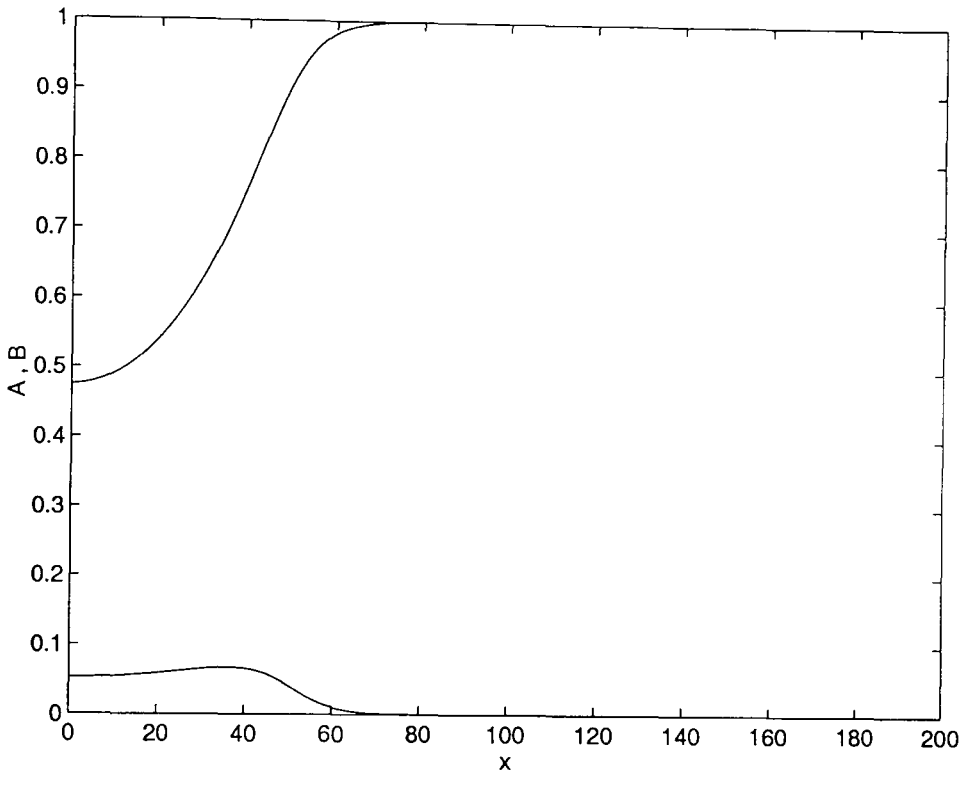

Figure 3.5: The solution profiles of α and β for the case of cubic autocatalysis and cubic decay for iii) $\kappa = 10.0$.

Case 3 : $r > s$

The numerical results confirmed that the travelling wave was not indicated in the reaction-diffusion problem (3.7), (3.8) unless $\beta_0 > \kappa^{\frac{1}{r-s}}$, irrespective of any additional condition on κ itself. The numerical solutions obtained are presented for $\kappa = 0.0465$ and $\beta_0 = 1.0$ in Tables 3.2, 3.3 and 3.4. It was observed that the behaviour of the numerical methods were very much consistent with the qualitative results for the reaction-diffusion system (see §3.2.1).

The numerical results are depicted in Fig. 3.6 where the wave profiles of α, β are given at time $t = 250$ using *Method* $\mathscr{C}_2(\phi)$ $(\phi = \frac{1}{2})$ with $h = 0.5$ and $\ell = 0.125$ for $\kappa = 0.02, 0.0465$. These profiles show that β quickly decays to zero everywhere (the rate of decay increases as κ increases) with α slowly (by diffusion) reverting back to its unreacted state.

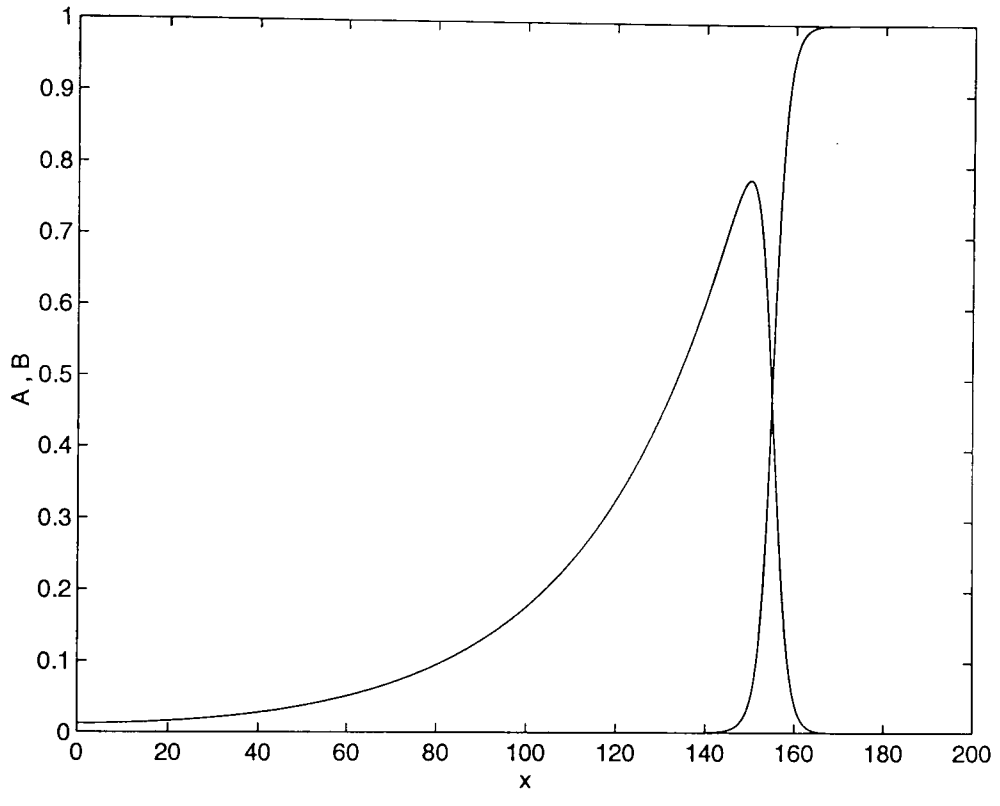

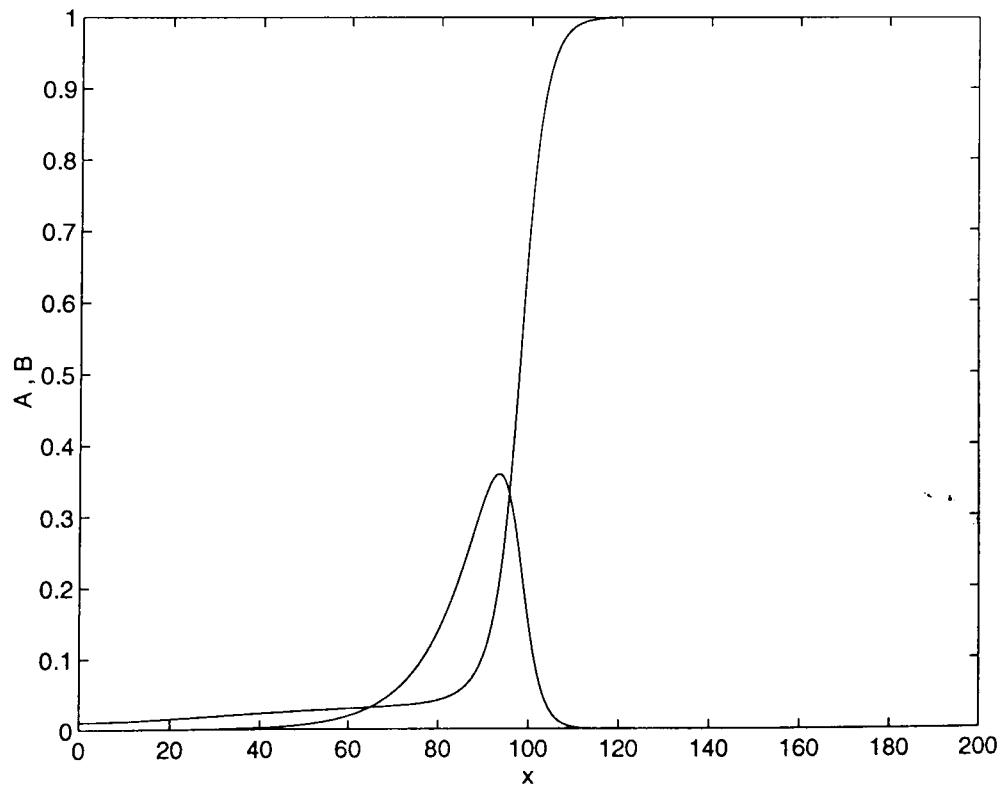

Figure 3.6: The solution profiles of α and β for the case of cubic autocatalysis and linear decay for i) $\kappa = 0.02$, ii) $\kappa = 0.0465$.

Specific Cases		Interval of Stability		
		Method $\mathscr{C}_1(\phi)$		
		$\phi = 0$	$\phi = \frac{1}{2}$	$\phi = 1$
$r = s$	$r = s = 1$	(0, 0.124)	(0, 2.0)	(0, 0.133)
	$r = s = 2$	(0, 0.124)	(0, 2.0)	(0, 0.117)
	$r = s = 3$	(0, 0.125)	(0, 2.0)	(0, 2.5)
$r < s$	$r = 1, s = 2$	(0, 1.6)	(0, 1.5)	(0, 1.8)
	$r = 2, s = 3$	(0, 0.9)	(0, 2.0)	(0, 2.5)
	$r = 1, s = 3$	(0, 0.9)	(0,2.0)	(0, 3.0)
$r > s$	$r = 2, s = 1$	(0, 0.113)	(0, 0.5)	(0, 2.0)
	$r = 3, s = 2$	(0, 0.117)	(0, 0.124)	(0, 1.5)
	$r = 3, s = 1$	(0, 0.119)	(0, 0.124)	(0, 0.49)

Table 3.2: Stability intervals of the numerical method, *Method* $\mathscr{C}_1(\phi)$.

Specific Cases		Interval of Stability		
		Method $\mathscr{C}_2(\phi)$		
		$\phi = 0$	$\phi = \frac{1}{2}$	$\phi = 1$
$r = s$	$r = s = 1$	(0, 0.129)	(0, ℓ_{large})	(0, 15.5)
	$r = s = 2$	(0, 0.133)	(0, ℓ_{large})	(0, ℓ_{large})
	$r = s = 3$	(0, 0.14)	(0, ℓ_{large})	(0, 10.0)
$r < s$	$r = 1, s = 2$	(0, 0.15)	(0, ℓ_{large})	(0, ℓ_{large})
	$r = 2, s = 3$	(0, 0.125)	(0, ℓ_{large})	(0, ℓ_{large})
	$r = 1, s = 3$	(0, 0.28)	(0,ℓ_{large})	(0, ℓ_{large})
$r > s$	$r = 2, s = 1$	(0, 0.133)	(0, ℓ_{large})	(0, ℓ_{large})
	$r = 3, s = 2$	(0, 0.135)	(0, ℓ_{large})	(0, ℓ_{large})
	$r = 3, s = 1$	(0, 0.134)	(0, ℓ_{large})	(0, ℓ_{large})

Table 3.3: Stability intervals of the numerical methods, *Method* $\mathscr{C}_2(\phi)$.

Specific Cases		Interval of Stability		
		Method $\mathscr{C}_3(\phi)$		
		$\phi = 0$	$\phi = \frac{1}{2}$	$\phi = 1$
$r = s$	$r = s = 1$	(0, 0.129)	(0, 4.0)	(0, ℓ_{large})
	$r = s = 2$	(0, 0.133)	(0, 10.0)	(0, ℓ_{large})
	$r = s = 3$	(0, 0.130)	(0, ℓ_{large})	(0, ℓ_{large})
$r < s$	$r = 1, s = 2$	(0, 0.15)	(0, ℓ_{large})	(0, ℓ_{large})
	$r = 2, s = 3$	(0, 0.117)	(0, ℓ_{large})	(0, ℓ_{large})
	$r = 1, s = 3$	(0, 0.133)	(0,ℓ_{large})	(0, ℓ_{large})
$r > s$	$r = 2, s = 1$	(0, 0.133)	(0, ℓ_{large})	(0, ℓ_{large})
	$r = 3, s = 2$	(0, 0.130)	(0, ℓ_{large})	(0, ℓ_{large})
	$r = 3, s = 1$	(0, 0.144)	(0, ℓ_{large})	(0, ℓ_{large})

Table 3.4: Stability intervals of the numerical methods, *Method* $\mathscr{C}_3(\phi)$.

3.4 Summary

Finite-difference schemes have been used to solve the reaction-diffusion system, (3.7)-(3.10), which models the possibility of travelling waves developing in the chemical system governed by general orders of autocatalysis and decay.

First- and second-order finite-difference approximations were developed to solve the well-stirred analogue to gain insight the reaction-diffusion system. The alternative explicit finite-difference schemes for the ordinary differential equations were easy to program and instability was easy to recognize. The other advantage of those explicit methods were they were regular methods, that is they do not produce spurious solutions. They also enjoy superior stability properties enabling a large time step ℓ to be used while still converging to qualitatively correct fixed points, unlike the Euler method which diverges for large values of ℓ. The second-order method attained a higher-order accuracy whilst maintaining good stability properties.

A family of numerical methods have been proposed, analysed, implemented and used to integrate the system, (3.7)-(3.10). One of these families of numerical methods is implemented sequentially whereas the others may be implemented on a parallel architecture using two processors. Two of the methods, (*Method* $\mathscr{C}_2(\phi)$, *Method* $\mathscr{C}_3(\phi)$), performed well being more economic and reliable with comparison to *Method* $\mathscr{C}_1(\phi)$.

The study also indicates that the well-stirred analogue was not sufficient to account accurately for the final outcome of the system. Therefore, one needs to consider the effect of diffusion on the results compared to the well-stirred system.

Chapter 4

Uncoupled Pooled Chemical Reaction

4.1 Introduction

In this chapter, which is a precursor to Chapter 5, the prototype chemical reaction scheme based upon the cubic autocatalator is

$$\text{precursor decay} \qquad \mathcal{P} \longrightarrow \mathcal{A} \qquad \text{rate} = k_0 p, \tag{4.1}$$

$$\text{autocatalysis} \qquad \mathcal{A} + 2\mathcal{B} \longrightarrow 3\mathcal{B} \qquad \text{rate} = k_1 a b^2, \tag{4.2}$$

$$\text{catalyst decay} \qquad \mathcal{B} \longrightarrow C \qquad \text{rate} = k_2 b. \tag{4.3}$$

The reaction takes place within a closed system, with the first intermediate $\mathcal{A}$ formed *via* the slow decay of a reactant or precursor species $\mathcal{P}$, initially in large excess. The reactant $\mathcal{A}$ is converted to $\mathcal{B}$ *via* a step in which $\mathcal{B}$ acts as its own catalyst. Then the autocatalyst $\mathcal{B}$ decays to a stable product $\mathcal{C}$. The reaction is called Pooled Chemical Reaction since the early period of the reaction is modelled with the precursor concentration assumed constant and set equal to its initial value (p_0) throughout.

Some previous works on models equivalent to reactions (4.1)-(4.3) have studied

the pool chemical, starting with Sel'kov [61], and by Tyson [68], Tyson and Kauffman [69] and Ashkenazi and Othmer [3]. Sel'kov derived from (4.1)-(4.3) a scheme of enzyme reactions proposed to account for the self-sustaining oscillations in glycolysis. Tyson and Kauffman [69] studied the scheme as a model of cell division or mitosis, with reaction taking place in two compartments coupled by diffusion through a semi-permeable membrane. Since autocatalytic rate-laws are also closely associated with almost all oscillatory reactions, this model is also important as the simplest "canonical form" for mechanistic interpretations of such behaviour. There are also many formal similarities with the extremely wide class of exothermic chemical reactions (Merkin and Needham [46]) where the reaction rate constants (k_1, etc.) show a strongly non-linear dependence on the (varying) temperature.

4.2 Mass-balance Equations and Dimensionless Groups

The mass-balance equations for the prototype pool chemical reaction scheme are

$$dp/d\bar{t} = -k_0 p, \tag{4.4}$$

$$da/d\bar{t} = k_0 p - k_1 a b^2, \tag{4.5}$$

$$db/d\bar{t} = k_1 a b^2 - k_2 b. \tag{4.6}$$

Two sets of dimensionless forms of these equations will be used. In the closed vessel situation, a_0 is interpreted as the initial concentration of species $\mathcal{A}$, that is, $a_0 = a(t = 0)$. In dimensionless form (4.4), (4.5) and (4.6) become

$$d\pi/d\tau = -\epsilon' \pi, \tag{4.7}$$

$$d\alpha/d\tau = \epsilon' \pi - \alpha\beta^2, \tag{4.8}$$

$$d\beta/d\tau = \alpha\beta^2 - \beta/\tau_2, \tag{4.9}$$

where

$$\alpha = a/a_0, \quad \beta = b/a_0, \quad \pi = p/a_0 \quad \text{and} \quad \tau = k_1 a_0^2 \bar{t}$$

$$\text{with} \quad \epsilon' = k_0/k_1 a_0^2 \quad \text{and} \quad \tau_2 = k_1 a_0^2/k_2.$$

Equations (4.7), (4.8) and (4.9) can be integrated to give

$$\pi = \pi_0 \exp\left(-\epsilon^{'} \tau\right), \tag{4.10}$$

where $\pi_0 = p_0/a_0$ in the dimensionless form for the initial concentration of $\mathcal{P}$. Two rate equations describing the evolution of the concentrations of $\mathcal{A}$ and $\mathcal{B}$ can be obtained in the form

$$d\alpha/d\tau = \epsilon^{'} \pi_0 e^{-\epsilon^{'} \tau} - \alpha\beta^2, \tag{4.11}$$

$$d\beta/d\tau = \alpha\beta^2 - \beta/\tau_2. \tag{4.12}$$

Since the initial concentration of $\mathcal{P}$ is very much larger than that of the reactant $\mathcal{A}$, π_0 may be very large compared with unity. At the same time the rate of the initiation step producing $\mathcal{A}$ from $\mathcal{P}$ will be slow on the chemical timescale t_{ch}. Thus $\epsilon^{'}$ will be small compared with unity. The product of the two terms,

$$\epsilon^{'} \pi_0 = \kappa \tag{4.13}$$

can be of order unity. So (4.11) and (4.12) can be written as

$$d\alpha/d\tau = \kappa e^{-\epsilon^{'} \tau} - \alpha\beta^2, \tag{4.14}$$

$$d\beta/d\tau = \alpha\beta^2 - \beta/\tau_2. \tag{4.15}$$

The initial conditions are

$$\alpha_{|\tau=0} = 1, \quad \beta_{|\tau=0} = \beta_0,$$

where

$$\beta_0 = b_0/a_0 \quad \text{is a constant.}$$

Making the transformations

$$x = \alpha\tau^{1/2}, \; y = \beta\tau_2^{1/2} \quad \text{and} \quad t = \tau/\tau_2, \tag{4.16}$$

where x and y are new dimensionless measures of the concentrations of $\mathcal{A}$ and $\mathcal{B}$, respectively, and t is a new dimensionless time $t = k_2\bar{t}$, equations (4.14) and (4.15) become

$$dx/dt = \mu e^{-\epsilon t} - xy^2, \tag{4.17}$$

$$dy/dt = xy^2 - y. \tag{4.18}$$

Here, $\mu = \kappa\tau_2^{3/2}$ is of order unity and $\epsilon = \tau_2\epsilon' = k_0/k_2$ is a small quantity, $\epsilon \leq 1$. Then the pool chemical reaction forms can be obtained by considering the limit in which ϵ' or ϵ become zero. This gives the dimensionless form of the pool chemical reaction equations to be

$$dx/dt = \mu - xy^2, \tag{4.19}$$

$$dy/dt = xy^2 - y. \tag{4.20}$$

4.3 Phase-plane Analysis

The qualitative character of the reaction kinetics (ODEs) can give some general results for ODEs before trying to solve them numerically Stuart and Humphries [65]. A geometrical device, the phase plane, is used for obtaining directly from the differential equation such properties as equilibrium, periodicity, stability, bifurcation and so on. The constant solutions are represented by equilibrium points obtained by solving the equations

$$\frac{dx}{dt} = \frac{dy}{dt} = 0$$

and near these points a linear approximation is applied to (4.19)-(4.20), and the local characters of the paths are determined. Such considerations are starting-points for global investigations of the solutions. Let the two species x and y satisfy reaction kinetics given by

$$dx/dt = f(x,y) \quad , \quad dy/dt = g(x,y), \tag{4.21}$$

where

$$f(x,y) = \mu - xy^2, \tag{4.22}$$

$$g(x,y) = xy^2 - y. \tag{4.23}$$

Steady-state solutions (x_{ss}, y_{ss}) of (4.21) are given by

$$f(x,y) = g(x,y) = 0,$$

of which only the positive solutions are of interest. For the simple pooled chemical reaction scheme (4.19) and (4.20)

$$(x_{ss}, y_{ss}) = (\frac{1}{\mu}, \mu) \tag{4.24}$$

is the only equilibrium point. Local stability is determined by considering the Jacobian, J, of the pair of equations (4.22) and (4.23). This is defined as

$$J = \begin{bmatrix} \partial f/\partial x & \partial f/\partial y \\ \partial g/\partial x & \partial g/\partial y \end{bmatrix}$$

and for (4.22) and (4.23)

$$J = \begin{bmatrix} -y^2 & -2xy \\ y^2 & 2xy - 1 \end{bmatrix}.$$

At the steady state J becomes

$$J = \begin{bmatrix} -\mu^2 & -2 \\ \mu^2 & 1 \end{bmatrix}.$$

The eigenvalues λ_1 and λ_2 of J are given by the roots of the quadratic equation

$$\lambda^2 - tr(J)\lambda + det(J) = 0$$

where $tr(J)$ is the trace of the Jacobian

$$tr(J) = (\partial f/\partial x)_{ss} + (\partial g/\partial y)_{ss}$$

and

$$det(J) = (\partial f/\partial x)_{ss}(\partial g/\partial y)_{ss} - (\partial f/\partial y)_{ss}(\partial g/\partial x)_{ss}.$$

Then the eigenvalues of J are obtained as

$$\lambda_{1,2} = \frac{1}{2}[tr(J) \pm [tr(J)^2 - 4det(J)]^{1/2}].$$

For the governing equations (4.22) and (4.23), evaluated using the stationary-state results, the eigenvalues become

$$\lambda_{1,2} = \frac{1}{2}[(1-\mu^2) \pm \left(1-5\mu^2\right)^{\frac{1}{2}}]. \tag{4.25}$$

Necessary and sufficient conditions for stability are

$$trJ = f_x + g_x < 0,\ |J| = f_x g_y - f_y g_x > 0$$

where the derivatives $f_x \equiv \partial f/\partial x, f_y \equiv \partial f/\partial y, g_x \equiv \partial g/\partial x, g_y \equiv \partial g/\partial y$ are evaluated at the steady-state (x_{ss}, y_{ss}) . The local stability and character properties of the steady-state solutions in terms of parametric values and the eigenvalues of the Jacobian are summarized in Table 4.1.

Table 4.1: Classification of local stability and character of stationary-state solutions.

$0 < \mu < 1$	UNSTABLE	$0 < \mu < \sqrt{2}-1$	Unstable Node	$\lambda \in \mathbb{R}(> 0)$
		$\sqrt{2}-1 < \mu < 1$	Unstable Spiral	$\lambda \in \mathbb{C},\ \Re(\lambda) > 0$
$\mu > 1$	STABLE	$1 < \mu < \sqrt{2}+1$	Stable Spiral	$\lambda \in \mathbb{C},\ \Re(\lambda) < 0$
		$\mu > \sqrt{2}+1$	Stable Node	$\lambda \in \mathbb{R}(> 0)$
$\mu = 1$	Hopf Bifurcation			$\lambda \in \mathbb{C}, \Re(\lambda) = 0$

4.4 Hopf Bifurcation Analysis and Oscillatory Behaviour

As may be observed from §4.3, when the trace of the Jacobian changes sign, the eigenvalues become imaginary. The change of the stationary state from an unstable to a stable focus associated with the condition

$$tr(J) = 0 \quad , \quad det(J) > 0$$

is characteristic of *Hopf bifurcation* phenomenon, Marsden and McCracken [35]. There are two important qualitative features that may arise at this point. One feature is a stable limit cycle which may emerge in the phase-plane and grow in size as the residence time, τ_{res}, increases beyond τ^*_{res} . This is known as a *supercritical* Hopf bifurcation. Alternatively, an unstable cycle may appear around the stable focus, growing in size as the residence time decreases. This bifurcation is termed *subcritical.* It is now shown formally that a Hopf bifurcation occurs in system (4.19)-(4.20). The eigenvalues $\lambda_{1,2}$ of the steady-state solution of (4.21) are determined. At $\mu = \mu^* = 1$ the eigenvalues are pure imaginary. Hence, in some open interval surrounding μ^*, the eigenvalues form a complex conjugate pair and can be written as

$$\lambda_1 = r(\mu) + i\Omega(\mu) \quad , \quad \lambda_2 = r(\mu) - i\Omega(\mu)$$

where

$$r(\mu) = \Re(\lambda_1(\mu)) = \Re(\lambda_2(\mu)),\ \Omega(\mu) = \Im(\lambda_1(\mu)) = -\Im(\lambda_2(\mu)).$$

It is readily seen that

$$r(\mu^*) = 0, \quad \Omega(\mu^*) \neq 0, \quad (dr/d\mu)(\mu^*) \neq 0.$$

Thus all the criteria of the Hopf bifurcation theorem are satisfied and it may be concluded that a limit cycle bifurcates out of the steady-state singularity (x_{ss}, y_{ss}) at the critical value $\mu = \mu^*$. To examine the stability of the limit cycle and decide which type of bifurcation occurs at the Hopf bifurcation point, equations (4.19) and (4.20) must first be written in the required canonical form. Then, following Gray and Scott [15], the *Floquet multiplier* should be calculated to determine the nature of the bifurcation. If this multiplier is negative the limit cycle will be stable and should correspond to observable oscillations; if it is positive the limit cycle will be unstable. From the Hopf bifurcation theorem and the stability calculation for the limit cycle, the bifurcation can be seen to be supercritical, creating a unique stable limit cycle surrounding the steady-state point (x_{ss}, y_{ss}) for $\mu < 1$, Merkin *et al.* [47]. As $\mu \to \mu^*$, the diameter of the closed orbit varies with $|\mu - 1|^{\frac{1}{2}}$ with period 2π. The

size and period of the oscillations, or of the corresponding limit cycle, varies with the dimensionless reactant concentration μ. Close to the Hopf bifurcation point the growth can be determined analytically but in general numerical computations should be applied.

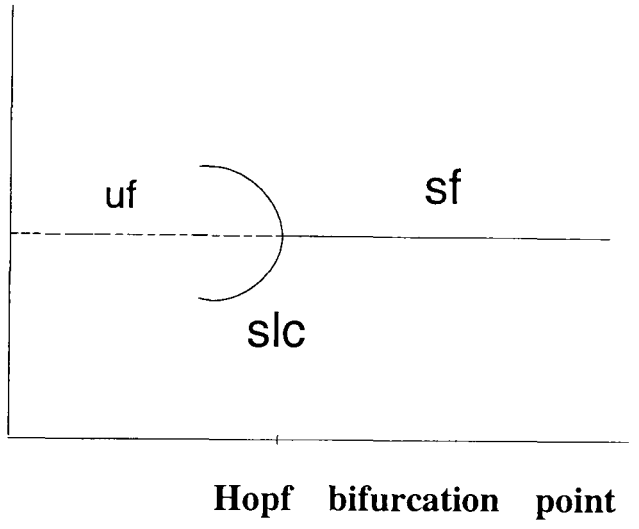

Figure 4.1: The development of the limit cycle at the Hopf bifurcation point **sf** represents stable focus, **uf** represents unstable focus, **slc** represents stable limit cycle. The x- axis presents μ values.

Figure 4.1 can be explained as follows. The straight line represent the locus of the steady-state solution; a solid line indicates stability, a broken line represents an unstable solution. Here $d(tr(J))/d\mu < 0$ and the Floquet multiplier is also negative; therefore the steady state loses stability as μ is decreased below μ^* and a stable limit cycle emerges in the same direction. The loss of local stability which occurs for a steady-state solution, as the real part of the eigenvalues changes from negative to positive, is closely linked to the conditions under which periodic oscillatory responses are born. The chemical system corresponding to the ODEs will therefore exhibit the onset of sustained oscillatory reaction as the residence time is increased through its critical value μ^*. According to the Hopf bifurcation theorem in Chapter 2, on page 15 which guarantees that as the parameter μ is varied through μ_1 and μ_2 a non-stationary or periodic state emerges; this periodic solution will exist over

some non-zero range of experimental conditions. These periodic solutions appear as sustained oscillations in the concentrations $x(t)$ and $y(t)$ and as closed loops or limit cycles in the xy- plane. The dependence of the amplitude of these oscillations in $x(A_x)$ on μ_0 can be observed in Fig 4.2.

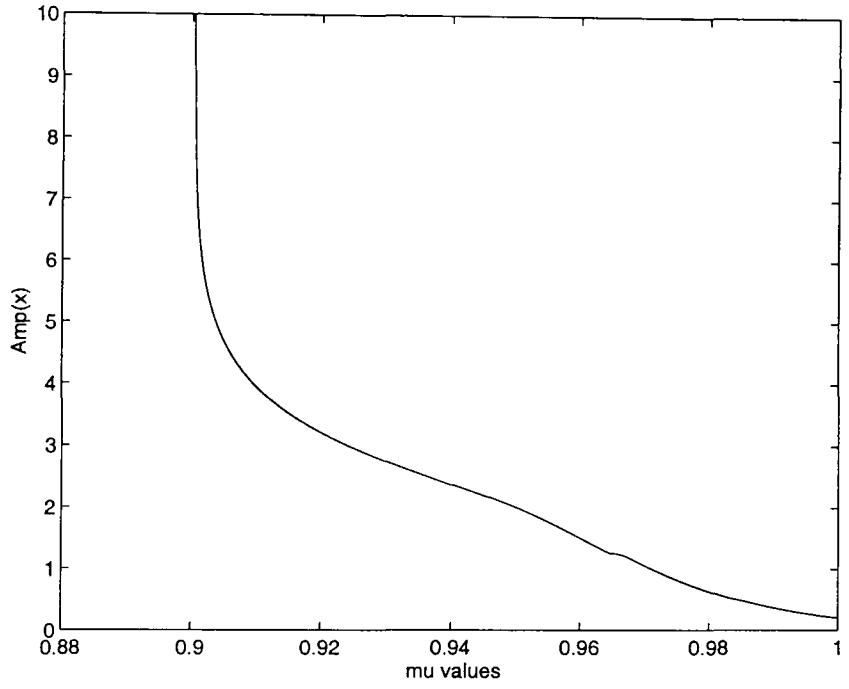

Figure 4.2: The amplitude A_x calculated from the numerical solution.

4.5 Numerical Methods

4.5.1 First-order numerical methods

The initial-value problem to be solved is given by

$$\frac{dx}{dt} = \mu - xy^2, \ t > 0 \tag{4.26}$$

$$\frac{dy}{dt} = xy^2 - y, \ t > 0 \tag{4.27}$$

with the given initial conditions

$$x \geq 0, \ y \geq 0, \ x(0) = 1, \ y(0) = y_0 \ \ at \ \ t = 0 \tag{4.28}$$

and $\mu = (k_1/k_2)^{1/2} k_0 p_0/k_2$ is a non-negative constant. First-order numerical methods are developed to solve ODEs (4.26)-(4.27) in the same way as in Chapter 3. The

theoretical solution of the system (4.26) and (4.27) at the point $t = t_n$ is denoted by $x(t_n)$ and $y(t_n)$ while the solution of an approximating numerical method will be denoted by X_n, Y_n at the same point t_n, where X and Y denote approximations to x and y respectively. Approximating the derivatives $dx(t)/dt$ and $dy(t)/dt$ by the first-order replacements (forward-difference approximants) at $t = t_n$ and evaluating x and y at the same base time level gives Method I (Euler)

$$X_{n+1} = (1 - \ell Y_n^2)X_n + \ell\mu \; ; \quad n = 0, 1, 2, \ldots \tag{4.29}$$

$$Y_{n+1} = Y_n + \ell(X_n Y_n - 1)Y_n \; ; \quad n = 0, 1, 2, \ldots \tag{4.30}$$

with $X_0 = x_0$ and $Y_0 = y_0$. The local truncation errors, LTEs, associated with (4.29) and (4.30) are given by

$$\begin{aligned} \mathscr{L}1_x[x(t), y(t); \ell] &= x(t+\ell) - x(t) - \ell\left(\mu - x(t)[y(t)]^2\right) \\ &= \frac{1}{2}\ell^2 x''(t) + O(\ell^3) \quad \text{as} \quad \ell \to 0, \end{aligned} \tag{4.31}$$

$$\begin{aligned} \mathscr{L}1_y[x(t), y(t); \ell] &= y(t+\ell) - y(t) - \ell\left(x(t)[y(t)]^2 - y(t)\right) \\ &= \frac{1}{2}\ell^2 y''(t) + O(\ell^3) \quad \text{as} \quad \ell \to 0. \end{aligned} \tag{4.32}$$

Replacing the derivatives in the ODEs (4.26) and (4.27) by the first-order approximations and evaluating the variables on the right-hand sides functions at time $t = t_n$ and $t = t_{n+1}$ leads to the implicit formulae

$$(X_{n+1} - X_n)/\ell = \mu - X_{n+1}Y_n^2, \tag{4.33}$$

$$(Y_{n+1} - Y_n)/\ell = X_{n+1}Y_nY_{n+1} - Y_{n+1}. \tag{4.34}$$

These can be rearranged to give Method II in explicit form,

$$X_{n+1} = (X_n + \ell\mu)/(1 + \ell Y_n^2); \quad n = 0, 1, 2, \ldots, \tag{4.35}$$

$$Y_{n+1} = Y_n/[1 - \ell(X_{n+1}Y_n - 1)]; \quad n = 0, 1, 2, \ldots \tag{4.36}$$

where $X_0 = x_0$ and $Y_0 = y_0$. The LTEs associated with Method II are obtained from (4.33) and (4.34) and are given by

$$\begin{aligned}\mathscr{L}2_x[x(t), y(t); \ell] &= x(t+\ell) - x(t) - \ell\left(\mu - x(t+\ell)[y(t)]^2\right) \\ &= (\frac{1}{2}x'' + x'y^2)\ell^2 + O(\ell^3) \quad \text{as} \quad \ell \to 0, \end{aligned} \tag{4.37}$$

$$\begin{aligned}\mathscr{L}2_y[x(t), y(t); \ell] &= y(t+\ell) - y(t) - \ell\left(x(t+\ell)y(t+\ell)y(t) - y(t+\ell)\right) \\ &= (\frac{1}{2}y'' - xyy' - x'y^2 + y')\ell^2 + O(\ell^3) \quad \text{as} \quad \ell \to 0. \end{aligned} \tag{4.38}$$

The numerical method, Method III can be developed by using the forward-difference approximants for the derivatives in the ODEs (4.26) and (4.27) as before and evaluating the variables on the RHS of (4.26) and (4.27) at time $t = t_n$ and $t = t_{n+1}$. Then the second pair of implicit formulae

$$(X_{n+1} - X_n)/\ell = \mu - X_{n+1}Y_n^2, \tag{4.39}$$

$$(Y_{n+1} - Y_n)/\ell = X_nY_n^2 - Y_{n+1} \tag{4.40}$$

are obtained. Method III can be implemented explicitly after rearranging (4.39) and (4.40) in the form

$$X_{n+1} = (X_n + \ell\mu)/(1 + \ell Y_n^2); \quad n = 0, 1, 2, \ldots, \tag{4.41}$$

$$Y_{n+1} = Y_n(1 + \ell X_nY_n)/(1 + \ell); \quad n = 0, 1, 2, \ldots. \tag{4.42}$$

The LTEs associated with Method III are obtained from (4.39) and (4.40) and are given by

$$\begin{aligned}\mathscr{L}3_x[x(t), y(t); \ell] &= x(t+\ell) - x(t) - \ell\left(\mu - x(t+\ell)[y(t)]^2\right) \\ &= (\frac{1}{2}x'' + x'y^2)\ell^2 + O(\ell^3) \quad \text{as} \quad \ell \to 0 \end{aligned} \tag{4.43}$$

$$\begin{aligned}\mathscr{L}3_y[x(t), y(t); \ell] &= y(t+\ell) - y(t) - \ell\left(x(t)[y(t)]^2 - y(t+\ell)\right) \\ &= (\frac{1}{2}y'' + y')\ell^2 + O(\ell^3) \quad \text{as} \quad \ell \to 0. \end{aligned} \tag{4.44}$$

The expressions {(4.31),(4.32)}, {(4.37),(4.38)} and {(4.43),(4.44)} show that all numerical methods Method I, Method II and Method III are first order.

4.5.2 Second-order methods

Second-order explicit methods can be developed for the numerical solution of the IVP

$$x' = \mu - xy^2, \tag{4.45}$$

$$y' = xy^2 - y. \tag{4.46}$$

These ODEs can be written as

$$x' - \mu + xy^2 = 0, \tag{4.47}$$

$$y' - xy^2 + y = 0 \tag{4.48}$$

and, differentiating with respect to t gives

$$x'' + x'y^2 + 2xyy' = 0, \tag{4.49}$$

$$y'' - x'y^2 - 2xyy' + y' = 0. \tag{4.50}$$

The second-order method is based on a linear combination of first-order numerical methods, some of which were mentioned in the previous section, and also on additional first-order methods which will be introduced. Even though the given ODE system in (4.26) and (4.27) is non-linear, it is possible to find their numerical solutions by solving a linear algebraic system at each time step.

Second-order method for X_{n+1}

The first-order methods previously discussed are given below along with the new first-order methods, named M_x^1, M_x^2 and M_x^3, and their associated LTEs, $\mathscr{L}1_x, \mathscr{L}2_x$ and $\mathscr{L}3_x$,

$$M_x^1 : (X_{n+1} - X_n)/\ell = \mu - X_{n+1}Y_n^2, \tag{4.51}$$

$$\mathscr{L}1_x[x(t), y(t); \ell] = (\frac{1}{2}x'' + x'y^2)\ell^2 + O(\ell^3) \quad \text{as} \quad \ell \to 0, \tag{4.52}$$

$$M_x^2 : (X_{n+1} - X_n)/\ell = \mu - X_nY_{n+1}Y_n, \tag{4.53}$$

$$\mathscr{L}2_x[x(t), y(t); \ell] = (\frac{1}{2}x'' + xyy')\ell^2 + O(\ell^3) \quad \text{as} \quad \ell \to 0, \tag{4.54}$$

$$M_x^3 : (X_{n+1} - X_n)/\ell = \mu - X_n Y_n^2, \tag{4.55}$$

$$\mathscr{L}3_x[x(t), y(t); \ell] = \frac{1}{2}x''\ell^2 + O(\ell^3) \quad \text{as} \quad \ell \to 0. \tag{4.56}$$

It follows from (4.52), (4.54) and (4.56) that $\mathscr{L}\mathcal{E}_x$ defined by

$$\mathscr{L}\mathcal{E}_x = \mathscr{L}1_x + 2\mathscr{L}2_x - \mathscr{L}3_x$$

gives

$$\mathscr{L}\mathcal{E}_x = (x'' + x'y^2 + 2xyy')\ell^2 + O(\ell^3), \quad \text{as} \quad \ell \to 0.$$

It follows from (4.49) that

$$\mathscr{L}\mathcal{E}_x = O(\ell^3) \quad \text{as} \quad \ell \to 0. \tag{4.57}$$

Then the second-order method for X_{n+1} can be seen to be

$$(2 + \ell Y_n^2)X_{n+1} + 2\ell X_n Y_n Y_{n+1} = 2\ell\mu + (2 + \ell Y_n^2)X_n. \tag{4.58}$$

Second-order method for Y_{n+1}

A similar procedure to that in developing second-order method for X_{n+1} can be applied to construct a second-order method for Y_{n+1} . The suitable first-order approximations, named M_y^1, M_y^2, M_y^3 and M_y^4, to the ODEs (4.26) and (4.27) with their LTEs, $\mathscr{L}1_y, \mathscr{L}2_y, \mathscr{L}3_y$ and $\mathscr{L}4_y$, can be given by

$$M_y^1 : (Y_{n+1} - Y_n)/\ell = X_{n+1}Y_nY_{n+1} - Y_n, \tag{4.59}$$

$$\mathscr{L}1_y[x(t), y(t); \ell] = (\frac{1}{2}y'' - x'y^2)\ell^2 + O(\ell^3) \quad \text{as} \quad \ell \to 0, \tag{4.60}$$

$$M_y^2 : (Y_{n+1} - Y_n)/\ell = X_nY_nY_{n+1} - Y_n, \tag{4.61}$$

$$\mathscr{L}2_y[x(t), y(t); \ell] = (\frac{1}{2}y'' - xyy')\ell^2 + O(\ell^3) \quad \text{as} \quad \ell \to 0, \tag{4.62}$$

$$M_y^3 : (Y_{n+1} - Y_n)/\ell = X_nY_nY_{n+1} - Y_{n+1}, \tag{4.63}$$

$$\mathscr{L}3_y[x(t), y(t); \ell] = (\frac{1}{2}y'' - xyy' + y')\ell^2 + O(\ell^3) \quad \text{as} \quad \ell \to 0. \tag{4.64}$$

$$M_y^4 : (Y_{n+1} - Y_n)/\ell = X_n Y_n^2 - Y_n, \tag{4.65}$$

$$\mathscr{L}4_y[x(t), y(t); \ell] = \frac{1}{2} y''\ell^2 + O(\ell^3) \quad \text{as} \quad \ell \to 0. \tag{4.66}$$

It can be easily seen from (4.60), (4.62), (4.64) and (4.66) that, defining a quantity $\mathscr{L}\mathcal{E}_y$ by

$$\mathscr{L}\mathcal{E}_y = \mathscr{L}1_y + \mathscr{L}2_y + \mathscr{L}3_y - \mathscr{L}4_y$$

gives

$$\mathscr{L}\mathcal{E}_y = (y'' - x'y^2 - 2xyy' + y')\ell^2 + O(\ell^3) \quad \text{as} \quad \ell \to 0$$

and, using (4.50) it follows that

$$\mathscr{L}\mathcal{E}_y = O(\ell^3) \quad \text{as} \quad \ell \to 0. \tag{4.67}$$

It is then possible to obtain a second-order method for Y_{n+1} which has the form

$$-\ell Y_n^2 X_{n+1} + (2 - 2\ell X_n Y_n + \ell) Y_{n+1} = -\ell X_n Y_n^2 + (2 - \ell) Y_n. \tag{4.68}$$

Solving the linear algebraic system (4.58) and (4.68) simultaneously for X_{n+1} and Y_{n+1} gives

$$X_{n+1} = \frac{(2+\ell)[2\ell\mu + X_n(2 + \ell Y_n^2)] - 2\ell(2-\ell)X_n Y_n^2 - 4\ell X_n Y_n (X_n + \ell\mu)}{(2+\ell)(2+\ell Y_n^2) - 4\ell X_n Y_n} \tag{4.69}$$

$$Y_{n+1} = \frac{2\ell\mu Y_n^2 + (2 + \ell Y_n^2)(2-\ell)Y_n}{(2+\ell)(2+\ell Y_n^2) - 4\ell X_n Y_n} \tag{4.70}$$

in which $n = 0, 1, 2, \ldots$.

4.5.3 Stability analysis of numerical methods

All the first- and second-order numerical methods which were mentioned in §4.5.1 and §4.5.2 have the same fixed point and stability properties as the ODEs (4.26) and (4.27). The fixed points of the numerical methods can be found by noting that they are one-point iteration functions of the forms

$$X_{n+1} = g_1(X_n, Y_n); \quad n = 0, 1, 2, \ldots \tag{4.71}$$

$$Y_{n+1} = g_2(X_n, Y_n); \quad n = 0, 1, 2, \ldots \tag{4.72}$$

and by considering the associated functions

$$X = g_1(X, Y) \text{ and } Y = g_2(X, Y),$$

where, for Method I

$$g_1(X, Y) = (1 - \ell Y^2)X + \ell\mu, \tag{4.73}$$

$$g_2(X, Y) = [1 + \ell(XY - 1)]Y, \tag{4.74}$$

for Method II

$$g_1(X, Y) = (X + \ell\mu)/(1 + \ell Y^2), \tag{4.75}$$

$$g_2(X, Y) = Y(1 + \ell Y^2)/(1 + \ell)(1 + \ell Y^2) - \ell Y(X + \ell\mu), \tag{4.76}$$

for Method III

$$g_1(X, Y) = (X + \ell\mu)/(1 + \ell Y^2), \tag{4.77}$$

$$g_2(X, Y) = Y(1 + \ell XY)/(1 + \ell), \tag{4.78}$$

and for the second-order method

$$g_1(X, Y) = \frac{(2 + \ell)[2\ell\mu + X(2 + \ell Y^2)] - 2\ell(2 - \ell)XY^2 - 4\ell XY(X + \ell\mu)}{(2 + \ell)(2 + \ell Y^2) - 4\ell XY} \tag{4.79}$$

$$g_2(X, Y) = \frac{2\ell\mu Y^2 + (2 + \ell Y^2)(2 - \ell)Y}{(2 + \ell)(2 + \ell Y^2) - 4\ell XY}. \tag{4.80}$$

It can be easily seen that $(x_{ss}, y_{ss}) = (\frac{1}{\mu}, \mu)$ is the only fixed point of all the numerical methods. The stability of this fixed point can be determined by analysing the eigenvalues of the matrix (Sandefur [59])

$$J = \begin{bmatrix} \partial g_1/\partial X & \partial g_1/\partial Y \\ \partial g_2/\partial X & \partial g_2/\partial Y \end{bmatrix}$$

at (x_{ss}, y_{ss}) for each method.

The Jacobian for Method I (Euler) is

$$J_{MI} = \begin{bmatrix} 1 - \ell Y^2 & -2\ell XY \\ \ell Y^2 & 1 + \ell \end{bmatrix}$$

which at $(x_{ss}, y_{ss}) = (\frac{1}{\mu}, \mu)$ becomes

$$J_{MI} = \begin{bmatrix} 1 - \ell\mu^2 & -2\ell \\ \ell\mu^2 & 1 + \ell \end{bmatrix}$$

The characteristic equation $\Phi_{MI}(\lambda)$ can be written in a simple form as

$$\Phi_{MI}(\lambda) \equiv \lambda^2 + \lambda[-2 + \ell(-1 + \mu^2)] + 1 + \ell^2\mu^2 - \ell(-1 + \mu^2) = 0.$$

The eigenvalues of $J_{MI_{|(x_{ss}, y_{ss})}}$ are obtained as

$$\lambda_{1,2} = \frac{1}{2}\left[2 + \ell(1 - \mu^2 \mp \sqrt{1 - 6\mu^2 + \mu^4}\right]. \tag{4.81}$$

The stability condition $\rho(J_{MI}) < 1$ where $\rho(J_{MI}) = max_{i=1,2}|\lambda_i|$ holds if

$$2 \leq \ell < \frac{2(\mu^2 - 1)}{\mu^4 - 4\mu^2 + 1} \quad \text{for} \quad \mu > 2. \tag{4.82}$$

The Jacobian for Method II is

$$J_{MII} = \begin{bmatrix} \dfrac{1}{1 - \ell Y^2} & \dfrac{2Y(X + \ell\mu)}{(1 - \ell Y^2)^2} \\ \dfrac{\ell Y^2(1 + \ell Y^2)}{[(1 + \ell)(1 + \ell Y^2) - \ell Y(X + \ell\mu)]^2} & \dfrac{(1 + \ell Y^2)^2(1 + \ell) - \ell^2 Y^2(X + \ell\mu)(3 - Y)}{[(1 + \ell)(1 + \ell Y^2) - \ell Y(X + \ell\mu)]^2} \end{bmatrix}$$

which at $(x_{ss}, y_{ss}) = (\frac{1}{\mu}, \mu)$ becomes

$$J_{MII} = \begin{bmatrix} \dfrac{1}{1 - \ell\mu^2} & \dfrac{2\ell(1 + \ell\mu^2)}{(1 - \ell\mu^2)^2} \\ \dfrac{\ell\mu^2}{1 + \ell\mu^2} & 1 + \ell \end{bmatrix}$$

The characteristic equation $\Phi_{MII}(\lambda)$ can be written in a simplified form as

$$\begin{aligned} \Phi_{MII}(\lambda) \equiv & \frac{1}{(-1 + \ell^2\mu^2)^2(1 + \ell^2\mu^2)}\Big\{\lambda^2\left[(-1 + \ell^2)(1 + \ell^2\mu^2)\right] \\ + & \lambda\left[(-1 + \mu^2)(2 + \ell(-1 + (-1 + \ell)\mu^2)(-1 + \ell\mu^2)\right] \\ + & \left[1 + \ell(1 - \ell\mu^2(4 + (1 + \ell)\mu^2)\right]\Big\} = 0. \end{aligned}$$

The eigenvalues of $J_{MII}|_{(x_{ss},y_{ss})}$ are obtained as

$$\begin{aligned}\lambda_{1,2} &= \frac{1}{2(-1+\ell^2\mu^2)^2(1+\ell^2\mu^2)} \\ &\quad \Big[2+\ell^3\mu^4+\ell^2(-2\mu^2-\mu^4)+\ell\Big(1+\mu^2 \\ &\mp \sqrt{(1+\mu^2(6+\mu^2+\ell(-4+6(3+\ell)\mu^2+(2+2(5-2\ell)\ell)\mu^4+(-1+\ell)^2\ell\mu^6)}\Big)\Big].\end{aligned} \tag{4.83}$$

The stability condition $\rho(J_{MII}) < 1$ where $\rho(J_{MII}) = max_{i=1,2}|\lambda_i|$ holds if

$$\frac{2+\sqrt{5}}{\mu^2} \leq \ell < \frac{4}{\mu^2-1} \quad \text{for} \quad \mu > 1. \tag{4.84}$$

The Jacobian for Method III is

$$J_{MIII} = \begin{bmatrix} \dfrac{1}{1+\ell Y^2} & \dfrac{-2\ell Y(X+\ell\mu)}{(1-\ell Y^2)^2} \\ \\ \dfrac{\ell Y^2}{1+\ell} & \dfrac{(1+2\ell XY}{1+\ell} \end{bmatrix}$$

which at $(x_{ss}, y_{ss}) = (\frac{1}{\mu}, \mu)$ becomes

$$J_{MIII} = \begin{bmatrix} \dfrac{1}{1+\ell\mu^2} & \dfrac{-2\ell}{1+\ell\mu^2} \\ \\ \dfrac{\ell\mu^2}{1+\ell} & \dfrac{1+2\ell}{1+\ell} \end{bmatrix}$$

The characteristic equation $\Phi_{MIII}(\lambda)$ can be written as

$$\Phi_{MIII}(\lambda) \equiv \lambda^2 - \Big(\frac{1}{1+\ell\mu^2} + \frac{1+2\ell}{1+\ell}\Big)\lambda + \frac{1+2\ell+2\ell^2\mu^2}{(1+\ell)(1+\ell\mu^2)} = 0.$$

The stability conditions $|\lambda_i| < 1$ can be carried out as if looking for the properties of the characteristic function, $\Phi_{MIII}(\lambda)$, continuous on a closed interval $[-1, 1]$. It can easily be seen that

$$\Phi_{MIII}(-1) \equiv 1 + \Big(\frac{1}{1+\ell\mu^2} + \frac{1+2\ell}{1+\ell}\Big) + \frac{1+2\ell+2\ell^2\mu^2}{(1+\ell)(1+\ell\mu^2)}$$

is always positive. In addition

$$\Phi_{MIII}(1) \equiv \ell^2\mu^2$$

is always positive also. Furthermore, the necessary condition for $\Phi_{MIII}(\lambda) = 0$ to have roots of magnitude less than unity is to check whether $\Phi_{MIII}(\lambda)$ has a minimum value such as $|\lambda_{min}| < 1$.

$$\frac{d\Phi_{MIII}(\lambda)}{d\lambda} = 2\lambda - \Big(\frac{1}{1+\ell\mu^2} + \frac{1+2\ell}{1+\ell}\Big) = 0$$

when

$$\lambda_{min} = \frac{1}{2}\Big(\frac{1}{1+\ell\mu^2} + \frac{1+2\ell}{1+\ell}\Big).$$

Thus, $|\lambda_{min}| < 1$ is true for all values of ℓ for $\mu > 1$. This result proves that Method III is unconditionally stable.

The Jacobian for the second-order method at the stationary state, (x_{ss}, y_{ss}), is

$$J_{sec} = \begin{bmatrix} \text{s1} & \text{s2} \\ \text{s3} & \text{s4} \end{bmatrix}$$

where the entries are given by

$$\begin{aligned}
\text{s1} &= -1 - \frac{4(-2+\ell)}{4-2\ell+\ell(2+\ell)\mu^2}, \\
\text{s2} &= -\frac{8\ell}{4-2\ell+\ell(2+\ell)\mu^2}, \\
\text{s3} &= \frac{4\ell\mu^2\left[4-2\ell-\ell\mu^2(-4+\ell)\right]}{4-2\ell+\ell(2+\ell)\mu^2}, \\
\text{s4} &= \frac{16+\ell\left[-4\ell+4(8+(-4+\ell)\ell)\mu^2-\ell(-4+\ell^2)\mu^4\right]}{4-2\ell+\ell(2+\ell)\mu^2}.
\end{aligned}$$

After some tedious calculations the eigenvalues of J_{sec} are obtained as

$$\begin{aligned}
\lambda_{1,2} = \frac{1}{2[4-2\ell+\ell(2+\ell)\mu^2)^3}\Big\{ &-2\Big[4-2\ell+\ell(2+\ell)\mu^2\Big] \\
&\Big[-16+\ell(-2(8+(-4+\ell)\ell)\mu^2+\ell^2(2+\ell)\mu^4 \pm 2 \\
&\Big(\pm 4+\sqrt{(4(-2+\ell)^2-4(-2+\ell)(-8+\ell(4+\ell))\mu^2} \\
&+(64+\ell(-240+\ell(128+(-12+\ell)\ell)))\mu^4 \\
&2\ell(2+\ell)(8+5(-4+\ell)\ell)\mu^6+\ell^2(2+\ell)^2\mu^8)\Big)\Big]\Big\}. \qquad (4.85)
\end{aligned}$$

The stability conditions for a given time step ℓ are obtained by substituting a parametric value μ in the stability condition $\left|\lambda_{1,2}\right| < 1$.

4.6 Numerical Experiments

The initial-value problem given by equations {(4.26),(4.27),(4.28)} is solved numerically by using Method I, Method II, Method III and the second-order method starting close to the equilibrium point at $t = 0$ for μ in the range $\mu \ll 1$ and $\mu > 1$. In the literature [47], this IVP has been solved using a Runge-Kutta method which can be compared with finite-difference methods to show the latter to be more economical and reliable.

It was found that while the stationary solutions are stable, $\mu > 1$, Method I (Euler) only produced convergence for $\mu > 2$ within the stability interval (4.82). Otherwise, divergence occurred.

The alternative method, Method II, showed convergence in the stability interval, (4.84), for $\mu > 1$. Throughout the numerical simulations divergence was not observed but instead oscillatory behaviour with large amplitudes occurred due to high global truncation error.

Method III was proven and seen to converge to the stable steady-state solution for any value of the time step ℓ.

Using the higher-order accurate numerical scheme, the second-order method, convergence was obtained for large values of ℓ up to the value $\ell = 20.0$ approximately. For larger values of ℓ the method shared the same feature with Method II.

Numerical experiments were performed for various values of μ and ℓ to observe the behaviour of the numerical methods. Here, the second-order method is chosen to illustrate some of the numerical results. While μ is decreased away from the Hopf bifurcation value, $\mu = 1$, the appearance of the stable limit cycle (periodic solutions) was observed at $\mu = 0.905$. This phenomenon is interpreted as a shift of stability from the original stationary solution to the periodic one. However, if the

mass-balance equations are integrated with $\mu = 0.9$, then no limit cycle behaviour is observed. Instead the concentration of Y tends to zero and that for X become infinitely large (growing linearly with time). The emerging stable limit cycle in the phase-plane and growing in size for $0.905 \leq \mu \leq 0.98$ shows that Hopf bifurcation is supercritical, Fig. (4.3). During the period of instability, $\mu < 1$, the system moves spontaneously away from the stationary state. For the pooled chemical reaction model, {(4.26),(4.27)}, there exists only one stationary state, $(x_{ss}, y_{ss}) = (\frac{1}{\mu}, \mu)$, so there is no other resting state for the system to move to. Since the concentrations of $\mathcal{A}$ and $\mathcal{B}$ must vary continuously in time they eventually tend to a periodic oscillatory motion around the unstable state, Fig. 4.4. If the concentrations of X and Y are plotted against each other, they draw out a closed curve around which the system circulates, Fig.4.5. This limit cycle surrounds the unstable pseudo-stationary state appropriate to μ. The amplitude of the oscillations is a measure of the size of this limit cycle. For a better illustration of the changes in the oscillations three-dimensional representations might be helpful, such as Figs. 4.6, 4.7. As μ increased further the stationary-state, (x_{ss}, y_{ss}), becomes stable for $\mu > 1$. A stable spiral surrounding the limit cycle is observed for $\mu = 1.1$ in Fig. 4.8.

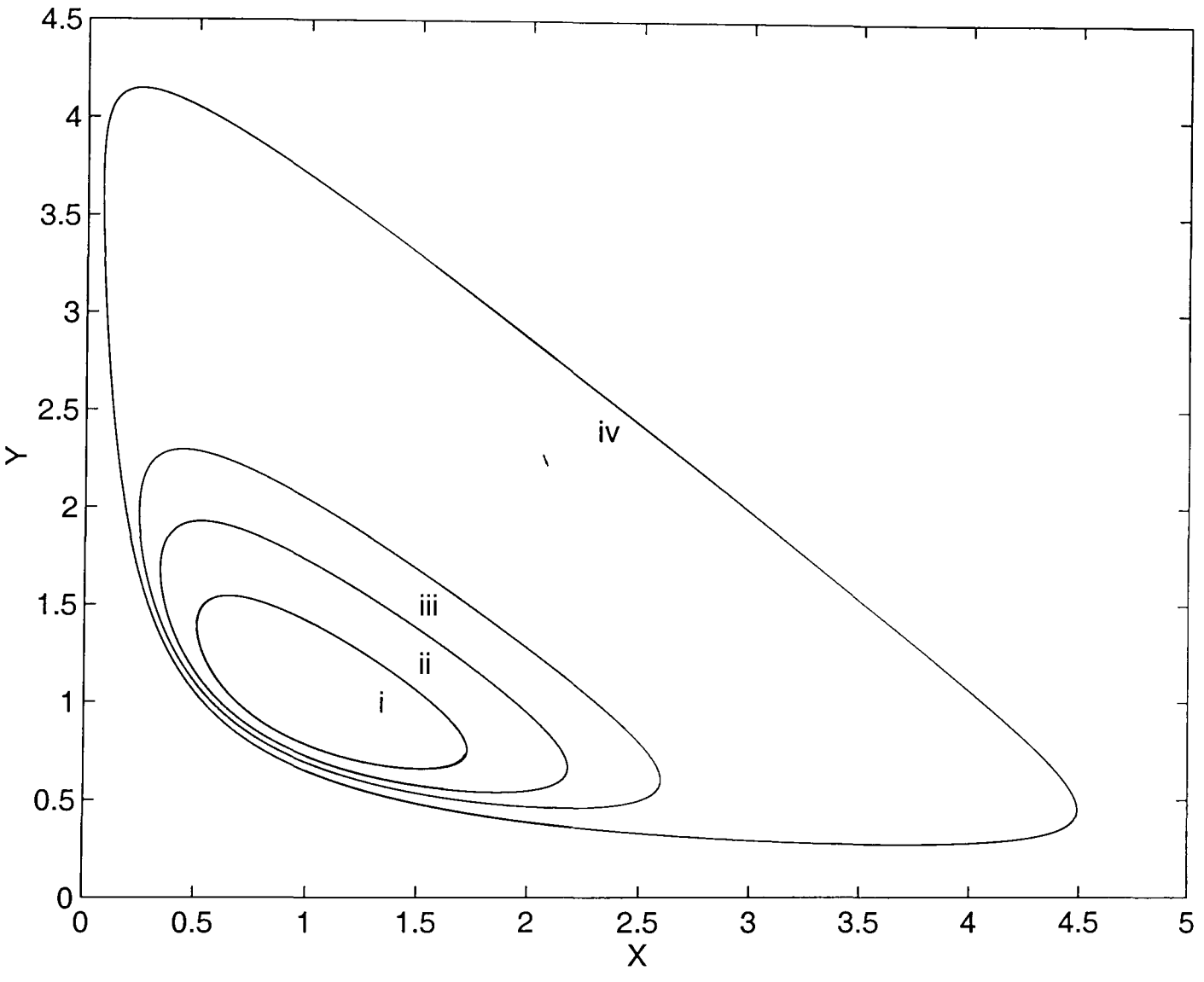

Figure 4.3: The limit cycles for different μ and ℓ values
i) $\mu = 0.98$, $\ell = 0.0016$, **ii)** $\mu = 0.96$, $\ell = 0.0017$,
iii) $\mu = 0.94$, $\ell = 0.0018$, **iv)** $\mu = 0.905$, $\ell = 0.0025$, $X(0) = 1.0, Y(0) = 0.78$.

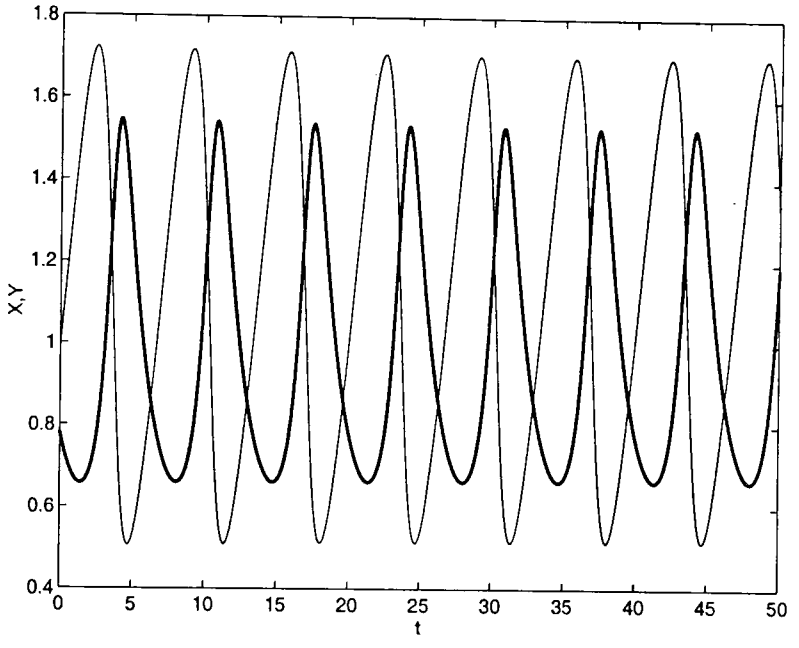

Figure 4.4: Period-one type of behaviour for $\mu = 0.98, \ell = 0.01$, $X(0) = 1.0, Y(0) = 0.78$ (bold one presents the concentration of Y).

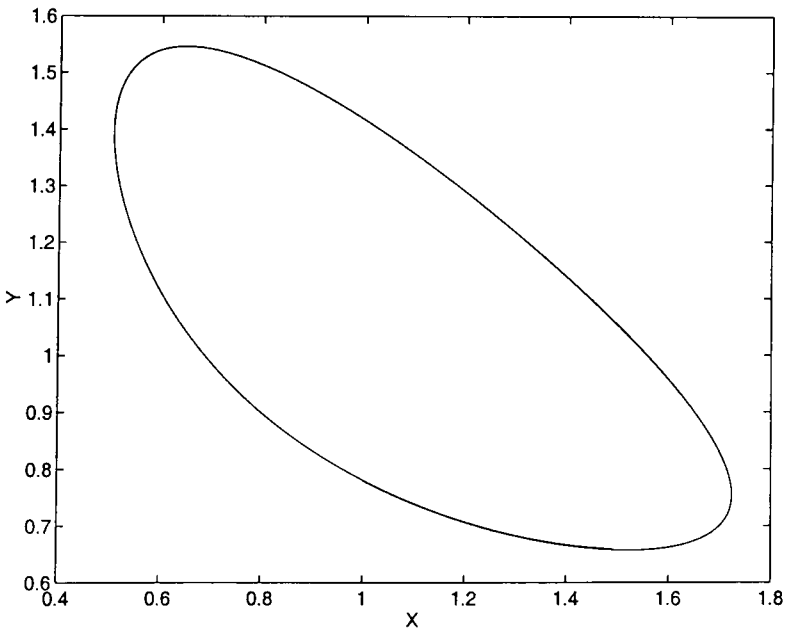

Figure 4.5: Limit cycle at $\mu = 0.98, \ell = 0.0016, X(0) = 1.0, Y(0) = 0.78$.

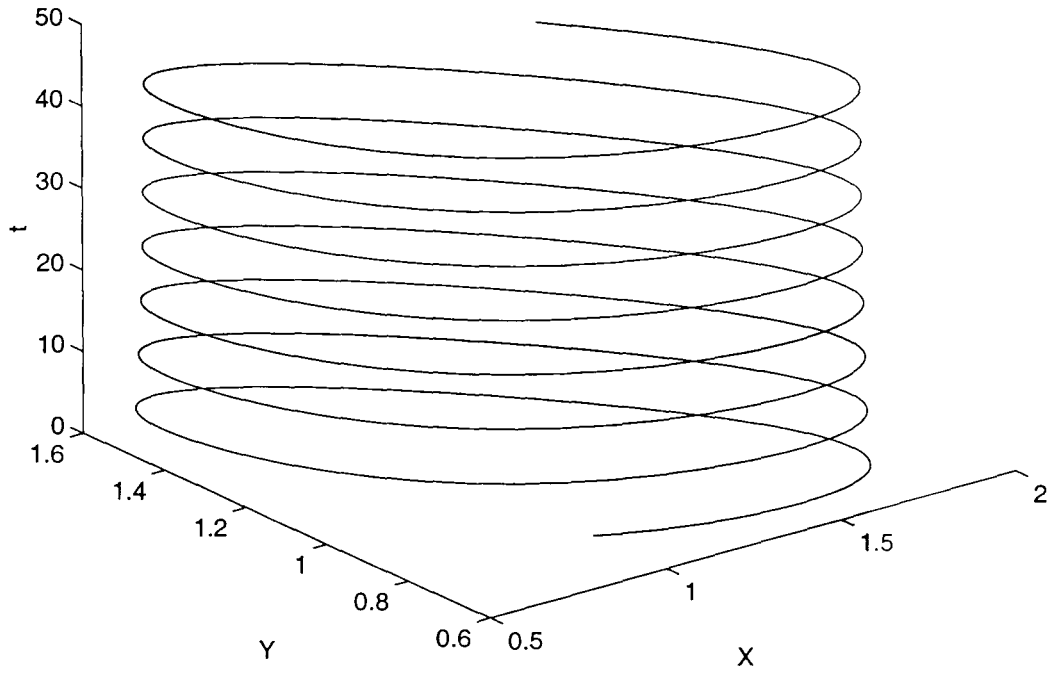

Figure 4.6: Periodic oscillations in $3D$ at $\mu = 0.98, \ell = 0.01, X(0) = 1.0$, $Y(0) = 0.78$.

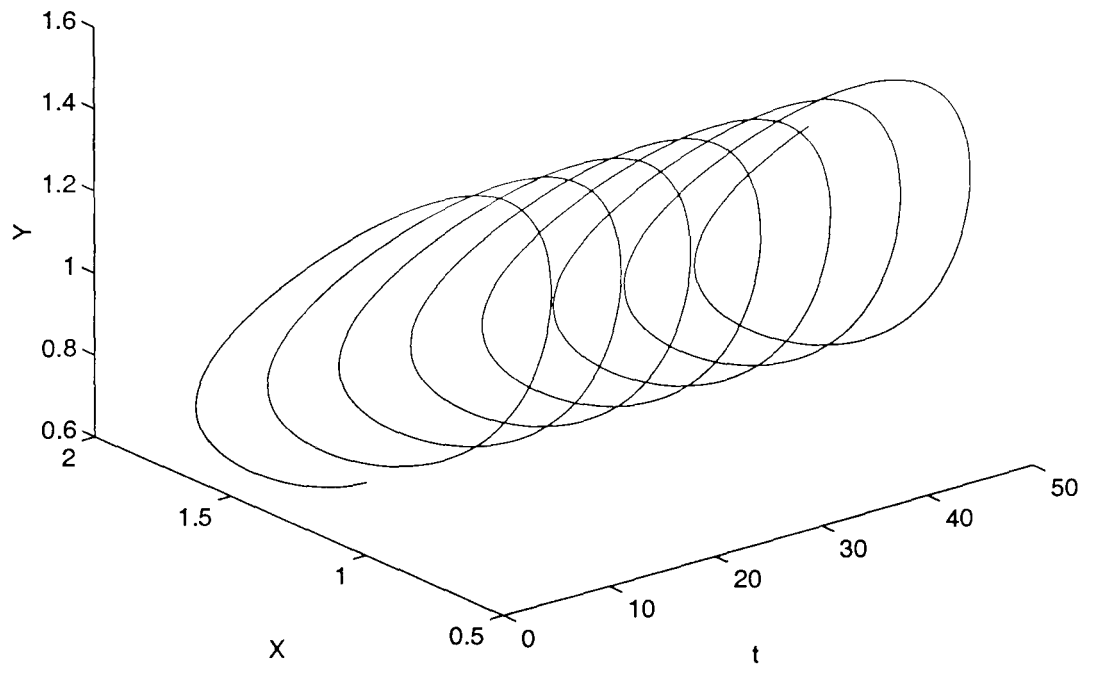

Figure 4.7: Periodic oscillations in $3D$ at $\mu = 0.98, \ell = 0.01, X(0) = 1.0$, $Y(0) = 0.78$.

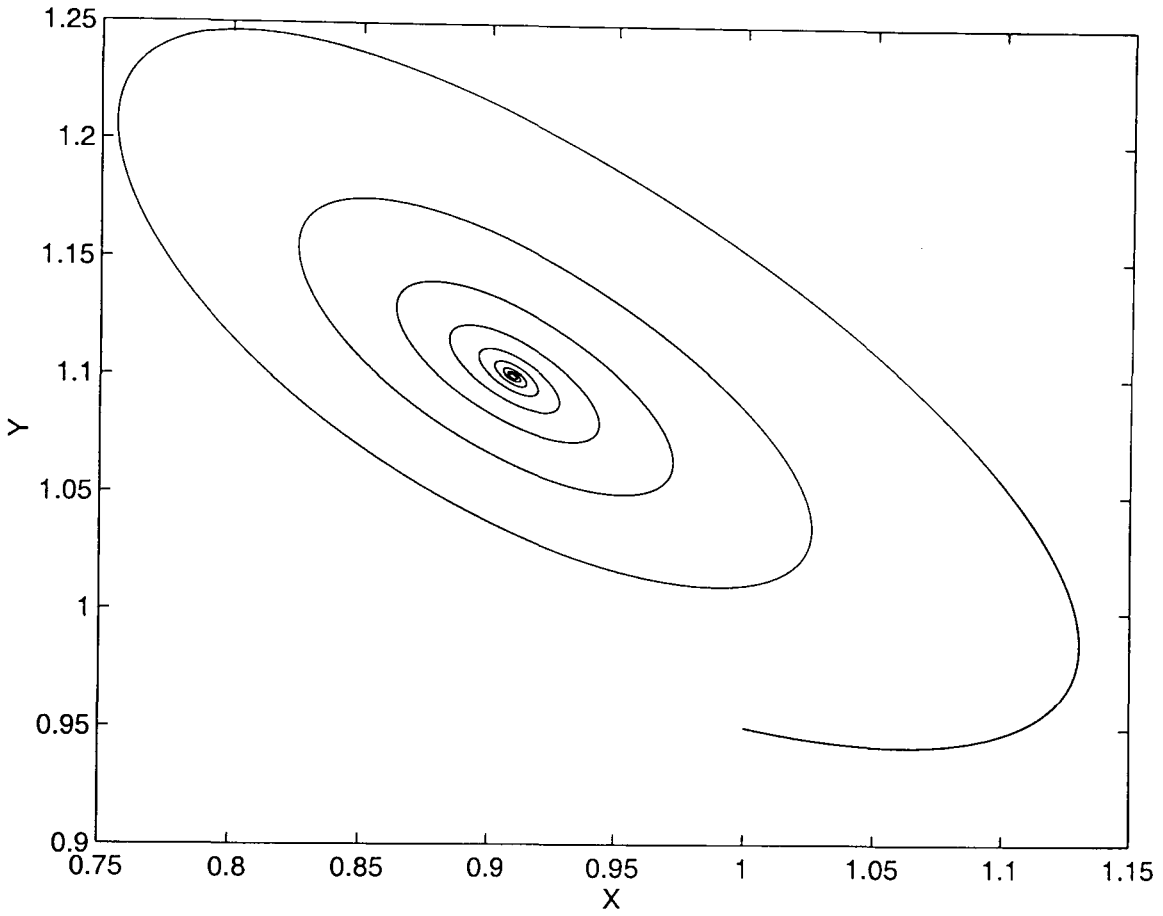

Figure 4.8: Stable spiral at $\mu = 1.1, \ell = 0.01, X(0) = 1.0, Y(0) = 0.95$.

4.7 Summary

First- and second-order finite-difference schemes were developed to study uncoupled pooled chemical reaction model, {(4.26),(4.27)}. The model shows many features observed in real life examples of oscillatory reactions such as a period of oscillatory behaviour leading to a supercritical Hopf bifurcation Gray *et al.* [14], Guckenheimer [16].

Among the proposed numerical methods, the first-order alternative finite-difference scheme and the second-order method discovered and illustrated a wealth of specific detail correctly and widely about the behaviour of the simple kinetic model studied here. Method III, especially, captured the phase portrait of ODEs successfully without any stability restrictions.

Chapter 5

Diffusion-coupled Isothermal Problem

5.1 Introduction

In the past two decades awareness has grown rapidly of the ability of producing complex dynamical behaviour of coupled chemical oscillators. This is due to the growing importance of using coupled bio-chemical oscillators to model physiological rhythms, spatio-temporal control of various developmental processes, cell division, contact inhibition, neurophysiology, neural networks, and many other phenomena in living organisms. A better understanding of coupled oscillating neurons may well hold the key to control complex behaviour such as in the heart or in consciousness. Chemical oscillators can be coupled physically through a membrane, by mass transport or electro-chemically Minorsky and Krieger [50]. Such studies provide a starting point for understanding certain types of more complex dynamical phenomena, such as multiple steady states, hysteresis, Hopf bifurcation, periodic motions, excitability, chaos, travelling waves, etc. José and Saletan [22]. The existence of such periodic motions is of crucial importance for the regulatory processes of biological organisms. Hopf bifurcation for systems of coupled oscillators illustrates important applications to the distinct patterns of leg-movement that animals employ at different speeds of

locomotion, known as gaits. For instance, humans walk, run, leap or hop; and horses walk, trot, canter; etc. These gait patterns can be modelled as symmetry-breaking oscillations of a network composed of a number of identical neural subcircuits.

In this chapter a mathematical model of a two-cell coupled non-linear isothermal chemical reactor problem is studied. The pooled chemical reaction scheme based on the cubic autocatalator and a simple first-order decay is

$$\left.\begin{array}{rcl} \mathcal{P} & \longrightarrow & \mathcal{A} \\ \mathcal{A}+2\mathcal{B} & \longrightarrow & 3\mathcal{B} \\ \mathcal{B} & \longrightarrow & \mathcal{C} \end{array}\right\} \tag{5.1}$$

The reaction scheme (5.1) is the same as in Chapter 4 but here it takes place in two similar cells which interact *via* diffusion past a semi-permeable membrane. Therefore the coupling between the cells is assumed to take place by a linear mass exchange of at least one chemical, either reactant $\mathcal{A}$ or autocatalyst $\mathcal{B}$. Each cell, at the beginning, is inert or dead in the sense that the concentrations of its enzymes achieve a constant equilibrium. After interaction, the cellular system pulses in the sense that the concentrations of enzymes in each cell might oscillate indefinitely. The chemical reaction (5.1) is a rather artificial and has been suggested by Sel'kov [61]; Ashkenazi and Othmer [3]; Tyson and Kauffman [68] as a simplified model of glycolysis, and has wide application in biology, particularly for enzyme reactions where cells can also interact by diffusion with some messenger molecule through semi-permeable membranes. Pavlidis [55] used a similar case to model physiological rhythms, spatio-temporal control of various developmental processes, cell division and other phenomena in living organisms. A similar coupling structure has been also used as a mathematical model of Turing's equations of cellular biology which will be examined in detail in Chapter 7.

5.2 Mathematical Model

The reaction scheme (5.1) is embodied in non-dimensional equations in the general form

$$\frac{dx_k}{dt} = R_1(x_k, y_k) \quad + \sum_{\substack{l \in \text{ set of} \\ \text{cells adjoining } k^{th} \text{ cell}}} \alpha(x_l - x_k) \tag{5.2}$$

$$\frac{dy_k}{dt} = \underbrace{R_2(x_k, y_k)}_{R(x_k, y_k)} \quad + \underbrace{\sum_l \beta(y_l - y_k)}_{D(y_l, y_k)} \tag{5.3}$$

where $k, l = 1, 2$. The mathematical model here shows how the linear coupling of two different kinds of processes, each process in itself stationary, can produce an oscillation. The term $R(x_k, y_k)$ is a transformation process which represents how the chemicals react with each other in the k^{th} cell while $D(y_l, y_k)$ is a transport process which describes the diffusion phenomenon between cells. Thus $(x_l - x_k)$ represents the difference of the concentrations of all the chemicals between the l^{th} and k^{th} cells. Here α and β are coupling constants which appear in the system according to exchange of chemicals.

5.2.1 The model equations

Due to the diffusion of one reactant passing through the semi-permeable membrane two cases may be observed. Coupling through reactant $\mathcal{A}$, by setting the coupling constant $\beta = 0$ in (5.3) gives

$$\frac{dx_1}{dt} = \mu - x_1 y_1^2 + \alpha(x_2 - x_1), \tag{5.4}$$

$$\frac{dy_1}{dt} = x_1 y_1^2 - y_1, \tag{5.5}$$

$$\frac{dx_2}{dt} = \mu - x_2 y_2^2 + \alpha(x_1 - x_2), \tag{5.6}$$

$$\frac{dy_2}{dt} = x_2 y_2^2 - y_2, \tag{5.7}$$

and coupling through autocatalyst $\mathcal{B}$, by taking the coupling constant $\alpha = 0$ in (5.2) gives

$$\frac{dx_1}{dt} = \mu - x_1 y_1^2, \tag{5.8}$$

$$\frac{dy_1}{dt} = x_1 y_1^2 - y_1 + \beta(y_2 - y_1), \tag{5.9}$$

$$\frac{dx_2}{dt} = \mu - x_2 y_2^2, \tag{5.10}$$

$$\frac{dy_2}{dt} = x_2 y_2^2 - y_2 + \beta(y_1 - y_2) \tag{5.11}$$

with some given initial conditions

$$x_k(0) = x_0, \qquad y_k(0) = y_0, \qquad x_0 > 0, y_0 > 0, \qquad k = 1, 2. \tag{5.12}$$

Here μ represents the initial concentration of the pooled chemical $\mathcal{P}$.

5.3 Case I: Coupling Through Reactant $\mathcal{A}$

5.3.1 Stationary states and investigation of linear stability

The investigation of linear stability is restricted in the positive quadrant of the phase space:

$$P = \{(x_1, y_1, x_2, y_2) \mid x_1 > 0, y_1 > 0, x_2 > 0, y_2 > 0\}.$$

The parameters α, β, μ satisfy the restrictions

$$\alpha > 0, \quad \beta > 0, \quad \mu > 0.$$

Analysis of the dynamics shows that the system has multiple stationary-state solutions

$$SS_i = (x_k, y_k, x_{k+1}, y_{k+1}), \quad i = 1, \ldots, 5, \ k = 1$$

in the set P. Solving the equations

$$\mu - x_1 y_1^2 + \alpha(x_2 - x_1) = 0, \tag{5.13}$$

$$x_1 y_1^2 - y_1 = 0, \tag{5.14}$$

$$\mu - x_2 y_2^2 + \alpha(x_1 - x_2) = 0, \tag{5.15}$$

$$x_2 y_2^2 - y_2 = 0, \tag{5.16}$$

the co-ordinates of the steady-state solutions SS_i can be obtained as

$$SS_1 = (\frac{1}{\mu}, \mu, \frac{1}{\mu}, \mu),$$

$$SS_2 = (\frac{1}{2\mu}, 2\mu, \frac{\mu}{\alpha} + \frac{1}{2\mu}, 0), \quad SS_3 = (\frac{\mu}{\alpha} + \frac{1}{2\mu}, 0, \frac{1}{2\mu}, 2\mu),$$

$$SS_{4,5} = (\frac{1}{2\alpha}(\mu \pm (\mu^2 - 2\alpha)^{\frac{1}{2}}), \mu \mp (\mu^2 - 2\alpha)^{\frac{1}{2}}, \frac{1}{2\alpha}(\mu \mp (\mu^2 - 2\alpha)^{\frac{1}{2}}), \mu \pm (\mu^2 - 2\alpha)^{\frac{1}{2}}).$$

The local attractivity (linear stability) of the equilibrium points are determined by the eigenvalues of the Jacobian of (5.4)-(5.7)

$$J = \frac{\partial(\dot{x_1}, \dot{y_1}, \dot{x_2}, \dot{y_2})}{\partial(x_1, y_1, x_2, y_2)} = \begin{bmatrix} -y_1^2 - \alpha & -2x_1 y_1 & \alpha & 0 \\ y_1^2 & 2x_1 y_1 - 1 & 0 & 0 \\ \alpha & 0 & -y_2^2 - \alpha & -2x_2 y_2 \\ 0 & 0 & y_2^2 & 2x_2 y_2 - 1 \end{bmatrix} \tag{5.17}$$

which corresponds to each of the five steady-state solutions. The characteristic equation for SS_1 can be written in the following form

$$[(1 - \lambda)(-\mu^2 - \alpha - \lambda) + 2\mu^2]^2 - \alpha^2(1 - \lambda)^2 = 0 \tag{5.18}$$

and it can be factorized as

$$\underbrace{[\lambda^2 + (\mu^2 - 1)\lambda + \mu^2]}_{(5.19)_1} \underbrace{[\lambda^2 + (\mu^2 + 2\alpha - 1)\lambda + \mu^2 - 2\alpha]}_{(5.19)_2} = 0 \tag{5.19}$$

Equation $(5.19)_1$ is also the characteristic equation for the uncoupled case [see Chapter 4]. A result of this linearization process shows that SS_1 is stable for $\mu > 1$, unstable for $\mu < 1$ and has a Hopf bifurcation at the value $\mu = 1$. To investigate the stability properties of SS_1, the corresponding characteristic equation, $(5.19)_2$, should be checked whether it has stable solutions at $\mu = 1$. The eigenvalues of $(5.19)_2$ are

$$\lambda = \frac{1}{2}\{1 - 2\alpha - \mu^2 \pm [(\mu^2 - 1 + 2\alpha)^2 - 4(\mu^2 - 2\alpha)]^{1/2}\}. \tag{5.20}$$

At $\mu = 1$, (5.20) becomes

$$\lambda = -\alpha \pm (\alpha^2 + 2\alpha - 1)^{1/2}. \tag{5.21}$$

To have a stable solution the eigenvalues given by (5.21) should have negative real parts; this only occurs when $0 \leq \alpha < \frac{1}{2}$. So

$$\mu = 1, \quad 0 \leq \alpha < \frac{1}{2}$$

is the only condition for a Hopf bifurcation for SS_1. The characteristic equation for each of the stationary-states SS_2 and SS_3 is

$$(\lambda + 1)\{\lambda^3 + (2\alpha + 4\mu^2 - 1)\lambda^2 + [4\mu^2(\alpha + 1) - 2\alpha]\lambda + 4\alpha\mu^2\} = 0. \tag{5.22}$$

It can easily be seen that $\lambda = -1$ is one of the roots of (5.22). The rest of (5.22) is a cubic equation and can be analysed using the Routh-Hurwitz theorem in Chapter 2, on page 16. According to the Routh-Hurwitz inequalities concerning the expression

$$\lambda^3 + (2\alpha + 4\mu^2 - 1)\lambda^2 + [4\mu^2(\alpha + 1) - 2\alpha]\lambda + 4\alpha\mu^2, \tag{5.23}$$

the steady-state solutions SS_2 and SS_3 are stable if

$$a_1 = 2\alpha + 4\mu^2 - 1 > 0 \tag{5.24}$$

$$a_3 = 4\alpha\mu^2 > 0 \tag{5.25}$$

$$a_1 a_2 - a_3 > 0 \tag{5.26}$$

where $a_2 = 4\mu^2(\alpha + 1) - 2\alpha$. The states SS_2 and SS_3 have a Hopf bifurcation at the values $\mu = \mu_{HB}$ satisfying the relation (for $\alpha \geq 0$).

$$\mu^2 = \frac{1}{8(1+\alpha)}\{1 + 2\alpha - 2\alpha^2 + [(1 + 2\alpha - 2\alpha^2)^2 + 8\alpha(1 + \alpha)(2\alpha - 1)]^{\frac{1}{2}}\}$$

which is the equation form of the condition (5.26) that seperates the region of instability from the region of stability.

The characteristic equation for $SS_{4,5}$ is

$$\lambda^4 - 2(1 + \alpha - 2\mu^2)\lambda^3 + (1 - 4\alpha + 4\alpha\mu^2)\lambda^2 - 2(2\mu^2 - 3\alpha - 4\alpha^2)\lambda + (8\alpha^2 - 4\alpha\mu^2) = 0. \tag{5.27}$$

Since the constant term $(8\alpha^2 - 4\alpha\mu^2)$ is negative, to satisfy the existence of $SS_{4,5}$, according to the Liénard-Chipart theorem in Chapter 2, on page 17, (5.27) is not a Routh-Hurwitz polynomial: that is, one of the roots of the characteristic equation (5.27) is positive. Therefore the states $SS_{4,5}$ are always unstable saddle points. A bifurcation analysis shows that all these Hopf bifurcations are supercritical while $\mu \leq \mu_{HB}$. During the analysis transitions from stable periodic behaviours with period one to period-two types of behaviour are observed. This transition occurs when eigenvalues of the iterated map (finite-difference schemes) pass out of the unit circle through -1 and this is known as a *flip-type bifurcation.* Neimark bifurcations (secondary Hopf bifurcations) are observed due to the transitions from periodic behaviour to quasi-periodic oscillations Kaplan and Glass [23]. This type of bifurcation occurs when the eigenvalues of the iterated map pass out of the unit circle as a pair of complex conjugates Kuznetsov [27].

5.3.2 First-order numerical methods

Discretizing the interval $t \geq 0$ at the points $t_n = n\ell$ $(n = 0, 1, 2, \ldots)$ the theoretical solution of {(5.4)-(5.7)} at the grid point t_n is denoted by $x_k(t_n), y_k(t_n)$. The solution of an approximating numerical method is denoted by X_k^n, Y_k^n. The general finite-difference scheme for {(5.4)-(5.7)} is

$$X_k^{n+1} = X_k^n + \ell[R_1(X_k^{n+1}, Y_k^n) + D_1(X_l^n, X_k^{n+1})], \tag{5.28}$$

$$Y_k^{n+1} = Y_k^n + \ell[R_2(X_k^{n+1}, Y_k^{n+1}) + D_2(X_l^n, X_k^{n+1})], \tag{5.29}$$

$k = 1, 2$. Evaluating x_k and y_k at the grid point t_n gives the Euler formulae

$$(X1_{n+1} - X1_n)/\ell = \mu - X1_n Y1_n^2 + \alpha(X2_n - X1_n), \tag{5.30}$$

$$(Y1_{n+1} - Y1_n)/\ell = X1_n Y1_n^2 - Y1_n, \tag{5.31}$$

$$(X2_{n+1} - X2_n)/\ell = \mu - X2_n Y2_n^2 + \alpha(X1_n - X2_n), \tag{5.32}$$

$$(Y2_{n+1} - Y2_n)/\ell = X2_n Y2_n^2 - Y2_n. \tag{5.33}$$

To prevent numerical instabilities and non-linearity, the non-linear terms in {(5.31)-(5.33)} are now modelled non-locally, that is $Y1_{n+1}^2$ and $Y2_{n+1}^2$ are evaluated at two different lattice points,

$$Y1_{n+1}^2 \to Y1_n Y1_{n+1}$$

$$Y2_{n+1}^2 \to Y2_n Y2_{n+1}.$$

This leads to the alternative finite-difference method

$$\begin{aligned}
(X1_{n+1} - X1_n)/\ell &= \mu - X1_{n+1}Y1_n^2 + \alpha(X2_n - X1_{n+1}), && (5.34)\\
(Y1_{n+1} - Y1_n)/\ell &= X1_{n+1}Y1_{n+1}Y1_n - Y1_{n+1}, && (5.35)\\
(X2_{n+1} - X2_n)/\ell &= \mu - X2_{n+1}Y2_n^2 + \alpha(X1_{n+1} - X2_{n+1}), && (5.36)\\
(Y2_{n+1} - Y2_n)/\ell &= X2_{n+1}Y2_{n+1}Y2_n - Y2_{n+1} && (5.37)
\end{aligned}$$

where $n = 0, 1, 2, \ldots$. The local truncation errors (LTEs) associated with the Euler formulae and the alternative finite-difference scheme are given by

$$\begin{aligned}
\mathscr{L}1_{x_k}[x_k(t), y_k(t); \ell] &= x_k(t+\ell) - x_k(t) - \ell[R_1(x_k(t), y_k(t)) + D_1(x_l, x_k)]\\
&= \frac{1}{2}x_k''(t)\ell^2 + O(\ell^3) \quad \text{as} \quad \ell \to 0, && (5.38)\\
\mathscr{L}1_{y_k}[x_k(t), y_k(t); \ell] &= y_k(t+\ell) - y_k(t) - \ell[R_2(x_k(t), y_k(t)) + D_2(x_l, x_k)]\\
&= \frac{1}{2}y_k''(t)\ell^2 + O(\ell^3) \quad \text{as} \quad \ell \to 0, && (5.39)
\end{aligned}$$

and

$$\begin{aligned}
\mathscr{L}2_{x_k}[x_k(t), y_k(t); \ell] &= x_k(t+\ell) - x_k(t) - \ell[R_1(x_k(t+\ell), y_k(t+\ell)) + D_1(x_l(t), x_k(t))]\\
&= (\frac{1}{2}x_k'' + x_k'y_k^2 + \alpha x_k')\ell^2 + O(\ell^3) \quad \text{as} \quad \ell \to 0, && (5.40)\\
\mathscr{L}2_{y_k}[x_k(t), y_k(t); \ell] &= y_k(t+\ell) - y_k(t) - \ell[R_2(x_k(t), y_k(t)) + D_2(x_l, x_k)]\\
&= (\frac{1}{2}y_k'' - x_k y_k y_k' - y_k^2 x_k' + y_1')\ell^2 + O(\ell^3) \quad \text{as} \quad \ell \to 0 && (5.41)
\end{aligned}$$

respectively with $k = 1, 2$. These results show that the numerical methods are first-order.

5.3.3 Second-order methods

The second-order methods are based on linear combinations of first-order numerical methods. The first-order methods previously discussed, named $\mathcal{M}^1_{x_1}, \mathcal{M}^2_{x_1}$ and $\mathcal{M}^3_{x_1}$, are given below along with alternative first-order methods and their associated LTEs, $\mathscr{L}^1_{x_1}, \mathscr{L}^2_{x_1}$ and $\mathscr{L}^3_{x_1}$,

$$\mathcal{M}^1_{x_1} : (X1_{n+1} - X1_n)/\ell = \mu - X1_{n+1}Y1_n^2 + \alpha(X2_{n+1} - X1_{n+1}) \tag{5.42}$$

$$\mathscr{L}^1_{x_1} = (\frac{1}{2}x_1'' + x_1'y_1^2 - \alpha x_2' + \alpha x_1')\ell^2 + O(\ell^3) \quad \text{as} \quad \ell \to 0, \tag{5.43}$$

$$\mathcal{M}^2_{x_1} : (X1_{n+1} - X1_n)/\ell = \mu - X1_nY1_nY1_{n+1} + \alpha(X2_n - X1_n) \tag{5.44}$$

$$\mathscr{L}^2_{x_1} = (\frac{1}{2}x_1'' + x_1'y_1y_1')\ell^2 + O(\ell^3) \quad \text{as} \quad \ell \to 0, \tag{5.45}$$

$$\mathcal{M}^3_{x_1} : (X1_{n+1} - X1_n)/\ell = \mu - X1_nY1_n^2 + \alpha(X2_n - X1_n) \tag{5.46}$$

$$\mathscr{L}^3_{x_1} = (\frac{1}{2}x_1'')\ell^2 + O(\ell^3) \quad \text{as} \quad \ell \to 0. \tag{5.47}$$

It can be shown that, obtaining a second-order method is possible since

$$\begin{aligned} \mathscr{L}^{\mathcal{E}}_{x_1} &= \mathscr{L}^1_{x_1} + 2\mathscr{L}^2_{x_1} - \mathscr{L}^3_{x_1} \\ &= O(\ell^3) \quad \text{as} \quad \ell \to 0, \end{aligned} \tag{5.48}$$

then method $\mathcal{M}^{\mathcal{E}}_{x_1}$ can be constructed as

$$\mathcal{M}^{\mathcal{E}}_{x_1} = \mathcal{M}^1_{x_1} + 2\mathcal{M}^2_{x_1} - \mathcal{M}^3_{x_1}. \tag{5.49}$$

Having applied a similar procedure for $X2, Y1$ and $Y2$, the second-order method for the system can be seen to be

$$\begin{aligned} &(2 + \alpha\ell + \ell Y_1^nY_1^n)X_1^{n+1} + 2\ell X_1^nY_1^nY_1^{n+1} - \alpha\ell X_2^{n+1} \\ &= (2 - \alpha\ell)X_1^n + \ell X_1^nY_1^nY_1^n + \alpha\ell X_2^n + 2\ell\mu \end{aligned} \tag{5.50}$$

$$\begin{aligned} &-\ell Y_1^nY_1^nX_1^{n+1} + (2 + \ell - 2\ell X_1^nY_1^n)Y_1^{n+1} \\ &= -\ell Y_1^nY_1^nX_1^n + (2 - \ell)Y_1^n \end{aligned} \tag{5.51}$$

$$(2+\alpha\ell+\ell Y_2^n Y_2^n)X_2^{n+1}+2\ell X_2^n Y_2^n Y_2^{n+1}-\alpha\ell X_1^{n+1}$$
$$=(2-\alpha\ell)X_2^n+\ell X_2^n Y_2^n Y_2^n+\alpha\ell X_1^n+2\ell\mu \tag{5.52}$$

$$-\ell Y_2^n Y_2^n X_2^{n+1}+(2+\ell-2\ell X_2^n Y_2^n)Y_2^{n+1}$$
$$=-\ell Y_2^n Y_2^n X_2^n+(2-\ell)Y_2^n \tag{5.53}$$

where $n=0,1,2,\ldots$.

5.3.4 Stability analysis of numerical methods

First- and second-order numerical methods which were studied in §5.3.2 and 5.3.3 retain all the equilibria of {(5.4)-(5.7)} as fixed points.

The numerical methods can be presented as one-point iteration algorithms of the forms

$$X_k^{n+1}=f_k(X_k^n,Y_k^n);\quad n=0,1,2,\ldots \tag{5.54}$$

$$Y_k^{n+1}=g_k(X_k^n,Y_k^n);\quad n=0,1,2,\ldots \tag{5.55}$$

and by considering the associated functions

$$X_k=f_k(X_k,Y_k) \text{ and } Y_k=g_k(X_k,Y_k),$$

where, for the Euler formulae

$$f_k(X_k,Y_k)=X_k+\ell[R_1(X_k,Y_k)+D_1(X_l,X_k)], \tag{5.56}$$

$$g_k(X_k,Y_k)=Y_k+\ell[R_2(X_k,Y_k)+D_2(X_l,X_k)], \tag{5.57}$$

and for the alternative finite-difference scheme

$$f_k(X_k,Y_k)=(X_k+\ell\mu+\ell\alpha X_{k+1})/(1+\ell Y_k^2+\ell\alpha), \tag{5.58}$$

$$g_k(X_k,Y_k)=Y_k/\Big[1-\ell\Big((X_k+\ell\mu+\ell\alpha X_{k+1})/(1+\ell Y_k^2+\ell\alpha)\Big)Y_k+\ell\Big]. \tag{5.59}$$

The Jacobian for the Euler method is

$$J_E = \begin{bmatrix} a_{11} & a_{12} & a_{13} & a_{14} \\ a_{21} & a_{22} & a_{23} & a_{24} \\ a_{31} & a_{32} & a_{33} & a_{34} \\ a_{41} & a_{42} & a_{43} & a_{44} \end{bmatrix} \tag{5.60}$$

where

$$\begin{aligned} a_{11} &= 1 - \ell(\alpha + Y1^2) & a_{12} &= -2\ell X1Y1 \\ a_{13} &= \alpha\ell & a_{14} &= 0 \\ a_{21} &= \ell Y1^2 & a_{22} &= 1 - \ell(1 - 2X1Y1) \\ a_{23} &= 0 & a_{24} &= 0 \\ a_{31} &= \alpha\ell & a_{32} &= 0 \\ a_{33} &= 1 - \alpha\ell - \ell Y2^2 & a_{34} &= -2\ell X2Y2 \\ a_{41} &= 0 & a_{42} &= 0 \\ a_{43} &= \ell Y2^2 & a_{44} &= 1 - \ell(1 - 2X2Y2) \end{aligned}$$

The matrix J_E becomes at $SS_1 = (\frac{1}{\mu}, \mu, \frac{1}{\mu}, \mu)$

$$J_{E_{|SS_1}} = \begin{bmatrix} 1 - \ell(\alpha + \mu^2) & -2\ell & \alpha\ell & 0 \\ \ell\mu^2 & 1 + \ell & 0 & 0 \\ \alpha\ell & 0 & 1 - \ell(\alpha + \mu^2) & -2\ell \\ 0 & 0 & \ell\mu^2 & 1 + \ell \end{bmatrix} \tag{5.61}$$

The characteristic equation $\Phi_E(\lambda) = 0$ can be written in a simple form as

$$\overbrace{\{\lambda^2 + \lambda[-2 + \ell(-1 + \mu^2)] + 1 + \ell^2\mu^2 - \ell(-1 + \mu^2)\}}^{\Phi_{11}}$$

$$\underbrace{\{\lambda^2 + \lambda[-2 + \ell(-1 + 2\alpha + \mu^2)] + 1 + \ell^2(-2\alpha + \mu^2) - \ell(-1 + 2\alpha + \mu^2)\}}_{\Phi_{12}} = 0. \tag{5.62}$$

The stability conditions $|\lambda_i| < 1$ can be carried out as if looking for the properties of the characteristic function, $\Phi_E(\lambda)$, continuous on a closed interval $[-1, 1]$. In particular, if the function has a positive value at one end of the interval and a negative

value at the other end, then it will vanish at least once within the interval. And the next step is examining whether these roots, minima or maxima, have magnitudes less than 1. Following these properties, since $\Phi_{11}(\lambda)$ is a degree two polynomial it would be enough to check whether the sign of $\Phi_{11}(1)$ and $\Phi_{11}(-1)$ are both the same. It can be easily seen that

$$\Phi_{11}(1) \equiv \ell^2\mu^2 > 0 \quad \text{is always true.}$$

On the other hand $\Phi_{11}(-1) \equiv \ell^2\mu^2 - 2\ell(\mu^2 - 1) + 4 > 0$ is true if $0 < \ell < 2$ provided $\mu > 1 + \sqrt{2}$.

Furthermore, the necessary condition for $\Phi_{11}(\lambda)$ to have zeros with magnitude less than 1 is to check whether $\Phi_{11}(\lambda)$ has a minimum value such as $|\lambda_{min}| < 1$. Now,

$$\frac{d\Phi_{11}(\lambda)}{d\lambda} = 2\lambda - 2 + \ell(\mu^2 - 1) = 0$$

when

$$\lambda_{min} = \frac{1}{2}[2 + \ell(1 - \mu^2)].$$

The condition $|\lambda_{min}| < 1$ is satisfied only if $0 < \ell < \dfrac{4}{\mu^2 - 1}$. The same procedure can be applied to $\Phi_{12}(\lambda)$ also. It can be observed that

$$\Phi_{12}(1) \equiv \ell^2(\mu^2 - 2\alpha) > 0$$

is always true since $\mu^2 > 2\alpha$ is a necessary condition for the existence of $SS_{4,5}$. Now,

$$\Phi_{12}(-1) \equiv (\mu^2 - 2\alpha)\ell^2 - 2(\mu^2 + 2\alpha - 1)\ell + 4 > 0$$

is true if

$$0 < \ell < 2 \quad \text{for} \quad \mu > 1 + \sqrt{2}$$

$$0 < \ell < \frac{4}{\mu^2 + 2\alpha - 1} \quad \text{for} \quad 1 < \mu < 1 + \sqrt{2}.$$

The function $\Phi_{12}(\lambda)$ has minimum value given by

$$\lambda_{min} = \frac{1}{2}[2 - \ell(\mu^2 + 2\alpha - 1)]$$

which has magnitude less than 1 if $0 < \ell < \dfrac{4}{\mu^2 + 2\alpha - 1}$. The overall stability condition is the intersection set of all the stability conditions for the characteristic polynomials $\Phi_{11}(\lambda)$ and $\Phi_{12}(\lambda)$, namely

$$0 < \ell < \frac{4}{\mu^2 + 2\alpha - 1} \quad \text{for} \quad \mu > 1. \tag{5.63}$$

The Jacobian associated with the alternative finite-difference scheme is given by

$$J_A = \begin{bmatrix} A_{11} & A_{12} & A_{13} & A_{14} \\ A_{21} & A_{22} & A_{23} & A_{24} \\ A_{31} & A_{32} & A_{33} & A_{34} \\ A_{41} & A_{42} & A_{43} & A_{44} \end{bmatrix} \tag{5.64}$$

where

$$A_{11} = \frac{1}{a},\ A_{12} = \frac{-2\ell bY1}{a^2},\ A_{13} = \frac{\alpha\ell}{a},\ A_{14} = 0,\ A_{21} = \frac{\ell aY1^2}{[a(1+\ell) - \ell Y1b]^2}$$

$$A_{22} = \frac{[1 + \ell(3Y1^2 + \alpha][a(1+\ell) - \ell bY1] - \ell aY1[2Y1(1+\ell) - b]}{(a - \ell bY1)^2}$$

$$A_{23} = \frac{\alpha\ell^2 aY1^2}{[a(1+\ell) - \ell bY1]^2},\ A_{24} = 0$$

$$A_{31} = \frac{\alpha\ell}{ac},\ A_{32} = \frac{-2\alpha\ell^2 bY1}{a^2},\ A_{33} = \frac{\alpha^2\ell^2 + a}{ac},\ A_{34} = \frac{-2\ell Y2(ad + \alpha\ell b)}{a^2c^2}$$

$$A_{41} = \frac{\alpha\ell^2 acY2^2}{[ac - \ell Y2(ad + \alpha\ell b)]^2}$$

$$A_{42} = \frac{2\ell cY1^2[(1+\ell)ac - \ell Y2(ad + \alpha\ell b) - 2\ell acY1[(1+\ell)c - 2\ell^2 Y2d]Y2}{[(1+\ell)ac - \ell Y2(ad + \alpha\ell b)]^2}$$

$$A_{43} = \frac{\ell acY2^2(a + \alpha^2\ell^2)}{\{a[(1+\ell)c - \ell Y2d] - \alpha\ell^2 bY2^2\}^2}$$

$$A_{44} = \frac{a\{[1+\ell(3Y2^2+\alpha)][(1+\ell)ac-(ad+\alpha\ell b)Y2]-cY2[2\ell aY2(1+\ell)-\ell(ad+\alpha\ell b)]\}}{[(1+\ell)ac-\ell Y2(ad+\alpha\ell b)]^2}$$

where

$$a = 1+\ell(\alpha+Y1^2), \quad b = X1+\ell(\mu+\alpha X2), \quad c = 1+\ell(\alpha+Y2^2), \quad d = X2+\ell\mu.$$

The matrix J_A at $SS_1 = (\frac{1}{\mu}, \mu, \frac{1}{\mu}, \mu)$ has the form

$$\frac{1}{e^2}\begin{bmatrix} e & -2\ell e^2 & \alpha\ell e^2 & 0 \\ \ell\mu^2 e^2 & e^3+\ell(1+\ell(\alpha-\mu^2))e^2 & \ell^2\alpha\mu^2 e^2 & 0 \\ \alpha\ell e & -2\alpha\ell^2 e & e^2+\alpha^2\ell^2 e & -2\ell e \\ \alpha\ell^2\mu^2 e & -2\alpha\ell^3\mu^2 e & \ell\mu^2(e+\alpha^2\ell^2)e & e^3+\ell(1+\ell(\alpha-\mu^2))e^2 \end{bmatrix} \tag{5.65}$$

where $e = 1+\ell(\alpha+\mu^2)$. The characteristic equation of J_A is a degree four polynomial equation of the form

$$\phi(\lambda) \equiv \alpha_0\lambda^4+\alpha_1\lambda^3+\alpha_2\lambda^2+\alpha_3\lambda+\alpha_4 = 0. \tag{5.66}$$

To be able to apply the Routh-Hurwitz criterion it is necessary to make the transformation from λ to z in $\phi(\lambda)$ where $\lambda = \frac{1+z}{1-z}$. After the transformation the polynomial equation can be obtained in the form

$$\Phi(\lambda) \equiv b_0\lambda^4+b_1\lambda^3+b_2\lambda^2+b_3\lambda+b_4 = 0 \tag{5.67}$$

where

$$\begin{aligned} b_0 = \frac{1}{(1+\ell(\alpha+\mu^2))^4} \; & (2(2+\ell)^2(1+\alpha\ell)^2(2+\alpha\ell(2+\alpha\ell)) \\ & +2\ell(2+\ell)(12+\ell(2+\alpha(26+\ell(1+\alpha(20+\ell+6\alpha\ell)))))\mu^2 \\ & -\ell^2(-52+\ell(-4+7\ell+6(-12+\ell^2)\alpha+\ell(-28+3\ell^2)\alpha^2))\mu^4 \\ & -4(-2+\ell)\ell^3(3+2\alpha\ell)\mu^6+(-2+\ell)^2\ell^4\mu^8) \\ b_1 = \frac{1}{(1+\ell(\alpha+\mu^2))^4} \; & (2\ell(-(2+\ell)(1+\alpha\ell)^2(4+(-2+\ell)\alpha(2+\alpha\ell)) \\ & 2(4+\ell(4(-2+5\alpha)+\ell(-3+\alpha(-4+24\alpha \end{aligned}$$

$$
\begin{aligned}
& & & +\ell(-1+\alpha-\alpha\ell+(8+\ell)\alpha^2)))))\mu^2 \\
& & & +\ell(20+\ell(-2+48\alpha+\ell(6+2\alpha\ell+(24+\ell^2)\alpha^2)))\mu^4 \\
& & & -2\ell^2(-8+\ell+2(-4+\ell)\alpha\ell)\mu^6-2(-2+\ell)\ell^3\mu^8)) \\
b_2 = & \frac{1}{(1+\ell(\alpha+\mu^2))^4} & & (2\ell^2(-(1+\alpha\ell)^2(-2+(4+\ell)\alpha(2+\alpha\ell)) \\
& & & -2(-2\alpha+\ell(-3+\alpha(2+\alpha\ell)(5+(-2+3\ell)\alpha)))\mu^2 \\
& & & +(2+\ell(-2-\ell+4(3+\ell^2)\alpha+2\ell(5+\ell^2)\alpha^2))\mu^4 \\
& & & +2\ell(2+3\ell+2\ell(2+\ell)\alpha)\mu^6-\ell^2(-2+(-2+\ell)\ell)\mu^8)) \\
b_3 = & \frac{1}{(1+\ell(\alpha+\mu^2))^4} & & (2\ell^3(\alpha(1+\alpha\ell)^2(2+\alpha\ell)-2(1+\ell(-1+\alpha)\alpha(1+\alpha\ell))\mu^2 \\
& & & -(-2+\ell(2+\alpha\ell(2+\alpha\ell)))\mu^4+2\ell(1+2\alpha\ell)\mu^6+2\ell^2\mu^8)) \\
b_4 = & \frac{1}{(1+\ell(\alpha+\mu^2))^4} & & (\ell^4\mu^2(-2\alpha(1+\alpha\ell)+\mu^2-\alpha\ell(2+\alpha\ell)\mu^2+\ell^2\mu^6))
\end{aligned}
$$

Demonstrating local stability involves verifying the following Routh-Hurwitz inequalities

$$
\begin{aligned}
b_i &> 0, \quad i=0,1,2,3,4 \\
b_5 &= b_1b_2b_3-b_0b_3^2-b_1^2b_4>0. \qquad (5.68)
\end{aligned}
$$

for given values of α, μ and ℓ.

5.3.5 Numerical experiments

The diffusion-coupled isothermal problem,{(5.2),(5.3)}, was studied for the case of coupling through $\mathcal{A}$ by using first- and second-order finite-difference schemes. The numerical results were produced using the alternative finite difference scheme {(5.34)-(5.37)} and the second-order method for various values of μ and α, to be able to illustrate most of the predicted phase-portrait. The following set of initial conditions were suggested throughout the numerical simulations

$$X1(0)=1.05,\ Y1(0)=0.8,\ X2(0)=1.08,\ Y2(0)=0.9\,. \qquad (5.69)$$

The symbol X may represent X_1 or X_2 and Y may represent Y_1 or Y_2 due to the inherent symmetry of the system. To show the different types of behaviour present,

two values of the coupling constant α were chosen, these being $\alpha = 0.05$ and $\alpha = 0.4$.

Using $\alpha = 0.05$ it was observed that as the parameter μ is decreased away from the Hopf bifurcation point, $\mu = 1$, a sequence of period doubling occurred, which was found to follow the Feigenbaum scenario. These results are depicted in Fig. 5.1 using the alternative finite-difference scheme for $\mu = 0.98$ and $\ell = 0.01$. The transition from the region of stable stationary state to a region of stable periodic oscillations is marked by the supercritical Hopf bifurcation. Following transitions from the region of periodic behaviour with one period to a region of stable periodic behaviour with two periods is known as flip-type bifurcation. Corresponding limit cycles are presented in Fig. 5.2 using second-order method with $\ell = 1.0$.

Using $\alpha = 0.4$, bifurcations to quasi-periodic behaviour following by strange attractor were observed. As μ is decreased away from the Hopf bifurcation point periodic behaviour at $\mu = 0.98$ to quasi-periodic transitions at $\mu = 0.943$ was observed. These results are depicted in Figs 5.3 and 5.4 using the second-order finite-difference scheme with $\ell = 1.0$. The curve of secondary Hopf bifurcation marks the transition from periodic behaviour to quasi-periodic oscillations. As μ was decreased further secondary Hopf bifurcation occurred and led to the emergence of a strange attractor at $\mu = 0.94$. These numerical results are illustrated in Fig. 5.5 for the second-order method with $\ell = 1.0$.

Throughout the numerical simulations it was observed that the alternative finite difference scheme {(5.34)-(5.37)} and the second-order method captured the qualitatively correct behaviour of the ODEs in §5.3.1 for large values of ℓ, such as $\ell \leq 20.0$. As ℓ was increased further divergence was not observed but instead oscillatory behaviour leading to convergence to a perturbed correct fixed point occurred. The Euler method converged to the correct steady-state solutions within the determined stability interval for rather restricted values of ℓ, otherwise divergence occurred. Moreover, the Euler method had difficulty in capturing some of the qualitative feature of the ODEs such as strange attractors.

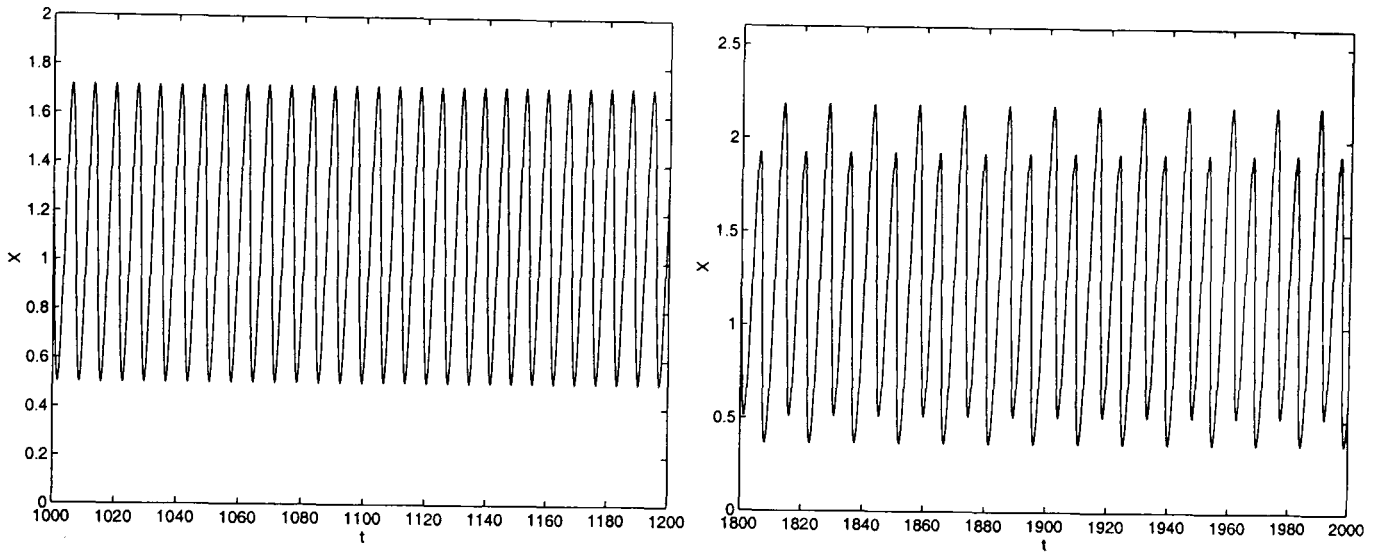

Figure 5.1: Period 1 $\rightarrow$ period 2 transitions.

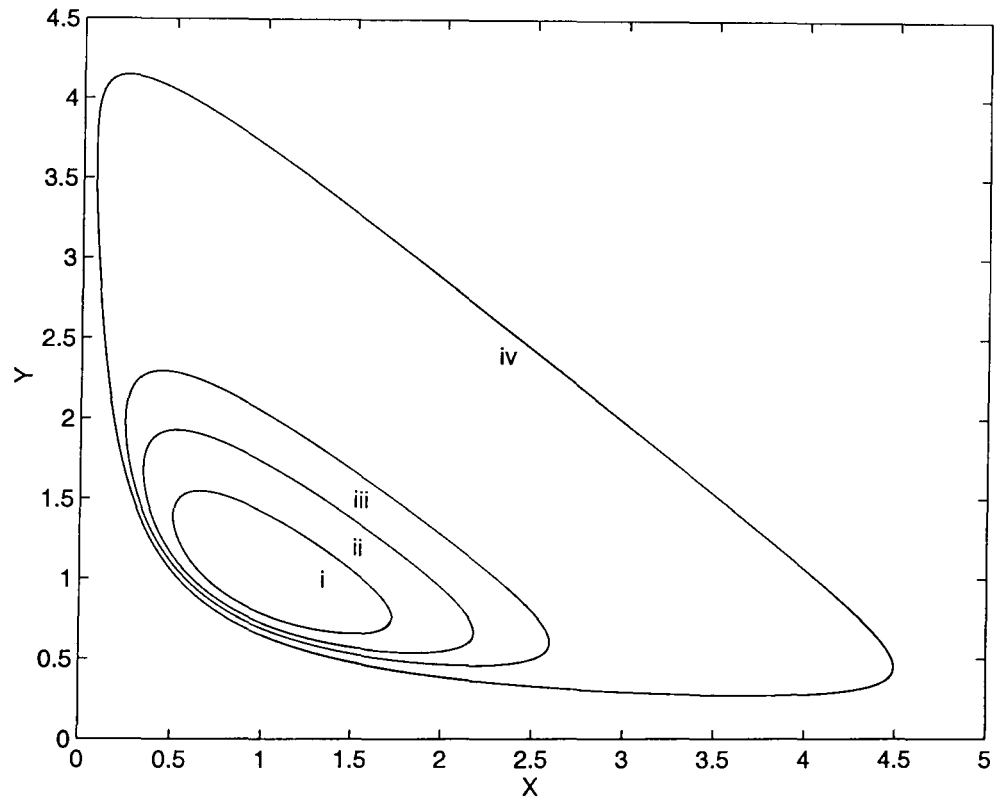

Figure 5.2: Stable limit cycles produced for various μ values:
$i)\mu = 0.98,\ ii)\mu = 0.975,\ iii)\mu = 0.960,\ iv)\mu = 0.95$.

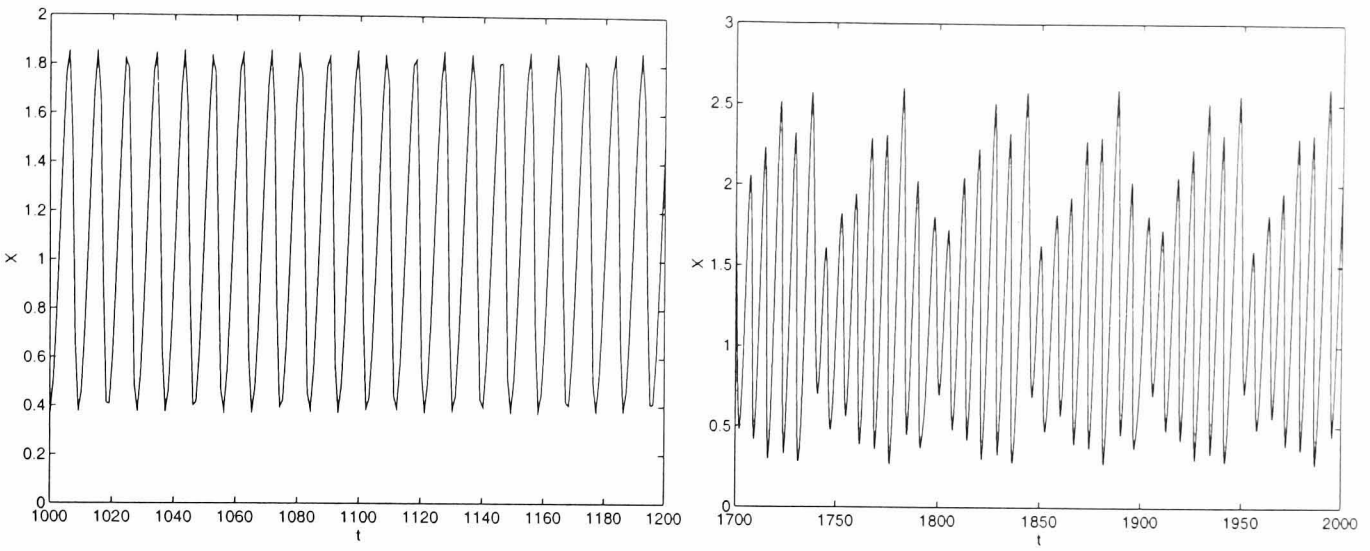

Figure 5.3: Periodic behaviour → quasi-periodic transitions.

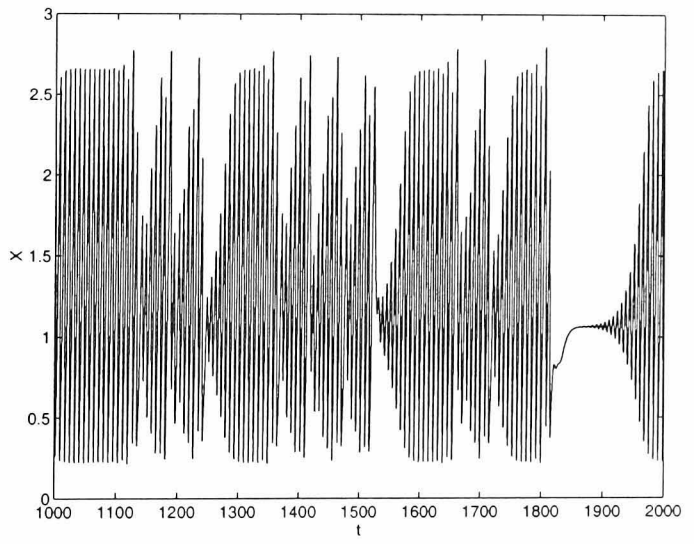

Figure 5.4: Quasi-periodic transitions.

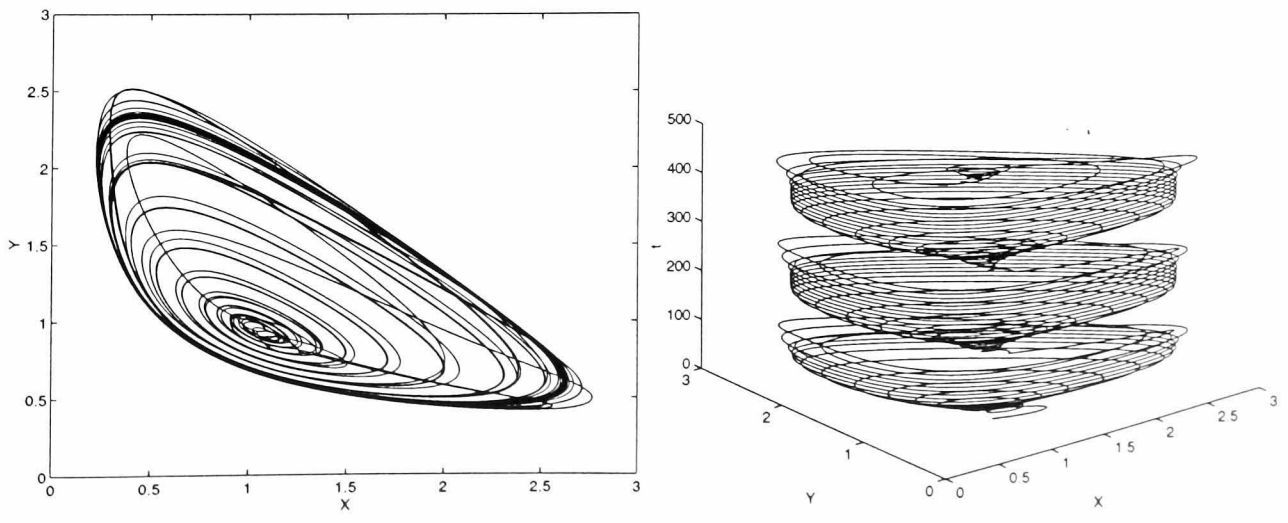

Figure 5.5: Strange attractors in $2D$ and $3D$.

5.4 Reduced System of Coupling Through Reactant $\mathcal{A}$

After analysing the local stability of the non-symmetric stationary-state points it can be easily seen that the system {(5.4)-(5.7)} can be reduced to

$$\frac{dx_1}{dt} = \mu - x_1 z^2 + \alpha(x_2 - x_1), \tag{5.70}$$

$$\frac{dz}{dt} = x_1 z^2 - z, \tag{5.71}$$

$$\frac{dx_2}{dt} = \mu + \alpha(x_1 - x_2) \tag{5.72}$$

due to the stationary-state points SS_2 and SS_3 having either $y_1 = 0$ or $y_2 = 0$. In that case y_1 or y_2 can be represented by z alone. Local stability analysis shows that the ODE system, (5.70)-(5.72), has only one steady-state point, SS_R,

$$SS_R = (\frac{1}{2\mu}, 2\mu, \frac{\mu}{\alpha} + \frac{1}{2\mu})$$

and has Jacobian

$$J_R = \begin{bmatrix} -z^2 - \alpha & -2x_1 z & \alpha \\ z^2 & 2x_1 z - 1 & 0 \\ \alpha & 0 & -\alpha \end{bmatrix} \tag{5.73}$$

The characteristic equation can be obtained for SS_R from (5.73): it is

$$\lambda^3 + (2\alpha + 4\mu^2 - 1)\lambda^2 + [4\mu^2(\alpha + 1) - 2\alpha]\lambda + 4\alpha\mu^2 = 0 \tag{5.74}$$

which is the same as $(5.22)_2$. The same phase portrait results are also valid for the reduced system, [see §5.3.1].

5.4.1 Numerical methods

First-order numerical methods are developed by approximating the derivatives $dx_k(t)/dt$ and $dz(t)/dt$ by first-order replacements (forward-difference approximants) as in previous sections. The resulting Euler-type scheme, $M1_R$, for {(5.70)-(5.72)}

is

$$(X1_{n+1} - X1_n)/\ell = \mu - X1_n Z_n^2 + \alpha(X2_n - X1_n), \tag{5.75}$$

$$(Z_{n+1} - Z_n)/\ell = X1_n Z_n^2 - Z_n, \tag{5.76}$$

$$(X2_{n+1} - X2_n)/\ell = \mu + \alpha(X1_n - X2_n). \tag{5.77}$$

Modelling the non-linear terms in (5.76) non-locally, that is using two different lattice points, gives

$$Z_{n+1}^2 \to Z_n Z_{n+1}.$$

This gives the alternative finite-difference method, $M2_R$,

$$(X1_{n+1} - X1_n)/\ell = \mu - X1_{n+1} Z_n^2 + \alpha(X2_n - X1_{n+1}), \tag{5.78}$$

$$(Z_{n+1} - Z_n)/\ell = X1_{n+1} Z_{n+1} Z_n - Z_{n+1}, \tag{5.79}$$

$$(X2_{n+1} - X2_n)/\ell = \mu + \alpha(X1_{n+1} - X2_{n+1}). \tag{5.80}$$

The associated local truncation errors, LTEs, for the Euler scheme and also the alternative finite-difference scheme are given by

$$\mathscr{L}1_{x_k}[x_k(t), z(t); \ell] = \frac{1}{2} x_k''(t)\ell^2 + O(\ell^3) \quad \text{as} \quad \ell \to 0, \tag{5.81}$$

$$\mathscr{L}1_z[x_k(t), z(t); \ell] = \frac{1}{2} z''(t)\ell^2 + O(\ell^3) \quad \text{as} \quad \ell \to 0, \tag{5.82}$$

$k = 1, 2$ and

$$\mathscr{L}2_{x_1}[x_1(t), z(t); \ell] = (\frac{1}{2} x_1'' + x_1' z^2 + \alpha x_1')\ell^2 + O(\ell^3) \quad \text{as} \quad \ell \to 0, \tag{5.83}$$

$$\mathscr{L}2_z[x_1(t), z(t), x_1(t); \ell] = (\frac{1}{2} z'' - x_1 z z' - z^2 x_1' + z')\ell^2 + O(\ell^3) \quad \text{as} \quad \ell \to 0, \tag{5.84}$$

$$\mathscr{L}2_{x_2}[x_1(t), z(t); \ell] = (\frac{1}{2} x_2'' - \alpha x_1' + \alpha x_2')\ell^2 + O(\ell^3) \quad \text{as} \quad \ell \to 0 \tag{5.85}$$

respectively.

5.4.2 Stability analysis of numerical methods

The Jacobian for $M1_R$ (Euler) is

$$J_{R_{M1}} = \begin{bmatrix} 1-\ell(Z^2+\alpha) & -2\ell X1Z & \alpha\ell \\ \ell Z^2 & 1+\ell(2X1Z-1) & 0 \\ \alpha\ell & 0 & 1-\alpha\ell \end{bmatrix} \tag{5.86}$$

which, at $SS_R = (\frac{1}{2\mu}, 2\mu, \frac{\mu}{\alpha} + \frac{1}{2\mu})$, becomes

$$J_{R_{M1}|_{SS_R}} = \begin{bmatrix} 1-\ell(\alpha+4\mu^2) & -2\ell & \alpha\ell \\ 4\ell\mu^2 & 1+\ell & 0 \\ \alpha\ell & 0 & 1-\alpha\ell \end{bmatrix} \tag{5.87}$$

After the transformation of, [see §5.3.4], the characteristic equation becomes

$$R(z) \equiv \rho_0 z^3 + \rho_1 z^2 + \rho_2 z + \rho_3 = 0, \tag{5.88}$$

where

$$\begin{aligned} \rho_0 &= -4(2+\ell)(-1+\alpha\ell) - 4\ell\mu^2(-2+\ell)(-2+\alpha\ell), \\ \rho_1 &= 4\ell(-1+2\alpha(1+\ell) + \mu^2(4+3\alpha\ell^2 - 4\ell(1+\alpha)), \\ \rho_2 &= -4\ell^2(\alpha+\mu^2(-2+\alpha(-2+3\ell))), \\ \rho_3 &= 4\alpha\ell^3\mu^2. \end{aligned}$$

The Routh-Hurwitz criteria give the following inequalities to ensure that the roots of the equation (5.88) lie inside the unit circle:

$$\begin{aligned} \rho_i &> 0, \quad i = 0,1,2,3 \\ \rho_4 &= \rho_1\rho_2 - \rho_3\rho_0 > 0. \end{aligned} \tag{5.89}$$

The Jacobian for $M2_R$, is

$$J_{R_{M2}} = \frac{1}{f}\begin{bmatrix} 1 & -2\ell bZ & \alpha\ell \\ \frac{\ell f Z^2}{[(1+\ell)-\frac{1}{f}\ell bZ]^2} & \frac{[f(1+\ell)-\ell bZ](1+3\ell Z^2+\alpha\ell)-\ell fZ[2Z(1+\ell)-b]}{[f^2[(1+\ell)-\frac{1}{f}\ell bZ]^2} & \frac{\alpha\ell^2 Z^2}{[(1+\ell)-\frac{1}{f}\ell bZ]^2} \\ \frac{\alpha\ell}{(1+\alpha\ell)} & \frac{2\ell Z[(X2+\ell\mu)(1-f)+\alpha\ell b]}{f(1+\ell)} & \frac{f+\alpha^2\ell^2}{(1+\alpha\ell)} \end{bmatrix} \tag{5.90}$$

where $f = 1 + \ell(\alpha + Z^2)$. The matrix $J_{R_{M2}}$ becomes, at $SS_R = (\frac{1}{2\mu}, 2\mu, \frac{\mu}{\alpha} + \frac{1}{2\mu})$,

$$J_{R_{M2}|_{SS_R}} = \frac{1}{g}\begin{bmatrix} 1 & -2\ell & \alpha\ell \\ 4\ell\mu^2 & g + \ell(1 + \ell(\alpha - 4\mu^2)) & 4\alpha\ell^2\mu^2 \\ \alpha\ell & -2\alpha\ell^2 & g + \alpha^2\ell^2 \end{bmatrix} \tag{5.91}$$

where $g = 1 + \ell(\alpha + 4\mu^2)$. Its characteristic equation can be expressed in the general form

$$\varrho_0 z^3 + \varrho_1 z^2 + \varrho_2 z + \varrho_3 = 0 \tag{5.92}$$

where

$$\begin{aligned}
\varrho_0 = \ & \tfrac{1}{(1+\alpha\ell)(1+\alpha\ell+4\ell\mu^2)} \ (-(2+\ell)(1+\alpha\ell)(4+\alpha\ell(4+\alpha\ell(2+\alpha\ell))) \\
& +4\ell(-12+\ell(-2+\alpha(-18+\ell(1+\alpha(-2+\ell)(5+2\alpha\ell)))))\mu^2 \\
& +16\ell^2(-8+\ell(2+\alpha(-6+9\ell+\alpha\ell(-2+4\ell+1))))\mu^4 \\
& +64\ell^3(-2+\ell(3+2\alpha\ell))\mu^6), \\
\varrho_1 = \ & \tfrac{1}{(1+\alpha\ell)(1+\alpha\ell+4\ell\mu^2)} \ (\ell(4+16\mu^2+\ell(\alpha(2+\alpha\ell)(4+\alpha\ell(1+\alpha\ell)) \\
& -4(-8+\alpha(-4+\ell(-5+\alpha\ell(5+2\alpha\ell))))\mu^2 \\
& -16(-4+\alpha\ell^2(9+4\alpha\ell+\alpha\ell))\mu^4 - 64\ell^2(3+2\alpha\ell)\mu^6))), \\
\varrho_2 = \ & \tfrac{1}{(1+\alpha\ell)(1+\alpha\ell+4\ell\mu^2)} \ (\ell^2((2+\ell)\alpha^2(1+\alpha\ell)(2+\alpha\ell) \\
& -4(1+\alpha\ell)(6+\alpha(-2+\ell)(3+2\alpha\ell))\mu^2 \\
& -16(-4+\ell(6+\alpha(-6+9\ell+\alpha\ell(-2+4\ell+1))))\mu^4 \\
& -64\ell(-2+\ell(3+2\alpha\ell))\mu^6)), \\
\varrho_3 = \ & \tfrac{1}{(1+\alpha\ell)(1+\alpha\ell+4\ell\mu^2)} \ (\ell^3(-\alpha^2(1+\alpha\ell)(2+\alpha\ell)+4\alpha(1+\alpha\ell) \\
& (3+2\alpha\ell)\mu^2+16(4+\alpha\ell(9+4\alpha\ell+\alpha))\mu^4 \\
& +64\ell(3+2\alpha\ell)\mu^6)).
\end{aligned}$$

The Routh-Hurwitz criteria give the following inequalities which must be satisfied if the roots of the equation (5.92) are to lie inside the unit circle:

$$\varrho_i > 0, \quad i = 0, 1, 2, 3, \tag{5.93}$$

$$\varrho_4 = \varrho_1\varrho_2 - \varrho_3\varrho_0 > 0. \tag{5.94}$$

5.4.3 Numerical experiments

Due to one of the eigenvalues associated with the non-symmetric stationary states, $SS_R = \left(\frac{1}{2\mu}, 2\mu, \frac{\mu}{\alpha} + \frac{1}{2\mu}\right)$, being $\lambda = -1$ the original system {(5.4)-(5.7)} is reduced to {(5.70), (5.71),(5.72)}.

First-order numerical methods, $M1_R$, $M2_R$, were tested in numerical experiments. It was observed that a supercritical Hopf bifurcation emanated at $\mu = 0.5$. This result was confirmed using $M2_R$ with $\alpha = 0.5$, $\ell = 1.0$ and the initial conditions $X1(0) = 1.02$, $Z(0) = 0.96$, $X2(0) = 2.2$. This period-one type of behaviour and the corresponding limit cycles are shown in Fig.5.6. As μ was increased further a succession of period doublings was observed which terminated when the infinite-period bifurcation was reached.

The Euler method managed to illustrate the supercritical Hopf bifurcation for $\ell < 0.5$ whereas the alternative finite-difference method $M2_R$ produced the correct phase-portait for $\ell < 10.0$. As ℓ was increased above these values, the Euler formulae showed divergence, while $M2_R$ approached a perturbed steady-state solution.

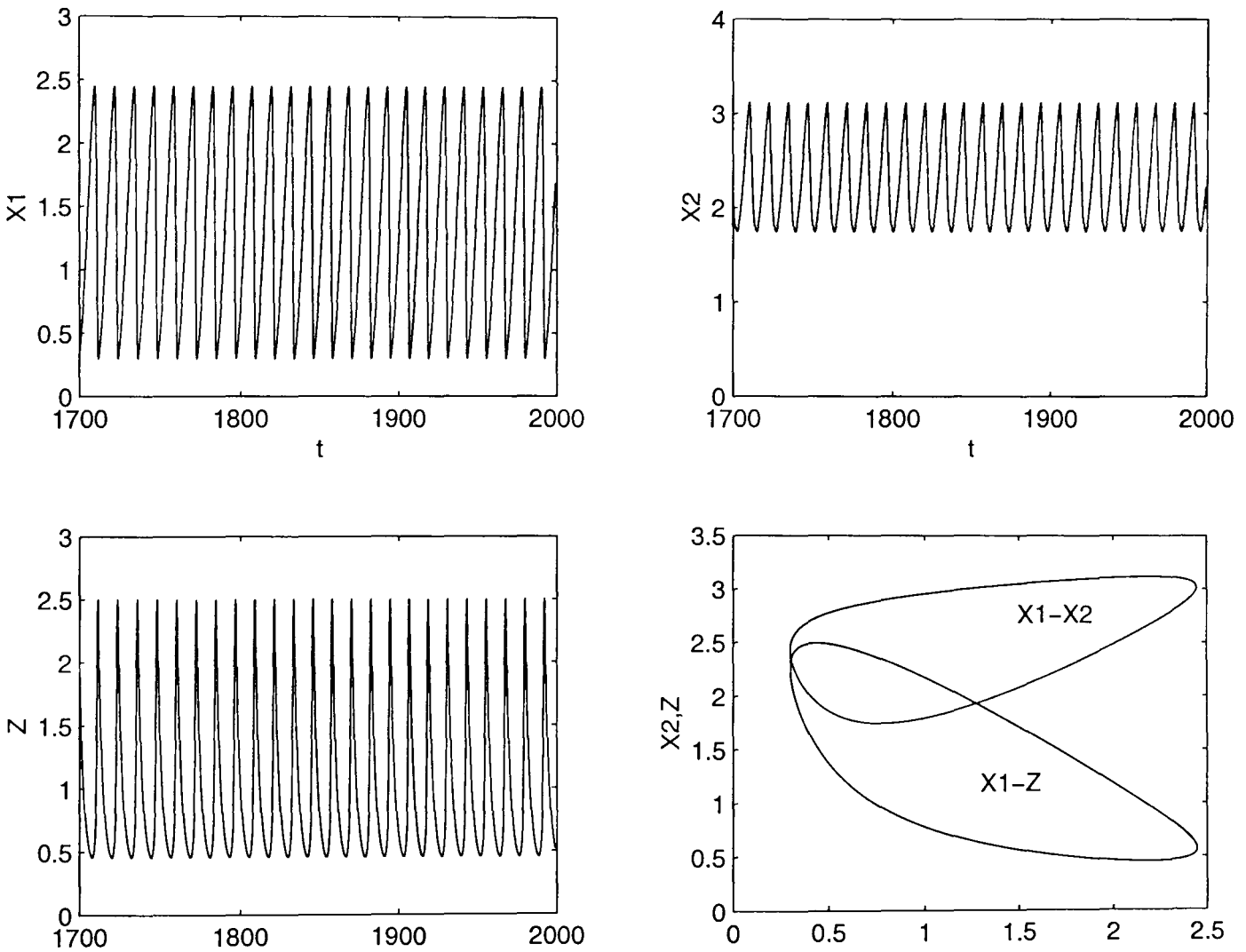

Figure 5.6: Period-one type solutions and corresponding limit cycles.

5.5 Case II: Coupling Through Autocatalyst $\mathcal{B}$

5.5.1 Stationary states and investigation of linear stability

Due to coupling through autocatalytic species $\mathcal{B}$ the ODE system {(5.8)-(5.11)} is obtained. The local stability of the system can also be bounded in the positive quadrant in §5.3.1 with positive parameters. According to the local stability analysis, {(5.8)-(5.11)} has no multiplicity of steady-state solutions as was observed in {(5.4)-(5.7)} and

$$SS_{\mathcal{B}} = (x_1, y_1, x_2, y_2) = (\frac{1}{\mu}, \mu, \frac{1}{\mu}, \mu)$$

is the only stationary-state solution. The Jacobian, $J_{\mathcal{B}}$, at $SS_{\mathcal{B}}$ becomes

$$J_{\mathcal{B}|_{SS_{\mathcal{B}}}} = \begin{bmatrix} -\mu^2 & -2 & 0 & 0 \\ \mu^2 & 1-\beta & 0 & \beta \\ 0 & 0 & -\mu^2 & -2 \\ 0 & \beta & \mu^2 & 1-\beta \end{bmatrix} \tag{5.95}$$

The characteristic equation for $SS_{\mathcal{B}}$ can be written in the following form

$$\begin{aligned} &\lambda^4 - 2(1-\beta-\mu^2)\lambda^3 + \lambda^2(1-2\beta+4\beta\mu^2+\mu^4) \\ &\quad - \ 2\mu^2(1-\mu^2-\beta\mu^2)\lambda + \mu^4(1+2\beta) = 0. \end{aligned} \tag{5.96}$$

An alternative way of dealing with the stability analysis is made possible due to the special form of the Jacobian $J_{\mathcal{B}}$, (5.95),

$$J_{\mathcal{B}}\Big|_{SS_{\mathcal{B}}} \equiv \begin{bmatrix} C_1 - D & \vdots & D \\ \cdots & & \cdots \\ D & \vdots & C_2 - D \end{bmatrix} \tag{5.97}$$

Let $T^A \equiv traceA$, $t^A \equiv detA$ for any 2×2 matrix A. The characteristic equation of $J_{\mathcal{B}}$ can be expressed in the form

$$\lambda^4 + \beta_1\lambda^3 + \beta_2\lambda^2 + \beta_3\lambda + \beta_4 = 0 \tag{5.98}$$

where

$$\begin{aligned} \beta_1 &= 2T^D - (T^{C_1} + T^{C_2}), \\ \beta_2 &= t^{C_1} + t^{C_2} + T^{C_1}T^{C_2} - 2T^D(T^{C_1} + T^{C_2}) + T^{C_1}D + T^{C_2}D + 4t^D, \\ \beta_3 &= -[T^{C_2}t^{C_1} + T^{C_1}t^{C_2} + T^{C_2}T^{C_1 D} + T^{C_1}T^{C_2 D} \\ &\quad -T^D(t^{C_2} + t^{C_1} + 2T^{C_1}T^{C_2}) + 2t^D(T^{C_1} + T^{C_2})], \\ \beta_4 &= t^{C_1}t^{C_2} - T^D(T^{C_1}t^{C_2} + T^{C_2}t^{C_1}) + T^{C_1 D}T^{C_2 D} \\ &\quad +T^{C_2 D}t^{C_1} + T^{C_1 D}t^{C_2} - T^{C_2 D}t^{C_1 D}. \end{aligned}$$

At $SS_{\mathcal{B}} = (\frac{1}{\mu}, \mu, \frac{1}{\mu}, \mu)$, the coefficients $\beta_i, \quad i = 1, 2, 3, 4$, become

$$\begin{aligned}
\beta_1 &= 2(-1 + \beta + \mu^2), \\
\beta_2 &= 1 - 2\beta(1 - 2\mu^2) + \mu^4, \\
\beta_3 &= 2\mu^2(-1 + (1 + \beta)\mu^2), \\
\beta_4 &= \mu^4(1 + 2\beta).
\end{aligned}$$

Applying the Routh-Hurwitz criteria, the conditions for stability can be determined as

$$\beta_i > 0, \quad i = 1, 2, 3, 4, \tag{5.99}$$

$$\beta_5 = \beta_1\beta_2\beta_3 - \beta_3^2 - \beta_4\beta_1^2, \tag{5.100}$$

so that

$$\beta_5 = 4\mu^2(-1 + \mu^2)(-1 + 2\beta + \mu^2)[1 - \beta + 2(-1 + \beta^2)\mu^2 + (1 + \beta)\mu^4]. \tag{5.101}$$

Here β_5 is the fifth Routh-Hurwitz inequality and it vanishes at $\mu = 1$. It can be easily seen that the condition (5.99) is also satisfied at $\mu = 1$. Since the Jacobian given in (5.95) has pair of eigenvalues with zero real part, the Hopf bifurcation occurs for the system {(5.8)-(5.11)} at $\mu = 1$ for all β.

5.5.2 Numerical methods

One-step methods are developed by approximating the derivatives $dx_k(t)/dt$ and $dy_k(t)/dt, k = 1, 2$, by first-order replacements (forward-difference approximants). The Euler formulae are given by

$$(X1_{n+1} - X1_n)/\ell = \mu - X1_n Y1_n^2, \tag{5.102}$$

$$(Y1_{n+1} - Y1_n)/\ell = X1_n Y1_n^2 - Y1_n + \beta(Y2_n - Y1_n), \tag{5.103}$$

$$(X2_{n+1} - X2_n)/\ell = \mu - X2_n Y2_n^2, \tag{5.104}$$

$$(Y2_{n+1} - Y2_n)/\ell = X2_n Y2_n^2 - Y2_n + \beta(Y1_n - Y2_n). \tag{5.105}$$

The alternative finite-difference formulae are developed by modelling the non-linear terms non-locally as in the previous sections, giving

$$(X1_{n+1} - X1_n)/\ell = \mu - X1_{n+1}Y1_{n+1}Y1_n, \tag{5.106}$$

$$(Y1_{n+1} - Y1_n)/\ell = X1_nY1_{n+1}Y1_n - Y1_{n+1} + \beta(Y2_n - Y1_{n+1}), \tag{5.107}$$

$$(X2_{n+1} - X2_n)/\ell = \mu - X2_{n+1}Y2_{n+1}Y2_n, \tag{5.108}$$

$$(Y2_{n+1} - Y2_n)/\ell = X2_nY2_{n+1}Y2_n - Y2_{n+1} + \beta(Y1_n - Y2_{n+1}) \tag{5.109}$$

where $n = 0, 1, 2, \ldots$ The general form of the local truncation errors associated with the Euler formulae and the alternative finite-difference scheme are given by

$$\mathscr{L}1_{x_k}[x_k(t), y_k(t); \ell] = \frac{1}{2}x_k''(t)\ell^2 + O(\ell^3) \quad \text{as} \quad \ell \to 0, \tag{5.110}$$

$$\mathscr{L}1_{y_k}[x_k(t), y_k(t); \ell] = \frac{1}{2}y_k''(t)\ell^2 + O(\ell^3) \quad \text{as} \quad \ell \to 0, \tag{5.111}$$

and

$$\mathscr{L}2_{x_k}[x_k(t), y_k(t); \ell] = (\frac{1}{2}x_k'' + x_k'y_k^2 + x_ky_ky_k')\ell^2 + O(\ell^3) \quad \text{as} \quad \ell \to 0, \tag{5.112}$$

$$\mathscr{L}2_{y_k}[x_k(t), y_k(t); \ell] = [\frac{1}{2}y_k'' - y_k'(x_ky_k - 1 - \beta)]\ell^2 + O(\ell^3) \quad \text{as} \quad \ell \to 0. \tag{5.113}$$

respectively, $k = 1, 2$.

5.5.3 Stability analysis of numerical methods

The Jacobian for $M1_{\mathcal{B}}$ (Euler) is

$$J_{\mathcal{B}_{M1}} = \begin{bmatrix} 1 - \ell Y1^2 & -2\ell X1Y1 & 0 & 0 \\ \ell Y1^2 & 1 - \ell(1 - 2X1Y1 + \beta) & 0 & \beta\ell \\ 0 & 0 & 1 - \ell Y2^2 & -2\ell X2Y2 \\ 0 & \beta\ell & \ell Y2^2 & 1 - \ell(1 - 2X2Y2 + \beta) \end{bmatrix} \tag{5.114}$$

At $SS_{\mathcal{B}} = (\frac{1}{\mu}, \mu, \frac{1}{\mu}, \mu)$, $J_{\mathcal{B}_{M1}}$ becomes

$$\begin{bmatrix} 1-\ell\mu^2 & -2\ell & 0 & 0 \\ \ell\mu^2 & 1+\ell(1-\beta) & 0 & \beta\ell \\ 0 & 0 & 1-\ell\mu^2 & -2\ell \\ 0 & \beta\ell & \ell\mu^2 & 1+\ell(1-\beta) \end{bmatrix} \tag{5.115}$$

and its characteristic equation $\Psi_{M1_{\mathcal{B}}}(\lambda) = 0$ can be expressed in a simplified form as

$$\overbrace{[(-1+\lambda)(-1-\ell+\lambda)+\ell(-1+\ell+\lambda)\mu^2]}^{\Psi_1}$$

$$\underbrace{\{(-1+\lambda)[-1+\ell(-1+2\beta)+\lambda]+\ell[-1+\ell(1+2\beta)+\lambda\mu^2]\}}_{\Psi_2} = 0. \tag{5.116}$$

The same structure of stability analysis in §5.3.3 can be applied here. The inequality

$$\Psi_1(-1) \equiv \ell^2\mu^2 + 2(1-\mu^2)\ell + 4 > 0$$

is true if $0 < \ell < 2$. On the other hand $\Psi_1(1) \equiv \mu^2\ell^2$ is always true. The other necessary condition, $\Psi_{1,2}(\lambda)$ has a minimum which has magnitude less than 1, is satisfied when

$$\frac{d\Psi_1(\lambda)}{d\lambda} = \ell(\mu^2-1) + 2(\lambda-1) = 0$$

that is when

$$\lambda_{min} = \frac{1}{2}[2+\ell(1-\mu^2)]$$

and $|\lambda_{min}| < 1$ is satisfied if $0 < \ell < \dfrac{4}{\mu^2-1}$. Now,

$$\Psi_2(-1) \equiv \mu^2(1+2\beta)\ell^2 - 2(\mu^2+2\beta-1)\ell + 4 > 0$$

is true if $0 < \ell < \dfrac{2}{1+2\beta}$ for $\mu > 1$ and $\Psi_2(1) \equiv \mu^2(1+2\beta)\ell^2 > 0$ is always true. The expression $\Psi_2(\lambda)$ has minimum value

$$\lambda_{min} = \frac{1}{2}[2-\ell(\mu^2+2\beta-1)]$$

which has magnitude less than 1 if $0 < \ell < \dfrac{4}{\mu^2+2\beta-1}$. The overall stability condition is

$$0 < \ell < \frac{4}{\mu^2+2\beta-1} \quad \text{for} \quad \mu > 1.$$

The Jacobian for the alternative finite-difference formulae, $M2_\beta$, is

$$J_{\mathcal{B}_{M2}} = \begin{bmatrix} b_{11} & b_{12} & b_{13} & b_{14} \\ b_{21} & b_{22} & b_{23} & b_{24} \\ b_{31} & b_{32} & b_{33} & b_{34} \\ b_{41} & b_{42} & b_{43} & b_{44} \end{bmatrix} \tag{5.117}$$

where

$$b_{11} = \frac{1}{[h+\ell(Y1+\ell\beta Y2)Y1]^2} \quad [h-\ell Y1(X1+\ell\mu)]$$
$$[h+\ell(Y1+\ell\beta Y2)Y1]+h\ell Y1(X1+\ell\mu)$$

$$b_{12} = \frac{1}{[h+\ell(Y1+\ell\beta Y2)Y1]^2} \quad -\ell X1(X1+\ell\mu)[h+\ell(Y1+\ell\beta Y2)Y1]$$
$$+\ell h(X1-2Y1-\ell\beta Y2)(X1+\ell\mu)$$

$$b_{13} = 0 \quad b_{14} = \frac{-h\ell^2\beta Y1(X1+\ell\mu)}{[h+\ell(Y1+\ell\beta Y2)Y1]^2}$$

$$b_{21} = \frac{\ell Y1(Y1+\ell\beta Y2)}{h^2} \quad b_{22} = \frac{h+\ell X1(Y1+\ell\beta Y2)}{h^2} \quad b_{23} = 0 \quad b_{24} = \frac{\ell\beta}{h}$$

$$b_{31} = 0 \quad b_{32} = \frac{-\beta\ell^2 kY2(X2+\ell\mu)}{[k+\ell Y2(Y2+\ell\beta Y1)]^2}$$

$$b_{33} = \frac{1}{[k+\ell(Y2+\ell\beta Y1)Y2]^2} \quad [k-\ell Y2(X2+\ell\mu)]$$
$$[k+\ell(Y2+\ell\beta Y1)Y2]+k\ell Y2(X2+\ell\mu)$$

$$b_{34} = \frac{1}{[h+\ell(Y2+\ell\beta Y1)Y2]^2} \quad -\ell X2(X2+\ell\mu)[k+\ell(Y2+\ell\beta Y1)Y2]$$
$$+\ell k(X2-2Y2-\ell\beta Y1)(X2+\ell\mu)$$

$$b_{41} = 0 \quad b_{42} = \frac{\ell\beta}{k}$$

$$b_{43} = \frac{\ell Y2(Y2+\ell\beta Y1)}{k^2} \quad b_{44} = \frac{k+\ell X2(Y2+\ell\beta Y1)}{k^2}$$

The matrix $J_{\mathcal{B}_{M2}}$ at $SS_{\mathcal{B}}$ may be expressed in a simpler form as

$$J_{\mathcal{B}_{M2}}\Big|_{SS_{\mathcal{B}}} = \begin{bmatrix} \mathcal{C} & \vdots & \mathcal{D} \\ \cdots & \cdots & \cdots \\ \mathcal{D} & \vdots & \mathcal{C} \end{bmatrix} \tag{5.118}$$

where

$$\mathcal{C} = \begin{bmatrix} \dfrac{1-\ell(\beta+\ell\mu^2)}{(1+\ell\beta)(1+\ell\mu^2)} & \dfrac{-\ell[2+\ell(1+\beta)]}{(1+\ell\beta)(1+\ell\mu^2)} \\ \dfrac{\ell\mu^2}{1+\ell\beta} & \dfrac{1+\ell}{1+\ell\beta} \end{bmatrix} \tag{5.119}$$

and

$$\mathcal{D} = \begin{bmatrix} 0 & \dfrac{-\ell^2\beta}{(1+\ell\beta)(1+\ell\mu^2)} \\ 0 & \dfrac{\ell\beta}{1+\ell\beta} \end{bmatrix} \tag{5.120}$$

The characteristic equation $\Pi_{M2_B}(\lambda) = 0$ can be expressed in a simplified form as

$$\Pi_{M2_B}(\lambda) \equiv \frac{1}{(1+\ell\beta)^2(1+\ell\mu^2)^2} \underbrace{\overbrace{(((-1+\lambda)^2+\ell^2(1+\beta(-1+\lambda)\lambda))\mu^2+\ell(-1+\lambda)(-1+\beta(-1+\lambda)+\lambda\mu^2))}^{\Pi_1} \underbrace{((-1+\lambda)^2+\ell^2(1+\beta\lambda(1+\lambda))\mu^2+\ell(-1+\lambda)(-1+\beta+\beta\lambda+\lambda\mu^2)))}_{\Pi_2} = 0.}_{} \tag{5.121}$$

A stability analysis similar to that in §5.3.1 can be applied here. Now,

$$\Pi_1(-1) \equiv \frac{[2+\ell(1+2\beta)](2+\ell\mu^2)}{(1+\ell\beta)^2(1+\ell\mu^2)^2} > 0$$

is always true and

$$\Pi_1(1) \equiv \frac{[\ell^2\mu^2}{(1+\ell\beta)^2(1+\ell\mu^2)^2} > 0$$

is always true as well. The other necessary condition, $\Pi_{1,2}(\lambda)$ has a minimum which has magnitude less than 1, is satisfied when

$$\frac{d\Pi_1(\lambda)}{d\lambda} = \frac{1}{(1+\ell\beta)^2(1+\ell\mu^2)^2} \{2(-1+\lambda) + \ell[-1-2\beta+2\beta\lambda+(1+\ell\beta)(-1+2\lambda)\mu^2]\} = 0,$$

that is, when

$$\lambda = \lambda_{min} = \frac{1}{2} + \frac{1+\ell\beta}{2[1+\ell(\beta+\mu^2+\ell\beta\mu^2)]}.$$

It is obvious that $\lambda_{min} > 0$, and also that $\lambda_{min} < 1$. Now,

$$\Pi_2(-1) \equiv (2+\ell)(2+\ell\mu^2) > 0$$

is always true as is the inequality

$$\Pi_2(1) \equiv \ell^2(1+2\beta)\mu^2 > 0.$$

The expression $\Psi_2(\lambda)$ has a minimum value

$$\frac{d\Pi_2(\lambda)}{d\lambda} = -2 - \ell + 2\lambda + 2\ell\beta\lambda + \ell[-1 + 2\lambda + \ell(\beta + 2\beta\lambda)]\mu^2$$

when

$$\lambda_{min} = \frac{2 + \ell(1 + \mu^2 - \ell\beta\mu^2)}{2[1 + \ell(\beta + \mu^2 + \ell\beta\mu^2)]}.$$

It can be easily seen that the condition $|\lambda_{min}| < 1$ is satisfied without any restrictions. This proves that method $M2_{\mathcal{B}}$ is unconditionally stable.

5.5.4 Numerical experiments

The diffusion-coupled isothermal problem {(5.2),(5.3)} was studied for the case of coupling through $\mathcal{B}$ by using first-order finite-difference schemes. The unconditionally stable finite-difference scheme, $M2_{\mathcal{B}}$, was tested and compared to the Euler method in a series of experiments.

The numerical results were produced using the alternative finite-difference method, $M2_{\mathcal{B}}$, with $\ell = 1.0$ and with the inital conditions $X1(0) = 1.05$, $Y1(0) = 0.8$, $X2(0) = 1.08$, $Y2(0) = 0.9$.

Using a strong coupling constant, $\beta \geq 0.3$, reduces the two-cell problem to the uncoupled problem which was studied in detail in Chapter 4.

A weak coupling constant, $\beta \leq 0.3$, was also used and as μ was increased away from the supercritical Hopf bifurcation point, $\mu = 1$, stable periodic behaviour was observed, Fig. 5.7, until the cyclic fold bifurcation was reached. This point is actually the point of collision of the stable and unstable periodic orbits. At $\mu = 0.935$ hysteresis occurred, Fig. 5.8, and a jump was made across the unstable periodic orbit to the co-existing stable periodic orbit at $\mu = 0.93$, Fig. 5.9. This phenomenon was then followed by a region of quasi-periodic behaviour bounded by secondary Hopf bifurcation, see Figs 5.10, 5.11.

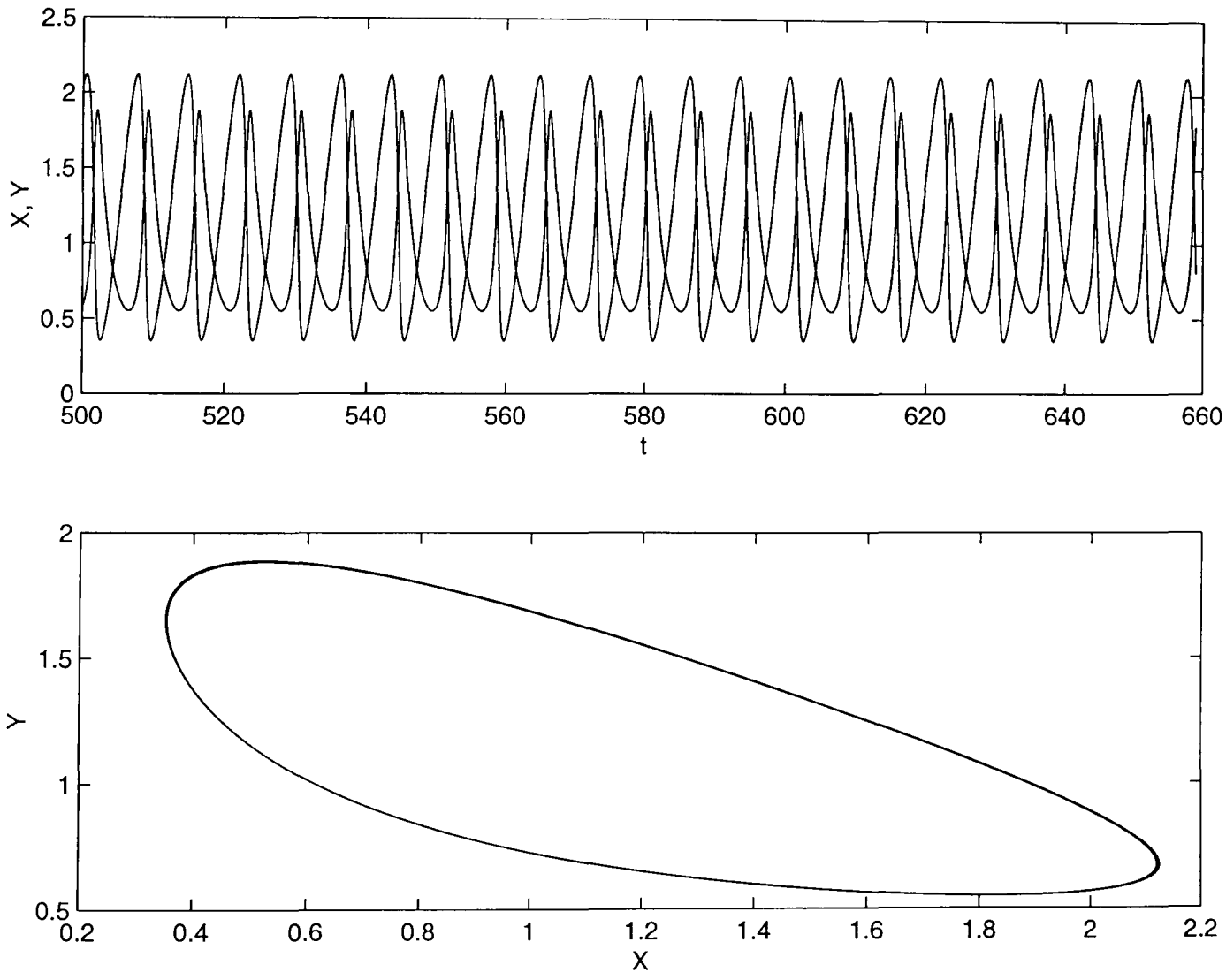

Figure 5.7: Period-one type solutions and corresponding limit cycle at $\mu = 0.96$.

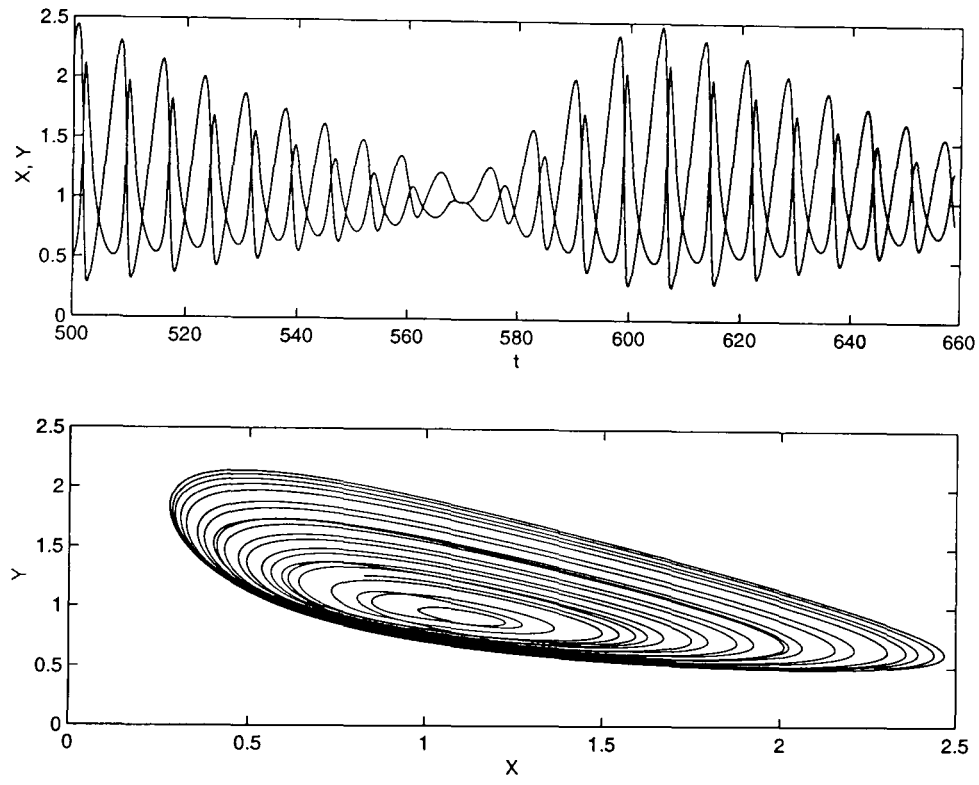

Figure 5.8: Hysteresis occurs at $\mu = 0.935$.

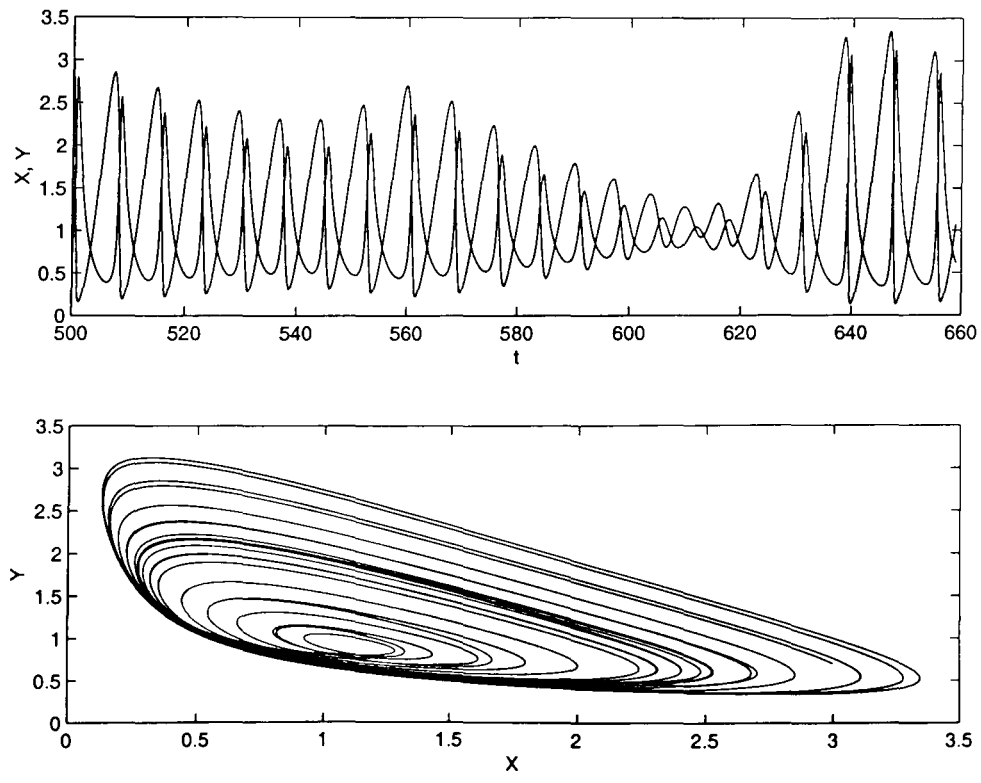

Figure 5.9: Hysteresis occurs at $\mu = 0.93$.

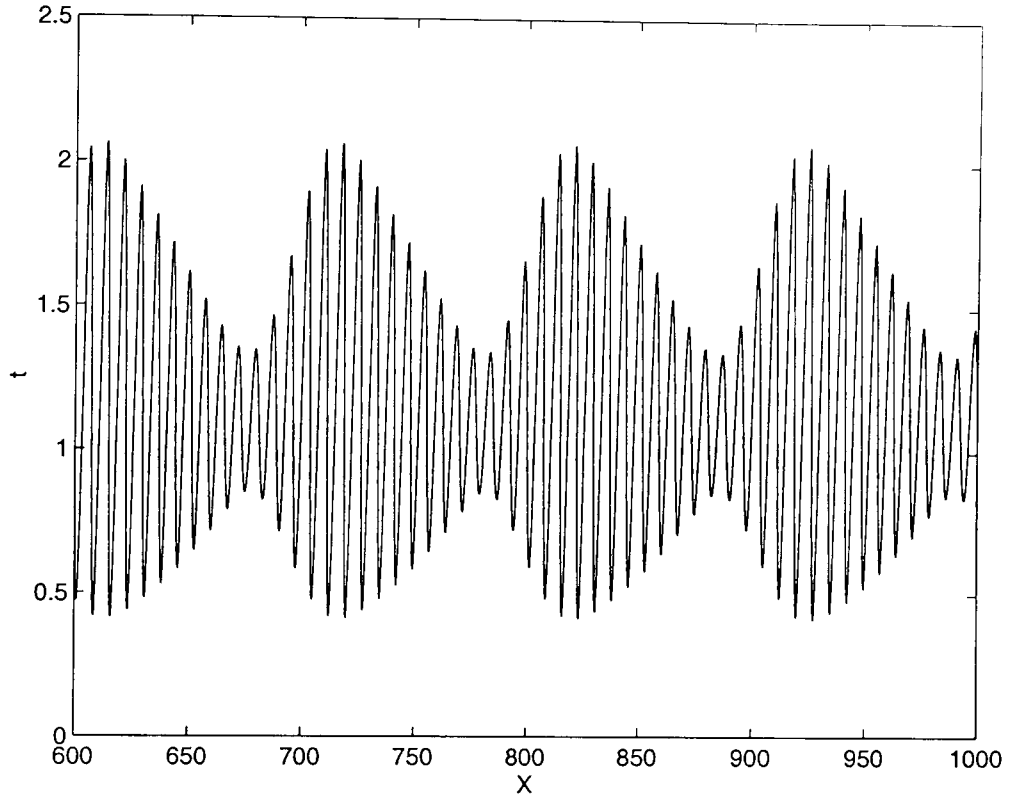

Figure 5.10: Quasi-periodic transitions in coupling through $\mathcal{B}$ at $\mu = 0.925$.

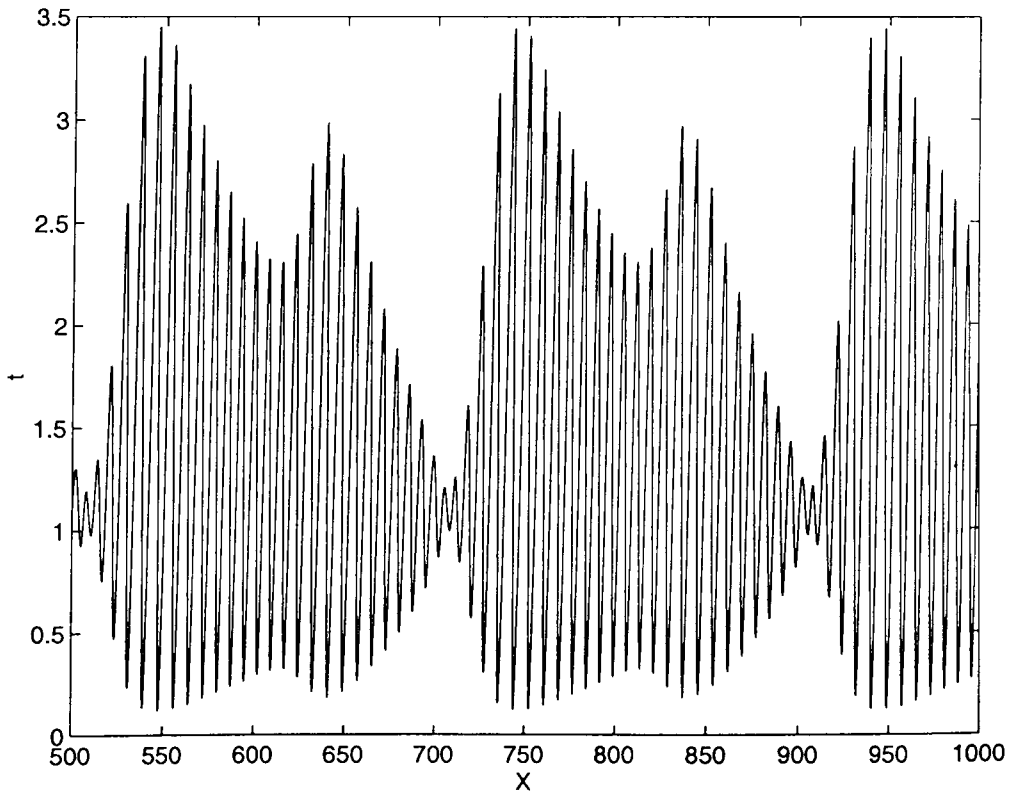

Figure 5.11: Quasi-periodic transitions in coupling through $\mathcal{B}$ at $\mu = 0.92$.

5.5.5 Summary

First- and second-order finite-difference schemes have been developed for the numerical solution of a diffusion-coupled oscillator problem, {(5.2),(5.3)}.

The coupling of two chemical oscillators *via* linear diffusive coupling produced a variety of complex behaviour and multiple stationary states. When coupling was arranged through the non-autocatalytic intermediate $\mathcal{A}$, multiple non-symmetric and symmetric stationary states, period doubling and flip, fold and also Hopf-type bifurcations occurred. When coupling is arranged through the autocatalytic species $\mathcal{B}$, the model did not show any multiple stationary states. A secondary Hopf bifurcation produced quasi-periodicity with its corresponding regular motion.

Some of the numerical results in the literature, such as Leach *et al.* [29], were used to establish the reliability of the alternative finite-difference schemes. The proposed numerical methods confirmed most of the complex dynamical behaviour of the coupled oscillator system. Although all the methods were implicit in nature, with the resulting improvements in stability, the methods were applied explicitly. It was also seen that all the numerical methods presented here are regular methods due to the fact that they don't have any spurious solutions. The resulting schemes can be extended into the long term dynamics of numerical methods incorporating local error control and adaptive stepsizes.

Chapter 6

The Development of Organisms

6.1 Introduction

Living organisms can be described by functional and morphological order. Roots, leaves, branches, skin and hair all appear with a well-defined order and relationship with respect to each other. This remarkable attribute of living species is engraved in tiny seeds and minute fertilized eggs. A fertilized egg is subject to cell division. It divides and multiplies into many thousands of cells. At the same time qualitative changes appear in the cell population. They transform, for example, into blood, skin, or liver cells. This process of transforming the fertilized egg into a grown adult organism is awesome. Many thousands of inter-related and co-ordinated chemical reactions are produced in order to keep the organism alive and functioning. Actually, this developmental processes reveals a well-defined time and space order in that different events follow each other in an orderly time sequence and at the same time spatial organization is observed in the embryo. In this way time and space coherence seems to be the rule in embryonic development. The birth of multi-cellular organisms consists of three aspects: cell differentiation, pattern formation and morphogenesis. Differentiated cells which have a well-defined spatial location organize themselves according to a well-defined pattern which is transmitted from one generation to the next. The phenomenon of morphogenesis is related to that of pattern formation.

It describes the mechanical processes by which organisms generate their specific form by the arrangement of their various tissues. The systems leading to embryonic development are very complex and contain many physical and chemical transformations which are mostly ill-defined. As a result the development of a comprehensive mathematical model might be impossible. The purpose of theories of morphogenesis is to find universal principles underlying developmental processes in multi-cellular embryos, based on a small number of rules governing cell behaviour. The important concept of morphogenetic fields, defined as an ensemble of functionally-coupled cells governed by the same regulatory processes, is the concept of positional information which suggests that the positions of cells are specified within this morphogenetic field with respect to various reference points. In each cell a genome reads its positional information within the field and differentiates accordingly. The idea that the fate of a cell in a developing embryo is defined by its position within the morphogenetic field was first studied by Driesch in 1890. In 1920, Child [6] used a similar idea and stated that physiological gradients were responsible for pattern formation in the development of species. Then, in 1952, Turing [67] supported these ideas by assuming that some biochemical reactions inside the developing organism may be of a catalytic or cross-catalytic nature and, moreover, that the various substances may diffuse throughout the organism. He could then show that mutual relations between chemical reactions and transport may generate spontaneously chemical concentration patterns within the embryo. In that way a physico-chemical basis for Driesch's hypothesis was found. Turing was a mathematician and his morphogenetic patterns arose from the solutions of a linear ODE and PDE systems which will be explained and discussed in detail in the next chapter. In this way, the reaction-diffusion equations as a source of pattern formation in multi-cellular systems was first recognized in biology. Similar ideas have been developed to describe polarity generation and cell differentiation in morphogenetic fields (Babloyantz [4]; Gierer and Meinhardt [12]).

6.2 Network Structures of Morphogenetic Fields

Network structure seems to be influenced by the interaction of intra-cellular chemical reactions and inter-cellular transfers, and thereby the stability of uniform stationary states of the network. General kinetic mechanism can be considered in both discrete and continuous systems. The former case is applicable at the cellular level, where there is a well-defined unit of structure, while the latter is appropriate to structureless reacting continua. Turing [67] was able to show his ideas for the growing embryo in an isolated ring of cells and also in a continuous tissue. In the literature the equations of concentration change of any number of chemical substances could be found in an arbitrary network, or in a lattice, of compartments or cells inter-connected by semi-permeable membranes, [see, Chapter 5] such as junctional membranes (Loewenstein [31], Furshpawn [11], Othmer *et al.* [54]). To be able to understand Turing's structure better, as described in the next chapter, basic network structures must be considered.

6.2.1 The discrete models

The prototype for a discrete system is a network of cells, coupled together *via* junctional membranes through which one or more of the reacting species can diffuse. The general structure of discrete forms can be described as

$$\frac{dc^{\mu}}{dt} = D\Delta^{\mu}c^{\mu} + R(c^{\mu}) \tag{6.1}$$

$$c^{\mu}(0) = c_0^{\mu}$$

where $\mu = 1, \ldots, N$ is the cell index, $c^{\mu} = (c_1^{\mu}, \ldots, c_n^{\mu})^T$ is the concentration vector and N is the number of cells. The difference operator Δ^{μ} is the appropriate version of the Laplacian and is defined by

$$\Delta^{\mu}c^{\mu} = \sum_{\upsilon}(c^{\upsilon} - c^{\mu}). \tag{6.2}$$

The diagonal matrix D is the diffusion matrix. $R(\mu)$ represents the reaction kinetics and satisfies Lipschitz condition.

6.2.2 A one-dimensional morphogenetic field

It can be considered that a piece of biological tissue with its hundreds of divided cells is actually different from a chemical vessel of the same size containing a homogeneous mixture. Since cell communication is mediated by highly non-linear biochemical processes, such as pumps, channels and gap junctions, a pair of dynamic equations is needed for each cell which express the passage of chemicals from one cell to the next. The formulation can be explained for a one-dimensional morphogenetic field; however, it may be extended easily to the actual three-dimensional tissues, [54]. Consider a multi-cellular system composed of N identical cells. In each cell there are m reacting chemical substances which interact according to kinetic laws which are noted by a function $f^l(X_i^1, \ldots, X_i^m)$. The concentration X_i^l of substance l in cell i changes in time for two reasons: firstly, X_i^l is consumed or produced inside the cell i, or is modified by losses or gains through interaction with its nearest neighbours, cells $i+1$ and $i-1$. Secondly, the complex inter-cellular communication processes are represented by contact functions $g^l(X_{i+1})$ and $g^l(X_{i-1})$ which are usually highly non-linear. Therefore, the most general kinetic equations for a one-dimensional morphogenetic field of N cells are:

$$\frac{dX_i^l}{dt} = f^l(X_i^l, \ldots, X_i^m) + g^l(X_{i+1}) + g^l(X_{i-1}),$$

$$l = 1, \ldots, m$$

$$i = 1, \ldots, N.$$

If the proportionality coefficient D describes the permeability of the membranes, and assuming the same permeability for all cells, the contact function for cell i becomes

$$g^l = D[X_{i+1}^l + X_{i-1}^l - 2X_i^l]. \tag{6.3}$$

Here, $-2DX_i^l$ describes the loss of X_i^l from cell i. If cells are arranged in a closed ring then, due to the symmetry of inter-cellular interactions, the contact function, g^l, given in (6.3), can be written as

$$D[X_{i+1} + X_{i-1} - 2X_i] = 2D[1 - \cos(\frac{2\pi k}{N})]X_i, \; k = 1, \ldots, N.$$

This relation reduces the characteristic equation to N second-degree polynomials. Turing's ring structure is a basic example of one-dimensional lattices, since a ring of N cells, each in contact with two neighbours, is also considered as a periodic, one-dimensional network with a period of N, that is $x^{\mu+N} = x^{\mu}$, Fig. 6.1.

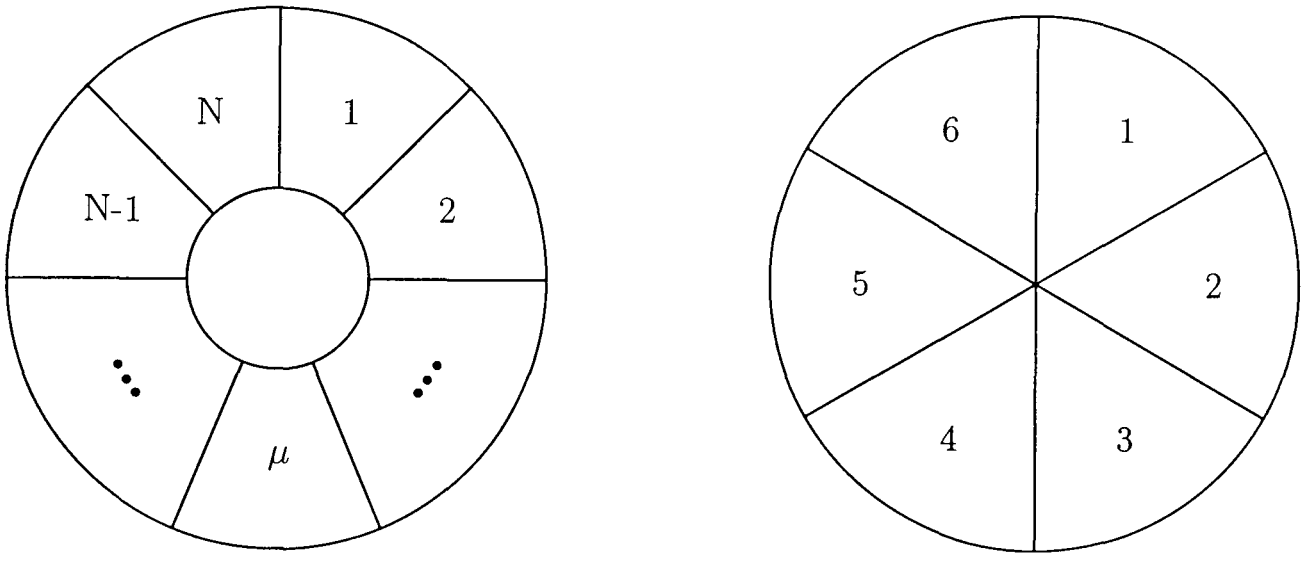

Figure 6.1: Examples of one-dimensional networks.

6.2.3 Two-dimensional morphogenetic field

One-dimensional lattices seem to be simple structures but may not be good enough to reflect real-life networks of living cells. Tissue culture cells generally begin assembling into a two-dimensional rather than one-dimensional network; examples can be found in D'Arcy Thompson's classic review, published in 1942 [66], on parenchymatous tissues and early stages of embryonic development and in Willmer [77] and Lucey and Curtis [32] on their work about epitheliocytes. The structure for one-dimesional lattices can also be applied to two-dimensional lattices with some modifications. The simplest is a doubly-periodic network in which each cell contacts four neighbours, as in Fig. 6.2. Then each cell can be indexed by a pair of co-ordinate

integers (μ, υ); the period is then M in μ and N in υ, that is

$$x^{\mu+M,\upsilon} = x^{\mu,\upsilon} = x^{\mu,\upsilon+N}.$$

The difference operator is defined by

$$\Delta^{\mu,\upsilon} x^{\mu,\upsilon} = x^{\mu+1,\upsilon} - 2x^{\mu,\upsilon} + x^{\mu-1,\upsilon} + x^{\mu,\upsilon+1} - 2x^{\mu,\upsilon} + x^{\mu,\upsilon-1} .$$

It can easily be seen that this is just the sum of the operators in two separate directions, that is $\Delta^{\mu+\upsilon} = \Delta^{\mu} + \Delta^{\upsilon}$.

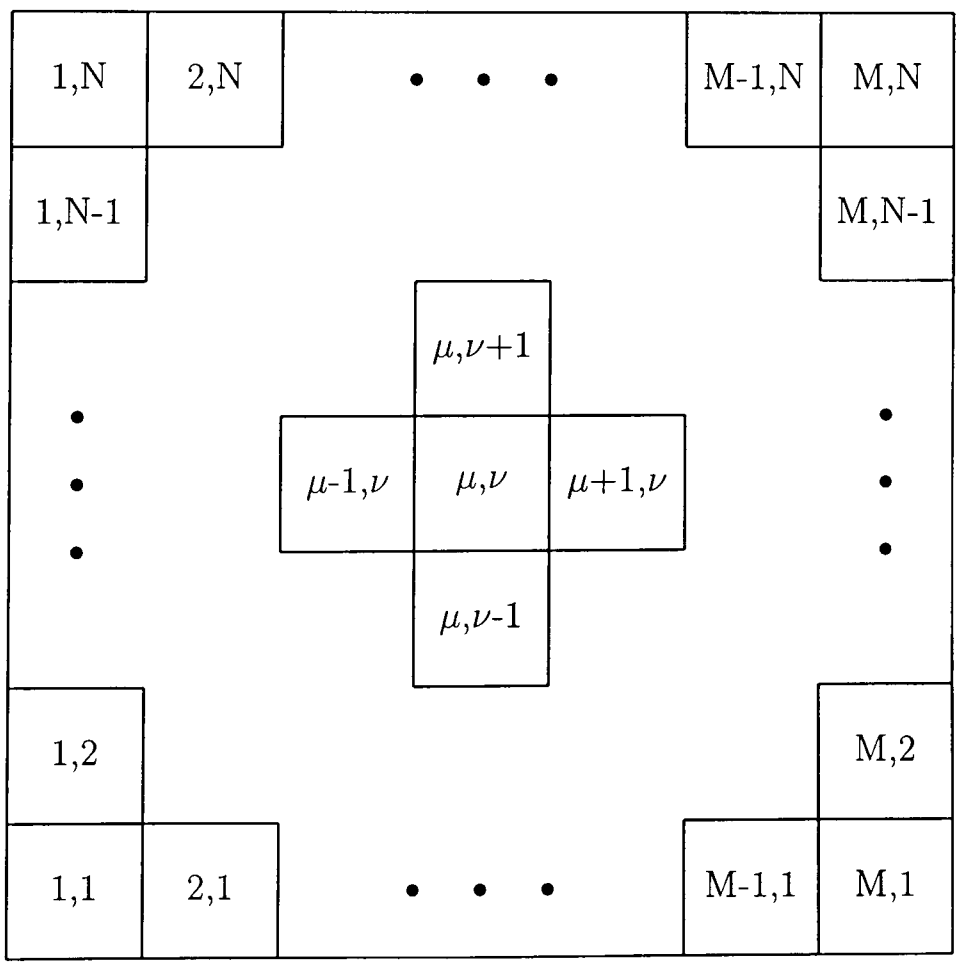

Figure 6.2: Examples of two-dimensional networks.

6.2.4 Polyhedral lattices

In some certain simple multi-cellular organisms, cell-grouping structures are to be observed as nearly spherical or topologically equivalent to a sphere, or some polyhedral network, Thompson [66], see Fig. 6.3.

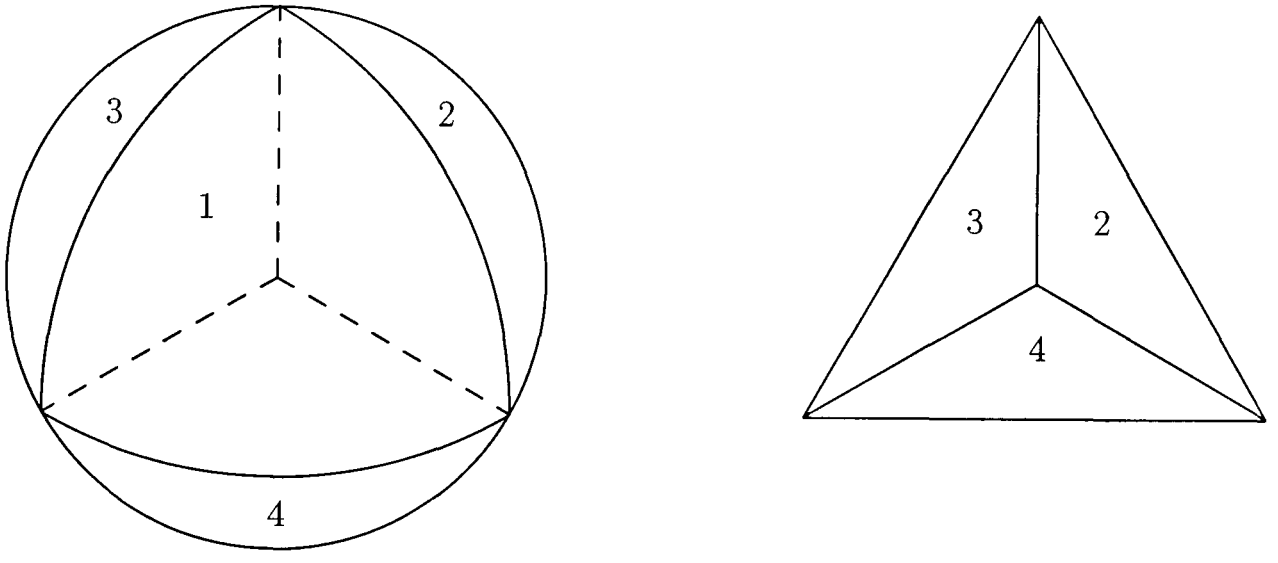

Figure 6.3: Polyhedral networks.

6.2.5 Continuum systems

General kinetic mechanisms in continuum systems are applicable for structureless reacting continua. Let Ω be a bounded region of $\mathbb{R}^p, p \leq 3$. It is assumed that transport in Ω occurs only by passive diffusion and that the flux of species i is given by $j_i = -\mathcal{D}\nabla_{c_i}$, where $\mathcal{D} > 0$ is a constant. If the zero-flux boundary conditions are taken into account then the continuum analogue of the discrete model is

$$\begin{aligned} \frac{\partial c}{\partial t} &= \mathcal{D}\nabla^2 c + R(c) \; in \; \Omega \\ n \cdot \nabla c &= 0 \; on \; \partial\Omega \\ c(r,0) &= c_r \; in \; \Omega, \end{aligned} \tag{6.4}$$

where $\mathcal{D} = diag\{\mathcal{D}_1, \ldots, \mathcal{D}_n\}$ and r is the space coordinate in Ω.

6.3 Summary

Basic network structures which make it possible to generate complete and complex organisms were introduced. A one-dimensional morphogenetic field will be used in the next chapter to explain Turing's theory of morphogenesis as a ring of cells structure.

By considering only linear contact functions and first-neighbour interactions such as Fig. 6.1 it is possible that large developmental field may be approximated quite satisfactorily by a single reaction-diffusion system. However, many fields of study, ranging from biology to the social sciences, focus on a wide variety of system, made a large number of units interconnected by highly non-linear contact functions. The human central nervous system is a very good example of such a complex organization. Each cell of the brain makes a few thousand contacts with the cells of the same tissue.

It seems desirable, therefore, to extend the concept of developing organisms in the multi-unit and multiply connected systems. Generating and implying finite-difference schemes for these type of non-rectangular meshes would be a quite interesting feature study Smith [64].

Chapter 7

Turing's Theory of Morphogenesis

7.1 Introduction

In a classic pioneering paper on biology in 1952 [67], Turing described a model of the growing embryo by discussing a possible mechanism by which the genes of a zygote may determine the anatomical structure of the resulting organism. Turing's theory was based on a consideration of the diffusibilities and reaction rates of substances which may be involved in growth and morphogenesis. He explained that a system of reacting and diffusing chemicals could spontaneously evolve the spatially heterogeneous patterns from an initially uniform state in response to infinitesimal perturbations. He also claimed that diffusion could drive a chemical system to instability, leading to a spatial pattern where no prior pattern existed. The theory introduces no new hypotheses. It makes use of well-known laws of physical chemistry, and, as Turing has shown, these seem likely to be sufficient to account for many of the facts of morphogenesis.

Turing imagined an idealized and simplified model of the embryo. The model takes two slightly different forms. In one form the system is considered as a ring of cells each in contact with its neighbours; in the other the matter of the organism is considered to be a continuous ring of tissue. In both forms Turing solved the equations for small perturbations about the uniform equilibrium solution and he found

that the structures are quite similar. As he pointed out, this is not surprising since the latter situation is a limiting case of the former. Turing also used the bifurcation properties of the solutions of differential equations to explain how a pattern appears in a region which has nothing to serve as a template. He constructed a system of simple PDEs that can plausibly be supposed to govern the concentration of some chemical substance, C say, throughout a region. The equations were designed in such a way that C = constant is always a solution, but it is not always stable. Then, simply by varying the value of a parameter (which in a real situation could correspond to the rate of some reaction or the size of the region), either a homogeneous distribution or else a definite and predictable pattern is obtained. Turing also showed that the model works whether the region is divided into cells or not. Whatever the fate of the reaction-diffusion model itself, these principles are certain to remain fundamental in biological modelling.

Turing specifically considered a system of two chemicals, pattern-forming substances, or morphogens, X and Y, as fundamental metabolites in a morphogenetic process. A third substance C, which is in the nature of an evocator and catalyst, is also involved. That is, one chemical, the activator, stimulates and enchances the production of the other chemical, which, in turn, depletes or inhibits the formation of the activator. It is necessary to assume that i) the morphogens, X and Y, are both diffusible and at different rates, ii) there are a number of reactions involving the substances X, Y and the catalyst C, these reactions not only use the chemicals X and Y, but also tend to produce them from other metabolic substances. Once the appropriate conditions are satisfied, namely that the concentration of the catalyst-evocator is initially at a low value but is slowly increasing, the following phenomena occur:

i) At the beginning there is a state of homogeneity, namely both X and Y are uniformly distributed, except some slight disturbances due to Brownian movement and the possibility of fluctuations in the number of the X and Y molecules that have reacted in different ways in different regions.

ii) The concentration of X and Y will change slowly while the system arranges itself towards the altering evocator concentration. This change will also result in the fluctuations of concentration smoothing themselves out more and more slowly where the system is unstable.

iii) Then the morphogen concentrations start to form an irregular wave pattern. The pattern will then regularize itself, and will eventually reach an equilibrium which is almost perfectly symmetrical. The resulting scheme might be called a stationary wave.

It might be difficult to visualize how, from an initial homogeneous distribution of metabolites in an embryonic region, a drift into instability can occur. Turing has pointed out how the instability may be triggered, for example by random disturbances in the distribution of morphogenetic substances, namely irregularities and statistical fluctuations in the number of molecules taking part in the various reactions. The determination of polarity in the fertilized ovum of Fucus, for instance, may be due to random changes, or to factors in the environment.

This phenomenon can be understood more easily with the following explanation due to Maini [34].

It can be considered that there exists a simple autocatalytic process $\mathcal{A}+\mathcal{B} \rightarrow 2\mathcal{B}$ in an unstirred reactor initially full of chemical $\mathcal{A}$ but not chemical $\mathcal{B}$. Then, no reaction would be observed. If the reaction domain is seeded with $\mathcal{B}$ at various local sites and if $\mathcal{A}$ can diffuse but $\mathcal{B}$ is immobilized, reaction will only occur where there has been seeding, with high concentrations of $\mathcal{B}$ building up at these points. Eventually, $\mathcal{A}$ would disappear and spots of $\mathcal{B}$ would be left. If, however, there is also a decay step for $\mathcal{B}$ to limit its growth, it may be possible to get a balance between supply and diffusion away from $\mathcal{A}$ balancing the decay of $\mathcal{B}$ in the spots, to give a steady-state, long-lived pattern, with high $\mathcal{A}$ concentrations in between the spots and high $\mathcal{B}$ concentration in the spots. The exact pattern of spots would still depend on the precise initial seeding, but Turing makes two predictions: first, this structure could develop spontaneously even from an initially almost homogeneous

distribution of $\mathcal{A}$ and $\mathcal{B}$ provided that $\mathcal{A}$ diffuses more rapidly than $\mathcal{B}$ and, second, the final pattern does not necessarily depend on the initial perturbation if $\mathcal{B}$ has a non-zero diffusivity. Then in this case the spots could arrange their position according to the demands of the local supply and demand due to diffusion and reaction.

That diffusion-reaction systems are present in all growing regions, in all living matter, is a fundamental fact of studies of metabolism. The novelty of Turing's theory is his demonstration that, under appropriate conditions, many different diffusion-reaction systems will eventually give rise to stationary waves and in fact, to a patternized distribution of metabolites.

7.2 Mathematical Model of the Growing Embryo

7.2.1 Reaction and diffusion in a ring of cells

As was mentioned in Chapter 6 there is a great variety of geometrical arrangement of cells which might be considered. That which Turing chose in his structure as a configuration is simple in its theory, and illustrates well the general principles. Turing developed an elegant mathematical solution arising from a circular (ring) configuration. In this he was not only simplifying the network structure but also avoiding the edge effects in a one-dimensional cell structure.

The system is considered as a ring of similar cells each in contact with its neighbours, Fig. 7.1. According to the cell model, the number and positions of the cells are provided, and so are the rates at which the various morphogens diffuse between the cells. It will be assumed that there are only two interacting, pattern-forming substances, or morphogens, X and Y. The concentrations of the two morphogens in cell r, where $1 \leq r \leq N$, will be denoted by X_r and Y_r, respectively. Cell 0 and cell $N+1$ are regarded as being synonymous with cell N and cell 1, respectively. The parameters μ and ν stand for the cell-to-cell diffusion constants for X

and Y, meaning that for unit concentration difference of X (or Y) for each cell the morphogen passes at a rate μ (or ν) from the cell with higher concentration to the neighbouring cell with the lower concentration. The most general assumption that can be made is that, for concentrations X and Y, chemical reactions are tending to increase X at the rate $f(X,Y)$ and Y at the rate $g(X,Y)$. Taking the chemical reaction components and diffusion into account, the deterministic behaviour of the system is then described by the $2N$ differential equations

$$\frac{dX_r}{dt} = f(X_r, Y_r) + \mu(X_{r+1} - 2X_r + X_{r-1}), \tag{7.1}$$

$$\frac{dY_r}{dt} = g(X_r, Y_r) + \nu(Y_{r+1} - 2Y_r + Y_{r-1}), \tag{7.2}$$

$r = 1, \ldots, N$.

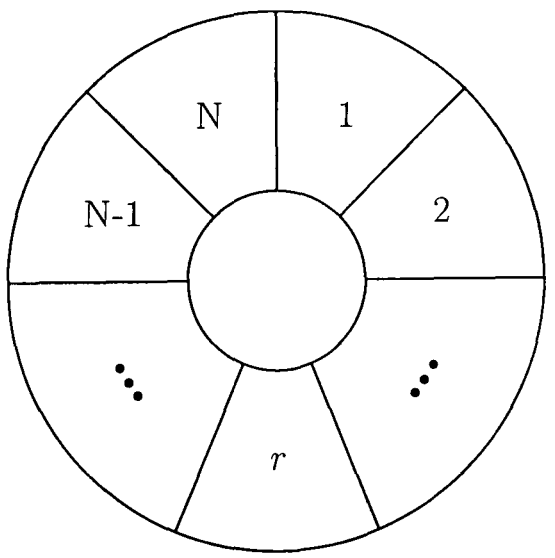

Figure 7.1: Ring of cells structure.

7.2.2 Linearization of rate functions

There is an equilibrium for each cell when the rate functions $f(X,Y)$ and $g(X,Y)$ are made to vanish for some positive values $X = X^*, Y = Y^*$, that is $f(X^*, Y^*) = g(X^*, Y^*) = 0$. The ring system also possesses an equilibrium, stable or unstable, in which each $X_r = X^*$ and $Y_r = Y^*$. Assuming that the departure from homogeneity is sufficiently small, the rate functions $f(X_r, Y_r)$ and $g(X_r, Y_r)$ can be safely taken

as linear functions. Since the ring system is not very far from this equilibrium, consideration of small perturbations x_r and y_r from equilibrium $X_r = X^* + x_r, Y_r = Y^* + y_r$ can be applied. Using Taylor's expansion of the rate function $f(X_r, Y_r)$ around the equilibrium conditions, (X^*, Y^*), gives

$$\begin{aligned} f(X_r, Y_r) &= f(X^* + x_r, Y^* + y_r) \\ &\simeq f(X^*, Y^*) + x_r \frac{\partial f(X^*, Y^*)}{\partial X_r} + y_r \frac{\partial f(X^*, Y^*)}{\partial Y_r} \\ &= 0 + ax_r + by_r \\ &= ax_r + by_r \end{aligned} \tag{7.3}$$

with a similar result for $g(X_r, Y_r)$. Then, for constant local reaction rates a, b, c, d, called marginal reaction rates by Turing, the rate functions f and g may be approximated by

$$f(X_r, Y_r) \simeq ax_r + by_r, \quad g(X_r, Y_r) \simeq cx_r + dy_r. \tag{7.4}$$

As a result of these linear approximations (7.1) and (7.2) take the much simpler forms

$$\frac{dx_r}{dt} = ax_r + by_r + \mu(x_{r+1} - 2x_r + x_{r-1}), \tag{7.5}$$

$$\frac{dy_r}{dt} = cx_r + dy_r + \nu(y_{r+1} - 2y_r + y_{r-1}), \tag{7.6}$$

where $r = 1, \ldots, N$.

7.2.3 Solution of the linearized equations

To solve the equations (7.5) and (7.6), the Fourier transformation of the x_r and y_r can be introduced by writing

$$\xi_r = \frac{1}{N} \sum_{s=1}^{N} x_s \exp(\frac{-2\pi irs}{N}), \tag{7.7}$$

$$\eta_r = \frac{1}{N} \sum_{s=1}^{N} y_s \exp(\frac{-2\pi irs}{N}), \quad i = +\sqrt{-1}. \tag{7.8}$$

These reactions can also be defined as

$$x_r = \sum_{s=0}^{N-1} \xi_s \exp(\frac{2\pi irs}{N}), \tag{7.9}$$

$$y_r = \sum_{s=0}^{N-1} \eta_s \exp(\frac{2\pi irs}{N}), \tag{7.10}$$

by using the equations

$$\sum_{s=1}^{N} \exp(\frac{2\pi irs}{N}) = 0 \quad if\ 0 < r < N, \tag{7.11}$$

$$\sum_{s=1}^{N} \exp(\frac{2\pi irs}{N}) = N \quad if\ r = 0\ or\ r = N. \tag{7.12}$$

In the first expression, (7.10), it is easy to see the result since the left hand side is a geometric series. In the second expression all the terms are equal to 1. Substituting for x_r and y_r from (7.9) and (7.10) in equations (7.5) and (7.6) gives

$$\frac{d\xi_s}{dt} = (a - 4\mu \sin^2 \frac{\pi s}{N})\xi_s + b\eta_s, \tag{7.13}$$

$$\frac{d\eta_s}{dt} = (d - 4\nu \sin^2 \frac{\pi s}{N})\eta_s + c\xi_s. \tag{7.14}$$

The sine terms occur because of Euler's relation $\exp(iz) = \cos(z) + i\sin(z)$, where $i = \sqrt{-1}$. These linear, constant coefficient, ordinary differential equations are quite manageable since, unlike equations (7.9) and (7.10), each pair contains just two variables, ξ_s and η_s. The standard solution form of (7.13) and (7.14) can be written as

$$\xi_s = A_s \exp(p_s t) + B_s \exp(p'_s t), \tag{7.15}$$

$$\eta_s = C_s \exp(p_s t) + D_s \exp(p'_s t), \tag{7.16}$$

where the coefficents A_s, B_s, C_s, D_s satisfy the relations

$$A_s(p_s - a + 4\mu \sin^2 \frac{\pi s}{N}) = bC_s, \tag{7.17}$$

$$B_s(p'_s - a + 4\mu \sin^2 \frac{\pi s}{N}) = bD_s, \tag{7.18}$$

and p_s, p'_s are the roots of the equations

$$(p_s - a + 4\mu \sin^2 \frac{\pi s}{N})(p_s - d + 4\mu \sin^2 \frac{\pi s}{N}) = bc. \tag{7.19}$$

Substituting these results back into (7.9) and (7.10), and replacing the local variables x_r, y_r by the actual concentrations X_r, Y_r, the solution can be written as

$$X_r = X^* + \sum_{1}^{N} [A_s \exp(p_s t) + B_s \exp(p'_s t)] \exp(\frac{2\pi irs}{N}), \tag{7.20}$$

$$Y_r = Y^* + \sum_1^N [C_s \exp(p_s t) + D_s \exp(p'_s t)] \exp(\frac{2\pi i r s}{N}). \tag{7.21}$$

Expressions (7.20) and (7.21) provide the general solution to the equations (7.1) and (7.2) under the assumption that perturbations from equilibrium are sufficiently small that the functions $f(X, Y)$ and $g(X, Y)$ can be replaced by their linear approximations.

7.2.4 Types of behaviour in the ring

The expressions (7.20) and (7.21) are the required mathematical solutions to equations (7.1) and (7.2) but their forms are not really informative. To be able to get more information about the behaviour of the solutions, their properties must be examined. Since the equations contain expressions of the form $\sum A \exp(bt)$, where the quantities A, b may be complex, it is possible to observe three basic types of behaviour as t increases:

a) If b is real and positive then $\exp(bt)$ grows indefinitely large,

b) If b is real and negative then $\exp(bt)$ decays to zero,

c) If b is imaginary, that is $b = i\beta$ for real β, then

$$\exp(bt) = \exp(i\beta t) = \cos(\beta t) + i \sin(\beta t)$$

and so $\exp(bt)$ oscillates.

After a lapse of time the solution pair (7.20) and (7.21) becomes dominated by the terms for which the corresponding p_s has the largest real part. Depending upon this dominant value, whether real or complex, two cases might arise. These are called the stationary and the oscillatory cases, respectively.

Stationary Case : After a sufficient lapse of time $X_r - X^*$ and $Y_r - Y^*$ approach asymptotically the forms

$$X_r - X^* = 2\mathcal{R} A_{s_0} \exp(\frac{2\pi i s_0 r}{N} + It), \tag{7.22}$$

$$Y_r - Y^* = 2\mathcal{R} C_{s_0} \exp(\frac{2\pi i s_0 r}{N} + It). \tag{7.23}$$

Here I represents the real part of p_{s_0} and $\mathcal{R}$ means "real part of". In the stationary case there are s_0 stationary waves arranged around the ring. The coefficients A_{s_0} and C_{s_0} are in a definite ratio (given by (7.17) and (7.18)), so that the pattern for one morphogen defines that for the other. Moreover, if there is genuine instability, that is if the real part of p_{s_0}, I, is positive, then the waves become more pronounced as time elapses.

Oscillatory Case : After a sufficient lapse of time $X_r - X^*$ and $Y_r - Y^*$ approach the forms

$$X_r - X^* = 2\exp(It)\mathcal{R}[A_{s_0}\exp(\frac{2\pi i s_0 r}{N} + iwt) + A_{N-s_0}\exp(-\frac{2\pi i s_0 r}{N} - iwt)], \tag{7.24}$$

$$Y_r - Y^* = 2\exp(It)\mathcal{R}[C_{s_0}\exp(\frac{2\pi i s_0 r}{N} + iwt) + C_{N-s_0}\exp(-\frac{2\pi i s_0 r}{N} - iwt)]. \tag{7.25}$$

In this case the interpretation is similar to that of the stationary case except that waves are not stationary but travelling; two wave trains move around the ring in opposite directions. Turing classifies the development of wave patterns for these two cases in the following caterogies.

a) Stationary case with extremely long wave-length : This case happens for example if

$$\mu = \nu = \frac{1}{4}, \quad b = c = 1, \quad a = d$$

then

$$p_s = a - \sin^2(\frac{\pi s}{N}) + 1 \tag{7.26}$$

is real, positive and takes its maximum value when $s = 0$. The contents of all the cells are the same; there is no resultant flow from cell to cell and so each behaves as if it is isolated. The general condition for this case might be summarized as

$$bc > 0, \quad \text{or}$$

$$bc < 0 \quad \text{and} \quad \frac{(d-a)}{\sqrt{(-bc)}} > \frac{(\mu' + \nu')}{\sqrt{(\mu'\nu')}}$$

or

$$bc < 0 \quad \text{and} \quad \frac{(d-a)}{\sqrt{(-bc)}} < -2\,.$$

The condition for instability is that either $bc > ad$ or $a + d > 0$.

b) Oscillatory case with extremely long wave-length : If

$$\mu = \nu = \frac{1}{4}, \quad b = -c = 1, \quad a = d,$$

then

$$p_s = a - \sin^2(\frac{\pi s}{N}) \pm i \tag{7.27}$$

which is complex and has greatest real part when $s = 0$. As in case **a)** each cell behaves as if it were isolated, with an oscillatory departure from equilibrium. The general condition is

$$bc > 0 \quad \text{and} \quad -2 < \frac{(d-a)}{\sqrt{(-bc)}} < \frac{4\sqrt{(\mu'\nu')}}{\mu' + \nu'}.$$

Instability occurs if, in addition, $a + d > 0$.

c) Stationary waves of extremely short wave-length : This case occurs, for instance, if

$$\nu = 0, \mu = 1, d = I, a = I - 1, b = -c = 1$$

then

$$p_s = I - \frac{1}{2} - 2\sin^2(\frac{\pi s}{N}) + \sqrt{[(2\sin^2\frac{\pi s}{N} + \frac{1}{2})^2 - 1]}, \tag{7.28}$$

and p_s is greatest when $\sin^2(\frac{\pi s}{N})$ is greatest. The general condition is that

$$bc > 0, \quad \mu' > \nu' = 0$$

with instability if, in addition, $a + d > 0$.

d) Stationary waves of finite wave-length : This is the case of greatest biological interest. It occurs, for example, if

$$a = I - 2, b = 2.5, c = -1.25, d = I + 1.5, \mu' = 1, \nu' = \frac{1}{2}$$

and

$$\frac{\mu}{\mu'} = \frac{\nu}{\nu'} = (\frac{N}{2\pi\rho})^2.$$

If $U = (\frac{N}{\pi\rho})^2 \sin^2(\frac{\pi s}{N})$ then equation (7.19) becomes

$$(p-I)^2 + (\frac{1}{2} + \frac{3}{2}U)(p-I) + \frac{1}{2}(U - \frac{1}{2})^2 = 0 \tag{7.29}$$

which has solution $p = I$ if $U = \frac{1}{2}$. If the radius of the ring ρ is chosen so that for some integer s_0,

$$\frac{1}{2} = U = (\frac{N}{\pi\rho})^2 \sin^2 \frac{\pi s_0}{N}$$

then there will be s_0 stationary waves around the ring since every other p_s will have a real part smaller than I. If the radius, ρ, is chosen so that

$$(\frac{N}{\pi\rho})^2 \sin^2 \frac{\pi s}{N} = \frac{1}{2}$$

in which s is not an integer, then the actual number of waves is one of the two nearest integers to s_0. The general condition for this case is

$$bc < 0 \quad \text{and} \quad \frac{4\sqrt{(\mu'\nu')}}{\mu' + \nu'} < \frac{(d-a)}{\sqrt{(-bc)}} < \frac{(\mu' + \nu')}{\sqrt{(\mu'\nu')}}$$

with instability occuring if in addition for $0 < \nu' \leq \mu'$

$$\frac{d}{\sqrt{(-bc)}}\sqrt{\frac{\mu'}{\nu'}} - \frac{a}{\sqrt{(-bc)}}\sqrt{\frac{\nu'}{\mu'}} > 2.$$

The case where $0 < \mu' \leq \nu'$ can be obtained by interchanging the two morphogens. The remaining other possibilities can only occur at the presence of at least three morphogens; with just one morphogen the only possibility is (a).

e) Oscillatory case with a finite wave-length : This means that there are two sets of travelling waves which may move around the ring, one travelling clockwise and the other anticlockwise.

f) Oscillatory case with extremely short wave-length : In this case metabolic oscillation occurs with neighbouring cells nearly 180° out of phase.

7.3 Numerical Examples

Turing has suggested two numerical examples in his original paper Turing [67]. The following details have to be given for any numerical example:

i) The number and dimensions of the cells of the ring, N, ρ,

ii) The diffusibilities of the morphogens, μ, ν,

iii) The reactions considered,

iv) The rates at which the reactions occur, f, g,

v) Information about random disturbances,

vi) Information about the distribution, in space and time, of those morphogens which are of the nature of evocators.

7.3.1 Six-cell problem

The general scheme of the system of autocatalytic chemical reactions between diffusing components proposed by Turing is

$$\begin{array}{ccccccc} \mathcal{A} & \longrightarrow & \mathcal{X} & \longrightarrow & \mathcal{C} & \longrightarrow & \mathcal{D} \\ & & \mathcal{B} & \xrightarrow{(\mathcal{C},\mathcal{W})} & \mathcal{Y} & \xrightarrow{(\mathcal{V},\mathcal{V}')} & \mathcal{E} \end{array}$$

Here two initial products, $\mathcal{A}$ and $\mathcal{B}$, are transformed into the final, or waste, products $\mathcal{D}$ and $\mathcal{E}$ through the intermediate products $\mathcal{X}$ and $\mathcal{Y}$ and by the action of the catalysts $\mathcal{C}, \mathcal{W}, \mathcal{V}, \mathcal{V}'$. More specifically, the set of chemical reactions are

$\mathcal{A} \to \mathcal{X}$	at the rate	$10^{-3}\mathcal{A}, \mathcal{A} = 10^{-3}$
$\mathcal{X} + \mathcal{Y} \to \mathcal{C}$	at the rate	$10^{3}\mathcal{X}\mathcal{Y}$
$\mathcal{C} \to \mathcal{X} + \mathcal{Y}$	at the rate	$10^{6}\mathcal{C}$
$\mathcal{C} \to \mathcal{D}$	at the rate	$62.5\mathcal{C}$
$\mathcal{B} + \mathcal{C} \to \mathcal{W}$	at the rate	$0.125\mathcal{B}\mathcal{C}, \mathcal{B} = 10^{3}$
$\mathcal{W} \to \mathcal{Y} + \mathcal{C}$	instantly	
$\mathcal{Y} \to \mathcal{E}$	at the rate	$0.0625\mathcal{Y}$
$\mathcal{Y} + \mathcal{V} \to \mathcal{V}'$	instantly	
$\mathcal{V}' \to \mathcal{E} + \mathcal{V}$	at the rate	$62.5\mathcal{V}'\mathcal{V}' = 10^{-3}\beta$

The effect of the reactions $\mathcal{X} + \mathcal{Y} \rightleftharpoons \mathcal{C}$ is $\mathcal{C} = 10^{-3}\mathcal{X}\mathcal{Y}$. The reaction $\mathcal{C} \to \mathcal{D}$ destroys $\mathcal{C}$ and hence both $\mathcal{X}$ and $\mathcal{Y}$, at the rate $\frac{1}{16}\mathcal{X}\mathcal{Y}$. The reaction $\mathcal{A} \to \mathcal{X}$ forms

$\mathcal{X}$ at the constant rate $\frac{1}{16}\beta$. The reactions $\mathcal{B}+\mathcal{C} \rightarrow \mathcal{W} \rightarrow \mathcal{Y}+\mathcal{C}$ forms $\mathcal{Y}$ at the rate $\frac{1}{8}\mathcal{X}\mathcal{Y}$, and $\mathcal{Y} \rightarrow \mathcal{E}$ destroys it at the rate $\frac{1}{16}\mathcal{Y}$. Thus, the reaction rate function is such that $\mathcal{X}$ is produced at the rate $f(X,Y) = \frac{1}{16}(16 - \mathcal{X}\mathcal{Y})$, and $\mathcal{Y}$ is produced at the rate $g(X,Y) = \frac{1}{16}(XY - Y - \beta)$. The diffusion constants will be $\mu = \frac{1}{4}$, $\nu = \frac{1}{16}$. The number of cells, N, is 6, and the parameter β gives a measure of the catalytic efficiency of $\mathcal{V}'$.

7.3.2 Mathematical model of the six-cell problem

The resulting deterministic equations for Turing's six-cell structure are

$$\frac{dX_r}{dt} = \frac{1}{16}(16 - X_rY_r) + \mu(X_{r+1} - 2X_r + X_{r-1}), \tag{7.30}$$

$$\frac{dY_r}{dt} = \frac{1}{16}(X_rY_r - Y_r - \beta) + \nu(Y_{r+1} - 2Y_r + Y_{r-1}) \tag{7.31}$$

where $r = 1, \ldots, 6$, $\beta = 12$ and with the given initial conditions such as

$$X_r(0) = X_0 > 0, \quad Y_r(0) = Y_0 > 0. \tag{7.32}$$

The range of values of β is $\beta_c = 12 \leq \beta < 16$ where β_c corresponds to the minimum value of the catalytic parameter β for which instability occur, Prigogine [58].

Equilibrium Point of the Isolated Cells :

The first assumption to be made concerning the parameters of the isolated cell is that it has only one equilibrium point and is stable. This unique equilibrium point could be calculated by solving the following equilibrium equations

$$\frac{1}{16}(16 - X_rY_r) = 0, \tag{7.33}$$

$$\frac{1}{16}(X_rY_r - Y_r - \beta) = 0. \tag{7.34}$$

As Turing pointed out the equilibrium condition gives $X_r^*Y_r^* = 16$ and $Y_r^* = 16 - \beta$, $r = 1, \ldots, 6$. The linear coefficients, (7.5)-(7.6) become

$$a = -\frac{1}{16}Y_r^*,\ b = -\frac{1}{16}X_r^*,\ c = \frac{1}{16}Y_r^*,\ d = \frac{1}{16}X_r^* - \frac{1}{16}.$$

The conditions are to be satisfied for the stationary waves of finite length sub-case d)

$$-\frac{1}{16}X_r^*\frac{1}{16}Y_r^* < 0 \quad \text{and} \quad \frac{4\sqrt{(\mu\nu)}}{\mu+\nu} < \frac{\frac{1}{16}X_r^* + \frac{1}{16}Y_r^* - \frac{1}{16}}{\sqrt{\frac{1}{256}X_r^*Y_r^*}} < \frac{\mu+\nu}{\sqrt{(\mu\nu)}}\,. \tag{7.35}$$

This condition could be summarized as

$$\frac{4}{Y_r^*} + \frac{Y_r^*}{4} < 2.75 \tag{7.36}$$

which will produce an instability if

$$\frac{8}{Y_r^*} + \frac{Y_r^*}{8} < \sqrt{3} + \frac{1}{2}. \tag{7.37}$$

Stability of the Equilibrium Point :

First, the local stability of the equilibrium point of an isolated cell is investigated. The stability problem is linear as Turing suggested and the linearized system around the equilibrium point, (X_r^*, Y_r^*), is asymptotically stable if the characteristic polynomial of the linear state equations

$$\frac{dX_r}{dt} = f_{X_r}X_r + f_{Y_r}Y_r, \tag{7.38}$$

$$\frac{dY_r}{dt} = g_{X_r}X_r + g_{Y_r}Y_r, \tag{7.39}$$

has both of its roots in the open left hand plane, where

$$f_{X_r} = \frac{\partial f}{\partial X_r}\Big|_{(X_r^*,Y_r^*)}, \quad f_{Y_r} = \frac{\partial f}{\partial Y_r}\Big|_{(X_r^*,Y_r^*)}, \quad g_{X_r} = \frac{\partial g}{\partial X_r}\Big|_{(X_r^*,Y_r^*)}, \quad g_{Y_r} = \frac{\partial g}{\partial Y_r}\Big|_{(X_r^*,Y_r^*)}$$

are the elements of the Jacobian matrix of $f(X_r, Y_r)$ and $g(X_r, Y_r)$. The corresponding linearized equations are

$$\frac{dX_r}{dt} = -\frac{1}{(16-\beta)}X_r - \frac{1}{16}(16-\beta)Y_r, \tag{7.40}$$

$$\frac{dY_r}{dt} = \frac{1}{16}(16-\beta)X_r + \frac{1}{16}\frac{\beta}{(16-\beta)}Y_r. \tag{7.41}$$

In terms of $f_{X_r}, f_{Y_r}, g_{X_r}, g_{Y_r}$ the characteristic polynomial is

$$det\begin{bmatrix} f_{X_r}-\lambda & f_{Y_r} \\ g_{X_r} & g_{Y_r}-\lambda \end{bmatrix} = 0$$

that is,

$$\lambda^2 - (f_{X_r} + g_{Y_r})\lambda + f_{X_r}g_{Y_r} - f_{Y_r}g_{X_r} = 0 \tag{7.42}$$

which has roots

$$\lambda_{1,2} = \frac{1}{2}\left(f_{X_r} + g_{Y_r} \pm \sqrt{(f_{X_r} - g_{X_r})^2 + 4f_{X_r}g_{Y_r}}\right). \tag{7.43}$$

To have both roots strictly in the left half plane, the following conditions should be fulfilled simultaneously

$$\begin{aligned} f_{X_r} + g_{Y_r} &< 0, \\ f_{X_r}g_{Y_r} - f_{Y_r}g_{X_r} &> 0. \end{aligned}$$

The first condition assures that, for complex roots, their real part is negative, and the second refers to real roots for which the greatest value should be negative. It is obvious that the values

$$f_{X_r} = -\frac{1}{4}, f_{Y_r} = -\frac{1}{4}, g_{X_r} = \frac{1}{4}, g_{Y_r} = \frac{3}{16}$$

correspond to a stable cell since the eigenvalues are

$$\lambda_{1,2} = \frac{1}{32}(-1 \mp i\sqrt{15}). \tag{7.44}$$

Interconnected Cells :

Since the resulting network (7.30)-(7.31) is much more complex than an isolated cell structure, much more complex dynamics and a diversity of equilibrium points are expected. It can easily be observed that (X^*, Y^*) is still an equilibrium point of the resulting connected cell system. In this case, the cells behave as if they were uncoupled. However, by the usual definition of a Turing pattern, this homogeneous equilibrium point, regarded as an equilibrium for the coupled case, must become unstable so that the array can evolve the other (stable) equilibria depending on the initial and boundary conditions.

Stability of the Interconnected Cells :

The resulting Jacobian for the non-linear case is the 12x12 matrix

$$\begin{bmatrix}
-\frac{1}{4}-2\mu & -\frac{1}{4} & \mu & 0 & \cdots & 0 & 0 & \mu & 0 \\
\frac{1}{4} & -\frac{3}{16}-2\nu & 0 & \nu & \cdots & 0 & 0 & 0 & \nu \\
\mu & 0 & -\frac{1}{4}-2\mu & -\frac{1}{4} & \cdots & 0 & 0 & 0 & 0 \\
0 & \nu & \frac{1}{4} & -\frac{3}{16}-2\nu & \cdots & 0 & 0 & 0 & 0 \\
\cdots & \cdots & \cdots & \cdots & \cdots & \cdots & \cdots & \cdots & \cdots \\
\mu & 0 & 0 & 0 & \cdots & \mu & 0 & -\frac{1}{4}-2\mu & -\frac{1}{4} \\
0 & \nu & 0 & 0 & \cdots & 0 & \nu & \frac{1}{4} & -\frac{3}{16}-2\nu
\end{bmatrix} \tag{7.45}$$

Table 7.1: Eigenvalues of six-cell problem.

Eigenvalues	
λ_1	-0.3750
λ_2	0.0000
λ_3	-0.9330
λ_4	-0.0670
λ_5	-1.1548
λ_6	-0.8690
λ_7	-0.4517
λ_8	-0.1212
λ_9	-0.0718
λ_{10}	0.0197
$\lambda_{11,12}$	$-0.0507 \mp 0.0815i$

It can be observed from Table 7.1 that two of the eigenvalues, λ_2 and λ_{10} are real and non-negative so that the homogeneous equilibrium point (regarded as an equilibrium for the connected cells) becomes unstable. This is exactly what Turing predicted (Turing [67], p.65).

7.3.3 Numerical methods

Development of numerical methods

The numerical methods are developed in the same way as in previous chapters by approximating the derivatives $dX_r(t)/dt$ and $dY_r(t)/dt$ by the first–order approximants

$$\frac{dX(t)}{dt} = \frac{X(t+\ell) - X(t)}{\ell} + O(\ell) \qquad \text{as} \qquad \ell \to 0, \tag{7.46}$$

$$\frac{dY(t)}{dt} = \frac{Y(t+\ell) - Y(t)}{\ell} + O(\ell) \qquad \text{as} \qquad \ell \to 0, \tag{7.47}$$

at $t = t_n$. For the given ODEs,

$$\frac{dX_r}{dt} = f(X_r, Y_r) + \mu(X_{r+1} - 2X_r + X_{r-1}), \tag{7.48}$$

$$\frac{dY_r}{dt} = g(X_r, Y_r) + \nu(Y_{r+1} - 2Y_r + Y_{r-1}), \tag{7.49}$$

evaluating X_r and Y_r at base time level, that is $t = t_n$, gives method $M1$ (Euler's method)

$$\mathcal{X}_r^{n+1} = \mathcal{X}_r^n + \ell f(\mathcal{X}_r^n, \mathcal{Y}_r^n) + \mu\ell(\mathcal{X}_{r+1}^n - 2\mathcal{X}_r^n + \mathcal{X}_{r-1}^n), \tag{7.50}$$

$$\mathcal{Y}_r^{n+1} = \mathcal{Y}_r^n + \ell g(\mathcal{X}_r^n, \mathcal{Y}_r^n) + \nu\ell(\mathcal{Y}_{r+1}^n - 2\mathcal{Y}_r^n + \mathcal{Y}_{r-1}^n). \tag{7.51}$$

where $n = 0, 1, 2, \ldots$. Replacing the function values f and g gives

$$\mathcal{X}_r^{n+1} = \mathcal{X}_r^n + \frac{\ell}{16}(16 - \mathcal{X}_r^n\mathcal{Y}_r^n) + \mu\ell(\mathcal{X}_{r+1}^n - 2\mathcal{X}_r^n + \mathcal{X}_{r-1}^n), \tag{7.52}$$

$$\mathcal{Y}_r^{n+1} = \mathcal{Y}_r^n + \frac{\ell}{16}(\mathcal{X}_r^n\mathcal{Y}_r^n - \mathcal{Y}_r^n - \beta) + \nu\ell(\mathcal{Y}_{r+1}^n - 2\mathcal{Y}_r^n + \mathcal{Y}_{r-1}^n). \tag{7.53}$$

The local truncation errors, LTEs, associated with (7.50) and (7.51) are given by

$$\begin{aligned}
\mathscr{L}1_{X_r}[X_r(t), Y_r(t); \ell] &= X_r(t+\ell) - X_r(t) - \ell f(X_r(t), Y_r(t)) \\
&- \mu\ell\,[X_{r+1}(t) - 2X_r(t) + X_{r-1}(t)] \\
&= \frac{1}{2}X_r''(t)\ell^2 + O(\ell^3) \quad \text{as} \quad \ell \to 0,
\end{aligned} \tag{7.54}$$

$$\begin{aligned}
\mathscr{L}1_{Y_r}[X_r(t), Y_r(t); \ell] &= Y_r(t+\ell) - Y_r(t) - \ell g(X_r(t), Y_r(t)) \\
&- \nu\ell\,[Y_{r+1}(t) - 2Y_r(t) + Y_{r-1}(t)] \\
&= \frac{1}{2}Y_r''(t)\ell^2 + O(\ell^3) \quad \text{as} \quad \ell \to 0.
\end{aligned} \tag{7.55}$$

This result shows that $M1$ is a first-order method.

Replacing the derivatives in the ODEs (7.48) and (7.49) by the same replacements as (7.46) and (7.47), evaluating the functions f and g as $f(\mathcal{X}_r^n, \mathcal{Y}_r^n)$ and $g(\mathcal{X}_r^n, \mathcal{Y}_r^{n+1})$ on the right–hand sides of (7.48) and (7.49) leads to the implicit formulae

$$\mathcal{X}_r^{n+1} = \mathcal{X}_r^n + \ell f(\mathcal{X}_r^n, \mathcal{Y}_r^n) + \mu\ell(\mathcal{X}_{r+1}^n - 2\mathcal{X}_r^n + \mathcal{X}_{r-1}^n), \tag{7.56}$$

$$\mathcal{Y}_r^{n+1} = \mathcal{Y}_r^n + \ell g(\mathcal{X}_r^n, \mathcal{Y}_r^{n+1}) + \nu\ell(\mathcal{Y}_{r+1}^n - 2\mathcal{Y}_r^n + \mathcal{Y}_{r-1}^n). \tag{7.57}$$

After rearrangement this alternative method, $M2$, can be written as

$$\mathcal{X}_r^{n+1} = \mathcal{X}_r^n + \frac{\ell}{16}(16 - \mathcal{X}_r^n\mathcal{Y}_r^n) + \mu\ell(\mathcal{X}_{r+1}^n - 2\mathcal{X}_r^n + \mathcal{X}_{r-1}^n), \tag{7.58}$$

$$\mathcal{Y}_r^{n+1} = \frac{[\mathcal{Y}_r^n - \frac{1}{16}\beta\ell + \nu\ell(\mathcal{Y}_{r+1}^n - 2\mathcal{Y}_r^n + \mathcal{Y}_{r-1}^n)]}{[1 - \frac{1}{16}\ell(\mathcal{X}_r^n - 1)]}. \tag{7.59}$$

The LTEs associated with $M2$ are obtained from (7.56) and (7.57) and are given by

$$\begin{aligned}
\mathscr{L}2_{X_r}[X_r(t), Y_r(t); \ell] &= X_r(t+\ell) - X_r(t) - \ell f(X_r(t), Y_r(t)) \\
&- \mu\ell\,[X_{r+1}(t) - 2X_r(t) + X_{r-1}(t)] \\
&= \frac{1}{2}X_r''(t)\ell^2 + O(\ell^3) \quad \text{as} \quad \ell \to 0,
\end{aligned} \tag{7.60}$$

$$\begin{aligned}
\mathscr{L}2_{Y_r}[X_r(t), Y_r(t); \ell] &= Y_r(t+\ell) - Y_r(t) - \ell g(X_r(t), Y_r(t+\ell)) \\
&- \nu\ell\,[Y_{r+1}(t) - 2Y_r(t) + Y_{r-1}(t)] \\
&= \frac{1}{2}[Y_r''(t) - \frac{1}{8}X_r(t)Y_r'(t) + \frac{1}{8}Y_r'(t)]\ell^2 + O(\ell^3) \quad \text{as} \quad \ell \to 0.
\end{aligned} \tag{7.61}$$

This result approves that $M2$ is a first-order method.

7.3.4 Stability analysis of numerical methods

The numerical methods {(7.52),(7.53)}, {(7.58),(7.59)} all have fixed points which will be denoted by $X_r = X_r^* = \frac{16}{16-\beta}$ and $Y_r = Y_r^* = 16 - \beta$. The stability of the fixed points are investigated by considering the associated functions

$$\mathcal{X}_r = h_1(\mathcal{X}_r, \mathcal{Y}_r) \quad \text{and} \quad \mathcal{Y}_r = h_2(\mathcal{X}_r, \mathcal{Y}_r)$$

where, for {(7.52),(7.53)},

$$h_1(\mathcal{X}_r, \mathcal{Y}_r) = \mathcal{X}_r + \frac{\ell}{16}(16 - \mathcal{X}_r\mathcal{Y}_r) + \mu\ell(\mathcal{X}_{r+1} - 2\mathcal{X}_r + \mathcal{X}_{r-1})$$

and

$$h_2(\mathcal{X}_r, \mathcal{Y}_r) = \mathcal{Y}_r + \frac{\ell}{16}(\mathcal{X}_r\mathcal{Y}_r - \mathcal{Y}_r - \beta) + \nu\ell(\mathcal{Y}_{r+1} - 2\mathcal{Y}_r + \mathcal{Y}_{r-1}),$$

for {(7.58),(7.59)}

$$h_1(\mathcal{X}_r, \mathcal{Y}_r) = \mathcal{X}_r + \frac{\ell}{16}(16 - \mathcal{X}_r\mathcal{Y}_r) + \mu\ell(\mathcal{X}_{r+1} - 2\mathcal{X}_r + \mathcal{X}_{r-1}),$$

$$h_2(\mathcal{X}_r, \mathcal{Y}_r) = \frac{[\mathcal{Y}_r - \frac{1}{16}\beta\ell + \nu\ell(\mathcal{Y}_{r+1} - 2\mathcal{Y}_r + \mathcal{Y}_{r-1})]}{[1 - \frac{1}{16}\ell(\mathcal{X}_r - 1)]}.$$

In order to examine the local stability of the fixed points, (X_r^*, Y_r^*), of $M1$ and $M2$, the eigenvalues of the matrix

$$\begin{bmatrix} \partial h_1(X_r^*, Y_r^*)/\partial \mathcal{X}_r & \partial h_1(X_r^*, Y_r^*)/\partial \mathcal{Y}_r \\ \partial h_2(X_r^*, Y_r^*)/\partial \mathcal{X}_r & \partial h_2(X_r^*, Y_r^*)/\partial \mathcal{Y}_r \end{bmatrix}$$

must be calculated.

Stability of the numerical methods may be analysed in the familiar way. First, the stability of the fixed point of an isolated cell is considered, that is, in the diffusion-free case where $\mu = \nu = 0$ in {(7.52),(7.53)} and {(7.58),(7.59)}. The resulting stability matrix for $M1$ for the isolated case at the fixed point $(X_r^*, Y_r^*) = (\frac{16}{16-\beta}, 16 - \beta)$ is

$$J_{M1_{is}} = \begin{bmatrix} 1 - \frac{\ell}{16}(16 - \beta) & -\frac{\ell}{(16 - \beta)} \\ \\ \frac{\ell}{16}(16 - \beta) & 1 + \frac{\ell\beta}{16(16 - \beta)} \end{bmatrix} \tag{7.62}$$

The eigenvalues of $J_{M1_{is}}$ for $\beta = 12$ are obtained as

$$\lambda_{1,2} = \frac{1}{32}[32 - \ell(1 - \mp i\sqrt{15})]. \tag{7.63}$$

Analysis of (7.63) reveals that the stability condition $\rho(J_{M1_{is}}) < 1$ where $\rho(J_{M1_{is}}) = \max_{i=1,2} |\lambda_i|$ is satisfied for $0 < \ell \leq 4$.

The resulting stability matrix for $M2$ for the isolated case at the fixed point $(X_r^*, Y_r^*) = (\frac{16}{16-\beta}, 16-\beta)$ is

$$J_{M2_{is}} = \begin{bmatrix} 1 - \dfrac{\ell}{16}(16-\beta) & -\dfrac{\ell}{(16-\beta)} \\ \dfrac{\ell(16-\beta-\frac{\ell}{16}\beta)}{16(1+\frac{\ell}{16}-\frac{\ell^2}{16-\beta}(16-\beta)} & \dfrac{1}{1+\frac{\ell}{16}-\frac{\ell}{16-\beta}} \end{bmatrix} \tag{7.64}$$

The eigenvalues of $J_{M2_{is}}$ for $\beta = 12$ are obtained as

$$\lambda_{1,2} = \frac{-128 + \ell\left(28 - 3\ell \mp \sqrt{-240 + 24\ell + 9\ell^2}\right)}{-128 + 24\ell}. \tag{7.65}$$

The stability condition $\rho(J_{M2_{is}}) < 1$ holds when

$$\left|\frac{-128 + \ell\left(28 - 3\ell + \sqrt{-240 + 24\ell + 9\ell^2}\right)}{-128 + 24\ell}\right| \leq 1 \tag{7.66}$$

In the case of interconnected cells, that is diffusion is present ($\mu \neq 0, \nu \neq 0$ in {(7.52),(7.53)} and {(7.58),(7.59)}), it is known from the qualitative analysis of the ODEs in §7.3.2 that the homogeneous equilibrium point (X_r^*, Y_r^*) should be unstable.

The resulting stability matrix $J_{M1_{in}}$ for $M1$ is a 12×12 version of (7.45): it is given by

$$J_{M1_{in}} = \begin{bmatrix}
a & b & c & 0 & 0 & 0 & 0 & 0 & 0 & 0 & c & 0 \\
c & d & 0 & e & 0 & 0 & 0 & 0 & 0 & 0 & 0 & e \\
c & 0 & a & b & c & 0 & 0 & 0 & 0 & 0 & 0 & 0 \\
0 & e & c & d & 0 & e & 0 & 0 & 0 & 0 & 0 & 0 \\
0 & 0 & c & 0 & a & b & c & 0 & 0 & 0 & 0 & 0 \\
0 & 0 & 0 & e & c & d & 0 & e & 0 & 0 & 0 & 0 \\
0 & 0 & 0 & 0 & c & 0 & a & b & c & 0 & 0 & 0 \\
0 & 0 & 0 & 0 & 0 & e & c & d & e & 0 & 0 & 0 \\
0 & 0 & 0 & 0 & 0 & 0 & c & 0 & a & b & c & 0 \\
0 & 0 & 0 & 0 & 0 & 0 & 0 & e & c & d & 0 & e \\
c & 0 & 0 & 0 & 0 & 0 & 0 & 0 & c & 0 & a & b \\
0 & e & 0 & 0 & 0 & 0 & 0 & 0 & 0 & e & c & d
\end{bmatrix}$$

where

$$a = 1 - \frac{3\ell}{4}, \quad b = -\frac{\ell}{4}, \quad c = \frac{\ell}{4},$$

$$d = 1 + \frac{\ell}{16}, \quad e = \frac{1}{16}.$$

The resulting characteristic equation may be written in a simplified form as

$$\begin{aligned} M1_{in}(\lambda) \equiv \frac{1}{67108864} & \left[(3\ell + 8(-1+\lambda)\right]^2 \\ & \left[\ell^2 + 16\ell(-1+\lambda) + 16(-1+\lambda)^2\right]^2 \\ & \left[\ell^2 + 4\ell(-1+\lambda) + 64(-1+\lambda)^2\right] \\ & \left[9\ell^2 + 84\ell(-1+\lambda) + 64(-1+\lambda)^2)(-1+\lambda)^2\right] = 0\,. \end{aligned} \tag{7.67}$$

The eigenvalues of $J_{M1_{in}}$ are summarized in Table 7.2.

Analysing the behaviour of the eigenvalues shows that instability occurs at $\ell = 1.7$ due to the magnitude of one of the eigenvalue exceeding unity: its value is 1.03116. This result illustrates that $M1$ behaves qualitatively wrongly by converging to the unstable homogeneous equilibrium point, (X_r^*, Y_r^*) which was proven in §7.3.2

Table 7.2: Eigenvalues of $J_{M1_{in}}$.

Eigenvalues	
$\lambda_{1,2}$	$\frac{1}{8}(8-3\ell)$
$\lambda_{3,4}$	$\frac{1}{4}[4-\ell(2+\sqrt{3})]$
$\lambda_{5,6}$	$\frac{1}{4}[4-\ell(2-\sqrt{3})]$
$\lambda_{7,8}$	$\frac{1}{32}[32-\ell(1\mp i\sqrt{15})]$
$\lambda_{9,10}$	1
$\lambda_{11,12}$	$\frac{1}{32}[32-\ell(21\mp 3\sqrt{33})]$

that it was unstable.

The Jacobian, $J_{M2_{in}}$, of $M2$ for the interconnected case is also a 12×12 version of (7.45): it is given by

$J_{M2_{in}} =$

$$\begin{bmatrix}
a' & b' & c' & 0 & 0 & 0 & 0 & 0 & 0 & 0 & c' & 0 \\
d' & e' & 0 & f' & 0 & 0 & 0 & 0 & 0 & 0 & 0 & f' \\
c' & 0 & a' & b' & c' & 0 & 0 & 0 & 0 & 0 & 0 & 0 \\
0 & f' & d' & e' & 0 & f' & 0 & 0 & 0 & 0 & 0 & 0 \\
0 & 0 & c' & 0 & a' & b' & c' & 0 & 0 & 0 & 0 & 0 \\
0 & 0 & 0 & f' & d' & e' & 0 & f' & 0 & 0 & 0 & 0 \\
0 & 0 & 0 & 0 & c' & 0 & a' & b' & c' & 0 & 0 & 0 \\
0 & 0 & 0 & 0 & 0 & f' & d' & e' & f' & 0 & 0 & 0 \\
0 & 0 & 0 & 0 & 0 & 0 & c' & 0 & a' & b' & c' & 0 \\
0 & 0 & 0 & 0 & 0 & 0 & 0 & f' & d' & e' & 0 & f' \\
c' & 0 & 0 & 0 & 0 & 0 & 0 & 0 & c' & 0 & a' & b' \\
0 & f' & 0 & 0 & 0 & 0 & 0 & 0 & 0 & f' & d' & e'
\end{bmatrix}$$

where

$$a' = 1 - \frac{3\ell}{4} \quad , \quad b' = -\frac{\ell}{4} \quad , \quad c' = \frac{\ell}{4}$$
$$d' = \ell \frac{4 - \frac{3\ell}{4}}{16(1 - \frac{3\ell}{16})^2} \, , \; e' = \frac{1 - \frac{\ell}{8}}{1 - \frac{3\ell}{16}} \, , \; f' = \frac{\ell}{16(1 - \frac{3\ell}{16})} \, .$$

The characteristic equation for $J_{M2_{in}}$ may be written in a simplified form as

$$\begin{aligned} M2_{in}(\lambda) \equiv & \frac{1}{64(16-3\ell)^6}\Big[(-1+\lambda)^2(32(-1+\lambda) - 3\ell(-6+\ell+2\lambda)\Big]^2 \\ & \Big[-16(-1+\lambda)^2 + \ell(-1+\lambda)(-19+3\lambda) + \ell^2(-4+3\lambda)\Big]^2 \\ & \Big[-64(-1+\lambda)^2 + \ell^2(-4+3\lambda) + 4\ell(-1+\lambda)(-4+3\lambda)\Big] \\ & \Big[12\ell(-8+\lambda)(-1+\lambda) - 64(-1+\lambda)^2 + 3\ell^2(-8+5\lambda))\Big] = 0. \end{aligned} \tag{7.68}$$

The eigenvalues obtained from (7.68) are summarized in Table 7.3.

Table 7.3: Eigenvalues of $J_{M2_{in}}$.

Eigenvalues	
$\lambda_{1,2}$	1
$\lambda_{3,4}$	$\dfrac{-32 + 18\ell - 3\ell^2}{-32 + 6\ell}$
$\lambda_{5,6}$	$\dfrac{-32 + \ell(22 - 3\ell - \sqrt{3}\sqrt{64 - 28\ell + 3\ell^2})}{2(-16 + 3\ell)}$
$\lambda_{7,8}$	$\dfrac{-32 + \ell(22 - 3\ell + \sqrt{3}\sqrt{64 - 28\ell + 3\ell^2})}{2(-16 + 3\ell)}$
$\lambda_{9,10}$	$\dfrac{-128 + \ell(28 - 3\ell \mp \sqrt{3}\sqrt{-80 + 8\ell + 3\ell^2})}{2(-64 + 12\ell)}$
$\lambda_{11,12}$	$\dfrac{-128 + \ell(108 - 15\ell \mp 3\sqrt{528 - 232\ell + 25\ell^2})}{2(-64 + 12\ell)}$

Method $M2$ also shows instability for $\ell > 1.4$ due to the magnitude of one of the complex conjugate eigenvalues exceeding unity with the value $1.00297 \mp i\, 0.203756$.

This result shows that $M2$ may also give qualitatively wrong results for some values of ℓ more precisely for $\ell \leq 1.4$.

7.4 Continuous Ring of Tissue

Turing [67] suggested a continuous ring of tissue as an alternative to a ring of seperate cells. In this case the position of a point of the ring is determined by the angle θ which a radius to the point makes with a fixed reference radius ρ. The morphogenetic field of N cells with two morphogens, X and Y, is described by the following reaction-diffusion equations

$$\frac{\partial X}{\partial t} = a(X - X^*) + b(Y - Y^*) + D_x \left(\frac{\partial^2 X}{\partial \rho^2} + \frac{1}{\rho} \frac{\partial X}{\partial \rho} + \frac{1}{\rho^2} \frac{\partial^2 X}{\partial \theta^2} \right), \quad (7.69)$$

$$\frac{\partial Y}{\partial t} = c(X - X^*) + c(Y - Y^*) + D_y \left(\frac{\partial^2 Y}{\partial \rho^2} + \frac{1}{\rho} \frac{\partial Y}{\partial \rho} + \frac{1}{\rho^2} \frac{\partial^2 Y}{\partial \theta^2} \right), \quad (7.70)$$

with the reaction-diffusion domain given by

$$\rho_i \leq \rho \leq \rho_0, \quad 0 \leq \theta < 2\pi$$

where $\rho_i, \rho_0 > 0$. Since ρ is fixed as a reference radius, that is $\dfrac{\partial}{\partial \rho} \equiv 0$, (7.69) and (7.70) become

$$\frac{\partial X}{\partial t} = a(X - X^*) + b(Y - Y^*) + D_x \frac{1}{\rho^2} \frac{\partial^2 X}{\partial \theta^2}, \quad (7.71)$$

$$\frac{\partial Y}{\partial t} = c(X - X^*) + d(Y - Y^*) + D_y \frac{1}{\rho^2} \frac{\partial^2 Y}{\partial \theta^2}, \quad (7.72)$$

in which

$$f(X, Y) = a(X - X^*) + b(Y - Y^*), \quad (7.73)$$

$$g(X, Y) = c(X - X^*) + d(Y - Y^*), \quad (7.74)$$

are linear rate functions. The terms a, b, c, d are the marginal rate functions as defined in previous sections, and

$$D_x = \mu', \quad D_y = \nu'$$

where μ', ν' are the diffusibilities of the two substances, X and Y, respectively. These are not quite the same as μ and ν of the last section, since μ and ν refer to a cell diameter as unit of length, whereas μ' and ν' are referred to a conventional unit, the same unit in which the radius ρ of the ring is measured. Thus

$$\mu = \mu'(\frac{N}{2\pi\rho})^2, \quad \nu = \nu'(\frac{N}{2\pi\rho})^2.$$

As the two morphogens must not flow out of the boundaries of the developing field, zero-flux boundary conditions are proposed

$$\frac{\partial X}{\partial \theta}\Big|_0 = \frac{\partial X}{\partial \theta}\Big|_{2\pi} = \frac{\partial Y}{\partial \theta}\Big|_0 = \frac{\partial Y}{\partial \theta}\Big|_{2\pi} = 0; \quad t > 0. \tag{7.75}$$

Here Turing's continuous ring of tissue model corresponds to polar coordinates. As he suggested, modelling the system either as a ring of cells each in contact with its neighbours or a continuous ring of tissue, have the same effects in the second numerical example, the twenty-cell problem. In this chapter the latter model will be studied.

7.4.1 Twenty-cell problem

Another general scheme of the system of autocatalytic chemical reactions between diffusing components proposed by Turing [67] is

$$\begin{aligned}
\mathcal{Y} + \mathcal{X} &\to \mathcal{W} && \text{at the rate } \frac{25}{16}\mathcal{Y}\mathcal{X} \\
2\mathcal{X} &\to \mathcal{W} && \text{at the rate } \frac{7}{64}\mathcal{X}^2 \\
\mathcal{A} &\to \mathcal{X} && \text{at the rate } \frac{1}{16} \times 10^{-3}\mathcal{A} \\
\mathcal{C}' &\to \mathcal{X} + \mathcal{C} && \text{at the rate } \frac{55}{32} \times 10^{-3}\mathcal{C}' \\
\mathcal{Y} &\to \mathcal{B} && \text{at the rate } \frac{1}{16}\mathcal{Y}
\end{aligned}$$

Four substances $\mathcal{A}, \mathcal{X}, \mathcal{Y}, \mathcal{B}$ are involved as isomeric subtances in the reactions. In addition to this the substances $\mathcal{C}, \mathcal{C}', \mathcal{W}$ are also considered. The substance $\mathcal{C}$ is in effect a catalyst for reaction $\mathcal{Y} \to \mathcal{X}$, and may also be regarded as an evocator, the

system being unstable if there is a sufficient concentration of $\mathcal{C}$. The reaction rate functions can be written as

$$f(X,Y) = \frac{1}{32}(-7X_r^2 - 50X_rY_r + 57 + 55\gamma), \tag{7.76}$$

$$g(X,Y) = \frac{1}{32}(7X_r^2 + 50X_rY_r - 2Y_r - 55 - 55\gamma), \tag{7.77}$$

where γ is a chance factor. The morphogens differ merely in the chance factors which were involved. The diffusion coefficients will be arbitrarily taken to be $\mu = \frac{1}{2}, \nu = \frac{1}{4}$. The number of cells, N, is 20.

7.4.2 Mathematical model of the twenty-cell problem

The resulting deterministic equations for Turing's twenty-cell structure are

$$\frac{dX_r}{dt} = \frac{1}{32}(-7X_r^2 - 50X_rY_r + 57 + 55\gamma) + \mu(X_{r+1} - 2X_r + X_{r-1}), \tag{7.78}$$

$$\frac{dY_r}{dt} = \frac{1}{32}(7X_r^2 + 50X_rY_r - 2Y_r - 55 - 55\gamma) + \nu(Y_{r+1} - 2Y_r + Y_{r-1}), \tag{7.79}$$

with the given initial conditions

$$X_r(0) = X_0 > 0, \quad Y_r(0) = Y_0 > 0 \tag{7.80}$$

where $r = 1, \ldots, 20$. The dimensionless quantity γ is often taken small, though values over as large a range as -0.5 to 0.5 may be considered. When $\gamma = 0$ there is an equilibrium state with $X_r = Y_r = 1$, $r = 1, \ldots, 20$. There are other stable equilibria with $\gamma = 0$, however, as Turing claimed. First, the behaviour of the system will be considered when γ remains permanently zero. In reality γ is different from 0 and is changing all the time. The equilibrium conditions for $\gamma = 0$ are

$$\frac{1}{32}(-7X_r^2 - 50X_rY_r + 57) = 0, \tag{7.81}$$

$$\frac{1}{32}(7X_r^2 + 50X_rY_r - 2Y_r - 55) = 0, \tag{7.82}$$

and the equilibrium points are obtained as $X^* = Y^* = 1$. The linear coefficients in (7.71), (7.72) are given the values

$$a = -2,\ b = -1.5625,\ c = 2,\ d = 1.5.$$

Then the continous model of the twenty-cell problem can be written as

$$\frac{\partial u}{\partial t} = a(u-e)+b(v-f)+D_u\frac{1}{\rho^2}\frac{\partial^2 u}{\partial\theta^2}, \tag{7.83}$$

$$\frac{\partial v}{\partial t} = c(u-e)+d(v-f)+D_v\frac{1}{\rho^2}\frac{\partial^2 v}{\partial\theta^2}, \tag{7.84}$$

where $(e,f)=(X^*,Y^*)$ in (7.71),(7.72) and $D_u=D_x$, $D_v=D_y$, $\rho=1$.

7.4.3 Numerical methods

The initial-boundary value problem,{(7.83),(7.84),(7.80),(7.75)}, may be solved using finite-difference techniques numerically, by discretizing the interval $0\le\theta\le 2\pi$ into $N+1$ subintervals each of width h and by discretizing the time interval $t\ge 0$ into steps each of length ℓ. The region $R=[0\le\theta<2\pi]\times[t>0]$ is covered by a mesh, the mesh points having co-ordinates $(\theta_m,t_n)=(mh,n\ell)$, with $m=0,1,\ldots,N+1$ and $n=0,1,2,\ldots$. The notations $\mathcal{U}_n^m$ and $\mathcal{V}_n^m$ will be used to distinguish the solution of an approximating finite-difference method from the theoretical solutions $u(\theta_m,t_n)$ and $v(\theta_m,t_n)$. The finite-difference methods are developed by approximating the time derivative in (7.83) by the first-order forward difference approximant

$$\partial u(\theta,t)/\partial t=(u(\theta,t+\ell)-u(\theta,t))/\ell+O(\ell)\quad\text{as}\quad\ell\to 0 \tag{7.85}$$

and the space derivative in (7.83) by the weighted second-order approximant

$$\begin{aligned}\partial^2 u(\theta,t)/\partial\theta^2 &= \frac{1}{h^2}\{\phi[u(\theta-h,t+\ell)-2u(\theta,t+\ell)+u(\theta+h,t+\ell)]\\ &+ (1-\phi)[u(\theta-h,t)-2u(\theta,t)+u(\theta+h,t)]\}+O(h^2),\end{aligned} \tag{7.86}$$

in which $\theta=\theta_m$ $(m=1,2,\ldots,N), t=t_n$ $(n=0,1,2,\ldots)$ and $\phi(0\le\phi\le 1)$ is a parameter. Similar approximations are used to approximate the derivatives in (7.84). The terms in (7.85)-(7.86) may be replaced in the following way

$$a(\mathcal{U}_m^n-e)+b(\mathcal{V}_m^n-f)\quad\text{and}\quad c(\mathcal{U}_m^n-e)+d(\mathcal{V}_m^n-f). \tag{7.87}$$

These approximations, together with the replacament for the derivatives of X and Y result in the numerical method, $\mathcal{M}(\phi)$, for the numerical solution of {(7.83)-(7.84)}

$$-\phi pD_u\mathcal{U}_{m-1}^{n+1}+(1+2\phi pD_u)\mathcal{U}_m^{n+1}-\phi pD_u\mathcal{U}_{m+1}^{n+1}=$$

$$(1-\phi)pD_u\mathcal{U}^n_{m-1}+[1-2(1-\phi)pD_u+a\ell]\mathcal{U}^n_{m+1}+(1-\phi)pD_u\mathcal{U}^n_m$$
$$+\ell(b\mathcal{V}^n_m-ae-bf), \tag{7.88}$$

$$-\phi pD_v\mathcal{V}^{n+1}_{m-1}+(1+2\phi pD_v)\mathcal{V}^{n+1}_m-\phi pD_v\mathcal{V}^{n+1}_{m+1}=$$
$$(1-\phi)pD_v\mathcal{V}^n_{m-1}+[1-2(1-\phi)pD_v+\ell d]\mathcal{V}^n_{m+1}+(1-\phi)pD_v\mathcal{V}^n_{m+1}$$
$$+\ell(c\mathcal{U}^n_m-ce-df), \tag{7.89}$$

in which $0\le\phi\le 1$, $p=\ell/h^2$, $m=0,\ldots,N$ and $n=0,1,2,\ldots$.

7.4.4 Local truncation errors

The local truncation error associated with (7.88) is given by

$$\begin{aligned}\mathscr{L}_u[u,v;h,\ell] &= \frac{1}{\ell}[u(\theta,t+\ell)-u(\theta,t)]\\ &- \frac{1}{h^2}\phi[u(\theta-h,t+\ell)-2u(\theta,t+\ell)+u(\theta+h,t+\ell)]\\ &- \frac{1}{h^2}(1-\phi)[u(\theta-h,t)-2u(\theta,t)+u(\theta+h,t)]\\ &- a\Big(u(\theta,t)-e\Big)-b\Big(v(\theta,t)-f\Big)\\ &- \left\{\frac{\partial u(\theta,t)}{\partial t}-\frac{D_u\partial^2u(\theta,t)}{\partial x^2}+a\Big(u(\theta,t)-e\Big)+b\Big(v(\theta,t)-f\Big)\right\}\\ &= -\frac{1}{12}h^2D_u\frac{\partial^4u}{\partial\theta^4}+(\frac{1}{2}\frac{\partial^2u}{\partial t^2}-\phi D_u\frac{\partial^3u}{\partial\theta^2\partial t})\ell+\ldots \quad \text{as} \quad h,\ell\to 0.\end{aligned} \tag{7.90}$$

The local truncation error associated with (7.89) is given by

$$\begin{aligned}\mathscr{L}_v[u,v;h,\ell] &= \frac{1}{\ell}[v(\theta,t+\ell)-v(\theta,t)]\\ &- \frac{1}{h^2}\phi[v(\theta-h,t+\ell)-2v(\theta,t+\ell)+v(\theta+h,t+\ell)]\\ &- \frac{1}{h^2}(1-\phi)[v(\theta-h,t)-2v(\theta,t)+v(\theta+h,t)]\\ &- c\Big(u(\theta,t)-e\Big)-d\Big(v(\theta,t)-f\Big)\\ &- \left\{\frac{\partial v(\theta,t)}{\partial t}-\frac{D_v\partial^2v(\theta,t)}{\partial x^2}+c\Big(u(\theta,t)-e\Big)+d\Big(v(\theta,t)-f\Big)\right\}\\ &= -\frac{1}{12}h^2D_v\frac{\partial^4v}{\partial\theta^4}+(\frac{1}{2}\frac{\partial^2v}{\partial t^2}-\phi D_v\frac{\partial^3v}{\partial\theta^2\partial t})\ell+\ldots \quad \text{as} \quad h,\ell\to 0.\end{aligned} \tag{7.91}$$

Hence, the local truncation error $\mathscr{L}[u(\theta,t), v(\theta,t); h, \ell]$ of the family of the numerical methods {(7.88),(7.89)} is seen to be $O(h^2 + \ell)$ as $h, \ell \to 0$.

7.4.5 Stability analysis

The von Neumann method of analysing stability is used to analyse the stability of the method $\mathcal{M}(\phi)$. Considering a small error Z_m^n of the form

$$Z_{u,m}^n = \mathcal{U}_m^n - \tilde{\mathcal{U}}_m^n = e^{\alpha n\ell} e^{i\beta mh}, \tag{7.92}$$

$$Z_{v,m}^n = V_m^n - \tilde{\mathcal{V}}_m^n = e^{\gamma n\ell} e^{i\delta mh}, \tag{7.93}$$

where $\alpha, \beta, \gamma, \delta$ are real and $i = +\sqrt{-1}$, will be considered. These errors will not grow if

$$|e^{\alpha\ell}| \leq 1 + M_u\ell \quad \text{and} \quad |e^{\gamma\ell}| \leq 1 + M_v\ell \tag{7.94}$$

where M_u and M_v are non-negative constants independent of h and ℓ. Equations (7.94) are the von Neumann necessary conditions for stability; they make no allowance for growing solutions if $M_u = 0$ and $M_v = 0$. The stability equation which is obtained by substituting $Z_{u,m}^n$ into (7.88) and linearization [19] is

$$(1 + 4\phi pD_u \sin^2 \frac{1}{2}\beta h)\xi_u = 1 - 4(1-\phi)pD_u \sin^2 \frac{1}{2}\beta h, \tag{7.95}$$

where $\xi_u = e^{\alpha\ell}$ is the amplification factor. The stability restrictions for $\mathcal{M}(\phi)$ with $M_u = 0$, are observed in the following form :

$$0 \leq \phi < \frac{1}{2}, \quad p \leq \frac{1}{2D_u(1-2\phi)}, \tag{7.96}$$

$$\phi = \frac{1}{2}, \quad p \leq \frac{1}{2D_u}, \tag{7.97}$$

$$\frac{1}{2} < \phi \leq 1, \quad p \geq \frac{-1}{2D_u(2\phi-1)}. \tag{7.98}$$

Substituting $Z_{v,m}^n$ into (7.89) and linearization [19] gives the (local) stability equation

$$(1 + 4\phi pD_v \sin^2 \frac{1}{2}\delta h)\xi_v = 1 - 4(1-\phi)pD_v \sin^2 \frac{1}{2}\delta h, \tag{7.99}$$

where $\xi_v = e^{\gamma\ell}$ is the amplification factor. The stability restrictions for $\mathcal{M}(\phi)$ with $M_v = 0$, are observed in the following form :

$$0 \leq \phi < \frac{1}{2}, \quad p \leq \frac{1}{2D_v(1-2\phi)}, \tag{7.100}$$

$$\phi = \frac{1}{2}, \quad p \leq \frac{1}{2D_v}, \tag{7.101}$$

$$\frac{1}{2} < \phi \leq 1, \quad p \geq \frac{-1}{2D_v(2\phi-1)}, \tag{7.102}$$

which, for $\phi = 0, 1$ or $\frac{1}{2}$ and $\alpha = 0$ give the stability conditions on an explicit, a fully implicit and Crank-Nicolson-type method for solving {(7.88)-(7.89)}.

7.4.6 Numerical experiments

Turing's theory of morphogenesis was studied by suggesting a family of finite-difference schemes which were developed for the initial-value problem, {(7.30),(7.31), (7.32)}, which is an example of an isolated ring-of-cells model and the reaction-diffusion system {(7.83),(7.84)}, which is an example of a continuous ring-of-tissue model. The well known Euler formula is used to compare the results of the alternative finite-difference scheme, $M2$. The qualitative analysis of {(7.30),(7.31)} in section §7.3.2 as well as some of the results given in Turing's paper [67] were used to establish the reliability of the suggested numerical methods.

The numerical methods, $M1$ and $M2$, all share the same fixed point, $(X_r^*, Y_r^*) = (4, 4)$ where $r = 1, \ldots, 6$, with the differential equations, {(7.30),(7.31)}. As was determined from the stability analysis of the numerical methods in §7.3.4 the Euler formulae converged to the stable homogeneous equilibrium point,(X_r^*, Y_r^*), for the diffusion-free case for $\ell < 4.0$. For interconnected cells it produced qualitatively correct results for $1.7 < \ell < 4.0$. As ℓ was increased further overflow occurred, whereas $M2$ converged to the stable fixed point,(X_r^*, Y_r^*), for large values of ℓ for isolated cells due to the $\lim_{\ell\to\infty} |\lambda_{1,2}| = \frac{4}{3}$ in (7.66). For the case of the presence of diffusion, $M2$ approached the unstable fixed point for $\ell \leq 1.4$. As ℓ was increased further the method converged to another stable equilibrium for $\ell \leq 5.0$. Here, the

time step ℓ must be chosen in such a way that the denominater in (7.59) does not vanish. The numerical results obtained from $M2$ are depicted in Figs. 7.2 and 7.3 for different sets of initial values which are summarized in Tables 7.4 and 7.5 for the six-cell problem as a ring configuration at time $t = 17.5$, with $\ell = 1.5$.

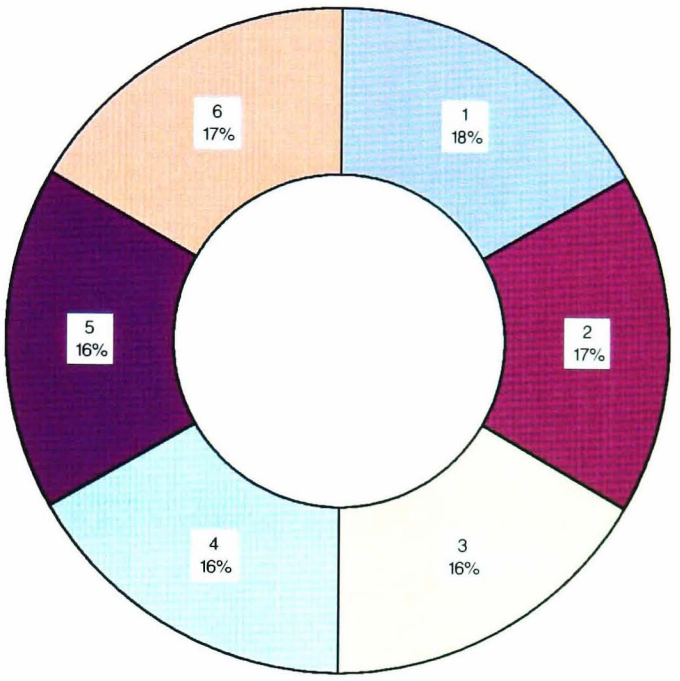

Figure 7.2: The concentration of morphogen X on the ring at $t = 17.5$.

Table 7.4: Initial values of six-cell problem.

	Initial Conditions		Initial Percentages	
Cell No	X_r	Y_r	X_r (%)	Y_r (%)
1	4.5	4.0	18.35	$16.\dot{6}$
2	4.0	4.0	16.33	$16.\dot{6}$
3	4.0	4.0	16.33	$16.\dot{6}$
4	4.0	4.0	16.33	$16.\dot{6}$
5	4.0	4.0	16.33	$16.\dot{6}$
6	4.0	4.0	16.33	$16.\dot{6}$

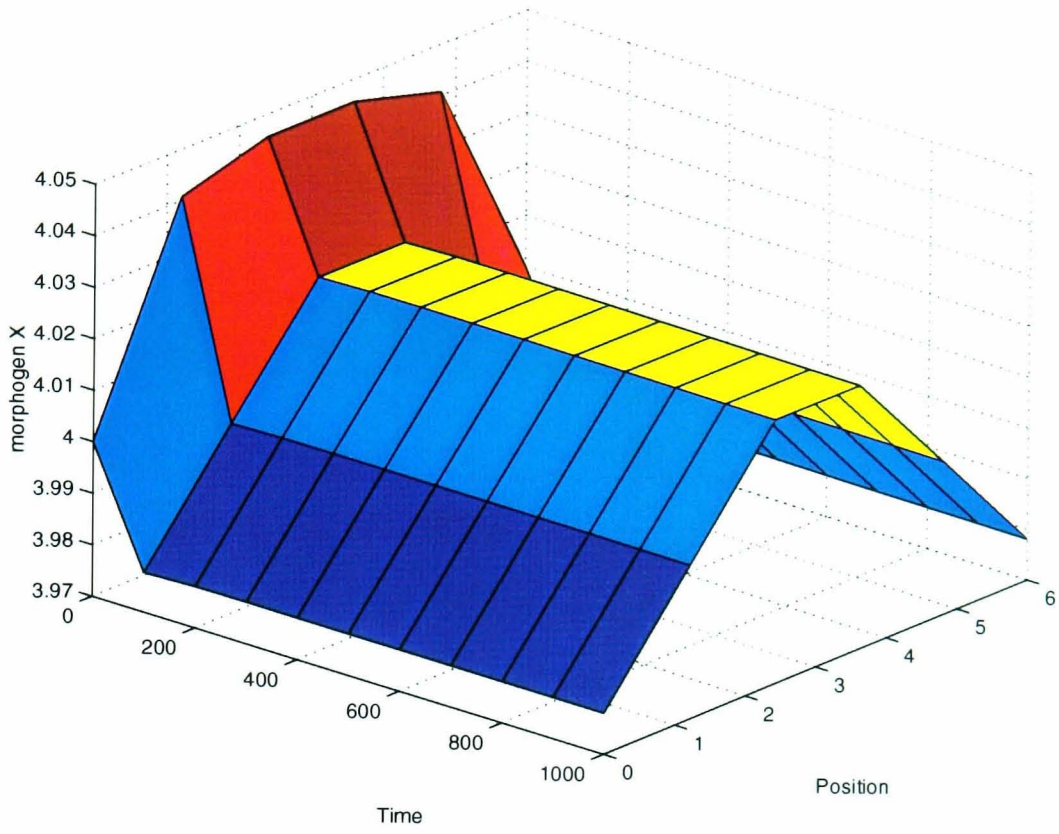

Figure 7.3: The concentration of morphogen X for the six-cell problem.

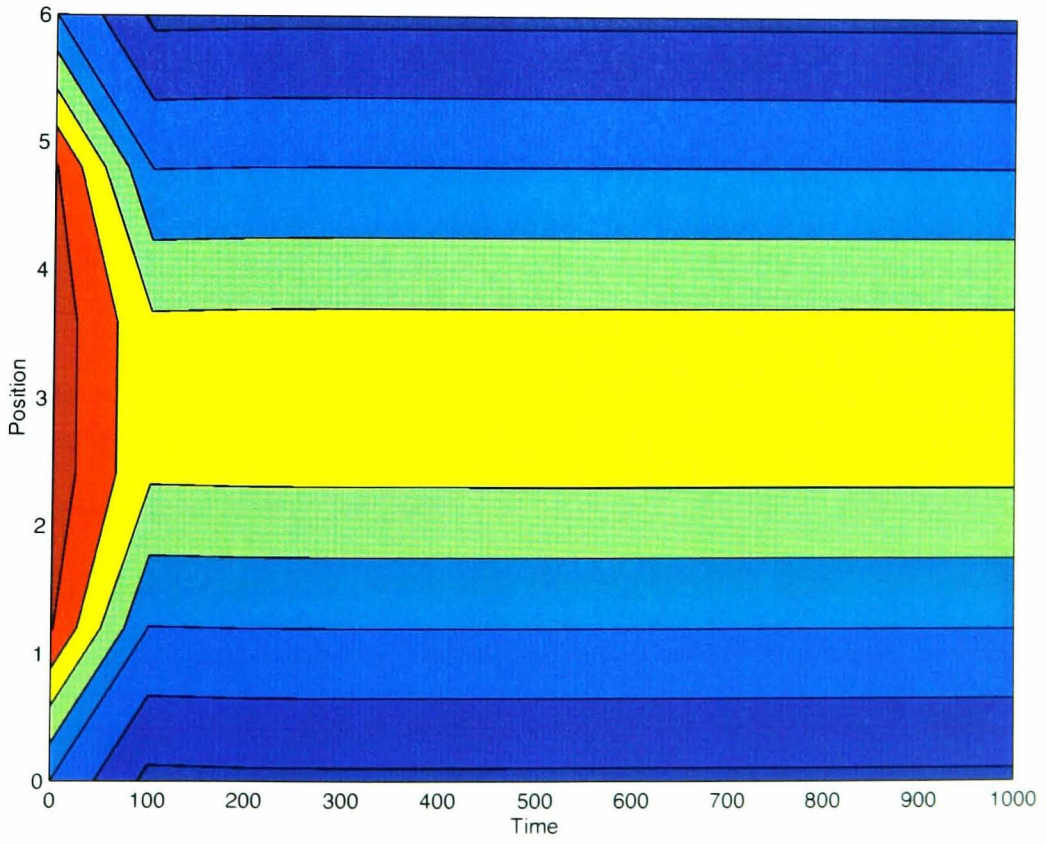

Figure 7.4: Contour plot of the concentration of morphogen X.

Table 7.5: Initial values of six-cell problem

	Initial Conditions
Cell No	X_r
1	4.00
2	4.04
3	4.045
4	4.045
5	4.04
6	4.00

Numerical experiments were carried out for the reaction-diffusion problem, {(7.83), (7.84)}, to see the behaviour of the suggested family of numerical methods, $\mathcal{M}(\phi)$, $(0 \leq \phi \leq 1)$ with $h = \frac{1}{2}$. Among them $\mathcal{M}(\phi = 0)$ and $\mathcal{M}(\phi = \frac{1}{2})$ produced convergence for $\ell < 8.0$. As ℓ was increased further overflow occurred. Using $\mathcal{M}(\phi = 1.0)$ convergence to a stable steady state was observed for $\ell \leq 10$. As ℓ increased further negative results leading to oscillatory behaviour with increasing amplitudes occurred.

With the uniform, near-equilibrium, starting configuration of

$$\mathcal{U}(0) = 1.0 + (1.0 - 2.0 \times RANDOM()) \times 0.02$$

and

$$\mathcal{V}(0) = 1.0 + (1.0 - 2.0 \times RANDOM()) \times 0.01$$

were tried to use throughout the numerical experiments. The reason for suggesting randomly distributed initial conditions is to create the effect of a trigger mechanism, which Turing has mentioned, such that the system is supposed to be in a stable homogeneous condition initially, but disturbed slightly from this state by some unspecified influences, such as Brownian movement or slight irregularities of form. The result of this near instability is that starting from the uniform equilibrium configuration, random effects soon give rise to large tentacles. This phenomenon can be observed from the numerical results of $\mathcal{M}(\phi = 1.0)$ with $\ell = 0.125$ for the twenty-cell

problem, in Fig. 7.5-7.10 with the initial conditions are

$$X_r(0) = 1.0 + (1.0 - 2.0 \times RANDOM()) \times 0.02$$

and

$$Y_r(0) = 1.0 + (1.0 - 2.0 \times RANDOM()) \times 0.01$$

Here the RANDOM() routine returns a uniformly distributed random number between 0.0D0 and 1.0D0.

Figure 7.10 is especially interesting in terms of pointing out the effect of the chance factor in {(7.78), (7.79)} which may affect the feature of the pattern in a totally different way when it is different from zero.

The numerical results illustrated in Figs. 7.11-7.14 were obtained as numerical solutions of the reaction-diffusion system {(7.83), (7.84)}. They were produced by using the numerical scheme $\mathcal{M}(\phi = 1.0)$ with $h = \frac{1}{2}$ for different diffusion coefficients, D_u and D_v, than previously shown results. It is interesting to see how instability can occur from a nearly homogeneous condition giving rise to patterns.

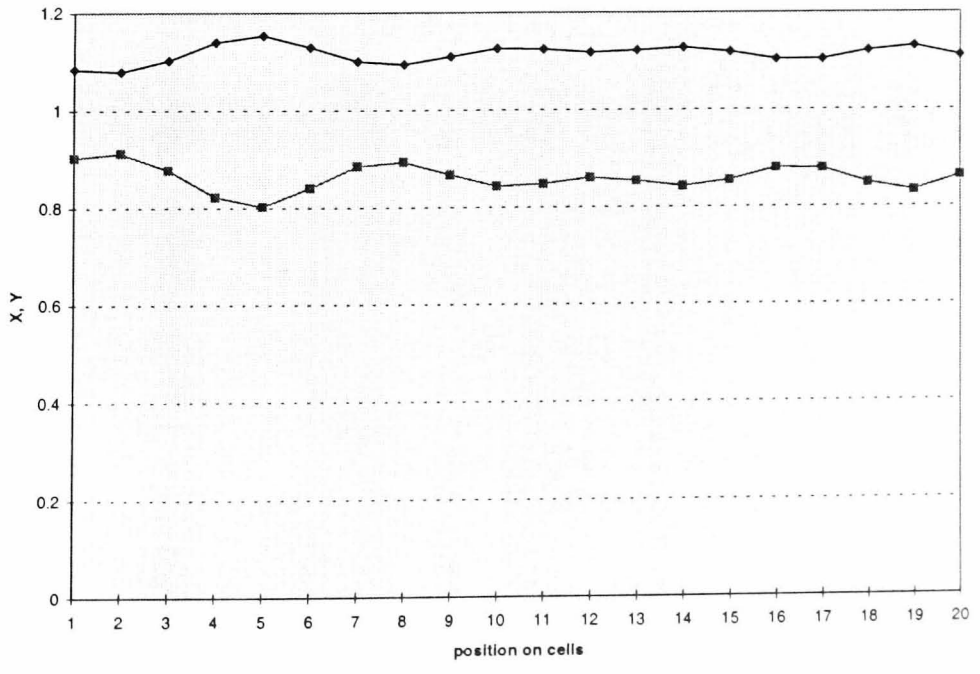

Figure 7.5: The stationary wave patterns at $t = 15$, $X - \Diamond, Y - \Box$.

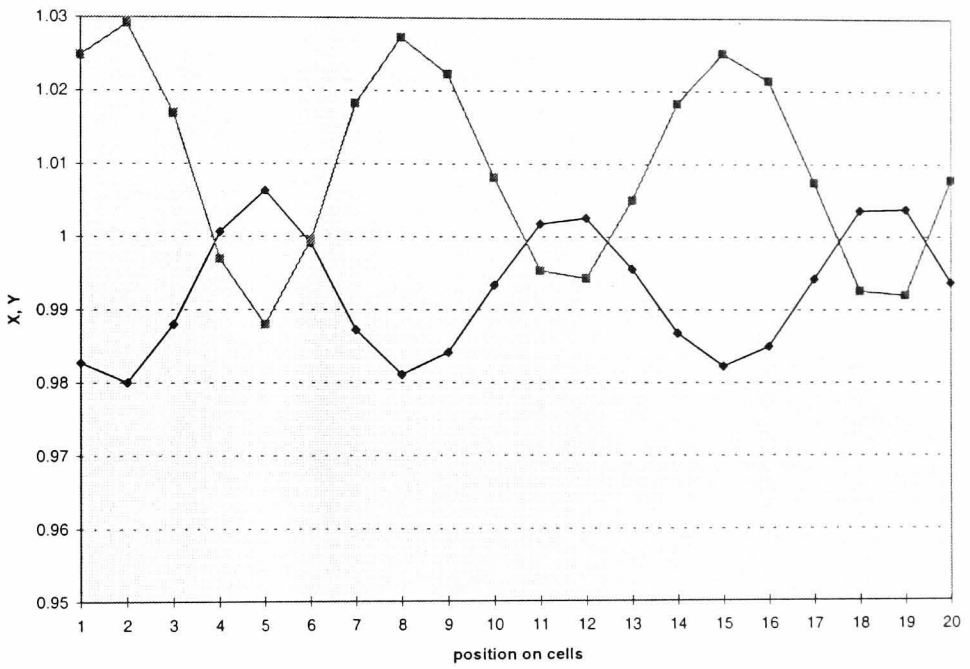

Figure 7.6: The stationary wave patterns at $t = 150$, $X - \Diamond, Y - \Box$.

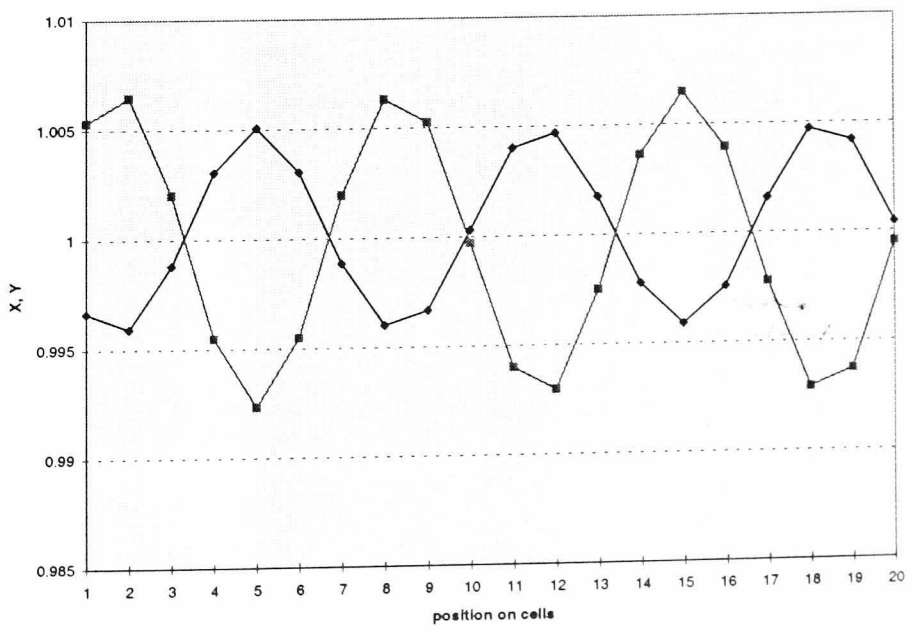

Figure 7.7: The stationary wave patterns at $t = 300$, $X - \Diamond, Y - \Box$.

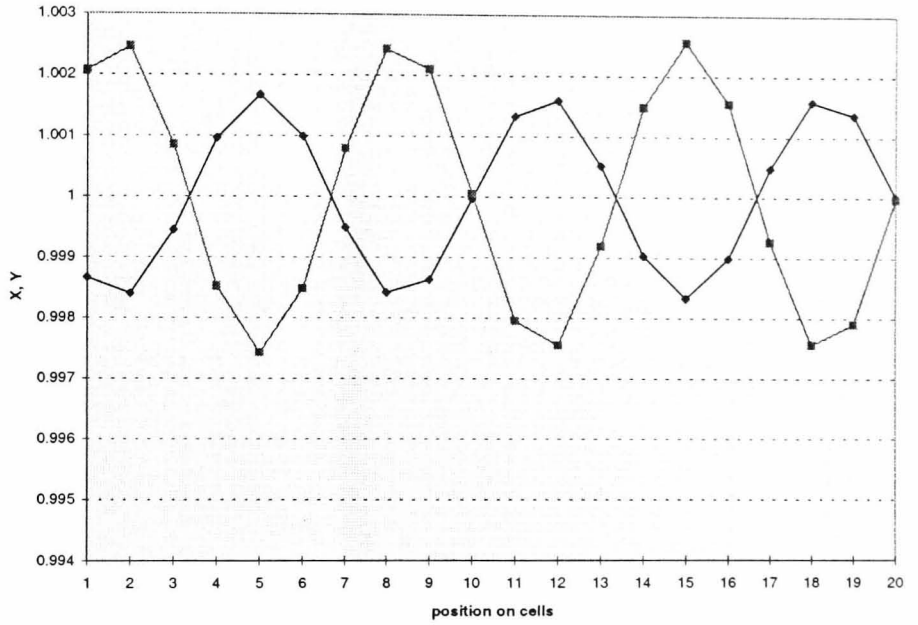

Figure 7.8: The stationary wave patterns at $t = 400$, $X - \Diamond, Y - \Box$.

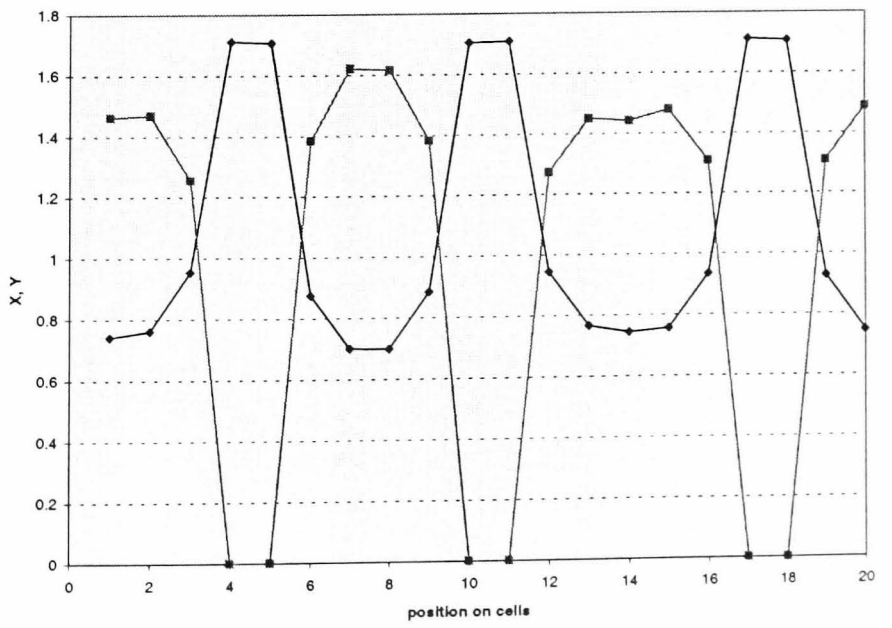

Figure 7.9: The final stationary wave patterns at $t = 1000$, $X - \Diamond, Y - \Box$.

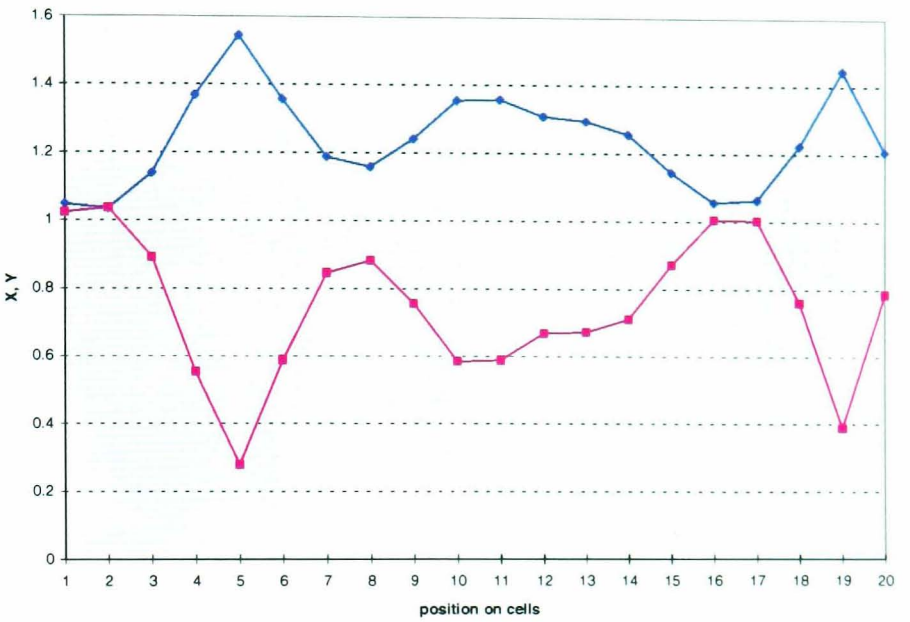

Figure 7.10: The stationary wave patterns at $t = 15$ with a chance factor $\gamma = 0.045$, $X - \Diamond, Y - \square$, [compare with Fig. 7.5 where $\gamma = 0$].

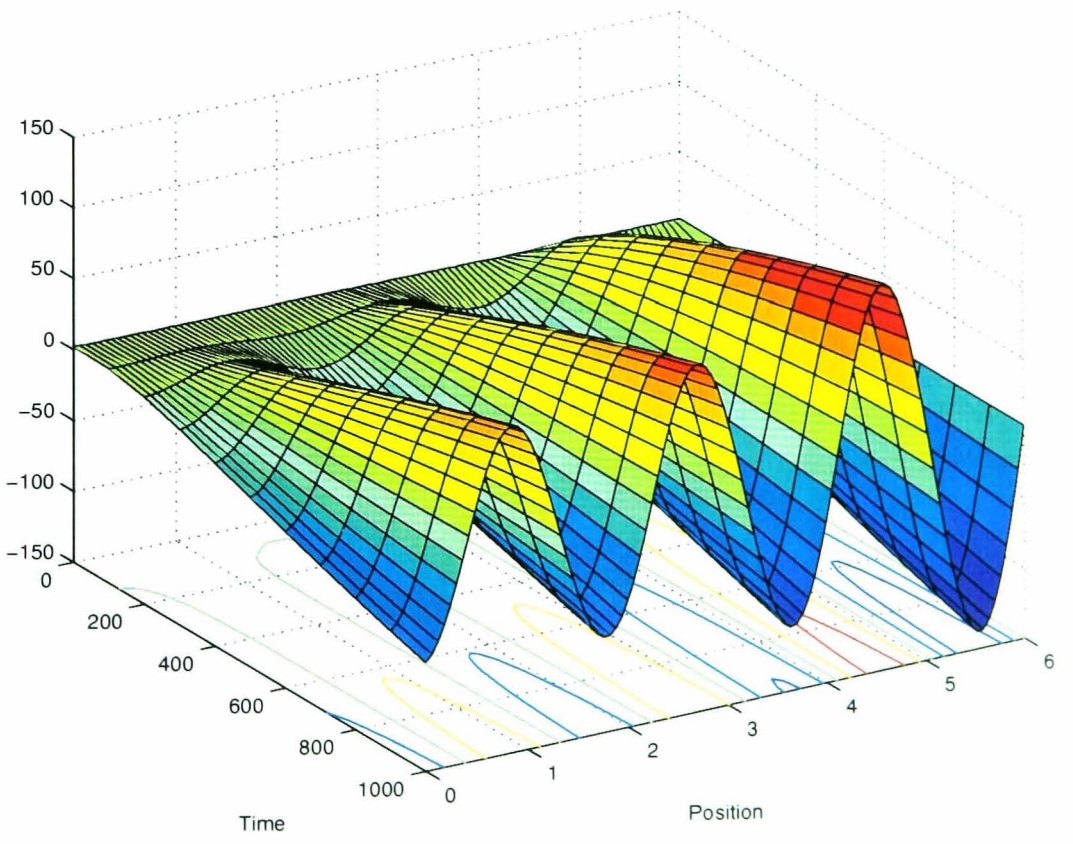

Figure 7.11: Time evolution of u at $t = 1000$, $\ell = 0.125$ with $D_u = 0.015$, $D_v = 0.025$.

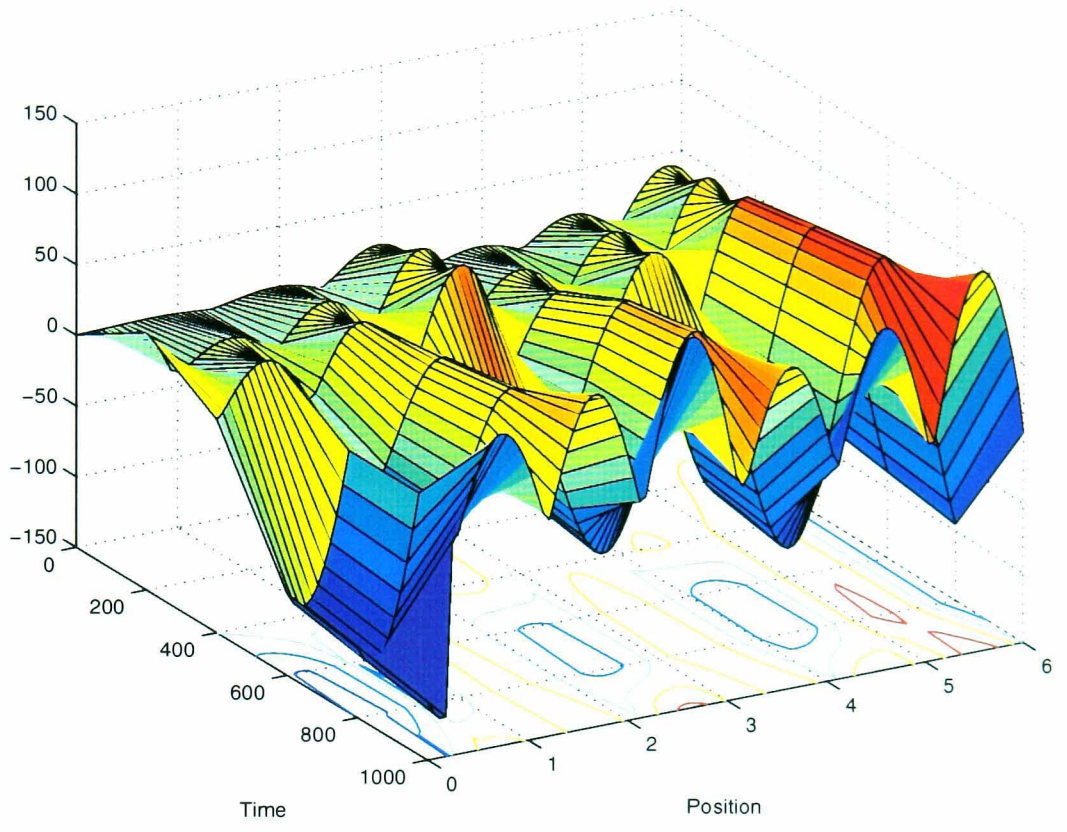

Figure 7.12: Time evolution of u at $t = 1000$, $\ell = 0.125$ with $D_u = 0.325$, $D_v = 0.1625$.

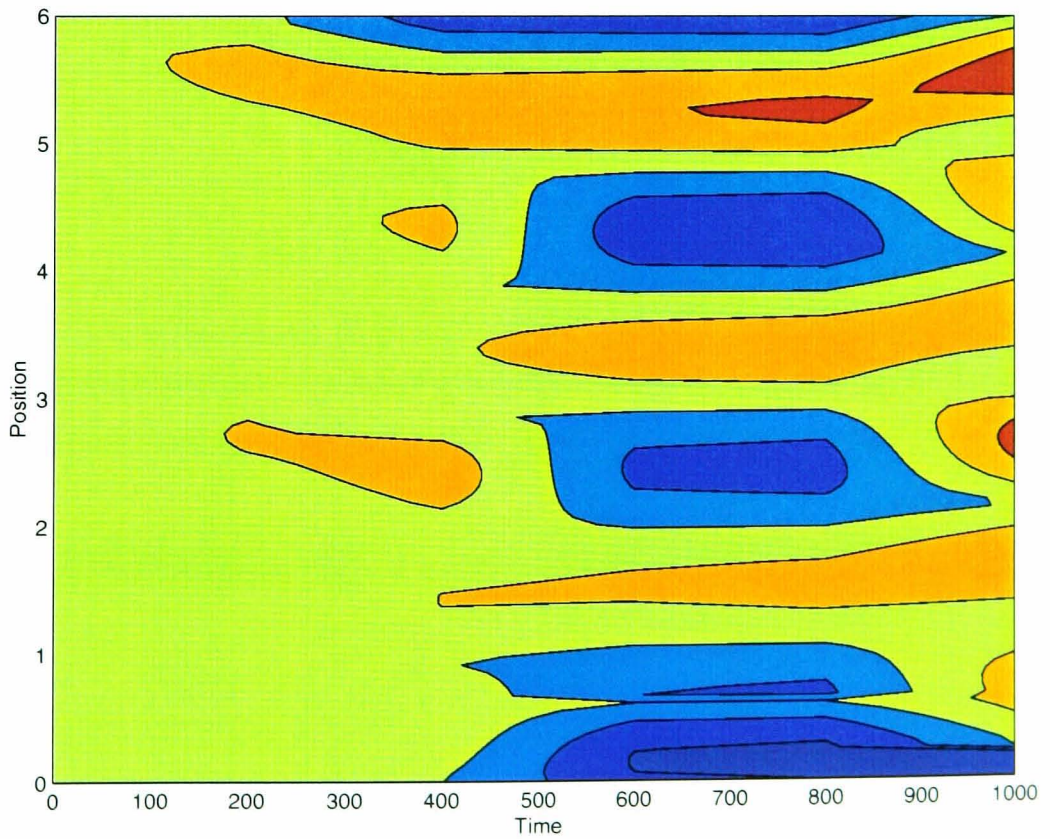

Figure 7.13: Projection of the surface plot in Figure 7.12.

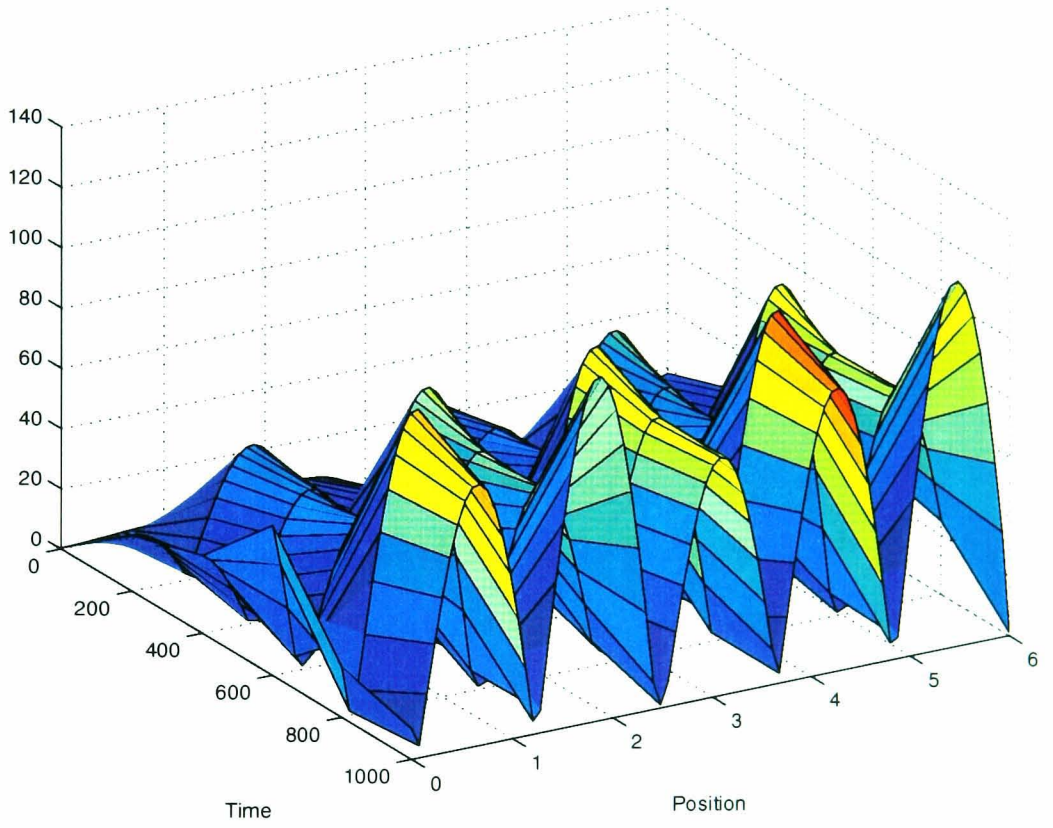

Figure 7.14: Time evolution of u at $t = 1000$, $\ell = 0.125$ with $D_u = 0.325$, $D_v = 0.1625$ with positive values of $u(\theta, t)$.

7.5 Summary

A family of finite-difference schemes has been developed and used to solve Turing's mathematical model of morphogenesis. The given systems considered were either a ring of cells in contact with their neighbours, or a continuous ring of tissue. The effects are indeed extremely similar in the two cases. The non-linear equations of the interconnected cells should have at least another equilibrium point different from that corresponding to the homogeneous case which is stable. In fact, depending on the parameters of the cells, the diffusion constants and the dimensions of the array, there may be many stable equlibria, each one corresponding to a different pattern. For this reason, both the ODEs and PDEs are very sensitive to initial conditions and the other parametric values, especially diffusion coefficients, therefore the mathematical models may not be well established for those particularly chosen examples. As a result the finite-difference schemes suffered from using quite restricted time step values.

Turing [67] hypothesized that, if certain chemicals are released in an embryo at certain times in that embryo's development, and these chemicals react with one another over a period of time, the chemicals produce a specific pattern which would be particular to the animal. As Turing predicted, diffusion-driven instability leading to spatial patterns is the fundamental result of the suggested models, and the finite-difference schemes managed to produce those predicted results.

Turing suggested a ring-of-cells model (ODEs) and a continuous ring of tissue (PDEs) which are thought to give a good approximation to the behaviour in certain kinds of chemical system. The differential equations have a number of parameters and it is neccessary to find values for these parameters which would make the model behave appropriately. The choice of the parameters is largely made on theoretical grounds, described in his paper, but in order to be sure that the differential equations really do describe development such as that mentioned in the paper, it is necessary to mimic its behaviour by computation. From this point of view the alternative

finite-difference schemes had the advantage of being easy to implement.

Considering the anatomical structure of the growing embryo problem and treating the problem in a hollow sphere of continuous tissue such as blastula would be a more reasonable approach. That is, solving the reaction-diffusion {(7.83), (7.84)} by using spherical polar coordinates.

Due to the random effects it is observed numerically that one should consider the stochastic feature of Turing's structure for a more realistic approach. The deterministic analysis which has been developed and applied in this chapter provides and predicts a more general qualitative knowledge to the stochastic one. That is why these two approaches should be taken into consideration together.

Chapter 8

A Model for Pattern Formation on Sea Shells

8.1 Introduction

The models describing shell patterning are special applications of the general problem of biological pattern formation in developing organisms the basic ideas of which were given in Chapter 6 and Chapter 7. Modelling the intricate and colourful patterns on sea shells not only provides more information about developing organisms but also helps in understanding dynamical systems in general. Mathematical modelling of pigmentation patterns was pioneered by Waddington and Cowe [76], who reproduced the tent-like patterns of *Oliva porphyria* using cellular automata and by Lindsday [30] for bivalved molluscs. A cellular automata phenomenological approach has also been discussed by Herman and Liu [20], by Wolfram [78] and by Plath and Schwietering [56]. Meinhardt [37],[38],[39] developed molecularly feasible models for pattern formation during the development of higher organisms by employing an activator-inhibitor reaction-diffusion model. Some of these models have now found direct support in molecular and genetic research.

It was not until 1972 that Meinhardt and his colleague Gierer [12] revealed that

short-ranged activation and long-ranged inhibition are the principal elements of Turing's patterns. Meinhardt and Gierer were able to formulate Turing's mechanism using more complicated and more physically motivated, non-linear equations, and to show how they could plausibly be related to the kinds of processes known to take place during real biological patterning and development. Meinhardt [40] has also shown in his beautiful book "The Algorithmic Beauty of Sea Shells" that the models proposed for shell patterning may establish a base for other important processes in development such as the formation of organizing regions and embryonic axes and the initiation of leaves. Close parallels between blood coagulation, cheomatactic orientation of cells and the spread of neuronal excitation become apparent to processes. In general sea shells show an enormous diversity of patterns throughout their development (Meinhardt [40]). Moreover, a structure, once formed, usually remains stable at least for a certain time interval. For the shell gets bigger by continual accretion of calcified material onto the outer edge, and so the pattern on the surface of the shell is a trace of the pigment distribution along a one-dimensional line at the shell's edge. Most patterns of shells result from the incorporation of pigments during the growth process. Once the patterns occur and remain unchanged they become historical records of what happens at the growing edge, that is, they are a time record of a pattern-forming process in a more or less linearly-arranged array of cells. Due to the space-time relation of the shell pattern, lines parallel to the direction of growth indicate the formation of a spatial periodic pattern of pigment production along the edge that is stable in time. At more or less regular distances, groups of cells in the mantle gland produce permanent pigment while cells in between do not. This is the usual situation in morphogenesis where particular structures such as leaves, hair or feathers become initiated at regularly spaced positions.

Since very little is known about the general mechanisms which would create the patterns on sea shells the models suggested here only describe the principle for such patterns.

8.2 The Activator-inhibitor Scheme

It was in 1952 that Turing published his landmark paper and then actually began to perceive the real key to his patterning mechanism, which is that it represents a competition between activation by compound $\mathcal{A}$ and inhibition by compound $\mathcal{B}$. Moreover, the inhibitor $\mathcal{B}$ must diffuse more rapidly than $\mathcal{A}$ for patterning to occur. Thus, while activation and autocatalytic production of $\mathcal{A}$ is a localized process, inhibition of $\mathcal{A}$ by $\mathcal{B}$ is long-ranged, because once formed in the vicinity of $\mathcal{A}$, $\mathcal{B}$ can rapidly diffuse away to inhibit the formation of $\mathcal{A}$ elsewhere. At the same time, this rapid diffusion of $\mathcal{B}$ ensures that it does not inhibit the local formation of $\mathcal{A}$. The whole scheme represents a subset of reaction-diffusion processes called "activator-inhibitor systems". A short-range substance, the activator, promotes its own production (autocatalysis) as well as that of its rapidly diffusing antagonist, the inhibitor. As a result the stripe patterns in the shells are a demonstration of a simple, periodic stationary pattern in one dimension, and also an analogue of the two-dimensional spot pattern, such as animal coat pattern.

A mathematical model which describes the pattern formation of the shell of *Lyria planicostata taiwanica* Fig. 8.1 (Meinhardt [40]), by describing a possible interaction between the autocatalytic activator $c = c(x,t)$ and its antagonist, the inhibitor $e = e(x,t)$, is demonstrated by the following PDE system :

$$\frac{\partial c}{\partial t} = s\left(\frac{c^2}{e} + e_c\right) - r_c\, c + D_c \frac{\partial^2 c}{\partial x^2}, \qquad 0 < x < \mathrm{S},\ \ t > 0, \tag{8.1}$$

$$\frac{\partial e}{\partial t} = sc^2 - r_e\, e + e_e + D_e \frac{\partial^2 e}{\partial x^2}, \qquad 0 < x < \mathrm{S},\ \ t > 0 \tag{8.2}$$

where t is time, x is the spatial coordinate, S is the length of the shell, D_c and D_e are the diffusion coefficients, and r_c and r_e the decay rates of c and e. A more detailed list of the individual terms might be more helpful to understand the mathematical model.

s : The source density. It describes the ability of the cells to perform the autocatalysis.

$\mathbf{s\frac{c^2}{e}}$: The production rate. There is an autocatalytic production of the activator c *via* production the rate term after which the production is slowed down by the inhibitor e.

$\mathbf{-r_c c}$: The rate of removal. The rate at which molecules saturate is, as a rule, proportional to the number of molecules present.

$\mathbf{e_c}$: Basic activator production. A small activator-independent activator production can initiate the system at low activator concentration. This term is necessary for regenerating patterns or for sustaining oscillations.

$\mathbf{e_e}$: Basic inhibitor production. A small activator-independent inhibitor production can cause a second homogeneous stable state at low activator concentrations. This term is necessary for simulation of travelling waves.

$\mathbf{D_c \frac{\partial^2 c}{\partial x^2}}$: The exchange by diffusion.

A possible simple chemical scheme behind the proposed mathematical model, (8.1), (8.2), may be suggested in the form

$$\begin{aligned}
\mathcal{A} &\xrightarrow{k_1} \mathcal{C} \\
\mathcal{D} &\xrightarrow{k_2} \mathcal{E} \\
\mathcal{C} &\xrightarrow{k_3} \mathcal{F} \\
\mathcal{E} &\xrightarrow{k_4} \mathcal{G} \\
\mathcal{E}+\mathcal{P} &\underset{k_6}{\overset{k_5}{\rightleftarrows}} \mathcal{C} \\
\mathcal{B}+\mathcal{C}+\mathcal{P} &\xrightarrow{k_7} \mathcal{P}+2\mathcal{C}
\end{aligned}$$

A morphogen $\mathcal{C}$ (activator c in (8.1), (8.2)) is produced from an initial product $\mathcal{A}$ at a constant rate $k_1\mathcal{C}$ as well as *via* an autocatalytic step that requires a third molecule $\mathcal{P}$. The morphogen $\mathcal{C}$ also catalyzes the production of its antagonist $\mathcal{E}$ (inhibitor e in (8.1), (8.2)) from a precursor molecule $\mathcal{D}$ at a rate $k_2\mathcal{D}\mathcal{C}^2$. In addition, $\mathcal{P}$ transforms $\mathcal{E}$ into $\mathcal{C}$. Since the intermediates $\mathcal{C}$ and $\mathcal{E}$ have finite lifetimes, they are either used up or degraded by the cells and leave the reaction medium *via* unimolecular steps. The products $\mathcal{F}$ and $\mathcal{G}$ are waste products.

The mathematical formulation of the sea-shell patterning problem is completed with given initial conditions such as

$$c(x,0) = c_0 > 0, \qquad e(x,0) = e_0 > 0, \tag{8.3}$$

and zero flux boundary (conditions suggested by Meinhardt [40]) which assume that the boundaries are closed and no loss or gain takes place through the boundary.

$$\frac{\partial c}{\partial x}\Big|_0 = \frac{\partial c}{\partial x}\Big|_S = \frac{\partial e}{\partial x}\Big|_0 = \frac{\partial e}{\partial x}\Big|_S = 0, \quad \text{for} \quad t > 0. \tag{8.4}$$

8.3 Numerical Methods

The initial-boundary value problem {(8.1),(8.2),(8.3),(8.4)} is solved using a finite-difference scheme, by discretizing the space interval $0 \leq x \leq S$ into $N+1$ subintervals, each of width $h > 0$ and by discretizing the time interval $t \geq 0$ at the points $t_n = n\ell (n = 0, 1, 2, \ldots)$. The open region $R = [0 \leq x \leq S] \times [t > 0]$ and its boundary ∂R consisting of the lines $x = S, x = 0$, and $t = 0$ are thus covered by a rectangular grid, the grid points have coordinates $(x_m, t_n) = (mh, n\ell)$ with $m = 0, 1, \ldots, N+1$ and $n = 0, 1, 2, \ldots$. The notations C_m^n and E_m^n will be used to distinguish the solution of an approximating finite-difference method from the theoretical solutions $c(x_m, t_n)$ and $e(x_m, t_n)$.

Introducing $\xi = \xi(x,t)$ as a differentiable function with respect to x and t in which ξ represents $c(x,t)$ or $e(x,t)$ in (8.1) and (8.2), a family of numerical methods is developed by approximating the time derivatives in {(8.1),(8.2)} by the first-order forward-difference replacement

$$\frac{\partial \xi(x,t)}{\partial t} = \frac{[\xi(x,t+\ell) - \xi(x,t)]}{\ell} + O(\ell) \quad \text{as} \quad \ell \to 0, \tag{8.5}$$

and the space derivatives in (8.1) and (8.2) by the second-order approximant

$$\begin{aligned} \partial^2 \xi(x,t)/\partial x^2 \;=\; & \frac{1}{h^2}\Big\{\phi\big[\xi(x-h,t+\ell) - 2\xi(x,t+\ell) + \xi(x+h,t+\ell)\big] \\ & + \; (1-\phi)\big[\xi(x-h,t) - 2\xi(x,t) + \xi(x+h,t)\big]\Big\} + O(h^2) \\ & \qquad \text{as} \quad h \to 0, \end{aligned} \tag{8.6}$$

in which $x = x_m$ $(m = 0, 1, 2, \ldots, N)$ and $t = t_n$ $(n = 0, 1, 2, \ldots)$.

Substituting (8.5) into (8.1) and (8.2), and evaluating the unknown functions $c(x,t)$ and $e(x,t)$ on the right hand sides of (8.1),(8.2) at time $t = t_n$ yields the following numerical scheme, *Method* $\mathscr{S}$ $(0 \le \phi \le 1)$

$$
\begin{aligned}
&-\phi p D_c C_{m-1}^{n+1} + (1 + 2\phi p D_c) C_m^{n+1} - \phi p D_c C_{m+1}^{n+1} = \\
&\quad (1-\phi) p D_c C_{m-1}^{n} + \Big[1 + \ell(s\frac{C_m^n}{E_m^n} - r_c) - 2(1-\phi) p D_c\Big] C_m^n + (1-\phi) p D_c C_{m+1}^n + \ell s e_c,
\end{aligned}
\tag{8.7}
$$

$$
\begin{aligned}
&-\phi p D_e E_{m-1}^{n+1} + (1 + 2\phi p D_e) E_m^{n+1} - \phi p D_e E_{m+1}^{n+1} = \\
&\quad (1-\phi) p D_e E_{m-1}^{n} + \Big[1 - \ell r_e - 2(1-\phi) p D_e\Big] E_m^n + (1-\phi) p D_e E_{m+1}^n + \ell[s(C_m^n)^2 + e_e],
\end{aligned}
\tag{8.8}
$$

in which $p = \ell/h^2, m = 1, \ldots, N$ and $n = 0, 1, 2, \ldots$.

8.3.1 Local truncation errors

The local truncation error associated with (8.7) is given by

$$
\begin{aligned}
\mathscr{L}_c[c, e; h, \ell] &= \frac{1}{\ell}[c(x, t+\ell) - c(x,t)] \\
&- \frac{1}{h^2}\phi[c(x-h, t+\ell) - 2c(x, t+\ell) + c(x+h, t+\ell)] \\
&- \frac{1}{h^2}(1-\phi)[c(x-h,t) - 2c(x,t) + c(x+h,t)] \\
&+ -s\left(\frac{[c(x,t)]^2}{e(x,t)} + e_c\right) + r_c c(x,t) \\
&- \left\{\frac{\partial c(x,t)}{\partial t} - \frac{D_c \partial^2 c(x,t)}{\partial x^2} - s\Big(\frac{[c(x,t)]^2}{e(x,t)} + e_c\Big) + r_c c(x,t)\right\} \\
&= -\frac{1}{12} h^2 D_c \frac{\partial^4 c}{\partial x^4} + \left(\frac{1}{2}\frac{\partial^2 c}{\partial t^2} - \phi \frac{\partial^3 c}{\partial x^2 \partial t}\right)\ell + \ldots \quad \text{as} \quad h, \ell \to 0.
\end{aligned}
\tag{8.9}
$$

The local truncation error associated with (8.8) is given by

$$
\mathscr{L}_e[c, e; h, \ell] = \frac{1}{\ell}[e(x, t+\ell) - e(x,t)]
$$

$$
\begin{aligned}
- \quad & \frac{1}{h^2}\phi[e(x-h,t+\ell)-2e(x,t+\ell)+e(x+h,t+\ell)] \\
- \quad & \frac{1}{h^2}(1-\phi)[e(x-h,t)-2e(x,t)+e(x+h,t)] \\
+ \quad & -s[c(x,t)]^2+r_e e(x,t)-e_e \\
- \quad & \left\{\frac{\partial e(x,t)}{\partial t}-\frac{D_e\partial^2 e(x,t)}{\partial x^2}-s[c(x,t)]^2+r_e e(x,t)-e_e\right\} \\
= \quad & -\frac{1}{12}h^2 D_e\frac{\partial^4 e}{\partial x^4}+\left(\frac{1}{2}\frac{\partial^2 e}{\partial t^2}-\phi\frac{\partial^3 e}{\partial x^2\partial t}\right)\ell+\ldots \quad \text{as} \quad h,\ell\to 0.
\end{aligned}
\tag{8.10}
$$

Hence, the local truncation error $\mathscr{L}[c(x,t),e(x,t);h,\ell]$ of the family of the numerical methods (8.7), (8.8) is seen to be $O(h^2+\ell)$ as $h,\ell\to 0$.

8.3.2 Numerical stability

The von Neumann method of analysing stability is used to analyse the stability of the numerical schemes, (8.7) and (8.8). Expressing the errors at $(x,t)=(mh,n\ell)$ in the unknowns C_m^n and E_m^n in the forms

$$
\begin{aligned}
Z_{c,m}^n &= C_m^n-\tilde{C}_m^n=e^{\zeta n\ell}e^{i\eta mh}, \\
Z_{e,m}^n &= E_m^n-\tilde{E}_m^n=e^{\sigma n\ell}e^{i\varsigma mh},
\end{aligned}
$$

where $\zeta,\eta,\sigma,\varsigma\in\mathbb{R}$; $i=+\sqrt{-1}$ and $\tilde{C}_m^n$ and $\tilde{E}_m^n$ are perturbed numerical solutions, a necessary condition for the error not to grow as $n\to\infty$ is

$$
|e^{\zeta\ell}|\le 1+K_c\ell \quad \text{and} \quad |e^{\sigma\ell}|\le 1+K_e\ell, \tag{8.11}
$$

where K_c and K_e are non-negative constants independent of h,ℓ.

Substituting $Z_{c,m}^n$ into (8.7) and linearization [19] leads to the stability equation

$$
\left(1+4\phi pD_c\sin^2\frac{1}{2}\eta h\right)\xi_c=1-4(1-\phi)pD_c\sin^2\frac{1}{2}\eta h+\ell(2s\frac{\tilde{C}_m^n}{\tilde{E}_m^n}-r_c), \tag{8.12}
$$

where $\xi_c=e^{\zeta\ell}$, with the consequent stability restrictions

$0 \leq \phi < \frac{1}{2}$,

$$p \leq \frac{2 + \ell(2s\frac{\tilde{C}_m^n}{\tilde{E}_m^n} - r_c)}{4D_c(1-2\phi)} \quad \text{and} \quad p \geq \frac{\ell(2s\frac{\tilde{C}_m^n}{\tilde{E}_m^n} - r_c)}{4D_c};$$

$\phi = \frac{1}{2}$,

$$\ell(r_c - 2s\frac{\tilde{C}_m^n}{\tilde{E}_m^n}) \leq 2 \quad \text{and} \quad p \geq \frac{\ell(2s\frac{\tilde{C}_m^n}{\tilde{E}_m^n} - r_c)}{4D_c};$$

$\frac{1}{2} < \phi \leq 1$,

$$p \geq \frac{-2 - \ell(2s\frac{\tilde{C}_m^n}{\tilde{E}_m^n} - r_c)}{4D_c(2\phi-1)} \quad \text{and} \quad p \geq \frac{\ell(2s\frac{\tilde{C}_m^n}{\tilde{E}_m^n} - r_c)}{4D_c}. \tag{8.13}$$

Substituting $Z_{e,m}^n$ into (8.8) and linearization [19] leads to the stability equation

$$\left(1 + 4\phi p D_e \sin^2\frac{1}{2}\varsigma h\right)\xi_e = 1 - 4(1-\phi)pD_e\sin^2\frac{1}{2}\varsigma h - \ell r_e, \tag{8.14}$$

where $\xi_e = e^{\sigma\ell}$, with the consequent stability restrictions

$$\begin{aligned} 0 \leq \phi < \frac{1}{2}, &\quad p \leq \frac{2-\ell r_e}{4D_e(1-2\phi)}; \\ \phi = \frac{1}{2}, &\quad \ell r_e \leq 2; \\ \frac{1}{2} \leq \phi < 1, &\quad p \geq \frac{\ell r_e - 2}{4D_e(2\phi-1)}. \end{aligned} \tag{8.15}$$

8.4 Implementation

Implementation of the boundary conditions, (8.4), would yield on $x = 0$ and $x = \mathrm{S}$

$$C_1^n = C_{-1}^n,\ E_1^n = E_{-1}^n \quad \text{and} \quad C_{N+1}^n = C_{N-1}^n,\ E_{N+1}^n = E_{N-1}^n\ (n = 0, 1, 2, \ldots) \tag{8.16}$$

to second order thus introducing the exterior grid points $(x_{-1}, t_n) = (-h, n\ell)$ and $(x_{N+1}, t_n) = ((N+1)h, n\ell)$.

Taking $m = 0$ in (8.7) and (8.8) and using (8.16) gives

$$(1 + 2\phi p D_c) C_0^{n+1} - 2\phi p D_c C_1^{n+1} =$$
$$[1 + \ell(s\frac{C_0^n}{E_0^n} - r_c) - 2(1-\phi)pD_c]C_0^n + 2(1-\phi)pD_c C_1^n + \ell s e_c, \tag{8.17}$$

and

$$(1 + 2\phi p D_e) E_0^{n+1} - 2\phi p D_e E_1^{n+1} =$$
$$[1 - \ell r_e - 2(1-\phi)pD_e]E_0^n + 2(1-\phi)pD_e E_1^n + \ell[s(C_0^n)^2 + e_e]. \tag{8.18}$$

The solution vectors $\mathbf{C}^{n+1}$ and $\mathbf{E}^{n+1}$ may be obtained using the following parallel algorithm:

$$\textbf{Processor 1}: \quad \text{solve} \quad A_1\mathbf{C}^{n+1} = A_2\mathbf{C}^n + \mathbf{q}_1 \quad \text{for} \quad \mathbf{C}^{n+1}, \tag{8.19}$$

$$\textbf{Processor 2}: \quad \text{solve} \quad I_1\mathbf{E}^{n+1} = I_2\mathbf{E}^n + \mathbf{q}_2 \quad \text{for} \quad \mathbf{E}^{n+1}, \tag{8.20}$$

where A_1 is a constant, tridiagonal matrix of order $N+1$ given by

$$A_1 = \begin{bmatrix} 1+2\phi pD_c & -2\phi p & 0 & \cdots & 0 \\ -\phi p & 1+2\phi pD_c & -\phi p & & \vdots \\ 0 & \ddots & \ddots & \ddots & 0 \\ \vdots & & -\phi p & 1+2\phi pD_c & -\phi p \\ 0 & \cdots & 0 & -2\phi p & 1+2\phi pD_c \end{bmatrix}$$

and $\mathbf{q}_1 = [\ell s e_c, \ldots, 0, \ell s e_c]^T$ is a constant vector of order $N+1$. The matrix

$$A_2 = A_2(\mathbf{E}^n) = \begin{bmatrix} a_0 & 2(1-\phi)pD_c & 0 & \cdots & 0 \\ (1-\phi)pD_c & a_1 & (1-\phi)pD_c & & \vdots \\ 0 & \ddots & \ddots & \ddots & 0 \\ \vdots & & (1-\phi)pD_c & a_{N-1} & (1-\phi)pD_c \\ 0 & \cdots & 0 & 2(1-\phi)pD_c & a_N \end{bmatrix}$$

with $a_i = 1 + \ell\left(s\frac{C_i^n}{E_i^n} - r_c\right) - 2(1-\phi)pD_c$, $i = 0, 1, \ldots, N$, is also a tridiagonal matrix of order $N+1$.

The matrix I_1 is also a constant, tridiagonal matrix of order $N+1$ given by

$$I_1 = \begin{bmatrix} 1+2\phi pD_e & -2\phi p & 0 & \cdots & 0 \\ -\phi p & 1+2\phi pD_e & -\phi p & & \vdots \\ 0 & \ddots & \ddots & \ddots & 0 \\ \vdots & & -\phi p & 1+2\phi pD_e & -\phi p \\ 0 & \cdots & 0 & -2\phi p & 1+2\phi pD_e \end{bmatrix}$$

and $\mathbf{q}_2 = \left[\ell(s(C_0^n)^2 + e_e), \ldots, \ell(s(C_N^n)^2 + e_e)\right]^T$ is a constant vector of order $N+1$. The matrix

$$I_2 = \begin{bmatrix} b & 2(1-\phi)pD_e & 0 & \cdots & 0 \\ (1-\phi)pD_e & b & (1-\phi)pD_e & & \vdots \\ 0 & \ddots & \ddots & \ddots & 0 \\ \vdots & & (1-\phi)p & b & (1-\phi)pD_e \\ 0 & \cdots & 0 & 2(1-\phi)pD_e & b \end{bmatrix}$$

with $b = 1 - \ell r_e - 2(1-\phi)pD_e$, is also a tridiagonal matrix of order $N+1$.

8.5 Numerical Experiments

A reaction-diffusion model, {(8.1),(8.2)}, of pigmentation patterns originated by Meinhardt [40] was studied. A family of numerical methods, *Method* $\mathscr{S}(\phi)$, $(0 \leq \phi \leq 1)$, has been developed, analysed and implemented. Numerical simulations based on the activator-inhibitor scheme {(8.1),(8.2)} were carried out using the explicit finite difference scheme {(8.7)-(8.8)}, *Method* $\mathscr{S}(\phi = 0)$. The reason explicit methods were chosen to illustrate the numerical results is that the adaptation of the equations into a form convenient for computer simulation is simple and also the implementation of

the numerical methods is easy. Throughout the numerical experiments two sets of parameter values were used, see Table 8.1.

Sets	D_c	D_e	r_c	r_c	e_c	e_e	s
S1	0.01	0.40	0.05	0.08	0.01	0.0	0.05
S2	0.05	0.40	0.01	0.015	0.05	0.0	0.3

Table 8.1: Sets of parameter values.

The initial conditions used with S1 are

$$C(0) = 1.5 + (1.0 - 2.0 \times RANDOM()) \times 0.03,$$

$$E(0) = 1.5 + (1.0 - 2.0 \times RANDOM()) \times 0.01$$

and with S2 are

$$C(0) = 1.0 + (1.0 - 2.0 \times RANDOM()) \times 0.02,$$

and

$$E(0) = 1.0 + (1.0 - 2.0 \times RANDOM()) \times 0.01.$$

Using *Method* $\mathscr{S}(\phi = 0)$ with the parameter values in set S1 and S2 stable periodic patterns were obtained for $\ell \leq 10.0$. As ℓ was increased further overflow was not observed but negative values leading to oscillatory behaviour with large amplitudes were observed. Concentrations of the activator and the inhibitor are plotted as functions of time at time $t = 1000$, $\ell = 0.01$ in Fig. 8.2 and Fig. 8.3, respectively. Stripes perpendicular to the growth edge of the shell were observed as a result of one-dimensional spatial patterning at the edge. A contour plot of the activator-inhibitor system as a space-time plot illustrates these stripes at the growing edge Fig. 8.4 [see also Fig. 8.1]. As observed in Chapter 7, relatively simple molecular interactions based on local self-enhancement and long range inhibiton allow the

formation of stable patterns starting from more or less homogeneous conditions, Fig. 8.7. The reason {(8.1),(8.2)} can generate the patterns in Fig. 8.4 is the fact that the inhibitor is assumed to diffuse much faster than the activator, that is the condition $D_e \gg D_c$ must be fulfilled: $D_e = 0.4, D_c = 0.01$ were used. This condition enables a new stable, steady-state pattern to be reached due to the action of the inhibitor driving the stabilization of the autocatalysis. In order to obtain a realistic approximation of the real situation very small time steps were used.

Throughout the numerical experiments it was observed that using small time steps was not practical especially if the total time frame was fairly long. Since shell patterns are formed over several years it is possible that a reaction-diffusion system may have some difficulties over such a long period. During the numerical simulations the explicit numerical scheme {(8.7),(8.8)} did not break down after running for a long time with small time step which was chosen by comprimising between speed and precision: $\ell = 0.01, t = 10000$ were used, see Fig. 8.4. Numerical instabilities occurred in step-by-step calculations when the diffusion rates, D_c, D_e, or the saturation term, s, was too high, Figs. 8.5, 8.6, 8.7. Since, when the concentration of the activator rises until it saturates (becomes limited by factors other than long-range inhibition), the spacing of the stripes becomes irregular and far different than the original pattern. Therefore, to avoid these instabilites the numerical values of the diffusion rates had to be taken as $D_c \leq 0.05$, $D_e \leq 0.4$. It was also observed that the width of the stripes and the gaps between them can be greatly sensitive to the model parameters, particularly the relative diffusion rates of activator and inhibitor. An increase in the diffusion rate of the activator to $D_c = 0.05$, broadened the stripes, Fig. 8.8, [see also Fig. 8.4 for $D_c = 0.01$], while an increase in the range of the inhibitor narrowed the stripes at the large distances. Moreover, the reaction-diffusion model was very sensitive to small changes in the initial conditions. Small differences in the initial conditions caused a completely different outcome.

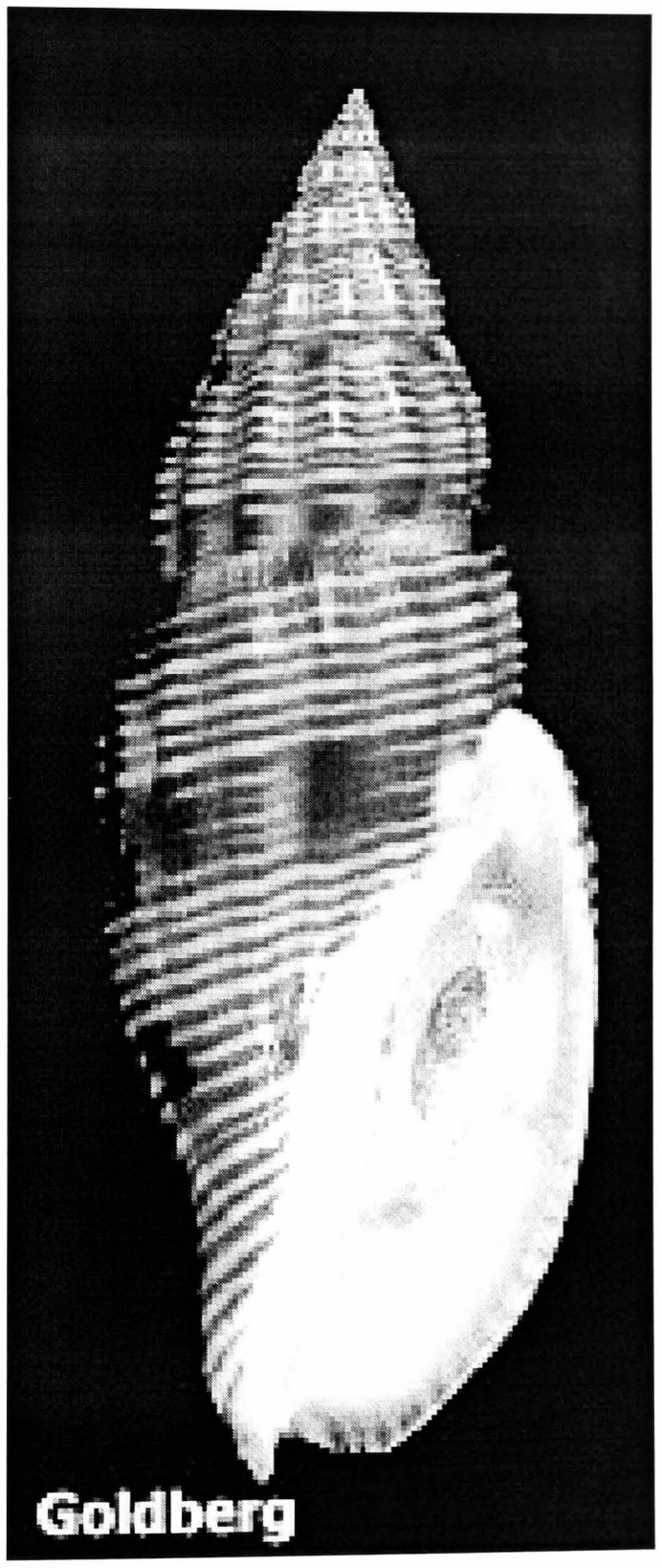

Figure 8.1: Shell of *Lyria planicostata taiwanica.* [79]

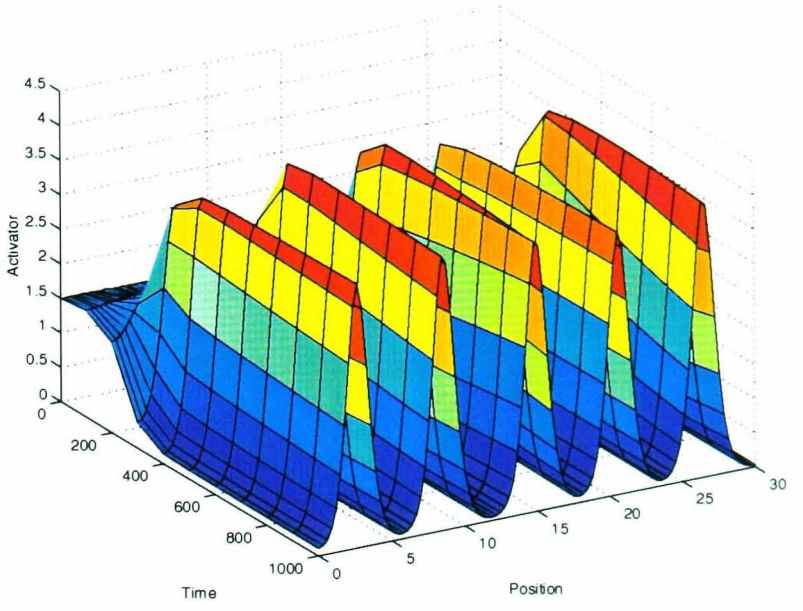

Figure 8.2: Concentrations of the activator as functions of time.

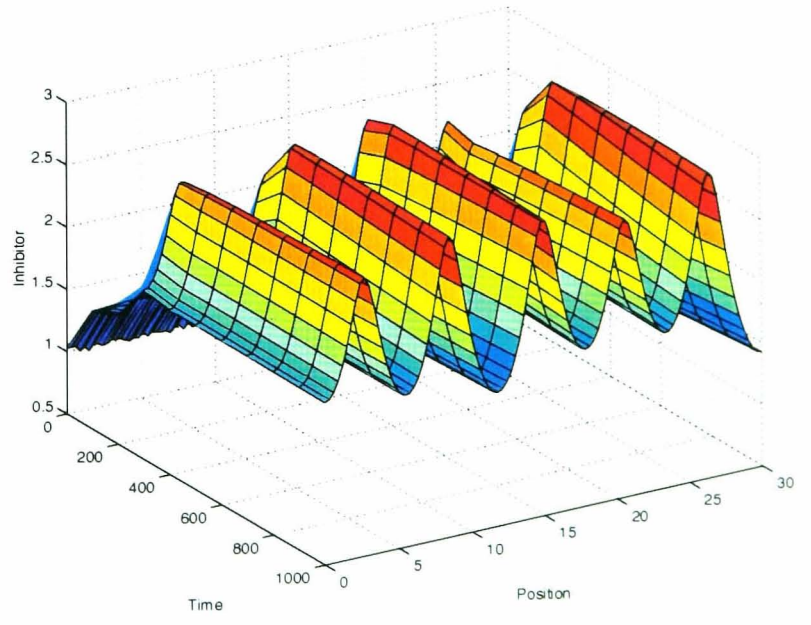

Figure 8.3: Concentrations of the inhibitor as functions of time.

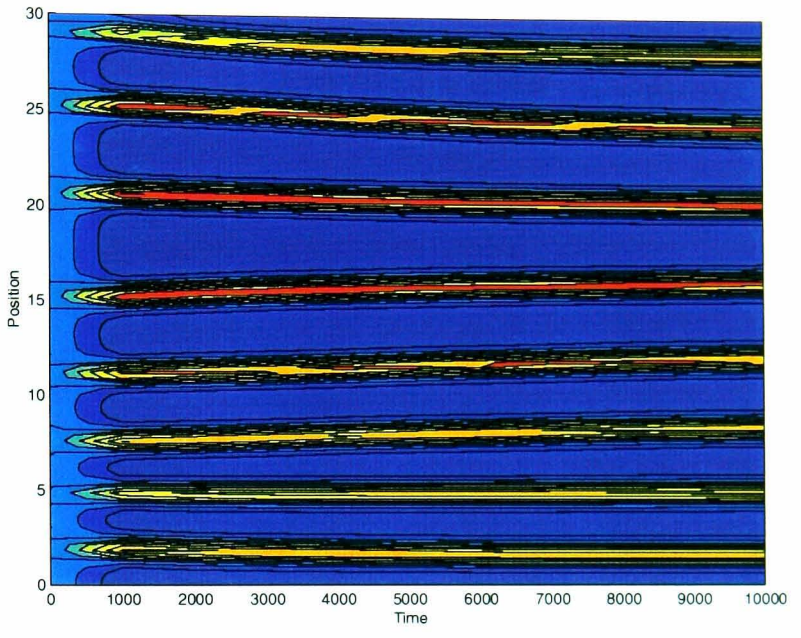

Figure 8.4: Contour plot of activator-inhibitor system.

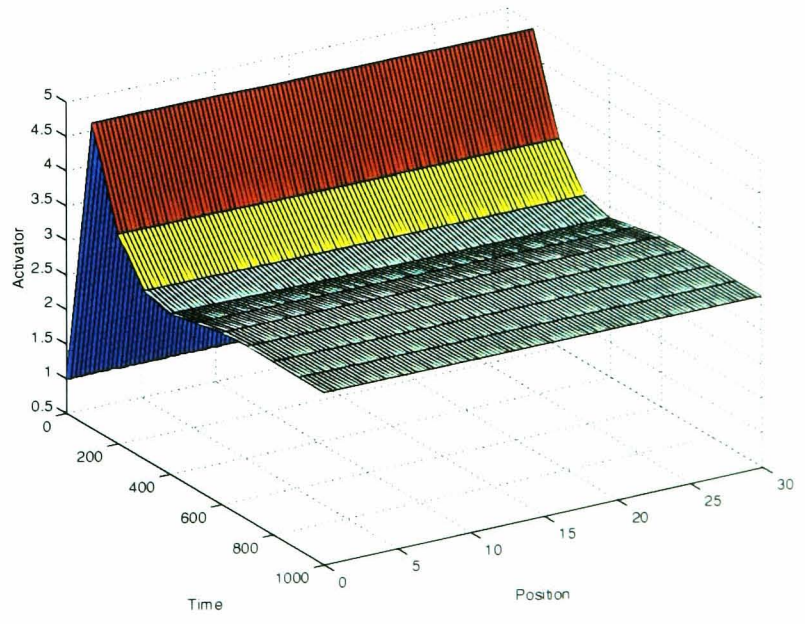

Figure 8.5: Concentration of the activator with $s_c = 0.3$.

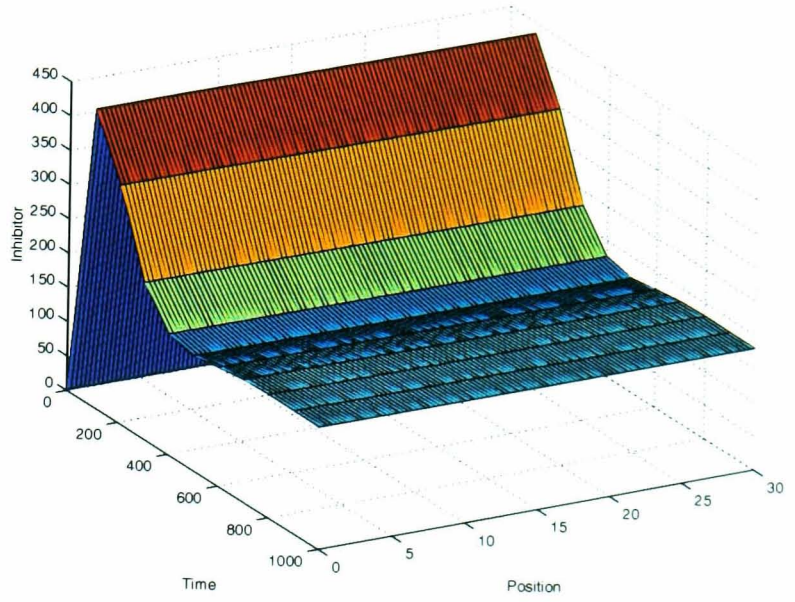

Figure 8.6: Concentration of the inhibitor with $s_c = 0.3$.

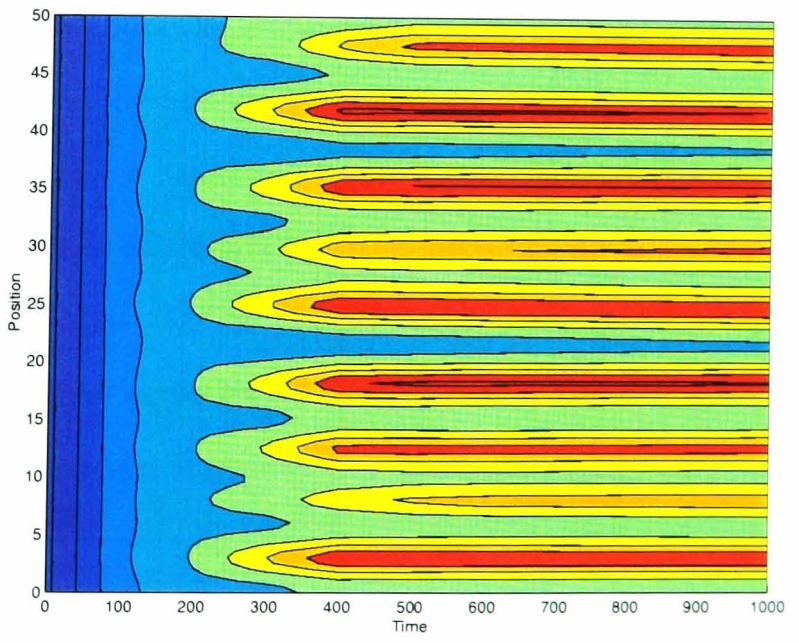

Figure 8.7: Saturation of the autocatalysis (s_c from 0.05 to 0.3) leads to broad stripes.

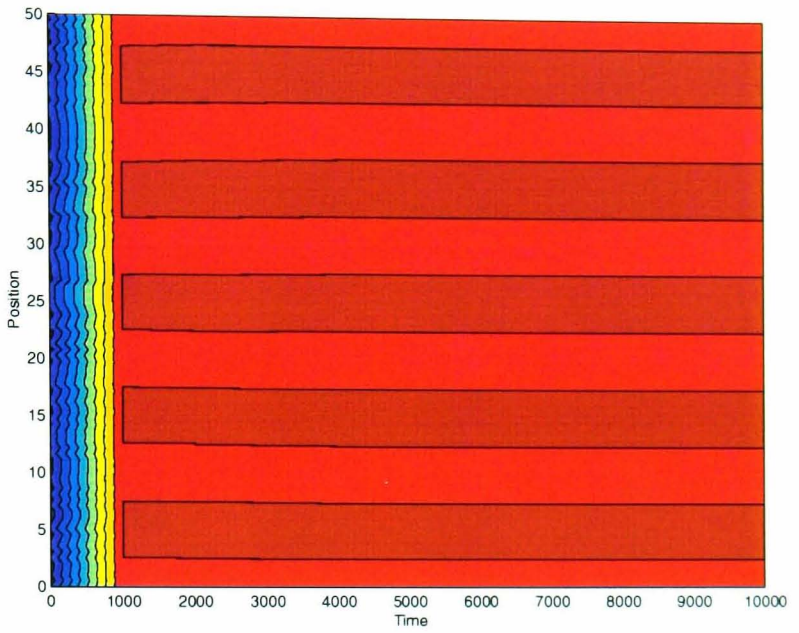

Figure 8.8: Higher activator diffusion leads to broad stripes, $D_c = 0.05$.

8.6 Summary

The generation of patterns on the sea shells by autocatalysis and long-range inhibition suggested by Meinhardt [40] has been studied as an extended study of Turing's theory of morphogenesis investigated in Chapter 7. A family of finite-difference schemes *Method* $\mathscr{S}(\phi), (0 \leq \phi \leq 1)$ was proposed. Explicit numerical methods $(\phi = 0)$ were used to show the reliability of the numerical scheme developed. Succesful simulations provided confirmation of the underlying finite-difference scheme, *Method* $\mathscr{S}(\phi = 0)$, as a valid description of the actual biological situation and compared well with the diagrams in Meinhardt [40].

It was observed that the patterns on the sea shells could be described with fundamentally the same equations that were derived to describe elementary steps in Turing's model for pattern formation.

Chapter 9

Conclusion

The aim of the thesis was fulfilled by developing accurate approximations to the solution of mathematical models of real life applications in chemistry and biology. It was found that the finite-difference schemes proposed, solved the solution profiles efficiently by being qualitatively well agreed to them.

The first- and second-order numerical methods suggested for the solution of ordinary differential equations (ODEs) and partial differential equations (PDEs) are characterized to be implicit. However, in each case it is observed that the numerical solution may be obtained explicitly. Throughout the numerical simulations, it was found that the proposed alternative finite-difference schemes to solve the ODEs have superior stability properties to those of the well-known, first-order, Euler method to which they are compared. For the numerical solution of the non-linear as well as one linear system of PDEs it was seen that the methods are inexpensive to implement and reliable. The numerical solutions were obtained by solving a linear system of algebraic equations at each time step, as opposed to solving a non-linear system which is the case most of the time when solving non-linear PDEs.

As a further study it would be valuable to develop further the mathematical theory of the stability of variable step-size codes to improve those finite-difference schemes studied in this thesis. Here the important question is whether the variation

of the time step according to local error control would automatically enforce some form of numerical stability, even for the explicit schemes. The idea behind this approach is that for the sake of efficiency, and to minimize the build up of round-off errors, being able to use the integration in the smallest number of steps, with the largest possible step size.

As a conclusion, it may be emphasized that studying the chemical reactions which might appear in some chemical and biological phenomena, similar to those studied here, may perhaps some day lead to a better understanding of the processes responsible for the origin of life.

References

[1] M. Al-Mannai, Finite-difference Methods For Some Non-linear reaction-diffusion Systems in Chemistry. Ph.D. thesis, Brunel University, 1998.

[2] D. K. Arrowsmith and C. M Place, *Dynamical Systems* , Chapman and Hall Mathematics, 1992.

[3] M. Ashkenazi and H. G. Othmer,Spatial patterns in coupled biochemical oscillators, *J. Math. Biol.* **5**, 305 (1978).

[4] A. Babloyantz, *Molecules, Dynamics, and Life: An Introduction to Self-Organization of Matter*, John Wiley and Sons, 1986.

[5] R. L. Burden, *Numerical Analysis*, PWS-Kent Publishing Company, Boston, 1993.

[6] C. M. Child, *Patterns and Problems of Development*, University of Chicago Press, 1941.

[7] J. Crank, *The Mathematics of Diffusion*, Clarendon Press, Oxford, 1975.

[8] Z. A. Çınar and E. H. Twizell, *Finite-difference methods for solving a pooled chemical reaction scheme*, technical report TR/33/96, Brunel University Department of Mathematics and Statistics, 1996.

[9] G. Dixon-Lewis, D. J. Williams, *In Comprehensive Chemical Kinetics*, vol. 17 (ed. C. H. Bamford and C. F. H. Tipper). Amsterdam:Elseiver, 1977.

[10] R. A. Fisher, *Ann. Eug.* , **7**, 355, 1937.

[11] E. J. Furshpawn and E. D. Potter, *In Current Topics in Developmental Biology*, (A. A. Moscona and A. Monroy, eds.) pp. 95-127, New York : Academic Press, 1968.

[12] A. Gierer and H. Meinhardt, *Kybernetik*, **12**, 30, 1972.

[13] P. Glendinning, *Stability, Instability and Chaos*, Chambridge University Press, 1995.

[14] P. Gray, S. R. Kay and S. K. Scott, Oscillations of an exothermic reaction in a closed system I. Approximate exponential represantation of Arrhenius reaction in a temperature-dependence,*Proc. R. Soc. Lond. A* **416**, 312 (1988).

[15] P. Gray and S. K. Scott, *Chemical Oscillations and Instabilities*, International Series of Monographs on Chemistry 21, Clarendon Press, Oxford, 1994.

[16] J. Guckenheimer and P. Holmes, *Nonlinear Oscillations, Dynamical Systems, and Bifurcation of Vector Fields*, Applied Mathematical Sciences 42, Springer-Verlag, 1986.

[17] A. Hanna, A. Saul and K. Showalter, Detailed studies of propogating fronts in the iodate oxidation of arsenous acid, *J. Am. chem. Soc.,* **104**, 3838, 1982.

[18] B. D. Hassard, N. D. Kazarinoff and Y. -H. Wan, *Theory and Applications of Hopf bifurcation*, Cambridge: Cambridge University Press, 1981.

[19] U. S. Herges, Finite-difference methods for computing the turning point of ignition in a tubular reactor operated adiabatically, *Comput. Methods Appl. Mech. Engrg.* **137**, 95, 1996.

[20] G. T. Herman and W. H. Liu, The dauther of Celia, the french flag and the firing quad: Progress report on a cellular linear iterative-array simulator, *Simulation* **21**, 33, 1973.

[21] D. W. Jordan, P. Smith *Non-linear Ordinary Differential Equations*. Clarendon Press, Oxford, 1987.

[22] J. V. José and E. J. Saletan, *Classical Dynamics. A Contemporary Approach*, Cambridge University Press 1998.

[23] D. Kaplan and L. Glass, *Understanding Nonlinear Dynamics*, Springer-Verlag New York 1995.

[24] D. G. Kendall, *Mathematical Models of the Spread of Infection.* In Mathematics and computer science in biology and medicine. Medical Research Council, 1965.

[25] W. O. Kermack, A. G. McKendrick, Propagating reaction-difussion waves in a simple isothermal quadratic autocatalytic chemical system, *Proc. R. Soc. Edinb. A. Math.* , **115**, 700, 1927.

[26] A. Kolmogorov, I. Petrovsky and N. Piscounov, *Moscow Univ. bull. Math.* , **1**, 1, 1937.

[27] Y. A. Kuznetsov, *Elements of Applied Bifurcation Theory*, Applied Mathematical Sciences **112**, Springer-Verlag, 1991.

[28] J. D. Lambert , *Numerical Methods for Ordinary Differential Systems* . John Wiley and Sons, Chichester, 1991.

[29] J. A. Leach, J. H. Merkin and S. K. Scott, An analysis of a two-cell coupled non-linear chemical oscillator, *Dynamics and Stability of Systems* **6** 341 (1991).

[30] D. T. Lindsday, A new programmatic basis for shell pigment patterns in the bivalue mollusc *Lioconcha castrensis*, *Differentiation* **21**, 32 (1982).

[31] W. R. Loewenstein, *In The Emergence of Order in Developing Systems.* (M. Locke, ed.; *Devl. Biol. Suppl.* No. 2.) pp. 151-183, New York: Academic Press, 1968.

[32] E. C. A. Lucey and A. S. G. Curtis, Med. biol. Illust. **9**, 86 (1959).

[33] D. G. Luenberger, *Introduction to Dynamical Systems. Theory, Models and Applications*, John Wiley and Sons, New York, 1979.

[34] P. K. Maini, K. J. Painter and H. N. P. Chau, Spatial pattern formation in chemical and biological systems, *J. Chem. Soc., Faraday Trans.* **93** 3601 (1997).

[35] J. E. Marsden and M. McCracken, *The Hopf Bifurcation and Its Applications*, Applied Mathematical Sciences 19, Springer-Verlag, 1976.

[36] R. M. May, *Stability and Complexity in Model Ecosystems*, Princeton University Press 1974.

[37] H. Meinhardt, *Models of Biological Pattern Formation*, Academic Press, London 1978.

[38] H. Meinhardt, Cell determination boundaries as organizing regions for secondary embryonic fields, *Devl. Biol.*, **76**, 115, 1983.

[39] H. Meinhardt, Models for positional signalling, the threefold subdivision of segments and the pigmentation pattern of molluscs, *J. Embryol. exp. Morph.*, **83**, (Supplement) 289, 1984.

[40] H. Meinhardt, *The Algorithmic Beauty of Sea Shells*, Springer Verlag 1998.

[41] J. H. Merkin, D. J. Needham, Propagating reaction-diffusion waves in a simple isothermal quadratic autocatalytic chemical system, *Journal of Engineering Mathematics,* **23**, 343, 1989.

[42] J. H. Merkin, D. J. Needham, The development of travelling waves in a simple isothermal chemical system. I. Quadratic autocatalysis with linear decay, *Proc. R. Soc. Lond. A,* **424**, 187, 1989.

[43] J. H. Merkin, D. J. Needham, The development of travelling waves in a simple isothermal chemical system. II. Cubic autocatalysis with quadratic and linear decay, *Proc. R. Soc. Lond. A,* **430**, 315, 1990.

[44] J. H. Merkin, D. J. Needham, The development of travelling waves in a simple isothermal chemical system with general orders of autocatalysis and decay, *Phil. Trans. R. Soc. Lond. A*, **337**, 261, 1991.

[45] J. H. Merkin, D. J. Needham, and S. K. Scott, A simple model for sustained oscillations in isothermal branched-chain or autocatalytic reactions in a well stirred open system, *Proc. Roy. Soc. London Ser. A* **398**, 101 (1985).

[46] J. H. Merkin, D. J. Needham, and S. K. Scott, Oscillatory chemical reactions in closed vessels, *Proc. Roy. Soc. London Ser. A* **406**, 299 (1986).

[47] J. H. Merkin, D. J. Needham, and S. K. Scott, On the creation, growth and extinction of oscillatory solutions for a simple pooled chemical reaction scheme, *Siam J. Appl. Math. Vol.* **47**, No. 5, 1040, 1987.

[48] J. H. Merkin, D. J. Needham, and S. K. Scott, The development of travelling waves in a simple isothermal chemical system. IV. Quadratic autocatalysis with quadratic decay, *Proc. Roy. Soc. London Ser. A* **343**, 531 (1991).

[49] R. E. Mickens, Construction of a novel finite-difference scheme for a non-linear difference equation, *Numerical Methods for Partial Diferential Equations* **5**, 299 (1991).

[50] N. Minorsky and R. E. Krieger, *Nonlinear Oscillations*, Malabarr, 1974.

[51] A. R. Mitchell, D. F. Griffiths, *Finite Difference Methods in Partial Differential Equations*, John Wiley and Sons, 1980.

[52] J. D. Murray, *Mathematical Biology* , Springer-Verlag, Volume 19, 1980.

[53] D. J. Needham, P. G. Chamberlain, Global similarity solutions to a class of semi-linear parabolic equations, *Proceedings of the royal Society of London Series A- Mathematical Physical and Engineering Sciences*, **454**, 1933 (1998).

[54] H. G. Othmer and L. E. Scriven, Instability and dynamic pattern in cellular networks, *J. theor. Biol.*, **32**, 507 (1971).

[55] T. Pavlidis, *Biological oscillators: Their Mathematical Analysis*, Academic, New York, 1973.

[56] P. J. Plath and J. Schwietering, *Improbable event in deterministically growing patterns. In: Fractal Geometry and Computer. Graphics (J. L. Encarnucao, H. O. Peitgen, Skas, G. englert, Eds.)*, Springer Verlag 1992.

[57] W.G. Price, Y. Wang and E. H. Twizell, A second-order, chaos-free, explicit method for the numerical solution of a cubic reaction problem in neurophysiology, *Numerical Methods for Partial Differential Equations,* **9**, 213, 1993.

[58] I. Prigogine and G. Nicolis, On symmetry-breaking instabilities in dissipative systems, *The Journal of Chemical Physics*, **46**, 507 (1967).

[59] J. T. Sandefur, *Discrete Dynamical Systems Theory and Applications*, Clarendon Press, Oxford, 1990.

[60] A. Saul and K. Showalter, *In Oscillations and travelling waves in chemical systems*, (ed. R. J. Field and M. Burger). New York: Wiley, 1984.

[61] E. E. Sel'kov, Self-oscillations in glycolysis, *Eur. J. Biochem* **4**, 79 (1968).

[62] R. Seydel, *From Equilibrium to Chaos*, Elseiver, 1988.

[63] E. L. Short, Private Communications, 1995.

[64] G. D. Smith *Numerical Solution of Partial Differential Equations: Finite Difference Methods*, Clarendon Press, Oxford, 1985.

[65] A. M. Stuart and A. R. Humphries, *Dynamical Systems and Numerical Analysis*, Cambridge Monographs on Applied and Computational Mathematics, 1996.

[66] Sir D'Arcy Thompson, *On Growth and Form*, 2nd ed. Cambridge University Press, 1942.

[67] A. M. Turing, The chemical basis of morphogenesis, *Phil. Trans. R. Soc.* **B 237**, 37 (1952).

[68] J. J. Tyson, Some further studies of non-linear oscillations in chemical systems, *J. chem. Phys.* **58**, 3919 (1973).

[69] J. J. Tyson and S. Kauffman, Control of mitosis by continuous biochemical oscillation: synchronization spatially inhomogeneous oscillation, *J. Math. Biol.* **1**, 289 (1975).

[70] E. H. Twizell, *Computational Methods for Partial Differential Equations*, Ellis Horwood, Chichester 1984.

[71] E. H. Twizell, *Numerical Methods, with Applications in the Biomedical Sciences*, Ellis Horwood, Chichester 1988.

[72] E. H. Twizell, Y. Wang and W.G. Price, Chaos-free numerical solutions of reaction-diffusion equations, *Proc. R. Soc. Lond.* **A**, **430**, 541, 1990.

[73] E. H. Twizell, Y. Wang, W.G. Price and F. Fakhr, Finite-difference methods for solving the reaction-diffusion equations of a simple isothermal chemical system, *Numerical Methods for Partial Differential Equations,* **10**, 435, 1994.

[74] F. Verhulst, *Nonlinear Differential Equations and Dynamical Systems*, Springer-Verlag 1989.

[75] V. G. Voronkov, N. N. Semenov, *Z. Fizic. Khim.* , **13**, 1695, 1939.

[76] C. Waddington and R. Cowe, Computer simulation of a molluscan pigmentation pattern, *J. Theor. Biol.* **25**, 219 (1969).

[77] E. N. Willmer, *Tissue Culture*, 3rd ed. London, 1958.

[78] S. Wolfram, Cellular automata as models of complexity, *Nature* **341**, 419 (1984).

[79] http://www.gastropods.com/shell_pages/p/Shell_Lyria_planicostata.html